INFORMATION TO USERS

This manuscript has been reproduced from the microfilm master. UMI films the text directly from the original or copy submitted. Thus, some thesis and dissertation copies are in typewriter face, while others may be from any type of computer printer.

The quality of this reproduction is dependent upon the quality of the copy submitted. Broken or indistinct print, colored or poor quality illustrations and photographs, print bleedthrough, substandard margins, and improper alignment can adversely affect reproduction.

In the unlikely event that the author did not send UMI a complete manuscript and there are missing pages, these will be noted. Also, if unauthorized copyright material had to be removed, a note will indicate the deletion.

Oversize materials (e.g., maps, drawings, charts) are reproduced by sectioning the original, beginning at the upper left-hand corner and continuing from left to right in equal sections with small overlaps.

Photographs included in the original manuscript have been reproduced xerographically in this copy. Higher quality 6" x 9" black and white photographic prints are available for any photographs or illustrations appearing in this copy for an additional charge. Contact UMI directly to order.

ProQuest Information and Learning
300 North Zeeb Road, Ann Arbor, MI 48106-1346 USA
800-521-0600

SOME ISSUES IN ENABLING TECHNOLOGIES FOR HIGH DATA RATE RELIABLE WIRELESS COMMUNICATIONS: OFDM AND ADAPTIVE ARQ

by

HLAING MINN
M.Eng., Asian Institute of Technology, 1997
B.E.(Hons.), Yangon Institute of Technology, 1995

A Dissertation Submitted in Partial Fulfillment of the Requirements
for the Degree of

DOCTOR OF PHILOSOPHY

in the Department of Electrical and Computer Engineering

We accept this dissertation as conforming
to the required standard

Dr. V. K. Bhargava, Supervisor, Dept. of Elect. & Comp. Eng.

Dr. P. Agathoklis, Dept. of Elect. & Comp. Eng.

Dr. W.-S. Lu, Dept. of Elect. & Comp. Eng.

Dr. N. Djilali, Outside Member, Associate Dean, Faculty of Engineering

Dr. M. Z. Win, External Examiner, AT&T Laboratories-Research.

Supervisor: Dr. V. K. Bhargava

ABSTRACT

Generation by generation, wireless communication has advanced in various ways and provided reliable communication services at higher and higher data rates to the needs of more and more advanced wireless applications. Two main issues towards future wireless communications are high-speed transmission technique to provide high data rate services and reliable communication to ensure the required performance. This dissertation focuses on these two issues. Since orthogonal frequency division multiplexing (OFDM) has emerged as an enabling technique for high-speed transmission in dispersive environments, major and fundamental issues in OFDM, namely, synchronization, channel estimation, and peak-to-average power ratio (PAPR) reduction are addressed. For the required reliability, automatic repeat request (ARQ) schemes must be applied. Due to large potential performance improvement, adaptive ARQ schemes have recently attracted much attention and are also addressed here.

We propose two improved OFDM timing synchronization methods which overcome the drawbacks of existing methods. We present a time-domain-based OFDM channel estimation which outperforms the existing time-domain-based approach and has a similar performance to the linear minimum mean square error estimator but with less complexity. For OFDM systems with transmit diversity, we present a reduced complexity channel estimation which has a comparable performance to the existing method for channels with relatively small delay spreads, but achieves much complexity saving. An approach to find the number of most significant channel taps is described for diverse channel environments. We analyze the effect of non-sample-spaced channel path on the channel estimation and propose a modification for further improvement.

Timing synchronization, frequency synchronization and channel estimation are usually addressed separately. Since they can affect each other, the idea of jointly addressing all of them together is much desirable and pursued here. This joint approach reflects the actual performance and gives an opportunity to exploit some information obtained from one task in another, hence promising more improvement. The proposed training preamble-based joint timing and frequency synchronization utilizes some information from the channel estimation. The sync detection is also considered. We

design the training symbol to achieve a better coarse timing synchronization. Methods to suppress or circumvent the interference in the frequency estimation caused by timing errors are presented. A new performance measure for OFDM timing synchronization is proposed which leads to obtaining optimal timing estimation setting. Next, we present a joint timing synchronization, frequency synchronization and channel estimation based on training preamble based maximum likelihood realization. Further complexity reduction by an adaptive scheme is also proposed.

We address some fundamental questions on peak factors, sampling theorem and sampling series. We present several bounds of bandlimited functions and peak factor ratio bound of a continuous signal and its sampled signal. Some discussion on the requirements of sampling theorems and related aspects on sampling series are presented. We study PAPR behavior of some Reed-Muller codes in OFDM systems in an attempt to find a code with good error correction, low PAPR, efficient encoding/decoding and reasonable code rate. Some regularities of the second and third-order cosets of first-order Reed-Muller codes with low PAPR are presented which indicates possibility of finding such code for OFDM.

The main issues in adaptive ARQ schemes are how to design the adaptive system parameters and how to effectively sense the channel conditions. We present an approach for designing the adaptive ARQ system parameters based on the throughput calculation and optimization. An alternative approach which avoids the tedious throughput calculation is also presented. An effective channel sensing algorithm which utilizes the error correcting capability is proposed. Incorporation of the adaptive frequency hopping concept into the ARQ scheme with adaptive error control is introduced which has a significant throughput improvement in slow fading channels.

Examiners:

Dr. V. K. Bhargava, Supervisor, Dept. of Elect. & Comp. Eng.

Dr. P. Agathoklis, Dept. of Elect. & Comp. Eng.

Dr. W.-S. Lu, Dept. of Elect. & Comp. Eng.

Dr. N. Djilali, Outside Member, Associate Dean, Faculty of Engineering

Dr. M. Z. Win, External Examiner, AT&T Laboratories-Research.

Table of Contents

List of Figures

List of Tables

List of Abbreviations

ACIS	Advanced Cellular Internet Services
ACK	Acknowledgement (message)
ADSL	Asymmetric Digital Subscriber Line
ANSI	American National Standards Institute
ARDIS	Advanced Radio Data Information Service
ARQ	Automatic Repeat reQuest
ATTC	Advanced Television Technology Center
AWGN	Additive White Gaussian Noise
BER	Bit Error Rate
BPSK	Binary Phase Shift Keying
BRAN	Broadband Radio Access Networks
CDPD	Cellular Digital Packet Data
CRC	Cyclic Redundancy Check
CSE	Channel State Estimator
CSI	Channel State Information
DAB	Digital Audio Broadcasting
DFT_N	N point Discrete Fourier Transform
DMT	Discrete Multi-Tone
DVB	Digital Video Broadcasting
ETSI	European Telecommunications Standardization Institute
FD	Frequency-Domain
FDM	Frequency Division Multiplexing
FEC	Forward Error Correction
FFT_N	N point Fast Fourier Transform
FH	Frequency Hopping
FPTA	Frequency-Pilot Time-Averaging method
GBN	Go-Back-N protocol
GPRS	General Packet Radio Services
GSM	Global System for Mobile communications

HD	Hard Decision
HiperLAN 2	High Performance Local Area Network - type 2
HT	Hilly Terrain
ICI	Inter-sub-Channel Interference
IEEE	Institute of Electrical and Electronics Engineers
IFFT_N	N point Inverse Fast Fourier Transform
iid	independent and identically distributed
ISDB-T	Terrestrial Integrated Services Digital Broadcasting
ISI	Inter-Symbol Interference
ITU-R	International Telecommunications Union - Radio
JTC	Joint Technical Committee
LAN	Local Area Network
LMMSE	Linear Minimum Mean Square Error (Estimator)
LS	Least Square
MAN	Metropolitan Area Network
ML	Maximum Likelihood
MMAC	Multimedia Mobile Access Communications
MMSE	Minimum Mean Square Error
mse	Mean Square Error
MST	Most Significant Taps
NACK	Negative Acknowledgement (message)
OFDM	Orthogonal Frequency Division Multiplexing
OFDMA	Orthogonal Frequency Division Multiple Access
PAPR	Peak to Average Power Ratio
PN-sequence	Pseudo Noise sequence
QoS	Quality of Service
QPSK	Quadrature Phase Shift Keying
RM	Reed-Muller code
RS	Reed-Solomon code
SC	Single Carrier
SER	Symbol Error Rate
SFN	Single Frequency Network

SIR	Signal-to-Interference Ratio
SNR	Signal-to-Noise Ratio
SOHO	Small Office Home Office
SW	Stop-and-Wait protocol
TD	Time-Domain
TU	Typical Urban
VLSI	Very Large Scale Integration
WSSUS	Wide Sense Stationary Uncorrelated Scattering
64-QAM	64-Quadrature Amplitude Modulation

Acknowledgement

First and foremost, I would like to express my deepest appreciation to my thesis supervisor and mentor, Prof. Vijay K. Bhargava. I greatly valued the freedom and flexibility with which he entrusted me, the generous support (both in terms of research assistantship and funding for attendance at many technical conferences) he has provided and for offering the finest lab on campus from which I could perform my research in a timely manner.

I am very grateful to Professors Ned Djilali, Panajotis Agathoklis and Wu-Sheng Lu for serving on my supervisory committee, and Dr. Moe Z. Win for agreeing to be the external examiner in my Ph.D. oral examination. Their time and effort are highly appreciated. Special thanks to Dr. M. Z. Win and Prof. V. K. Bhargava for their many helpful suggestions which have improved the presentation of this thesis.

My sincere thanks are extended to my colleagues at Prof. Bhargava's lab for their friendship and co-operation in various ways. I also wish to express my thanks and appreciation to Professors Khaled Ben Letaief, Chinthananda Tellambura and Dr. Mao Zeng for their useful suggestions and constructive criticism at several points throughout my research. My thanks also go to Professor Aaron T. Gulliver for allowing me to use his computer resources. I also thank to Mohamed Watheq El-Kharashi for his help in Latex formatting. It is impossible to mention all the people that have in some way influenced this work, and I apologize to those individuals whose names are omitted.

Last but not the least, I deeply thank my family for their love and devoted support throughout my life. In particular, my parents have always been there for me and supported me in every way possible.

Dedication

To My Beloved Parents

Chapter 1

Introduction

Starting from Maxwell's prediction of electromagnetic radiation in 1864, Hertz's verification of Maxwell's theory in 1887, Oliver Lodge's demonstration of wireless communication over a distance of 150 yards in 1894, Marconi's first transatlantic wireless signal transmission in 1901, Fessenden's transmission of speech and music by radio in 1905, the wireless communication has been developed in various aspects. Through the developments of the first generation analog mobile wireless communication in the 1980's, the second generation digital mobile wireless communication in the 1990's, the wireless communication has recently entered into its third generation (3G). Researchers around the world start looking into further improvements for the 3G systems, and issues for the beyond-3G systems. As the popularity of the wireless internet and wireless multimedia communications increases, one of the major challenges for those 3G and beyond-3G systems is to establish a reliable wireless communication link with a sufficiently high data rate in a hostile wireless radio channel environment.

For the issue of achieving a desired reliability, error control techniques such as automatic repeat request (ARQ) schemes have to be incorporated in the system design in addition to the other performance improvement techniques such as error correcting codes , antenna diversity, etc. For a time-varying mobile wireless channel, adaptive ARQ schemes, which change some parameters such as code rate, modulation format, packet length according to the channel conditions, have recently achieved much attention due to their potentially significant performance improvement. Those adaptive ARQ schemes typically require to sense the channel conditions. Hence, how to design an effective adaptive ARQ scheme and how to efficiently sense the channel conditions are of great interest for further performance improvement.

For the issue of high data rate transmission in a hostile dispersive multipath fading

channel, orthogonal frequency division multiplexing (OFDM) technology has emerged as one of the favored transmission techniques. Although the popularity of OFDM is quite recent, the basic concept of OFDM appeared in the research literature as early as in 1966 when Chang published his work [1] on the synthesis of band-limited orthogonal signals for multichannel data transmission. It was followed by Saltzberg's work [2] on its performance analysis in 1967. In these works, banks of subcarrier oscillators were used in both transmitting and receiving the multicarrier signal. The realization of a frequency division multiplexing (FDM) system by means of the discrete Fourier transform (DFT) was proposed by Darlington [3] in 1970. Subsequently, the use of DFT as a baseband modulation and demodulation technique for the multicarrier signal was proposed by Weinstein and Ebert [4] in 1971 which eliminated the need of banks of subcarrier oscillators. They used a null guard interval in the case of a dispersive multipath channel. The next contribution to OFDM technology is due to Peled and Ruiz [5] where they used a cyclic extension of the OFDM symbol to fill the null guard interval. With this cyclic prefix, the effect of the multipath channel to the multicarrier signal in the time domain turns into a circular convolution type rather than the usual linear convolution type. In the subcarrier (frequency) domain, each subcarrier just experiences a flat (complex) channel response which makes the equalization task in an OFDM system much easier than that in a single carrier system which usually has to use a computationally expensive time-domain equalization for a dispersive multipath channel.

In fact, earlier than the above works, OFDM technology was used in military high-frequency (HF) communication systems such as the KINEPLEX system [6] [7] from Collins Radio Co. (USA), the ANDEFT/SC-320 system [8] from General Dynamics Corp. (USA) and the AN/GSC-10 KATHRYN system [9] [10] from General Atronics Corp. (USA). Another application of OFDM was found in high-speed voice-band data communication modems [11] [12] at NEC Corp. (Japan) where the motivation was to alleviate the degradations caused by an impulsive noise environment. Further works in OFDM such as [13] [14] [15] motivate much interest in OFDM technology and applications. Due to the advances in signal processing and VLSI technology, the efficient implementation of DFT by means of fast Fourier transform (FFT) algorithm makes the OFDM technology enjoy a renaissance.

Based on the works such as [14] [16] [17] [18] [19], the OFDM technology has been adopted in European Digital Audio Broadcasting (DAB) standard which is suited for mobile receivers and the total data rate is 1.7 Mbps. This has led to ITU-R system recommendations for terrestrial digital sound broadcasting [20] [21]. Moreover, works such as [22] [23] [24] [25] [26] have led to the adoption of OFDM in European Digital Video Broadcasting (DVB) standard which has a net data rate of more than 20 Mbps. Also in Japan, OFDM has been chosen for terrestrial integrated services digital broadcasting (ISDB-T) [27] [28]. It must be also mentioned that OFDM has been adopted in wireline applications such as Asymmetric Digital Subscriber Line (ADSL) by ANSI [1] [29] where it is better known by the name discrete multi-tone (DMT).

Current wireless data systems may be categorized into two groups [30] [31]. The first group covers wide-area services offering limited bit rates on the order of 10-100 kbps. These include RAM Mobile Data, Advanced Radio Data Information Service (ARDIS), Cellular Digital Packet Data (CDPD) and the emerging digital cellular data services like the General Packet Radio Service (GPRS) for GSM. The second group provides much higher data rates (1-10 Mbps) but has small coverage areas, usually limited to within a building. These include WaveLAN and RangeLAN2. There have been several recent activities addressing the need to transmit higher data rates or cover wider areas. To provide wireless internet services with higher data rates than 3G systems, AT&T has proposed Advanced Cellular Internet Services (ACIS) [31] where OFDM is adopted and data rates of 2 to 5 Mbps in macro-cellular environments, and up to 10 Mbps in micro-cellular and indoor environments are described [32]. For broadband communications, OFDM has been chosen for High Performance Local Area Networks (HIPERLAN) type 2 standard in 5GHz band with the data rate ranging from 6 to 54 Mbps by the ETSI-BRAN [2] [33]. Similarly, the IEEE 802.11 standards group has chosen OFDM for wireless LANs operating at bit rates ranging from 6 to 54 Mbps in the 5 GHz band [34]. In Japan, the Ministry of Post and Telecommunications started a standardization effort of Multimedia Mobile Access Communication (MMAC) [35] which also adopted OFDM for its physical layer

[1] American National Standards Institute

[2] ETSI= European Telecommunications Standardization Institute, BRAN=Broadband Radio Access Networks

standard [36]. MMAC's target specification includes wireless access and wireless LAN in the 5 GHz band (similar to HiperLAN/2 and IEEE 802.11a) with the bit rates of 20 to 25 Mbps, high speed wireless access in 25/40/60 GHz bands with the bit rate of 30 Mbps, wireless home-link in 5/25/40/60 GHz bands with the bit rates of 30 to 100 Mbps and ultra high speed wireless LAN in 60 GHz band with the bit rate of 156 Mbps. It should be noted that all wireless access and wireless LAN standards in the 5 GHz band from IEEE, ETSI and Japan have adopted the same physical layer technology OFDM, hence, paving the way for global applicability of OFDM wireless LAN products.

Currently, the IEEE 802.16 Wireless Metropolitan Area Networks (Wireless MAN) group is carrying out the standardization activities for broadband wireless access in 10 to 66 GHz bands and licensed and unlicensed bands in the 2 to 11 GHz. The group for licensed and unlicensed bands in the 2 to 11 GHz has adopted both single carrier and OFDM physical layer technologies. In fact, in the single carrier technology, frequency domain equalization, which was originated in OFDM technology, is an essential part. There are some other projects/activities which have adopted OFDM. For example, the WIND-FLEX project [37] in Europe is developing a very flexible wireless indoor modem with a bit rate between 64 Kbps to 100 Mbps for the small office home office (SOHO) environment with low mobility in the 17 GHz band and OFDM has been adopted for the air interface.

The basic principle of OFDM is as follows. The transmission bandwidth is divided into many narrow band subchannels and data are transmitted parallel on the subchannels. Hence, the OFDM symbol has much longer interval and suffers from much less inter-symbol interference (ISI) than the single carrier case. Moreover, the spectra of the subchannels overlap and hence, improving the bandwidth efficiency of the system. The baseband subcarriers are orthogonal to each other over an OFDM symbol duration (the reciprocal of the subcarrier spacing). This fact facilitates the recovery of the transmitted data at the receiver and allows the efficient DFT implementation. The FFT implementation also eradicates the need of banks of subcarrier oscillators and simplifies in generating and retrieving the OFDM signal. By cyclically extending the OFDM symbol (in other words, by inserting a cyclic prefix), the effect of ISI can, in principle, be totally avoided and the effect of the channel to the

data in the frequency domain becomes just like a flat fading. The equalization in a dispersive multipath environment becomes just a complex multiplication on each subcarrier data, hence, achieving much complexity saving for the equalization. For a conventional single carrier system in a similar dispersive multipath environment, the required equalization to combat the ISI can be computationally prohibited.

Another advantageous flexibility with OFDM is that according to the subchannel responses, adaptive power distribution and/or adaptive bit loading (adaptive modulation) can be applied across the subcarriers based on the Gallager's water-pouring theorem. By applying this, bit error rate (BER) or data throughput or power consumption can be significantly improved.

The desirable features and advantages of OFDM also come with some disadvantages. Being a multi-carrier system, OFDM is much more sensitive to synchronization errors, particularly frequency offset errors. Frequency offset errors cause the loss of orthogonality among the subcarriers and result in inter-subchannel interference (ICI) which can degrade the system performance. Other synchronization tasks such as timing synchronization can affect the frequency synchronization performance. Hence, synchronization is an important issue in OFDM for ensuring its advantages. For a coherent OFDM system or an OFDM system with adaptive power allocation or bit loading, or a coherent OFDM system with space-time coding, the channel estimation becomes a crucial task and receives much research attention. Another issue in OFDM with transmit diversity is channel estimation complexity. For a time-varying channel if the channel estimates have to be tracked quite closely, the required complexity can be quite large and it demands a reduced complexity algorithm.

Another disadvantage of OFDM system is a high peak-to-average power ratio (PAPR) of the signal. Having high PAPR can cause nonlinear distortion at the transmit power amplifier and result in in-band and out of band distortion. The PAPR problem is more serious in an OFDM system with a larger number of subcarriers. In the above, the background, application, basic principle, and research issues in our focus areas are presented. The following sections will concentrate on our research contributions.

1.1 Significance of Research

In this dissertation, we address two main research areas namely OFDM and adaptive ARQ. The significance of OFDM technology has been justified by its adoption in many standards as described above. In OFDM, we address main research issues such as synchronization, channel estimation, joint synchronization and channel estimation, reduced complexity channel estimation, and PAPR. Regarding the timing synchronization in OFDM, the existing methods are associated with one or more drawbacks such as limited operation range, non-robustness, large estimation error, etc. We propose two timing synchronization methods which avoid those drawbacks and achieve better timing estimation performance. A better timing estimation can not only save some system overhead by means of smaller cyclic prefix guard interval but also help other synchronization and channel estimation tasks to achieve a better performance. In other words, a better timing synchronization can improve both system capacity and system performance.

Channel estimation is an important research area in OFDM. In order to effectively employ performance enhancement techniques such as adaptive power distribution or adaptive bit loading, high performance channel estimation is quite essential. At the same time, reduced complexity methods are much desirable particularly for mobile terminals. We propose a time-domain-based channel estimation which achieves a better performance than the existing time-domain-based method, and a similar performance to linear minimum mean square error estimator but with reduced complexity. A better channel estimation can not only improve the system performance but also facilitate the employment of performance and capacity enhancement techniques which in turn improve the system capacity.

In counteracting the impairment of mobile wireless channels, diversity techniques such as transmit/receive diversity are favorable approaches since no extra system resources such as time slots or frequency bands are required. Space-time coding is a form of transmit diversity combined with some coding aspects such that both diversity gain and coding gain are maximized. Space-time coding has recently achieved a great attention due to its high peak data rate transmission capability and it will play an important role for future wireless system with transmit diversity. For OFDM systems with space-time coding, the required channel estimation task for a time-varying

channel can be computationally expensive especially for mobile terminals. In order to implement the space-time coding in mobile terminals commercially successfully, reduced complexity channel estimation methods for systems with transmit diversity are highly desirable. We propose a reduced complexity channel estimation for an OFDM system with transmit diversity which has a similar performance to the existing method in channel environments with relatively small delay spreads, but achieves much complexity saving. In the existing channel estimation method for OFDM with transmit diversity, the knowledge of the number of most significant channel taps is required. For channel environments where this knowledge is unavailable, other mechanism to find the number of most significant taps is required. We present an approach to find the number of most significant taps. The proposed approach has similar performance to the case with known knowledge of this number and can achieve some complexity saving under some conditions. We also propose a modification to the existing method which can yield a significant performance improvement without requiring any added complexity.

Generally, timing synchronization, frequency synchronization and channel estimation are addressed separately. In some timing synchronization methods, a perfect carrier frequency recovery is assumed. In most separate frequency synchronization methods, a perfect timing is assumed. Since perfect synchronization is not always be achieved in practice and errors in one task can affect the other, the performance of separate methods would not reflect the actual situations. Hence, joint timing and frequency synchronization approach is much desirable. Moreover, little attention has been given to the sync detection. For a reliable communication link, very low probabilities of false detection and missed detection are essential. We propose a joint timing and frequency synchronization which has a robust sync detection capability. Other practical issue such as peak factor of the training symbol is also taken into account in the proposed method. Previous channel estimation methods assume perfect synchronization which cannot be guaranteed. The synchronization errors can affect the channel estimation performance. Hence, it is much desirable to address the synchronization and channel estimation tasks together since it will reflect a more practical situation. Moreover, the information from one task can be utilized in another task to achieve further improvement. We also propose a joint synchronization

and channel estimation in this trend. The performance is quite promising and the proposed method is rather general.

Timing synchronization performance is usually evaluated by timing estimation variance. However, in OFDM systems, as long as the timing offset is within the ISI-free interval, it will just introduce phase shifts on the subcarrier symbols. These phase shifts will be taken care by the channel estimation and hence, there will be no performance degradation caused by the timing offset. Hence, a more performance-oriented measure for the timing synchronization performance is desirable. Timing offset introduced interference power appears to be a good measure. However, it depends on the timing estimation parameter such as the mean of the timing offset. In this dissertation, we present a new performance measure for the timing synchronization performance. This new performance measure yields a simple and effective way of how to optimally design the timing estimation setting such as the timing estimate shift for a considered mobile wireless channel. In fact, in the research literature, no works have been observed for designing the timing estimation setting. Our results show that proper design of the timing estimation setting can considerably improve the system performance. Hence, the proposed performance measure and the proposed timing estimation setting design will be much useful in OFDM modem design.

Another major issue in OFDM is its high PAPR which has been the main unfavorable obstacle for a wider acceptance of OFDM. Several techniques have been proposed to tackle this PAPR problem at the expense of performance degradation, power backoff penalty, code rate, high computational complexity with no guaranteed PAPR limit, etc. Since error correcting code is an essential part for a reliable wireless communication, the idea of finding a code with good error correcting capability and low PAPR is one of the promising techniques. In fact, to find a code with good error correcting capability, low PAPR, reasonable code rate and efficient encoding/decoding process for an OFDM system with any number of subcarriers is really ambitious objective and an open problem. A recent breakthrough in this trend is the use of second-order cosets of the first-order Reed-Muller code which enjoys good error correction capability, low PAPR and efficient encoding/decoding process. However, for an OFDM system with a large number of subcarriers, this approach has a very low code rate. Hence, the problem is still open. We follow a similar trend and

study the PAPR behavior of higher order cosets of the first-order Reed-Muller code. Our results show that some regularities exist for those codes with low PAPR. This indicate that it is possible to include higher order cosets in order to increase the code rate. Although our results do not solve the open problem, it indicates the posibility to alleviate the problem and motivates further research in a similar trend.

In most communications texts to our reach, the statement on sampling theorem usually says that for a finite energy signal whose spectrum is zero for the frequencies $|f| > W$, it can be represented by its samples obtained with the sampling frequency $f_s = 2W$. This theorem is quite often applied to the periodic signal too. However, the detailed analysis of the applicability of this theorem to the periodic signal is missing. In this dissertation, we discuss this sampling issue for both non-periodic and periodic signals. Moreover, related to the peak factors of the continuous signal and its sampled signal, other fundamental questions also arise. These questions are: "under what condition, if any, can a bandlimited function take infinite values between finite samples ?", "does an arbitrary sequence represent the samples of a bandlimited function of interest for communications systems ?", "how much can the peak factors of a continuous signal and its sampled signal differ ?", and "what are the bounds of the amplitude and variations of a bandlimited periodic or non-periodic function ?". These fundamental questions will also be discussed in this dissertation.

The second part of this dissertation focuses on adaptive ARQ schemes. Adaptive ARQ schemes, which change some parameters such as code rate, modulation formats according to the channel condition, are in principle quite effective in time-varying wireless environment and have significant potential throughput performance improvement. However, in actual implementation, two issues, have to be solved. They are how to design the adaptive system parameters and how to efficiently sense the channel condition. Previous adaptive ARQ schemes usually use heuristically chosen adaptive system parameters or are designed based on an assumed channel model with known characteristics. Their applicability in a practical time-varying mobile wireless channel needs further investigation. Improper adaptive system parameters and/or unreliable channel sensing not only lose the potential throughput improvement but also can render a worse performance than a non-adaptive system. We address these two issues in this dissertation. The efficiency and applicability of our proposed approaches are

evaluated by computer simulation for a typical time-varying mobile wireless channel characterized by the Rayleigh fading and lognormal shadowing. Moreover, we introduce another dimension into adaptive ARQ scheme's parameters which yields substantial throughput improvement in slow fading environments. The throughput expression of an adaptive ARQ scheme is conventionally expressed as the average of the throughputs in individual modes of the adaptive system. However, we point out that this conventional throughput expression is not an exact but an approximate one. We also outline an exact throughput calculation of an adaptive ARQ scheme.

1.2 Thesis Outline

This thesis consists of eleven chapters. Chapter 2 to 8 are related to OFDM and Chapter 9 and 10 are related to adaptive ARQ schemes. In Chapter 2, we present two improved timing synchronization methods for OFDM systems which overcome the drawbacks of previous methods. In Chapter 3, we present a time-domain-based channel estimation for OFDM systems which employs intra-symbol averaging and most significant tap selection. The relationship to other existing methods, the similarities and the differences are discussed. The proposed method has a better performance than the existing time-domain-based method namely frequency-pilot time-average method (FPTA) and a similar performance to a LMMSE method but with less complexity.

In Chapter 4, we present a reduced complexity channel estimation for OFDM systems with transmit diversity. The BER performance and computational complexity comparison between the proposed method and the existing method are presented. An approach to find the number of most significant channel taps required in the channel estimation is also proposed. The effect of non-sample-spaced channel path on the sample-spaced channel estimation is analyzed. Based on this, a modification to the existing method and the proposed reduced complexity method is proposed which achieves further improvement without any added complexity.

In Chapter 5, a robust timing and frequency synchronization for OFDM systems is presented. In order to achieve a better coarse timing synchronization, the OFDM training symbol is designed to have a steep roll-off timing metric trajectory. In order to

avoid the nonlinear distortion of the training symbol at the transmit power amplifier, the training symbol is designed to have a low PAPR. In the consideration of the timing metric, a robust sync detection capability is taken into account. Existing performance measures for OFDM timing synchronization are discussed and a new performance measure is proposed. Based on this, an optimal design for the timing estimation setting is presented. An approach to suppress the timing error introduced interference in the frequency estimation is proposed. A maximum likelihood based frequency estimation which does not suffer from the timing error introduced interference is also presented. Further improvement in the synchronization performance by means of utilizing some information from the channel estimation is discussed.

In Chapter 6, we present a maximum likelihood (ML) based timing and frequency synchronization and channel estimation for OFDM systems using a training sequence based approach. The ML realization is obtained by two stages namely coarse stage and fine stage. Performance analyses of frequency estimation and channel estimation are presented. Discussions on the non-ideal situations in the practical implementation are given. Simulation results in a frequency selective multipath fading channel for the sync detection performance, timing synchronization performance, frequency synchronization performance, channel estimation performance and BER performance are presented. An adaptive scheme which reduces some complexity is also outlined.

In Chapter 7, we discuss on the peak factors of continuous signal and its sampled signal. Several bounds for bandlimited periodic or non-periodic functions are presented. Based on them, bounds on the peak factor ratio of the continuous periodic or non-periodic signal and its sampled signal are given. Related aspects on the sampling theorem and sampling series are also discussed. In Chapter 8, we study some PAPR behavior of the second and third-order cosets of first-order Reed-Muller code for OFDM systems. Some regularities of the second and third-order cosets with low PAPR are presented.

In Chapter 9, a simple and efficient adaptive ARQ scheme is presented. An exact throughput calculation for adaptive ARQ scheme is outlined. An approach of how to design the adaptive system parameters is presented where the parameters are obtained by optimization of the adaptive system's throughput based on a static channel environment. The tracking capability of the proposed approach to the time-varying

channel conditions is illustrated by the short-term throughput performance. The applicability of the proposed approach in a time-varying channel is investigated and confirmed by the average throughput performance in time-varying channels characterized by Rayleigh fading and lognormal shadowing.

In Chapter 10, an alternative adaptive ARQ scheme is presented. The task of the throughput calculation and optimization required in the method proposed in Chapter 9 can be quite tedious for adaptive system with many modes. An adaptive ARQ scheme which circumvents this tedious task is described. An effective channel sensing method which exploits the error correcting capabilities of the adaptive modes is presented. The concept of adaptive ARQ scheme with adaptive frequency hopping is proposed which achieves substantial throughput improvement in slow fading environments.

Finally in Chapter 11, conclusions and suggestions for future work are presented.

Chapter 2

Timing Offset Estimation for OFDM Systems

Synchronization in OFDM usually includes symbol timing synchronization, carrier frequency synchronization and sampling clock synchronization. The first two are more dominant factors and usually performance of frequency synchronization also depends on the accuracy of symbol timing synchronization. Hence, high accuracy of symbol timing synchronization is much desirable and in this chapter, only symbol timing synchronization is considered.

Regarding symbol timing synchronization, [38]-[39] propose to use the correlation of the cyclic prefix with its copy part. [40] also uses the correlation of the cyclic prefix in a two stage timing estimation but it has long acquisition time. Since the guard interval (cyclic prefix) is usually affected by intersymbol interference (ISI), the result of the methods using the correlation of the cyclic prefix depends on the *á priori* assumption about the channel. Hence, [41]-[42] use a larger guard interval where ISI-free part of the guard interval is used for the timing estimation. However, it fails under some channel conditions and they propose a second method where by making use of the channel estimate, the timing metric is maximized by a search varying the position of the FFT window. However, its acquisition time may not allow a burst mode transmission and the behavior of tracking loop in a mobile environment remains subject to further investigation.

In [43], an m-sequence or chirp synchronization burst is used which is correlated at the receiver with locally generated one. Due to the frequency offset, the locally generated synchronization burst would be different from the received one. Hence, the timing estimation would not be reliable in the presence of a large frequency offset.

To avoid these problems in the timing estimation, Schmidl & Cox [44] proposes a robust method using a training symbol with two identical halves which can be applied in either a continuous or burst mode transmission. However, the timing metric plateau inherent in it causes uncertainty in choosing the best timing point, hence, causing a large timing estimator variance. In [45], a differential approach in frequency detection together with raising fourth power of the signal to cancel the QPSK modulation format is applied. However, an initial timing offset is required to be within one-eighth of the FFT size. Alternatively in [46], the cyclic prefix and pilot symbols used for the channel estimation are exploited for the timing estimation.

In brief, most of the previous timing estimation methods have one or more of the following drawbacks:

- not applicable for both burst mode and continuous mode transmission,
- depending on the *á priori* assumption about the channel ,
- restricted to some modulation formats,
- limited for small frequency offset cases, and
- having tendency of estimator performance degradation caused by timing metric plateau.

In this chapter, we present two timing estimation methods as modifications to [44]. By eliminating the timing metric plateau, the proposed methods achieve some improvement in the timing estimation and avoid the drawbacks described above. This chapter is organized as follows. Section 2.1 briefly describes the considered system and the timing estimation method of [44]. Section 2.2 presents the two proposed timing estimation methods. In Section 2.3, the performances of the proposed methods and [44] [46] are compared in terms of the estimator variance obtained by computer simulation. Finally, conclusions are given in Section 2.4.

2.1 System Description

The samples of the transmitted baseband OFDM symbol can be given by

$$s(k) = \frac{1}{\sqrt{N}} \sum_{n=0}^{N_u-1} c_n \, exp(j2\pi kn/N), \; -N_g \leq k \leq N-1, \tag{2.1}$$

where c_n is the modulated data on the n^{th} subcarrier, N is the number of inverse Fast Fourier Transform (IFFT) points, $N_u(\leq N)$ is the number of subcarriers, N_g is the number of the guard samples, $j = \sqrt{-1}$ and the sampling period is T_u/N with $1/T_u$ being the subcarrier spacing. Consider a discrete-time channel characterized by

$$h(k) = \sum_{l=0}^{K-1} h_l \, \delta(k - \tau_l) \tag{2.2}$$

where $\delta(k)$ represents the Dirac-Delta function, $\{h_l\}$ the complex path gains, $\{\tau_l\}$ the path time delays which are assumed in multiple of OFDM samples, and K the total number of paths.

The received samples, assuming a perfect sampling clock, can be given by

$$r(k) = exp(j\phi) \; exp(j2\pi kv/N) \sum_{l=0}^{K-1} h_l \; s(k - \tau_l) + n(k) \tag{2.3}$$

where v is the carrier frequency offset normalized by the subcarrier spacing, ϕ is an arbitrary carrier phase factor, and $n(k)$ is the sample of zero mean complex Gaussian noise process with variance σ_n^2. The timing point for the start of the FFT window is determined by the timing synchronization at the sample $r(\varepsilon)$ where ε is a timing offset in unit of OFDM samples.

Suppose the sample indexes of a perfectly synchronized OFDM symbol be $\{-N_g$, ... , -1, 0, 1, ... , $N-1\}$ and the maximum channel delay spread be τ_{max}. Then if $\varepsilon \in \{-N_g + \tau_{max}, -N_g + \tau_{max} + 1, \ldots, 0\}$, the orthogonality among the subcarriers will not be destroyed and the timing offset will only introduce a phase rotation in every subcarrier symbol Y_m at the FFT output as

$$Y_m = exp(j2\pi m\varepsilon/N) \; c_m \; H_m + n_m, \quad -N_g + \tau_{max} \leq \varepsilon < 0 \tag{2.4}$$

where m is the subcarrier index, H_m is the channel frequency response to the m^{th} subchannel, i.e., $\{H_m\} = DFT_N(h(k))$, and n_m is a complex Gaussian noise term. For a coherent system, this phase rotation is compensated in the channel equalization which sees it as a channel introduced phase shift.

If the timing estimate is outside the above range, the orthogonality among the subcarriers will be destroyed by the resulting ISI and an additional inter-subchannel interference (ICI) will be introduced. Thus, the guard interval should be long enough

for the timing estimate to lie within the range described above. On the other hand, a longer guard interval translates into a greater loss in the system capacity due to the overhead. Hence, a high performance timing synchronization is much desirable for higher system performance and capacity efficiency. The smaller the variance of timing estimator is, the shorter the guard interval can be designed, and consequently, the less overhead and hence, the increased capacity efficiency can be obtained. With this aspect, the performance of the symbol timing synchronization algorithms will be evaluated by the timing estimator variance.

The symbol timing estimator finds the start of the OFDM symbol. The correct symbol timing point will be taken as the start of the useful part of the OFDM symbol (i.e., the start of FFT window for demodulation). Let the training symbol (excluding cyclic prefix) contain two identical halves in time domain each having $L = N/2$ samples. At the receiver there will be a phase difference between the samples in the first half and their replica in the second half caused by the carrier frequency offset. Training data is usually a PN sequence. Then the Schmidl & Cox's timing estimator [44] takes as the start of the symbol the maximum point of the timing metric given by

$$M(d) = \frac{|P(d)|^2}{R^2(d)} \tag{2.5}$$

where d is a time index corresponding to the first sample in a window of $2L$ samples and $P(d)$ is the correlation metric given by

$$P(d) = \sum_{m=0}^{L-1} r^*(d+m) \cdot r(d+m+L) \tag{2.6}$$

where $(\cdot)^*$ represents a complex conjugation and $R(d)$ represents the energy of half OFDM symbol and is included for normalization of the correlation metric in account for the large fluctuation of the OFDM sample amplitudes and given by

$$R(d) = \sum_{m=0}^{L-1} |r(d+m+L)|^2. \tag{2.7}$$

The above timing metric reaches a plateau (see Fig. 2.2) which leads to some uncertainty as to the start of the frame. To alleviate this, [44] proposes an averaging method where the maximum point is first found and then two points with 90% of the

maximum value, one to the left and the other to the right of the maximum point, are found. The timing estimate is taken as the average of the two 90% points.

2.2 Proposed Methods

In this section, we present two methods to reduce the uncertainty due to the timing metric plateau and thus improve the timing offset estimation scheme proposed by Schmidl & Cox.

2.2.1 Sliding Window Method

Firstly, in calculation of the half symbol energy $R(d)$, all samples over one symbol period (excluding the guard interval) are used instead of those over the second half symbol period. Secondly, instead of 90% points averaging approach, the timing metric is simply averaged over a window of length $N_g + 1$ samples. Then the timing metric is given by

$$M_1(d) = \frac{1}{N_g + 1} \sum_{k=-N_g}^{0} M_f(d+k), \tag{2.8}$$

where $M_f(d)$ can be calculated as

$$M_f(d) = \frac{|P(d)|^2}{{R_f}^2(d)} \tag{2.9}$$

and

$$R_f(d) = \frac{1}{2} \sum_{m=0}^{N-1} |r(d+m)|^2 \tag{2.10}$$

and $P(d)$ is given by (2.6).

2.2.2 Training Symbol Method

The samples of the training symbol (excluding cyclic prefix) are designed to be of the form

$$\boldsymbol{s} = [\boldsymbol{A} \;\; \boldsymbol{A} \;\; -\boldsymbol{A} \;\; -\boldsymbol{A}] \tag{2.11}$$

where $\boldsymbol{A}$ represents samples of length $L = N/4$ generated by $N/4$ point IFFT of $N_u/4$ length modulated data of a PN sequence. The abrupt amplitude change due to sign conversion in the training symbol can easily be avoided, if desired, by modifying the PN sequence such that the sum of the corresponding modulated data equals zero. Then the timing metric is given by

$$M_2(d) = \frac{|P_2(d)|^2}{{R_2}^2(d)} \tag{2.12}$$

where

$$P_2(d) = \sum_{k=0}^{1} \sum_{m=0}^{L-1} r^*(d + 2Lk + m) \cdot r(d + 2Lk + m + L) \tag{2.13}$$

and

$$R_2(d) = \sum_{k=0}^{1} \sum_{m=0}^{L-1} |r(d + 2Lk + m + L)|^2. \tag{2.14}$$

In both methods, $P_2(d)$ and $R_2(d)$ or $P(d)$ and $R_f(d)$ can be calculated iteratively.

The training symbol patterns of [44] and the proposed training symbol method are shown in Fig. 2.1. Also shown is the elimination of the timing metric plateau inherent in [44] by a proper design of the training symbol in the proposed training symbol method. There is no difference in the correlation values of [44] between two scenarios where the start of the correlation window is, for the first scenario (left figure), at the correct timing point and, for the second scenario (right figure), just before the correct timing point. This causes the correlation metric peak plateau. In contrast, the correlation values of the proposed training symbol method are different for the two scenarios. When the start of the correlation window is some amount off the correct timing point, the correlation of some samples results in negative values as shown in Fig. 2.1, hence, eliminating the correlation metric peak plateau.

In Fig. 2.2, the timing metric trajectories of Schmidl & Cox (2.5), and the proposed methods (2.8)(2.12) are shown for the system parameters given in Section 2.3 and under a noiseless and distortionless condition. The correct timing point (index 0 in the figure) is taken as the start of the useful part of the training symbol (after the cyclic prefix). For the training symbol of [44], the correlation metric has its peak for the whole interval of the cyclic prefix (under noiseless and distortionless condition)

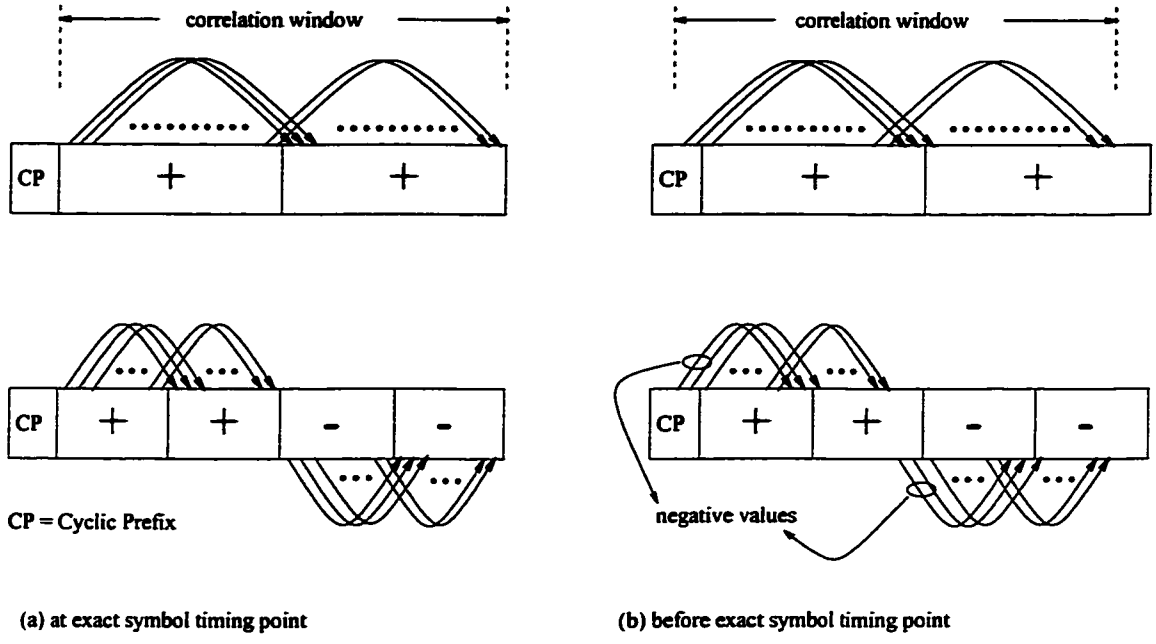

Figure 2.1. *Correlation of the training symbol: Schmidl & Cox's method (upper), Proposed training symbol method (lower)*

while both proposed methods have the correlation metric peak at the correct FFT window starting point. The training symbol method has a sharper roll-off in the timing metric trajectory.

In calculation of half symbol energy in the [44] and the proposed training symbol method, N samples instead of $N/2$ samples can be used to get more reliable result. Then for both methods, $R(d)$ and $R_2(d)$, respectively, can be replaced by $R_f(d)$ given in (2.10).

2.3 Simulation Results and Discussion

Performance of the timing offset estimators have been investigated by computer simulation for six cases:

(I) Schmidl & Cox method (2.5) with 90% maximum points averaging,

(II) Modified Schmidl & Cox method (same as (I), except that $R(d)$ is replaced by $R_f(d)$),

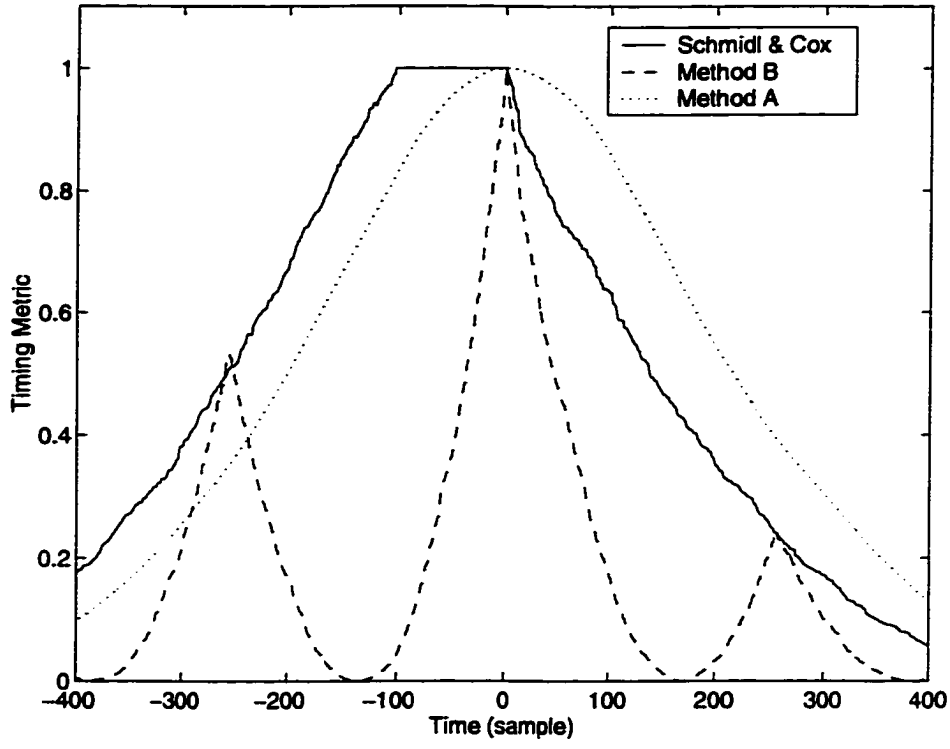

Figure 2.2. *Timing metric trajectory under a noiseless and distortionless condition*

(III) Proposed Method A (2.8),

(IV) Proposed Method B (2.12),

(V) Modified Proposed Method B (same as IV except that $R_2(d)$ is replaced by $R_f(d)$), and

(VI) Landström method [46].

The system used is 1000 subcarriers OFDM system with 1024 point FFT, 10% guard interval (102 samples), a carrier frequency offset of 12.4 subcarrier spacing, QPSK subcarrier modulation, and 10 000 simulation runs. Two channel conditions are considered:

a) An AWGN channel with no inter-symbol interference (ISI) (it will be called AWGN channel) and

b) An ISI channel with AWGN (it will be called ISI channel).

The ISI channel is modelled as sixteen paths with path delays τ_i of $0, 4, 8, \ldots, 60$ samples and path gains given by

$$h_i = \frac{exp(-\tau_i/60)}{\sqrt{\sum_{k=0}^{15} exp(-\tau_k/30)}}, \quad i = 0,\ 1,\ \ldots,\ 15. \tag{2.15}$$

For the timing estimator of [46], the additional parameters are: one pilot every $40th$ subcarrier and dummy SNR value $\tilde{SNR} = 5\ dB$.

Figs. 2.3 and 2.4 show the means and variances of the timing offset estimates in an AWGN channel and an ISI channel, respectively. For the AWGN channel, the means of timing offsets for the cases I and II are about the middle of the timing metric plateau (within the cyclic prefix) while the means for the cases III, IV, V and VI are about the correct timing point. For the ISI channel, the means are observed to be shifted to the right in the time axis (i.e., delayed) by some amount depending on the shapes of the timing metric trajectory and the ISI channel. Note that if the timing estimate is desired to lie within the guard interval, then the means for the cases III, IV, V and VI can easily be shifted to the left (i.e., advanced) by some appropriate design amount.

As for the variances, the following are observed:

- In the AWGN channel, cases I, II and VI show floor in estimator variance curves

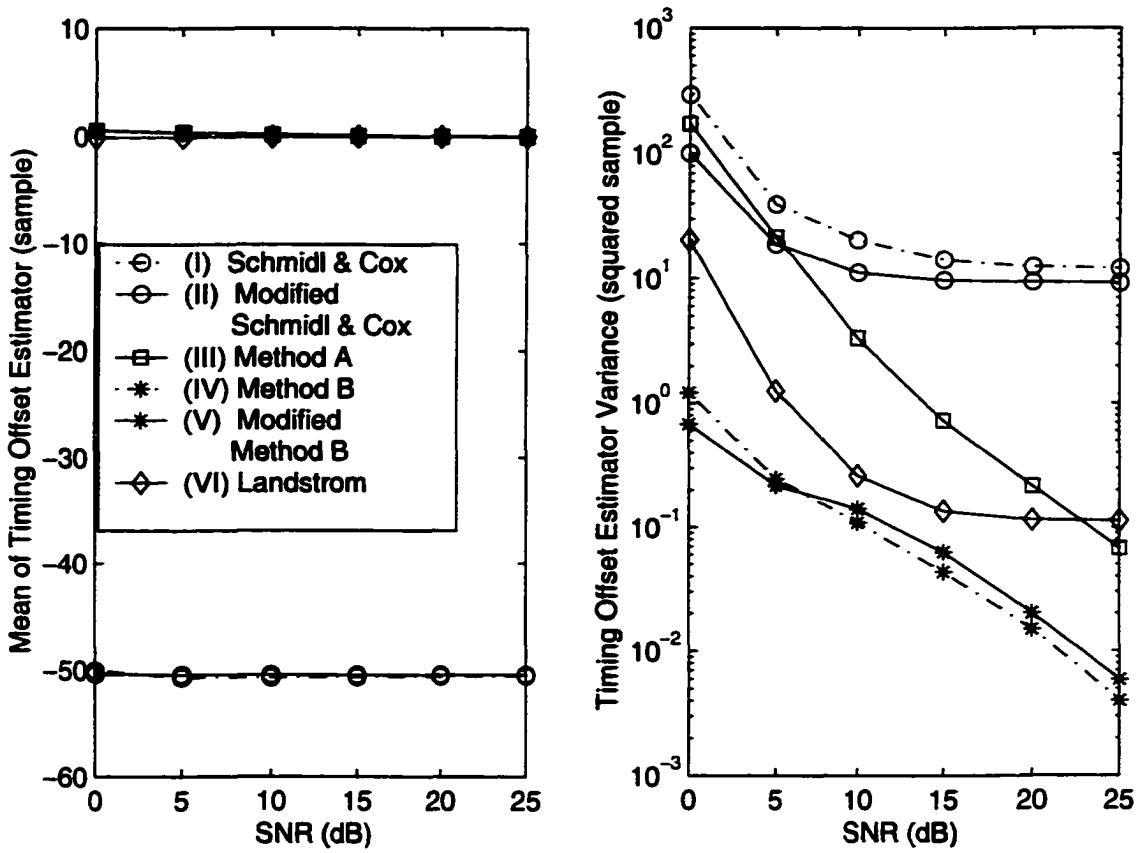

Figure 2.3. *Mean and variance of timing offset estimators in an AWGN channel*

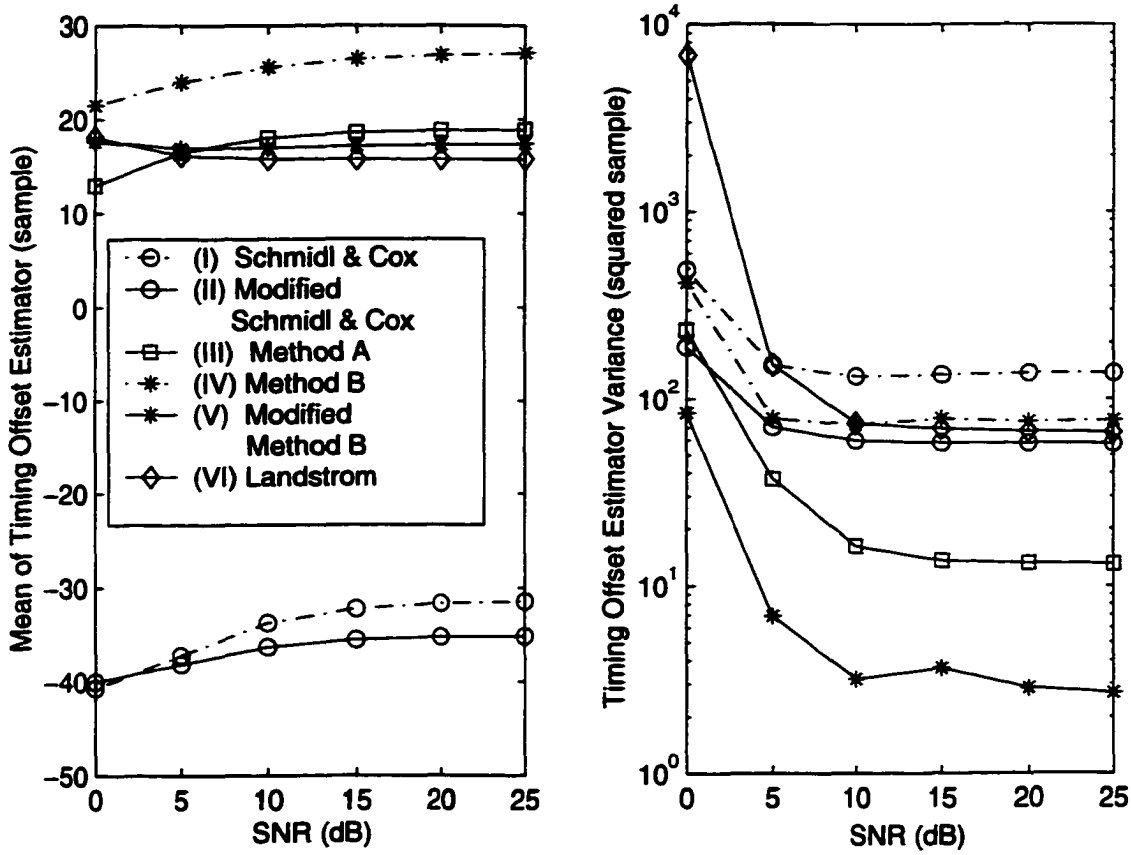

Figure 2.4. *Mean and variance of timing offset estimators in an ISI channel*

while the proposed methods (cases III, IV and V) do not. In the ISI channel, all methods have estimator variance floor.

- Performance of case II is better than case I for all conditions considered, at the expense of some additional complexity. The smaller variance of case II is due to using more samples to calculate the half symbol energy used in the timing metric.
- Proposed methods (cases III, IV and V) have significantly smaller estimator variance than Schmidl & Cox's method (case I) for all conditions considered. The better performance of the proposed methods is generally due to the absence of timing metric plateau.
- As comparison of proposed methods to case VI, in the AWGN channel, cases IV and V have significantly smaller estimator variance but case III has larger variance than case VI for SNR values less than about 23 dB ; while in the ISI channel, case IV has slightly larger variance for SNR values greater than 10 dB but cases III and V have significantly smaller variances.
- In the AWGN channel, the slope of the timing metric off the correct timing point determines the estimator variance (see cases I and II vs cases III, IV and V in Fig. 2.3).
- In the ISI channel, using all the samples over one symbol period (excluding cyclic prefix) to calculate the half symbol energy (i.e. using R_f) has more effect on reducing the estimator variance than the slope of the timing metric (see case IV vs. cases II, III and V in Fig. 2.4).
- As an overall evaluation for both channel conditions, case V (proposed method B using R_f) performs the best.

The cases II, III and V have some additional complexity due to using R_f as compared to case I. However, cases IV and V do not need averaging of timing metric as required in cases I, II and III. Hence, case IV has even smaller complexity than case I.

2.4 Conclusions

Two timing offset estimation methods for OFDM systems are presented as modifications to Schmidl & Cox's method [44] where a training symbol containing two identical halves was used. The first method uses two modifications: (a) all samples over one symbol period (excluding guard interval), instead of over half symbol period, are used in calculation of the half symbol energy required in the timing metric and (b) averaging of the timing metrics over a window of the guard interval length is used instead of 90% maximum points averaging. The second method uses a training symbol containing four equal length parts: the first two are identical and the last two are negative of the first two. Modification (a) can also be applied in the second method and gives robustness to the ISI channel. The simulation results show that both proposed methods have significantly smaller estimator variance than [44] under both the AWGN channel and the ISI channel. The performance of the method in [46] is also included in the comparison as another reference. As an overall performance for both channels, the second proposed method with modification (a) gives the best result.

Chapter 3

A Time-Domain-Based Channel Estimation for OFDM Systems

As similar to a single carrier system, an OFDM system can be either noncoherent or coherent. For a noncoherent OFDM system, the channel estimation can be avoided and the system complexity will be reduced at the cost of 3-4 dB performance loss [47]. If a coherent OFDM system is adopted, channel estimation becomes a requirement and usually pilot tones are used for channel (frequency response) estimation. Pilot tones can be inserted in all subcarriers of a particular OFDM symbol forming an OFDM training symbol, in which case training symbols are transmitted at an appropriate regular rate determined by the time varying nature of the wireless channel. A decision-directed approach can be used for the channel estimation based on the data symbols. If complexity is affordable, a time interpolation (e.g., [48]) can be used to improve the performance.

Another approach is that, instead of using all subcarriers, the pilot tones are multiplexed with data to form OFDM symbols. The subcarrier spacing between pilot tones is usually determined by the frequency selectivity of the wireless channel. The pilot multiplexing can be allowed for all OFDM symbols (i.e., all the time of transmission) or at an appropriate rate depending on the time selectivity of the wireless channel. If the pilot tone multiplexing is used, a frequency interpolation has to be performed to get all subchannel response estimates [49]-[50]. Similarly, a time-domain interpolation can be performed at the cost of complexity.

Most of the channel estimation approaches may be viewed as DFT-based approaches [51] [52] [47] [48], where LS (Least square) channel (frequency response) estimates are fed to the IFFT block to get the time domain channel impulse response

estimate, and then appropriately processed and transformed back to the frequency domain by FFT. A DFT-based approach for an OFDM system with transmit and receive antenna diversity has been discussed in [47].

In this chapter, we investigate a time-domain channel estimation approach, namely FPTA (Frequency Pilot Time Average) [53] which applies intra-symbol time-domain averaging of identical parts of the pilot signal. We show that the time domain pilot to noise ratio defined in [53] is not an appropriate measure for the channel estimation. We also propose a time-domain approach for OFDM channel estimation which achieves performance gain over FPTA approaches. The relationship, similarities, and differences between the proposed approach and the existing methods are presented. The proposed method is also extended to an LMMSE-based approach. The rest of this chapter is organized as follows. In Section 3.1, the OFDM system and LS channel estimation are presented for notational description. The method of time-averaging the identical parts of a pilot signal is briefly presented in Section 3.2, and our analysis on this intra-symbol time-averaging is given in Section 3.3. Section 3.4 presents the proposed time-domain channel estimation and its relation to the DFT-based approaches are discussed in Section 3.5. Simulation results are discussed in Section 3.6 and conclusions are given in Section 3.7.

3.1 System Description

Suppose the pilot tones $P[k]$ are multiplexed with data $D[k]$ in all OFDM symbols at a pilot ratio $1/K$ (ratio of the number of pilot tones to the total number of subcarriers) where k is subcarrier index $(0, 1, ..., N-1)$ with N being the total number of subcarriers, and $P[k]$ and $D[k]$ are zeros except at their corresponding subcarriers. Then the transmitted OFDM signal in discrete-time domain, excluding guard-interval, can be expressed as

$$s[n] = IFFT_N\{P[k]\} + IFFT_N\{D[k]\} = p[n] + d[n] \tag{3.1}$$

where $IFFT_N\{\ \}$ is N-point inverse Fast Fourier transform and n is the time-domain index $(0, 1, ..., N-1)$ of an OFDM symbol. Suppose the wireless channel has a

discrete-time impulse response given by

$$h[n] = \sum_{l=0}^{L-1} \alpha_l \, \delta[n - \tau_l] \tag{3.2}$$

where α_l is complex path gain of l^{th} path, τ_l is the delay of l^{th} path, and L is the total number of channel paths. For simplicity, time dependence nature of the channel impulse response is suppressed in the notation.

After passing through a multipath wireless channel, the time-domain received samples of an OFDM symbol, if appropriate cyclic prefix guard samples are used, is given by

$$r[n] = s[n] \otimes h[n] + w[n] \tag{3.3}$$

where $\otimes$ represents N-point circular convolution, $\{w[n]\}$ are independent and identically distributed (*iid*) AWGN samples with zero mean and variance of σ_t^2. Assuming a perfect synchronization, the FFT output frequency-domain subcarrier symbols can be expressed as

$$R[k] = FFT_N\{r[n]\} = H[k] \; P[k] + H[k] \; D[k] + W[k] \tag{3.4}$$

where $\{W[k]\} = FFT_N\{w[n]\}$ are frequency-domain AWGN noise samples with zero mean and variance $\sigma_f^2 = N\sigma_t^2$. Then the channel frequency response at the pilot tones can be estimated by

$$\hat{H}[m] = \frac{R[m]}{P[m]} = H[m] + \frac{W[m]}{P[m]} \tag{3.5}$$

where m is the subcarrier index for pilot tones. This channel estimate is called LS (least square) estimate. The channel responses at other subcarriers can be obtained by interpolation.

3.2 Frequency Pilot Time Average (FPTA) Method

In FPTA [53] approach, positive and negative alternatively polarized pilot tones are multiplexed with data at a pilot ratio of $1/K$. The frequency-domain pilot tones can be expressed as

$$P[k] = \begin{cases} (-1)^m A & , k = Km \\ 0 & , k = Km + i \end{cases} \tag{3.6}$$

where K, m and i are integers, $1 \leq i \leq K-1$, $0 \leq m \leq M-1$, A is pilot amplitude and $M = N/K$ is an integer. The corresponding time-domain pilot samples can be expressed as

$$\begin{aligned} p[n] &= IFFT_N\{P[k]\} = \frac{1}{N}\sum_{k=0}^{N-1} P[k]\, W_N^{-nk} \\ &= \frac{A}{K}\sum_{r=0}^{K-1} \delta[n - Mr - M/2] \end{aligned} \tag{3.7}$$

where $W_N = exp(-j2\pi/N)$.

In FPTA approach, since there are K identical parts of time-domain pilot samples, the corresponding parts of received samples are averaged over K parts. This intra-symbol time-domain averaging reduces the variance of noise samples by K times, i.e., $\sigma_{t,avg}^2 = \sigma_t^2/K$. Based on this observation, [53] defined time-domain pilot to noise ratio as $p[n]/\sigma_{t,avg}$ and compared it with frequency domain pilot to noise ratio $P[k]/\sigma_f$ resulting in the following expression

$$\frac{p[n]/\sigma_{t,avg}}{P[k]/\sigma_f} = \sqrt{\frac{N}{K}} \tag{3.8}$$

which was mentioned as the gain of FPTA approach over frequency domain approach such as LS estimation discussed in Section 3.2. However, this result is optimistic and more details on it will be discussed in the following section.

3.3 Analysis of Intra-Symbol Time Averaging in FPTA

In order to investigate the pilot to noise ratio insightfully, we neglect the data part and consider only the pilot affected by multipath channel and Gaussian noise. Then the time-domain received samples vector of an OFDM signal can be given by

$$\boldsymbol{r} = \boldsymbol{p}' + \boldsymbol{w} \tag{3.9}$$

where $\boldsymbol{r} = [\boldsymbol{r}_0, \boldsymbol{r}_1, \ldots, \boldsymbol{r}_{K-1}]$ with $\boldsymbol{r}_i = [r_i[0], r_i[1], \ldots, r_i[M-1]]$, $\boldsymbol{p}'$ is N-point circular convolution of pilot signal $\boldsymbol{p}$ and channel impulse response $\boldsymbol{h}$ and can be

expressed as $\boldsymbol{p}' = [\boldsymbol{p}'_0, \boldsymbol{p}'_1, \ldots, \boldsymbol{p}'_{K-1}]$ with $\boldsymbol{p}'_i = [p'_i[0], p'_i[1], \ldots, p'_i[M-1]]$ and $\boldsymbol{w} = [w[0], w[1], \ldots, w[N-1]]$ is *iid* Gaussian noise samples.

Then averaging the received samples over K parts, assuming that the channel impulse response is constant over the OFDM symbol interval, gives

$$\boldsymbol{r}_{avg} = \frac{1}{K} \sum_{l=0}^{K-1} \boldsymbol{r}_l = \boldsymbol{p}'_0 + \boldsymbol{w}_{avg} \tag{3.10}$$

where $\boldsymbol{w}_{avg} = [w_{avg}[0], w_{avg}[1], \ldots, w_{avg}[M-1]]$ with $w_{avg}[i] = \frac{1}{K}\sum_{j=0}^{K-1} w[i+jM]$. Since $\{w[n]\}$ are *iid* zero mean complex Gaussian random variables with variance σ_t^2, $\{w_{avg}[i]\}$ are *iid* zero mean complex Gaussian random variables with variance $\sigma_{t,avg}^2 = \frac{\sigma_t^2}{K}$.

Now, we investigate two possible approaches for channel estimation using intra-symbol time-averaged received samples. The first approach, which will be denoted by FPTA-1 in the rest, is to reconstruct the received samples of length N by repeating the $\boldsymbol{r}_{avg}$, K times. Then the reconstructed samples $\boldsymbol{y}$ can be expressed as

$$\boldsymbol{y} = [\boldsymbol{r}_{avg}, \boldsymbol{r}_{avg}, \ldots, \boldsymbol{r}_{avg}] = \boldsymbol{p}' + \boldsymbol{v} \tag{3.11}$$

where $\boldsymbol{v} = [\boldsymbol{w}_{avg}, \boldsymbol{w}_{avg}, \ldots, \boldsymbol{w}_{avg}]$ is K times repeated version of $\boldsymbol{w}_{avg}$. The corresponding frequency domain samples are

$$Y[k] = FFT_N\{y[n]\} = H[k]\ P[k] + V[k] \tag{3.12}$$

where $\{P[k]\}$ are original pilot tones, $H[k]$ is channel frequency response and $V[k] = FFT_N\{\boldsymbol{v}\}$ is frequency-domain zero mean Gaussian noise term. The channel frequency responses at pilot tones can be estimated by

$$\hat{H}[m] = Y[m]/P[m] = H[m] + V[m]/P[m] \tag{3.13}$$

where $m = 0,\ K,\ 2K,\ \ldots,\ (M-1)K$.

The variance of $V[m]$ can be given as follows:

$$\begin{aligned}
var\{V[m]\} &= E\{V[m]\ V^*[m]\},\quad m = 0,\ K,\ 2K,\ \ldots,\ (M-1)K \\
&= E\{\sum_{i=0}^{N-1} v[i]\ W_N^{mi} \sum_{j=0}^{N-1} v^*[j]\ W_N^{-mj}\} \\
&= E\{\sum_{i=0}^{M-1} v[i] \sum_{l=0}^{K-1} W_N^{m(i+lM)} \sum_{j=0}^{M-1} v^*[j] \sum_{n=0}^{K-1} W_N^{-m(j+nM)}\} \\
&= \sum_{i=0}^{M-1}\sum_{j=0}^{M-1} E\{v[i]\ v^*[j]\} \sum_{l=0}^{K-1} W_N^{m(i+lM)} \sum_{n=0}^{K-1} W_N^{-m(j+nM)} \\
&= \sum_{i=0}^{M-1} \sigma_{t,avg}^2 \left|\sum_{l=0}^{K-1} W_N^{m(i+lM)}\right|^2 \\
&= \sum_{i=0}^{M-1} \sigma_{t,avg}^2 K^2 = N\sigma_t^2 \qquad (3.14)
\end{aligned}$$

which is the same as the variance of frequency-domain noise term without intra-symbol time-averaging (i.e., $W[k]$ in (3.4)). The pilot to noise ratio is also the same, given by $\frac{A}{\sqrt{N\sigma_t^2}}$.

The second possible approach, which will be denoted by FPTA-2 in the rest, is to use $FFT_N\{\boldsymbol{r}_{avg}\}$ together with $FFT_N\{\boldsymbol{p}_0\}$ where $\boldsymbol{p}_0$ is one of the identical parts of time-domain pilot samples. The channel frequency response is estimated as follows:

$$P_0[k] = FFT_N\{p_0[n]\} = A/K,\ for\ k = 0,\ 1,\ \ldots,\ N-1 \qquad (3.15)$$

$$R_{avg}[k] = FFT_N\{r_{avg}[n]\} = H[k]\ P_0[k] + W_{avg}[k] \qquad (3.16)$$

$$\hat{H}[k] = R_{avg}[k]/P_0[k] = H[k] + W_{avg}[k]/P_0[k] \qquad (3.17)$$

where $\{W_{avg}[k]\}$ are zero mean complex Gaussian noise terms and $\{P_0[k]\}$ are the equivalent pilot tones for this approach. It can be shown that the variance of $W_{avg}[k]$ is $M\sigma_{t,avg}^2 (= \frac{M}{K}\sigma_t^2)$. The pilot to noise ratio is the same as the previous case.

The channel estimation error is given by $e_H = \hat{H}[k] - H[k]$ which is the second term in $\hat{H}[k]$ equation. Since its mean is zero, the mean square error (MSE) of the channel estimate, $MSE\{\hat{H}[k]\} = E[e_H e_H^*]$, is equal to the variance of the second term. Hence, the channel estimation MSE's of LS method and intra-symbol time-averaging methods are the same and equal to $\frac{N\sigma_t^2}{A^2}$.

The above discussion also indicates that intra-symbol time-averaging alone does not achieve channel estimation performance gain and the result in (3.8) is optimistic. Another way of explanation for the result in (3.8) is that it considers only one time-domain sample (after averaging) while other samples also affect the channel estimate. The result would be appropriate if $p[n]/\sigma_{t,avg}$ in (3.8) is obtained by averaging over all M samples (after averaging). In the rest, the gain of a channel estimation method over another (if not mentioned, LS method is assumed) will be expressed by the MSE gain (i.e., the ratio of MSE's) or the (frequency-domain) pilot-to-noise power ratio instead of the pilot amplitude to noise standard deviation ratio.

3.4 Most Significant Taps Approach

For practical multipath wireless channels, there are not so many channel paths with significant energy (if compared to the FFT size N). Hence, among N samples (taps) of the channel impulse response estimate, many samples (taps) will have little or no energy at all except noise perturbation. Neglecting those nonsignificant channel taps in the channel estimation may introduce some performance degradation if some of the channel energy is missed, but at the same time it will eliminate the noise perturbation from those taps. Usually total noise perturbation from those neglected channel estimate taps is much higher than the multipath energy contained in them, especially for low SNR values. Hence, neglecting those nonsignificant channel estimate taps can improve the channel estimation performance significantly and this fact is applied in the proposed method as shown in Fig. 3.1.

We consider the same scenario as in [53] where pilot tones are multiplexed with data in each OFDM symbol at a pilot ratio of $1/K$. The pilot tone used in the proposed MST approach is

$$P[k] = \sum_{m=0}^{M-1} A\,\delta[k - mK]\ ,\ k = 0,\ 1,\ \ldots,\ N-1 \tag{3.18}$$

and the corresponding time-domain samples contain K identical parts and are given by

$$p[n] = \sum_{m=0}^{K-1} \frac{A}{K}\,\delta[n - mM]\ ,\ n = 0,\ 1,\ \ldots,\ N-1. \tag{3.19}$$

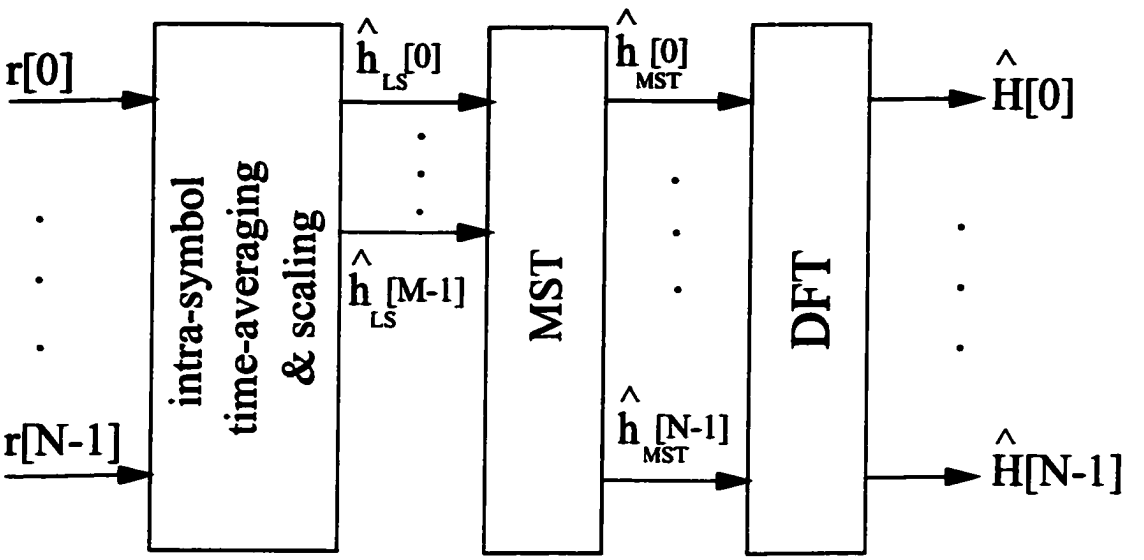

Figure 3.1. *Most Significant Taps (MST) Method*

If the maximum channel delay spread is less than the length of an identical part, which can be designed to satisfy this, then the time-domain received samples corresponding to the time-domain pilot samples contain K parts, each representing a scaled channel impulse response for the respective part corrupted by AWGN. If the channel path gains remain essentially the same over an OFDM symbol interval, which is usually the case since OFDM systems are usually designed to satisfy this in order to maintain orthogonality among subcarriers, then the received samples corresponding to time-domain pilot samples contain K repeated versions of scaled channel impulse response which are independently corrupted by AWGN.

In order to choose most significant channel taps, those K parts can be averaged so that the noise variance is reduced by K times and more reliable most significant channel taps can be obtained. In mathematical expression, the time-domain received

samples corresponding to time-domain pilot samples [1] can be given by

$$\begin{aligned} r[n] &= h[n] \otimes p[n] + w[n] \\ &= \frac{A}{K} \sum_{m=0}^{K-1} h[n - mM] + w[n] \ , \ n = 0, \ 1, \ \ldots \ , \ N-1. \end{aligned} \tag{3.20}$$

After averaging, we have the noise-corrupted scaled channel impulse response

$$r_{avg}[n] = \frac{A}{K} \, h[n] + w_{avg}[n], \ n = 0, \ 1, \ \ldots \ , \ M-1. \tag{3.21}$$

Then the raw channel impulse response estimate is given by

$$\hat{h}_{LS}[n] = \frac{K}{A} \, r_{avg}[n] = h[n] + \frac{K}{A} \, w_{avg}[n], \ n = 0, \ 1, \ \ldots \ , \ M-1. \tag{3.22}$$

Now, the most significant J channel taps are chosen as the J largest amplitude channel taps. Let the channel tap indexes for those most significant J taps be denoted by $n_0, n_1, \ldots, n_{J-1}$. Then the time-domain channel impulse response estimate of the proposed MST method is obtained by setting the other channel tap gains to zero as shown below:

$$\hat{h}_{MST}[n] = \sum_{i=0}^{J-1} \hat{h}_{LS}[n_i] \ \delta[n - n_i], \ n = 0, \ 1, \ \ldots \ , \ N-1. \tag{3.23}$$

The channel frequency response estimate is directly obtained by applying FFT to $\{\hat{h}_{MST}[n]\}$ as

$$\begin{aligned} \hat{H}_{MST}[k] &= FFT_N\{\hat{h}_{MST}[n]\}, \ k = 0, \ 1, \ \ldots \ , \ N-1 \\ &= H[k] - H_{res}[k] + W_{avg}[k] \end{aligned} \tag{3.24}$$

where

$$\begin{aligned} H[k] &= \sum_{n=0}^{N-1} h[n] \ W_N^{kn} \\ H_{res}[k] &= \sum_{l=0}^{N-J-1} h[n'_l] \ W_N^{kn'_l} \\ W_{avg}[k] &= \frac{K}{A} \sum_{i=0}^{J-1} w_{avg}[n_i] \ W_N^{n_i k} \end{aligned}$$

[1] For simplicity, data part is neglected in the received samples expression. The mean of the data part after averaging is zero.

with $\{n_i\}$ being the most significant channel tap indexes and $\{n_l'\}$ being the indexes of the other channel taps.

By using a suitable number of most significant taps, $H_{res}[k]$ can be kept very small (or zero) and hence, the channel estimation error is mostly dominant (or totally caused) by the noise term $W_{avg}[k]$. For this case, the MSE of the channel estimate can be approximated (or expressed) as

$$\begin{aligned} MSE\{\hat{H}[k]\} &= E\{W_{avg}[k]\, W_{avg}^{*}[k]\} = \frac{K^2}{A^2}\, J\, \sigma_{t,avg}^2 \\ &= \frac{K\, J\, \sigma_t^2}{A^2} = \frac{K\, J}{N}\, MSE\{\hat{H}_{LS}[k]\}. \end{aligned} \tag{3.25}$$

Hence, the MSE performance gain of the proposed MST method over LS method (similarly over FPTA method) is ideally $\frac{N}{JK}$. The actual MSE performance gain would be less than this amount due to the interference from data part and some (if any) excluded channel taps of nonsignificant energy.

The choice of the number of most significant taps J in the channel estimation depends on the application scenario. Broadcasting environment such as single frequency network can have larger number of multipaths with significant energy than non-broadcasting cases such as wireless LANs environment. In any case, J should be chosen larger than the (designed) number of multipaths in order to prevent channel estimation error caused by missed channel taps. The channel estimation error caused by the noise from an additional tap in the channel estimation is much less than that caused by missing one of the multipaths. A suitable choice for J may be two times or more of the (designed) number of multipaths (as will be seen in the simulation results) in order to ensure no channel energy missing.

Another MST tap selection approach can be implemented by selecting the channel taps whose energies are above a threshold. The threshold may be set as η times the maximum channel tap's energy in the raw channel estimate. The suitable choice of η depends on the operating SNR and more details will be discussed in the simulation results section.

3.5 Similar Approaches in DFT-based methods

In this section, we relate the proposed MST method to the DFT-based approaches [51] [52] [47]. Essentially, due to the one-to-one relationship of DFT and IDFT, the MST method can be related to DFT-based approach as shown in Fig. 3.2. Consider the system with training symbol (i.e., pilot tones on all subcarriers). First, LS estimates are obtained and then input to IFFT block resulting in N samples LS estimate of the channel impulse response. The largest amplitude J channel taps among the N samples (taps) are chosen as J most significant channel taps and the other taps are set to zero. The resulting MST channel impulse response estimate is input to FFT block to get the MST channel frequency response estimate. This MST's dual form DFT-based approach has been applied in [47]. A similar concept by using singular value decomposition can be found in [54].

The difference between the proposed MST approach and its dual form DFT-based approach is that MST uses pilot-data multiplexed approach while its dual form DFT based approaches use training symbol approach. It can be shown that the potential gain of the latter approach is N/J. Using total pilot power of NA^2, the latter approach achieves potential gain of N/J whereas MST achieves potential gain of $N/(JK)$ with total pilot power of NA^2/K; hence, on the basis of the same total pilot power, both methods have the same potential gain for the channel estimation.

Another difference is the complexity. In MST approach, operations involved are time-averaging, most significant channel taps selection and one FFT operation whereas its dual form DFT-based approach requires LS estimation, one IFFT operation, most significant channel taps selection and one FFT operation. Hence, the proposed MST approach saves some complexity.

One approach which is similar to MST's dual form DFT-based approach is the method of [52]. The difference is that [52] uses the first N_{cp} channel taps where N_{cp} is the number of cyclic prefix samples whereas MST's dual form DFT-based approach uses only J most significant channel taps, $(J < N_{cp})$. Since multipath channels usually have much less channel taps than N_{cp}, [52] has more noise perturbation than MST.

Other DFT-based approaches use linear minimum mean square error (LMMSE) estimators or approximate LMMSE estimators with reduced complexity [51]. If com-

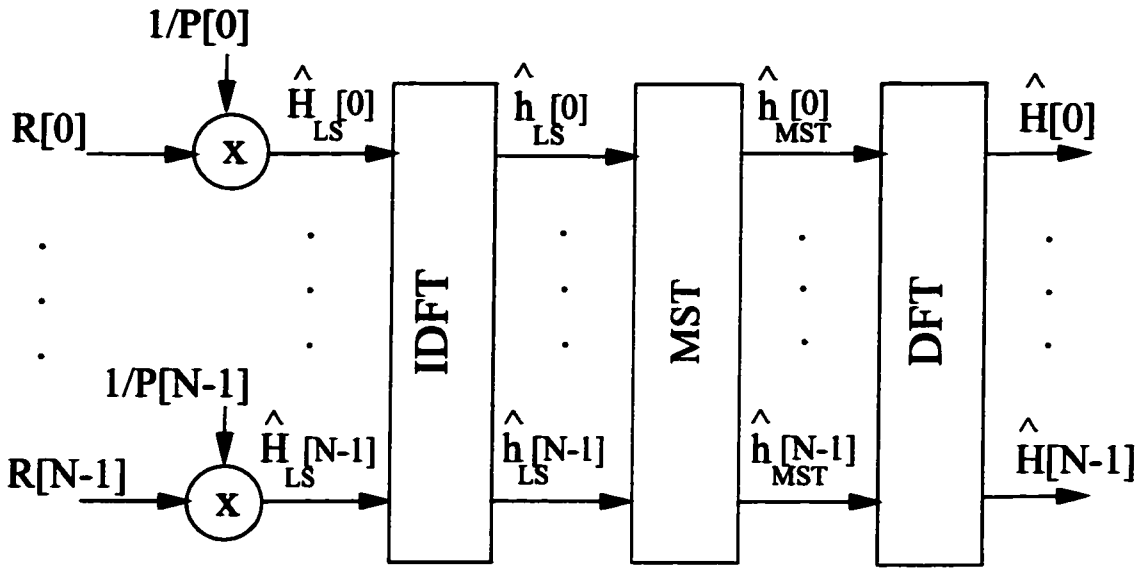

Figure 3.2. *MST's dual form DFT-based method*

plexity can be afforded, these LMMSE or approximate LMMSE estimators can be implemented in MST approach. Let us consider a wide-sense stationary uncorrelated scattering (WSSUS) multipath channel with power delay profile given by $\sigma_{h_i}^2$ at delays of i OFDM sample intervals. Due to the uncorrelated multipaths, the correlation matrix of the channel impulse response becomes a diagonal matrix with the diagonal elements given by the power delay profile. Then the LMMSE's matrix multiplication (or scalar multiplication on corresponding channel taps) is performed as follows [55] [51]:

$$\hat{h}_{LMMSE} = diag\{\frac{\sigma_{h_0}^2}{\sigma_{h_0}^2 + \beta/SNR}, \frac{\sigma_{h_1}^2}{\sigma_{h_1}^2 + \beta/SNR}, \cdots, \frac{\sigma_{h_{N-1}}^2}{\sigma_{h_{N-1}}^2 + \beta/SNR}\} \hat{h}_{LS} \tag{3.26}$$

where $diag\{a_0, a_1, \ldots, a_{N-1}\}$ is a diagonal matrix with diagonal elements $[a_0, a_1, \ldots, a_{N-1}]$.

In DFT-based LMMSE approach, the first symbol is composed of all pilot tones of equal amplitude and the following data symbols are composed of M-ary QAM symbols on all subcarriers. Then for the initial channel estimation based on the

training symbol, SNR/β in (3.26) is replaced by the pilot-to-noise power ratio. For the following channel estimation operated in the decision directed mode, β in (3.26) is given by $\beta = E[|X|^2]\ E[|X|^{-2}]$ where X is M-ary QAM symbol. For 64-QAM, $\beta = 2.6854$. For MST-LMMSE, SNR/β is replaced by its pilot-to-noise power ratio (which is $1/K$ times that of DFT-based LMMSE due to its pilot ratio of $1/K$).

There is a delicate difference between DFT-based LMMSE and MST-LMMSE. In DFT-based LMMSE, all N samples of $\hat{h}_{LS}$ are corrupted by *iid* AWGN noise samples of zero mean and variance σ_t^2/A^2. In MST-LMMSE, the first M samples of $\hat{h}_{LS}$ are corrupted by *iid* AWGN noise samples of zero mean and variance $K\sigma_t^2/A^2$ and the rest are zeros. Hence, if compared for the training symbol alone, DFT-based LMMSE will have a better channel estimation performance due to the larger pilot power used in channel estimation. But for the following data symbols, DFT-based LMMSE has to use decision directed approach which may degrade the channel estimation performance and BER performance due to the decision directed errors. For MST-LMMSE, the channel estimation and BER performances remain the same for all symbols.

In LMMSE implementation, since multipath channel correlation and SNR are usually unknown at the receiver, some fixed values have to be used for them. In [54], it is suggested to use high dummy SNR value and uniform multipath channel correlation which are robust to the channel correlation mismatch. If high dummy SNR value is used and uniform multipath channel correlation is assumed over guard interval, then LMMSE approach would be similar to [52] 's method. From (3.26) with high dummy SNR value, the LMMSE approach can be viewed as setting the channel taps with no energy to zeros and bypassing the other taps. Since most practical multipath channels have only a few significant paths (if compared to N), a suitable way of implementing an approximate LMMSE is choosing a predefined number of most significant taps and setting the others to zero which is the underlying idea of MST method. In complexity aspect, MST-LMMSE estimator still saves one N-point IFFT operation if compared to DFT-based LMMSE estimators.

3.6 Channel Estimation Performance Evaluation by Simulation

The proposed MST channel estimation is evaluated by computer simulation for two multipath fading channel models, namely Channel-A and Channel-B. The Channel-A is the ATTC (Advanced Television Technology Center) and the Grand Alliance DTV laboratory's ensemble E model whose channel impulse response for the static case is given by

$$h[n] = \delta[n] + 0.3162\,\delta[n-2] + 0.1995\,\delta[n-17] + 0.1296\,\delta[n-36] + 0.1\,\delta[n-75] + 0.1\,\delta[n-137] \quad (3.27)$$

where unit delay is assumed to be the same as OFDM sample period. The Channel-B is a simplified version of DVB-T channel model P_1 [56] and its channel impulse response for the static case is given in Table 3.1. In the simulation, the given channel tap gains of both channels represent the standard deviations of the gains of the complex Gaussian random variables.

The OFDM system parameters are as follows: the number of subcarriers $N = 8192$, pilot ratio $1/K = 1/8$, and the guard interval ratio $= 1/8$. Two sub-carrier modulation formats, BPSK and 64-QAM, are considered. For BPSK modulation, two scenarios, one is a static multipath channel and the other is a time-varying multipath fading channel both based on Channel-A, are considered. The first scenario might be considered as the case with a stationary reception of the broadcast signal and the second scenario a mobile user case. For 64-QAM modulation, two quasi-static multipath fading channels based on Channel-A and Channel-B are considered. They might be considered as cases at a base station receiver in a Single Frequency Network (SFN), where many base stations receive and retransmit the signal, or at a slow-moving mobile receiver in a SFN network. A perfect synchronization is assumed in order to observe the channel estimation performance alone. The considered methods are MST, FPTA-1, FPTA-2, MST-LMMSE, DFT-based LMMSE and [52]. In the last two methods, one OFDM symbol is used for training symbol (pilot tones on all subcarriers) in every K OFDM symbols (i.e., the same pilot ratio $1/K$).

In both LMMSE methods, ideal channel correlation and SNR values are used in order to evaluate the relative performance of MST method. For OFDM with BPSK,

Table 3.1. *Channel impulse response for Channel-B*

Delay (OFDM samples)	Gain	Phase (radians)
0	0.2478	-2.5694
1	0.1287	-2.1208
3	0.3088	0.3548
4	0.4252	0.4187
5	0.4900	2.7201
7	0.0365	-1.4375
8	0.1197	1.1302
12	0.1948	-0.8092
17	0.4187	-0.1545
24	0.3170	-2.2159
29	0.2055	2.8372
49	0.1846	2.8641

10^4 independent simulation runs are used for all SNR values except that for 20 dB SNR in the static channel, 10^5 independent simulation runs are used. For OFDM with 64-QAM, the same pilot tone symbol of $7+j7$ signal point in 64-QAM constellation is used in all methods. For SNR of 40 and 50 dB, 10^5 independent simulation runs are used and for the other SNR values, 10^4 independent runs are used.

3.6.1 Performance for OFDM with BPSK

Fig. 3.3 shows the channel estimation MSE performance of the proposed MST method and time-averaged methods (FPTA-1 and FPTA-2) for an OFDM system with BPSK modulation in a static channel with tap gains given by (3.27). LS estimation is also included as a reference. Since pilots are multiplexed with data, the required interpolation in FPTA-1 and LS methods are performed using Matlab's default *interp* function. Due to some noise reduction of this interpolation, the MSE of FPTA-1 and LS are slightly less than FPTA-2. MST method with 6 taps, which is the same as the number of channel taps, has approximately 18 to 22 dB MSE gain over LS and FPTA-1, FPTA-2 approaches. Even when MST method uses 4 more taps than the actual number of channel taps, it still achieves about 14 dB MSE gain. The less improvement of MST-10 taps case is due to the noise contribution from 4 taps with no channel energy.

The actual MSE gain of MST method is slightly less than the potential gain of MST method described in the previous section since data signal interference to training signal is neglected in the derivation of the potential gain. The actual MSE gain is less in low SNR region than high SNR region. The reason is that most significant channel taps selection would be more likely to choose some channel taps with no energy at low SNR region than at high SNR region, resulting in less MSE gain at low SNR region. This simulation results also confirm that intra-symbol time-averaging only would not achieve channel estimation MSE gain and the time-domain pilot-to-noise ratio as defined in [53] is not an appropriate measure for the channel estimation performance.

Fig. 3.4 shows the corresponding BER performance of the system using MST, FPTA-1, FPTA-2 and LS methods. Due to much better channel estimation performance, the MST method has significantly better BER performance than the others.

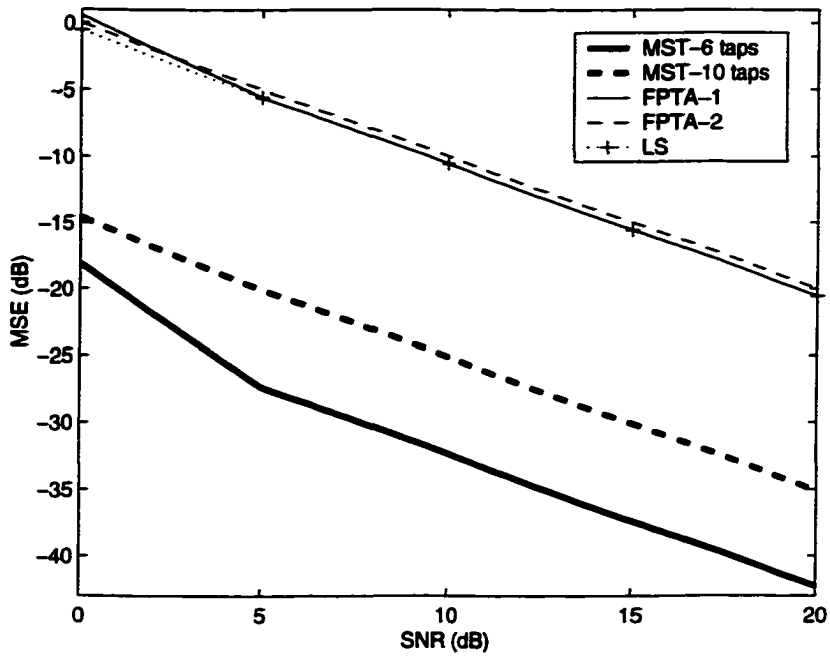

Figure 3.3. *Channel estimation mean square error (MSE) for an OFDM system with BPSK modulation in a static multipath channel*

The BER performance for MST-10 taps system is almost the same as MST-6 taps system although their MSE performances are somewhat different. This also indicates that when the channel estimation MSE's become very small (relative to the noise level), the BER performance becomes insensitive to some MSE deviation.

Furthermore, the performance of the proposed MST method for an OFDM system with BPSK modulation is evaluated in a time-varying Rayleigh fading multipath channel with power delay profile given by $|h[n]|^2$ from (3.27) and $f_D\ T = 0.005$ where f_D is the Doppler frequency and $1/T$ is the OFDM subcarrier spacing. The method of Chini [52], LS approach, and DFT-based LMMSE approach [51] are also included for comparison where one OFDM symbol is used for the training symbol (pilot tones on all subcarriers) in every K OFDM symbols (i.e., the same pilot ratio $1/K$). The MST-LMMSE approach is also evaluated. In both LMMSE methods, ideal channel correlation and SNR values are used in order to evaluate the relative performance of MST method. The MSE performances are shown in Fig. 3.5 and the BER performances are given in Fig. 3.6.

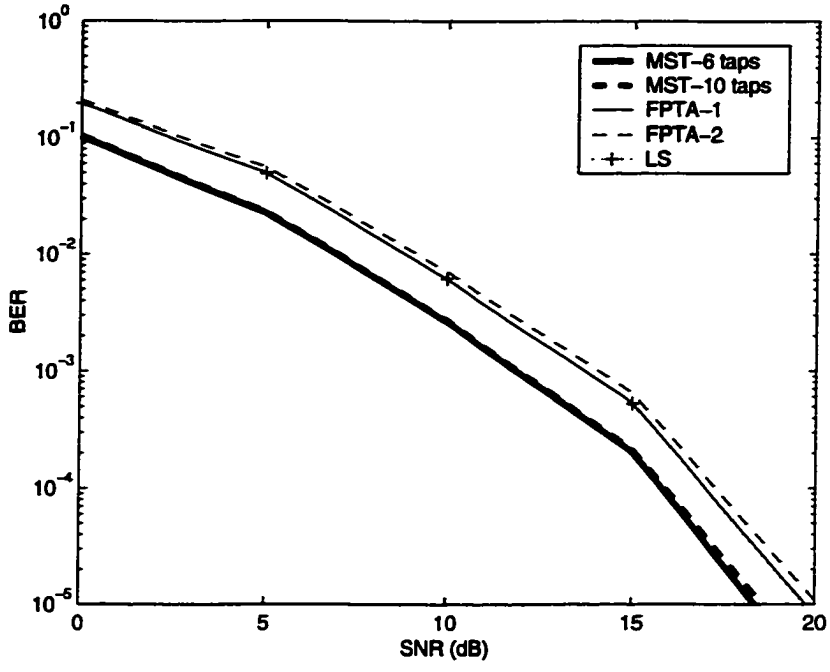

Figure 3.4. *BER performances of an OFDM system with BPSK modulation for different channel estimation methods in a static multipath channel*

The method of Chini [52] achieves about 10 to 15 dB MSE gain over LS method while MST with 10 taps achieves about 15 to 20 dB and MST with 6 taps achieves about 18 to 25 dB MSE gain over LS method. MST with 5 taps has a slightly better MSE performance than 6 taps and 10 taps cases at very low SNR region but it shows an MSE floor at high SNR region. It can be explained as follows. At very low SNR region, noise effect is more dominant and the MSE performance gain achieved by suppressing the noise perturbation from channel taps with insignificant energy is greater than the MSE performance loss caused by neglecting those taps with insignificant energy. At high SNR region, noise effect becomes insignificant and the missing channel energy from the neglected channel tap(s) causes the MSE floor. For the considered channel, the missing channel energy in MST-5 taps case is about 1% of the total channel energy and the MSE floor is at about -28 dB. However, this MSE floor does not result in a significant degradation of BER performance as can be seen in Fig. 3.6.

The DFT-based LMMSE approach has slightly worse MSE performance than

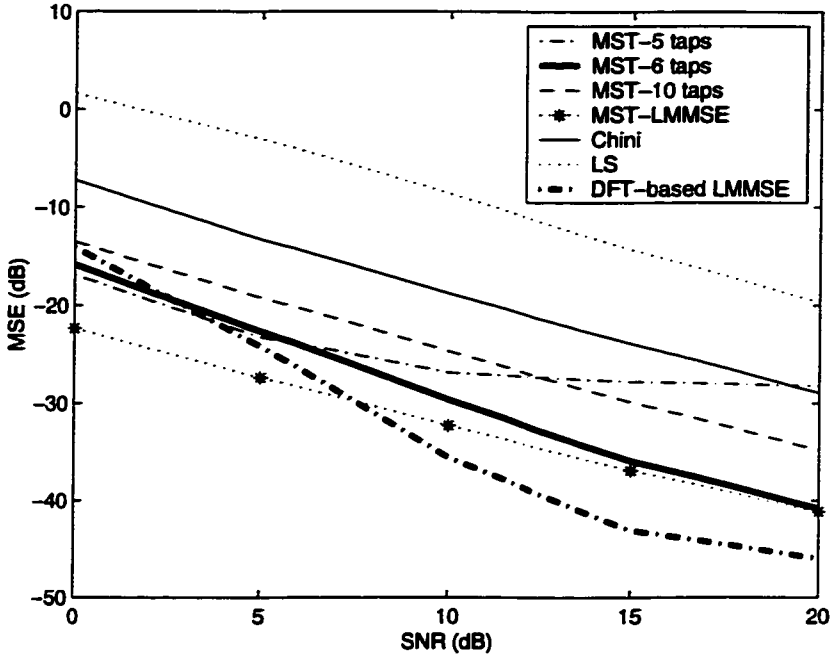

Figure 3.5. *Channel estimation mean square error (MSE) for an OFDM system with BPSK modulation in a time-varying multipath fading channel*

MST methods at very low SNR region but better MSE performance at high SNR region. Since decision-directed approach is used in DFT-based LMMSE, the less reliable decision-directed reference subcarrier symbols at lower SNR region cause the slightly worse channel estimation MSE. At high SNR region, this drawback diminishes and the DFT-based LMMSE achieves better channel estimation MSE than MST approaches. However, this better MSE does not translate into a better BER performance as can be seen in Fig. 3.6. The reason can be explained as follows. The DFT-based LMMSE uses the channel estimate obtained from the previous symbol to equalize the current symbol but the time-varying nature of the multipath mobile wireless channel causes some variation in the channel responses to the previous symbol and the current symbol, depending on the fading rate of the mobile channel. This channel estimate mismatch causes the better MSE performance of the DFT-based LMMSE not to bring about a better BER performance. For the considered channel, MST approach has even a very slightly better BER performance.

When comparing MST-LMMSE with MST-6taps, the former has better MSE per-

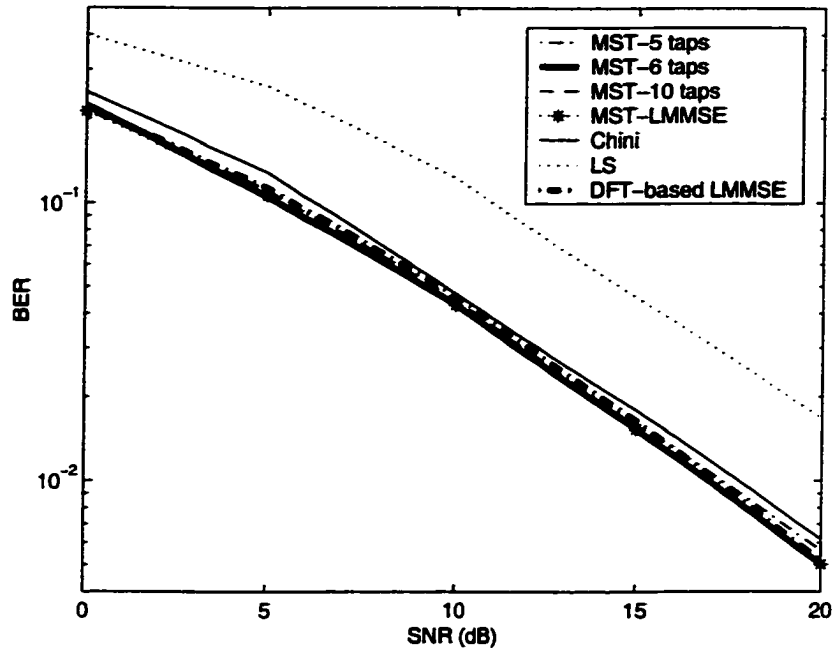

Figure 3.6. *BER performances of an OFDM system with BPSK modulation for different channel estimation methods in a time-varying multipath fading channel*

formance than the latter especially at low SNR region. Since ideal channel statistics and particularly ideal noise statistics are used in MST-LMMSE whereas MST does not use noise statistics, MST-LMMSE achieves more improvement in MSE performance for the noise dominant SNR region. For high SNR region, the two MSE performances becomes very close. This reflects that MST with the same number of taps as in the channel well-approximates an LMMSE at high SNR region. In terms of BER performance, both MST-LMMSE and MST approaches have almost the same performance (MST-LMMSE is just marginally better). In terms of complexity, MST approach has less complexity than the others except the LS method.

3.6.2 Performance for OFDM with 64-QAM

Fig. 3.7 shows the MSE performances of different channel estimation methods for an OFDM system with 64-QAM in Channel-A where a quasi-static fading is assumed. Similar to BPSK case, the MSE of FPTA-1 is slightly less than FPTA-2. The method of Chini [52] has some improvement over FPTA approaches even though it is asso-

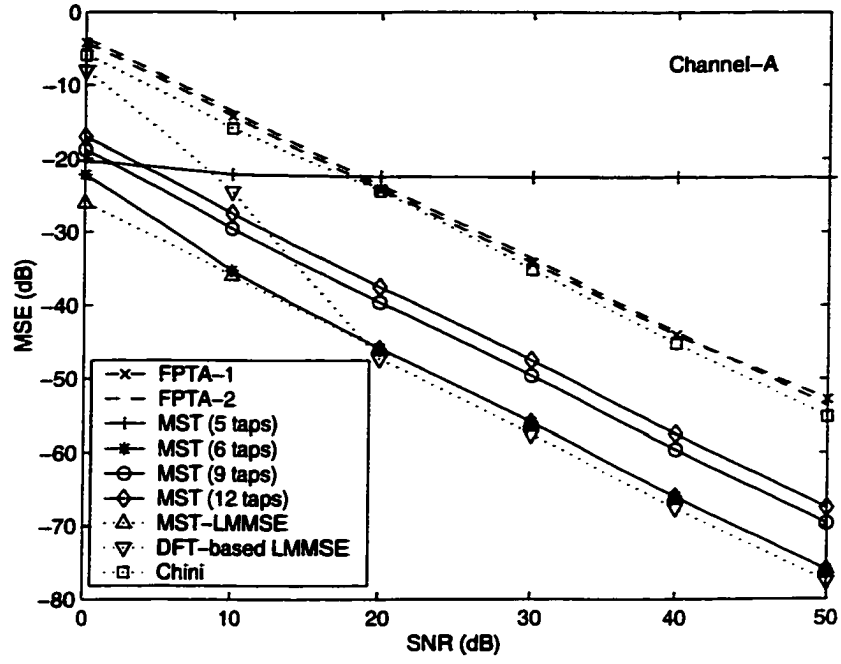

Figure 3.7. *Channel estimation mean square error (MSE) in Channel-A for an OFDM system with 64-QAM modulation*

ciated with decision directed errors. MST method with 6 taps, which is the same as the number of taps in Channel-A, has approximately 18 to 22 dB MSE gain over FPTA approaches. MST with 5 taps shows an irreducible channel estimation error floor caused by missing some of the channel energy. It has a better performance than FPTA approaches for SNR less than 20 dB since for this SNR region the gain in noise suppression is greater than the loss of the channel energy missing. However, for higher SNR region where noise has smaller impact than the channel energy missing, the channel estimation error floor results in a worse performance for MST with 5 taps. For the cases of MST with larger number of taps than the actual channel taps, MST achieves performance gain over FPTA and [52] approaches. The channel estimation performance gains are not as high as MST with 6 taps case due to the additional noise perturbation from the extra taps.

Also shown in Fig. 3.7 are the performances of MST-LMMSE and DFT-based LMMSE methods. LMMSE's approaches are of similar performance to MST with 6 taps case. For SNR less than 20 dB, DFT-based LMMSE has a worse performance

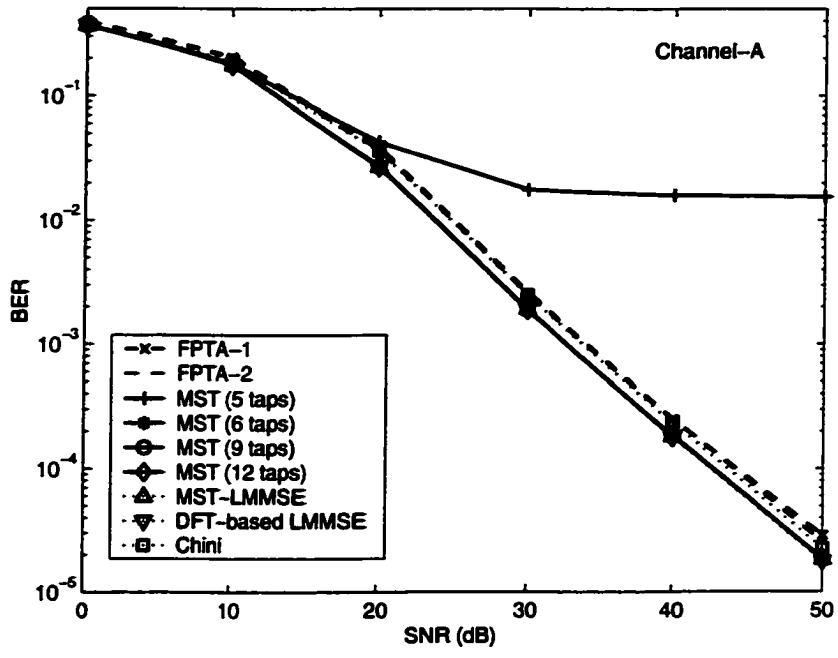

Figure 3.8. *BER performances of an OFDM system with 64-QAM modulation for different channel estimation methods in Channel-A*

Table 3.2. *BER of an OFDM system with 64-QAM modulation for different channel estimation methods in Channel-A*

SNR (dB)	0	10	20	30	40	50
FPTA-1	0.3926	0.2015	3.7501×10^{-2}	2.5364×10^{-3}	2.4960×10^{-4}	2.8721×10^{-5}
FPTA-2	0.3957	0.2049	3.9122×10^{-2}	2.6389×10^{-3}	2.5513×10^{-4}	2.5377×10^{-5}
MST (5 taps)	0.3693	0.1814	4.262×10^{-2}	1.7651×10^{-2}	1.5964×10^{-2}	1.5441×10^{-2}
MST (6 taps)	0.3689	0.1770	2.7049×10^{-2}	1.8693×10^{-3}	1.8358×10^{-4}	1.8309×10^{-5}
MST (9 taps)	0.3695	0.1776	2.7291×10^{-2}	1.8841×10^{-3}	1.8505×10^{-4}	1.8502×10^{-5}
MST (12 taps)	0.3700	0.1781	2.7487×10^{-2}	1.8958×10^{-3}	1.8598×10^{-4}	1.8574×10^{-5}
MST-LMMSE	0.3689	0.1753	2.7023×10^{-2}	1.9081×10^{-3}	1.8309×10^{-4}	1.8299×10^{-5}
DFT-based LMMSE	0.3670	0.1762	2.7051×10^{-2}	1.8911×10^{-3}	1.8052×10^{-4}	1.7851×10^{-5}
Chini [52]	0.3711	0.1887	3.6529×10^{-2}	2.4789×10^{-3}	2.3445×10^{-4}	2.2593×10^{-5}

than MST with 6 taps due to the decision directed errors. For higher SNR region, it has a slightly better performance due partly to the fact that its decision directed errors become insignificant and partly to the fact that MST suffers some interference from data part. MST-LMMSE has a slight performance gain over MST with 6 taps case for low SNR region and almost the same performance for high SNR region. This slight performance gain of MST-LMMSE in low SNR region is due to the utilization of (ideal) channel and noise statistics in MST-LMMSE approach by which the selection of channel taps are always correct, whereas in MST approach, the selection of channel taps may not be always correct due to the large noise perturbation.

Due to the same reasons as in BPSK modulation, the actual MSE gain of MST method is slightly less than the potential gain of MST method described in the previous section and the actual MSE gain is less in low SNR region than in high SNR region.

In Fig. 3.8, the BER performances of an OFDM system with 64-QAM modulation in Channel-A are presented for different channel estimation methods. For BPSK modulation case, it was observed in Figs. 3.5 and 3.6 that the MST with 5 taps has an MSE floor but no BER floor. However, for 64-QAM case, Figs. 3.7 and 3.8 show that the MST with 5 taps has both MSE floor and BER floor. The reason is due to the larger BER-sensitity of 64-QAM to the channel estimation errors. The method of [52] is slightly better than FPTA approaches as is the case in the corresponding MSE performance. The other MST and LMMSE approaches have better BER performances than FPTA and [52] approaches, but among themselves, the BER performances are just slightly different and hence, their BER curves are almost the same.

For a better presentation of their slight differences, their BER values are tabulated in Table. 3.2. These slight differences can be ascribed to the corresponding different channel estimation performances. It is also noted that when the channel estimation MSE is much smaller than 1/SNR, then some deviation in channel estimation MSE does not significantly affect the BER performance since noise is the dominant contributor to BER in this case.

The channel estimation performance and BER performance of the considered methods for an OFDM system with 64-QAM modulation in Channel-B, where a quasi-static fading is assumed, are plotted in Figs. 3.9 and 3.10, respectively, and the

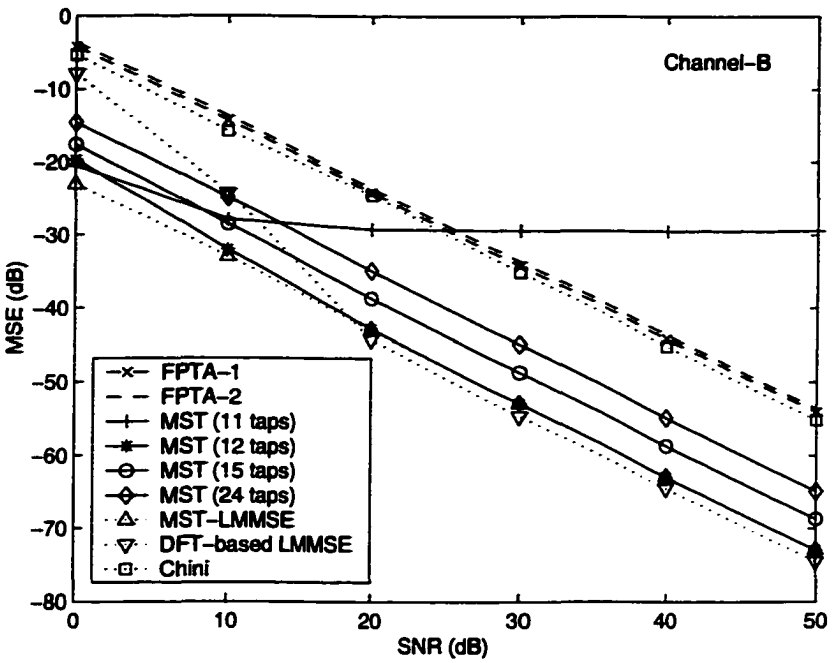

Figure 3.9. *Channel estimation mean square error (MSE) in Channel-B for an OFDM system with 64-QAM modulation*

Table 3.3. *BER of an OFDM system with 64-QAM modulation for different channel estimation methods in Channel-B*

SNR (dB)	0	10	20	30	40	50
FPTA-1	0.4014	0.2250	6.1986×10^{-2}	8.0725×10^{-3}	8.3867×10^{-4}	8.6296×10^{-5}
FPTA-2	0.4041	0.2283	6.3793×10^{-2}	8.3684×10^{-3}	8.6701×10^{-4}	8.6831×10^{-5}
MST (11 taps)	0.37828	0.2019	5.3833×10^{-2}	1.2092×10^{-2}	6.7836×10^{-3}	6.2976×10^{-3}
MST (12 taps)	0.3785	0.2011	4.9783×10^{-2}	6.1269×10^{-3}	6.2924×10^{-4}	6.3026×10^{-5}
MST (15 taps)	0.3790	0.2017	5.0082×10^{-2}	6.1707×10^{-3}	6.3410×10^{-4}	6.3421×10^{-5}
MST (24 taps)	0.3805	0.2032	5.0749×10^{-2}	6.2714×10^{-3}	6.4442×10^{-4}	6.4503×10^{-5}
MST-LMMSE	0.3781	0.2011	4.9847×10^{-2}	6.1509×10^{-3}	6.3000×10^{-4}	6.3806×10^{-5}
DFT-based LMMSE	0.3775	0.2018	4.969×10^{-2}	6.1261×10^{-3}	6.2774×10^{-4}	6.2568×10^{-5}
Chini [52]	0.3809	0.2123	5.9644×10^{-2}	7.7969×10^{-3}	8.0554×10^{-4}	8.0195×10^{-5}

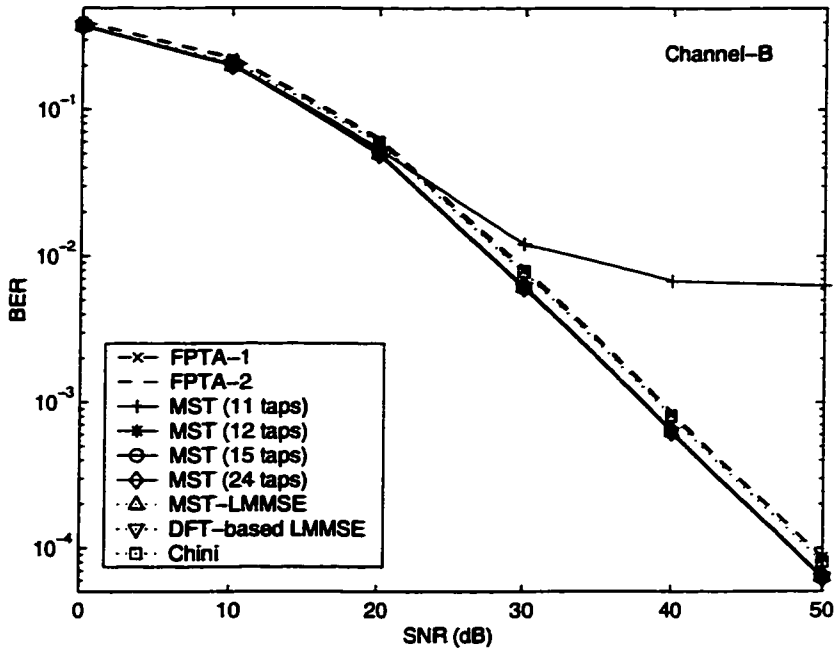

Figure 3.10. *BER performances of an OFDM system with 64-QAM modulation for different channel estimation methods in Channel-B*

BER values are given in Table. 3.3 for the sake of clarity. The performances are of the same trend as in Channel-A. It is also noted that the channel estimation and BER performances in Channel-B are worse than those in Channel-A except for the case of missing some of the channel energy (i.e., MST with 5 taps in Channel-A and MST with 11 taps in Channel-B). This exception is due to the larger percentage of the channel energy missed in Channel-A than in Channel-B.

From the simulation results, it is clear that the number of MST taps J should not be smaller than the number of actual channel taps. On the other hand, using more taps may slightly degrade the BER performance due to the more noise perturbation. However, even up to double of the number of actual channel taps, MST has almost the same BER performance as using the number of actual channel taps. Hence, a suitable choice for J might be double of the (designed) number of channel taps for the considered channel environment.

Another way of selecting MST taps by threshold decision is also evaluated in Channel-B. The corresponding channel estimation MSE and BER results are shown

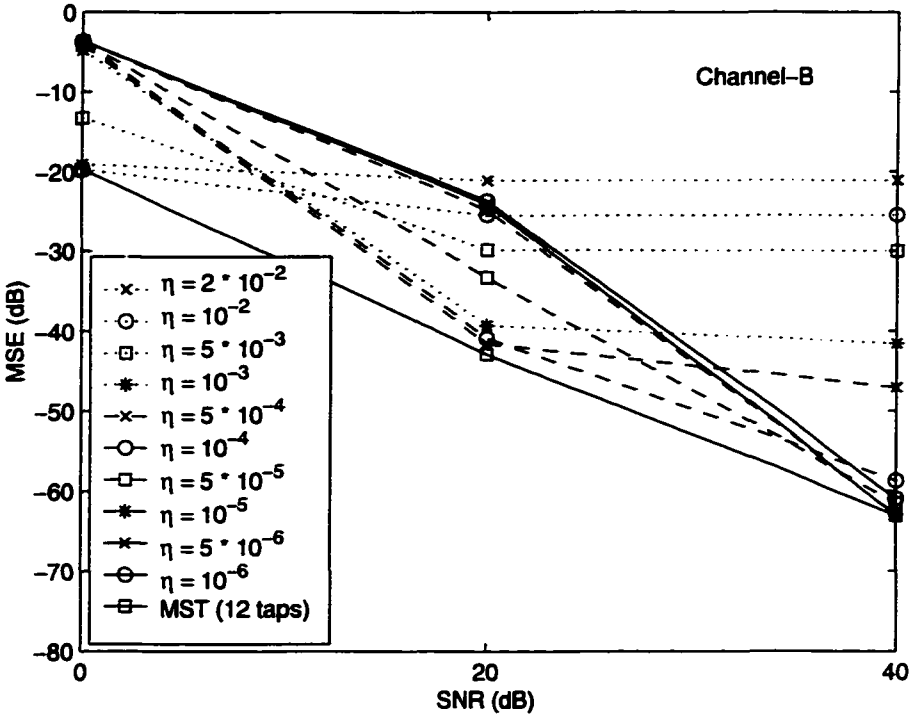

Figure 3.11. *Channel estimation mean square error (MSE) of MST with threshold setting η for an OFDM system with 64-QAM modulation*

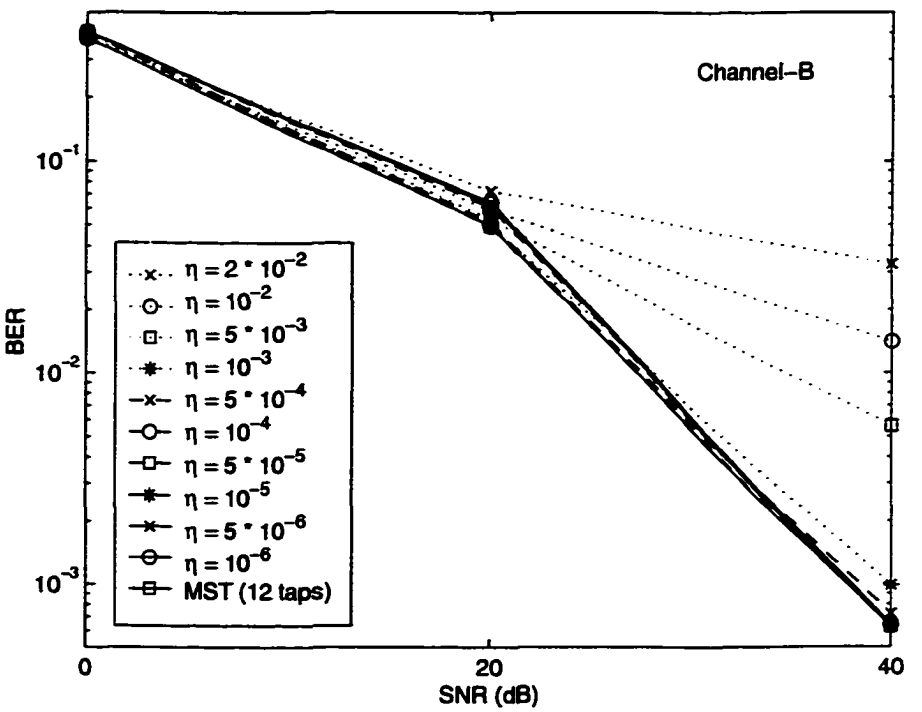

Figure 3.12. *BER performance of MST with threshold setting η for an OFDM system with 64-QAM modulation*

in Figs. 3.11 and 3.12 respectively. The performance of MST with 12 taps is also included for a reference. It is observed that a suitable choice of the threshold also depends on the operating SNR, as expected. The results also indicate that almost the same performance as MST with 12 taps case can be obtained if the threshold for an operating SNR is set within approximately 20 to 23 dB below the operating 1/SNR. This low value of the threshold in ensuring no channel energy miss is also due to the gain variations in the channel taps.

It is also remarked that for relatively slow fading environments, the decision feedback approaches such as [52] and LMMSE can increase spectrum efficiency by using smaller pilot ratio. Similarly, MST approach can increase the spectrum efficiency by not inserting pilot tones in every OFDM symbol. For this case, the decision feedback approach as used in MST's dual form DFT-based approach can easily be applied for pure data symbols.

3.7 Conclusions

In this chapter, intra-symbol time-domain averaging approaches for time-domain channel estimation of OFDM system are investigated. As an approximation to LMMSE type estimator, a time-domain approach, called MST, is proposed where intra-symbol time-domain averaging and most significant taps selection are applied. The similarities and differences of the proposed MST method versus DFT-based LMMSE methods are discussed. Two approaches for MST taps selection are described where the first uses a fixed number of taps while the second chooses all taps above a threshold. The simulation results suggest that a suitable choice for the fixed number of MST taps is using double of the (designed) number of channel taps for the considered channel environment. And a suitable choice of the threshold is within the range of approximately 20 to 23 dB below the operating 1/SNR. In terms of BER performance in multipath fading channels, MST without channel energy missing and LMMSE approaches have almost the same performance which is better than the other considered approaches. In terms of complexity, the proposed MST approach keeps the minimum complexity among the considered methods.

Chapter 4

A Reduced Complexity Channel Estimation for OFDM Systems with Transmit Diversity in Mobile Wireless Channels

One of the desirable features of OFDM is its robustness to the multipath induced inter-symbol interference. On the other hand, due to the frequency selective fading of the dispersive wireless channel, some subchannels may face deep fades and degrade the overall system performance. In order to compensate the frequency selectivity, techniques such as error correcting code and diversity have to be used [47] [57] [30]. Transmit diversity for wireless systems has been studied in research literature (e.g., [58], [59]). For OFDM systems, transmit diversity combined with Reed-Solomon code has been proposed for clustered OFDM in [57]. Recently, space-time coding [60] has been shown to give high code efficiency and good performance. Application of space-time coding in OFDM systems has been studied in [61] with perfect channel knowledge at the receiver.

The channel estimation for OFDM systems without transmit diversity has been studied by many researchers (e.g., [51] [54] [48]). However, for systems with transmit diversity, the received signal is a superposition of the different transmitted signals from all transmit antennas and consequently, the channel estimation becomes more complicated. Recently, the channel estimation for OFDM systems with transmit diversity using space-time coding has been proposed in [47]. In order to reduce the complexity associated with the matrix inverse operation, [47] also proposed a simpli-

fied approach. In this chapter, we focus on reduced complexity channel estimation for OFDM systems with transmit diversity.

We propose a channel estimation method which has less complexity than the simplified method of Li [47]. By decoupling the effect of different transmit antennas, the sizes of the matrix inverse and FFT's required in the channel estimation for every OFDM data symbol are reduced by half. The significant tap catching approach of Li [47] requires the knowledge of the number of significant taps. In this chapter, we describe an alternative approach which adaptively finds this number. Moreover, we investigate the impact of non-sample-spaced channel paths on the channel estimation and propose a simple modification which reduces the channel energy leakage lost in the channel estimation of both Li [47] and the reduced complexity method. This modified approach achieves a substantial performance improvement without any added complexity.

The rest of this chapter is organized as follows. In Section 4.1, the system and the channel considered are described. In Section 4.2, the reduced complexity channel estimation is derived and adaptively finding the number of significant taps is described. The performance in terms of the channel estimation mean square error (MSE) and the complexity comparison are presented in Section 4.3. The energy leakage of the channel path with non-sample-spaced delay is investigated in Section 4.4. Based on this, a modified approach is proposed for further improvement. Simulation results are discussed in Section 4.5 and finally, conclusions are given in Section 4.6.

4.1 System and Channel Description

The considered OFDM system with two-branch transmit diversity and two-branch receive diversity using a space-time code is described in Fig. 4.1. At a transmission time n, a binary data block $\{b[n,k] : k = 0\ 1,\ \ldots\}$ is space-time-coded (in fact, space-frequency-coded) into two blocks of frequency-domain subcarrier symbols, $\{s_i[n,k] : k = 0,\ 1,\ \ldots\}$ for $i = 1,\ 2$, which are simultaneously transmitted from the two antennas.

The DFT output frequency-domain subcarrier symbols from receive antenna j can

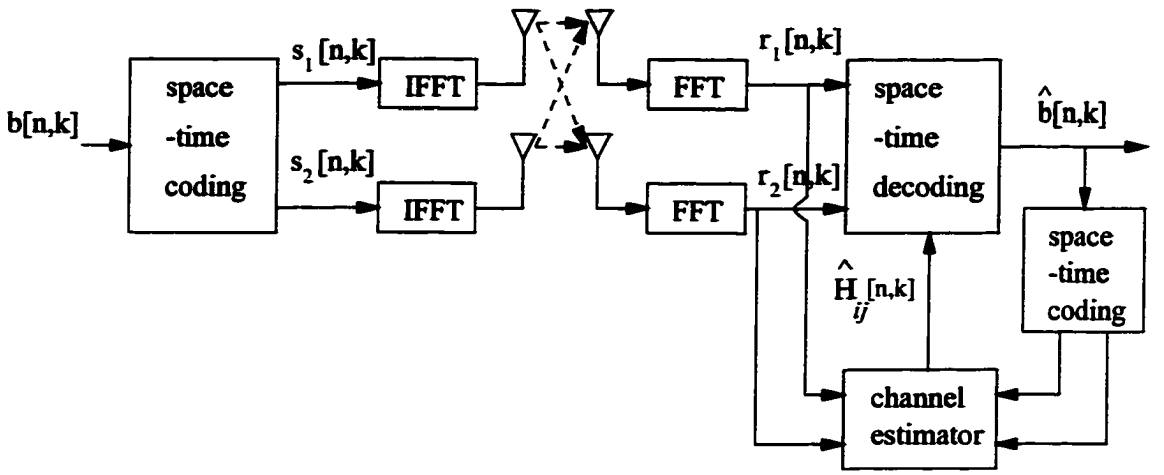

Figure 4.1. *The considered OFDM system with two-branch transmit diversity and two-branch receive diversity using a space-time code*

be expressed as

$$r_j[n,k] = \sum_{i=1}^{2} H_{ij}[n,k]\ s_i[n,k] + w_j[n,k] \tag{4.1}$$

where $w_j[n,k]$ is the additive white complex Gaussian noise with zero mean and variance σ_n^2, on the j^{th} receive antenna, that is uncorrelated for different n's, k's, or j's, and $H_{ij}[n,k]$ is the channel frequency response for the k^{th} tone at time n, corresponding to the i^{th} transmit antenna and the j^{th} receive antenna. For a system with L-transmit diversity, the average SNR at the receiver is defined as

$$SNR \triangleq \frac{E\left\{\sum_{i=1}^{L} |H_{ij}[n,k]|^2\right\}}{\sigma_n^2} \tag{4.2}$$

where $E\{\cdot\}$ represents the expectation and $E\{|s_i|^2\} = 1$ is assumed. In our simulation, the channels are modeled such that $E\{|H_{ij}[n,k]|^2\} = 1$.

The channel impulse response of the mobile wireless channel can be given by

$$h(t,\tau) = \sum_{k} \gamma_k(t)\ \delta(\tau - \tau_k) \tag{4.3}$$

where τ_k is the delay of the k^{th} path, $\gamma_k(t)$ is the corresponding complex gain, $\delta(\tau)$ is the Dirac Delta function. The antenna indexes i, j are omitted for simplicity. The

frequency response at time t is

$$H(t,f) \triangleq \int_{-\infty}^{\infty} h(t,\tau)\, e^{-j2\pi f\tau}\, d\tau = \sum_{k} \gamma_k(t)\, e^{-j2\pi f\tau_k}. \tag{4.4}$$

The path gains $\gamma_k(t)$'s are modeled as independent wide-sense stationary (WSS), narrowband complex Gaussian processes with the time-domain correlation defined by the classical Doppler spectrum. The frequency-domain correlation of the channel is defined by the channel power delay profile.

With tolerable leakage, the channel frequency response can be expressed as [1]

$$H[n,k] \triangleq H(nT_f, k\Delta f) = \sum_{l=0}^{K_0-1} h[n,l]\, W_K^{kl} \tag{4.5}$$

where $h[n,l] \triangleq h(nT_f, lt_s)$, $W_K = exp(-j2\pi/K)$, K_0 is the total number of sample-spaced channel taps, K is the number of tones (including guard tones), T_f and Δf are the total OFDM symbol interval and the tone spacing of the OFDM system, respectively, and $t_s = 1/(K\Delta f)$.

The considered channel power delay profile models are two-ray (equal average power on each ray), the Global System for Mobile communication (GSM)'s typical urban (TU) (6 taps), GSM's hilly terrain (HT) (6 taps), and the Joint Technical Committee (JTC)'s indoor office channel model A (3 taps) [62].

4.2 Reduced Complexity Channel Estimation

Since the channels considered have independent responses to different receive antennas, the channel estimation is independently performed for each receive antenna. The receive antenna index j will be omitted in the following. The frequency-domain subcarrier symbols from each receive antenna can be expressed as

$$r[n,k] = \sum_{i=1}^{2} H_i[n,k]\, s_i[n,k] + w[n,k]. \tag{4.6}$$

Due to the limited delay spread of the channel, the channel subcarrier responses are correlated. Generally, the smaller the ratio of the channel delay spread to the OFDM

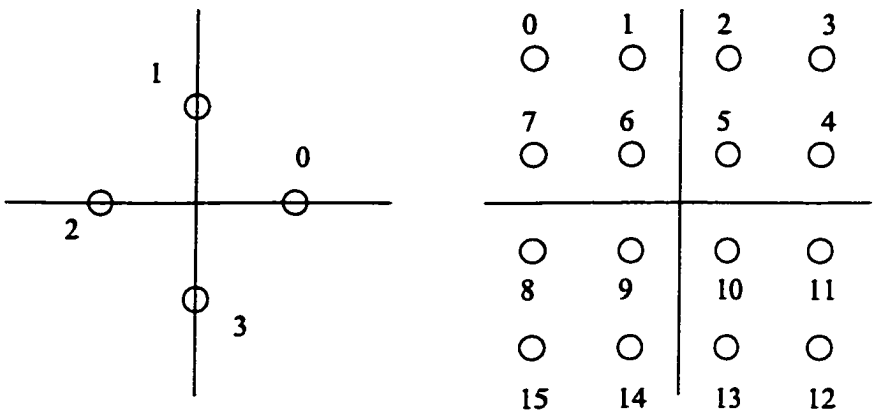

Figure 4.2. *Signal constellations of 4-PSK and 16-QAM.*

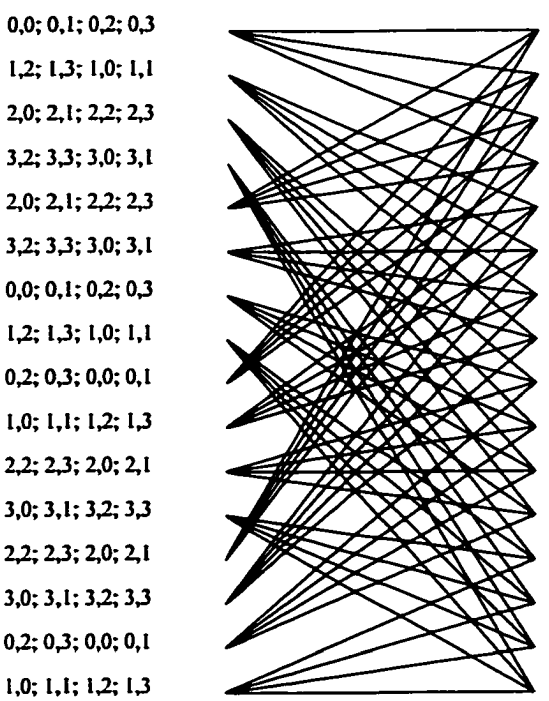

Figure 4.3. *Trellis diagram of a 16-states 2 branch space-time code with 4-PSK*

Figure 4.4. *Trellis diagram of a 16-states 2 branch space-time code with 16-QAM*

symbol interval, the more correlated the adjacent subcarrier responses are. In this chapter, we attempt to find a reduced complexity channel estimation by exploiting the correlation of the subcarrier responses. In particular, we will assume in the derivation of the reduced complexity channel estimation that

$$H_i[n, 2m] = H_i[n, 2m + 1]. \tag{4.7}$$

The above assumption would be a good approximation for the case with a very small ratio of channel delay spread to OFDM symbol interval. We will also investigate the applicability of this assumption for different channels with different delay spreads.

Let us define the following:

$$z_1[n,m] \triangleq \frac{r[n,2m]}{s_2[n,2m]} - \frac{r[n,2m+1]}{s_2[n,2m+1]} \tag{4.8}$$

$$z_2[n,m] \triangleq \frac{r[n,2m]}{s_1[n,2m]} - \frac{r[n,2m+1]}{s_1[n,2m+1]} \tag{4.9}$$

$$\varpi_1[n,m] \triangleq \frac{w[n,2m]}{s_2[n,2m]} - \frac{w[n,2m+1]}{s_2[n,2m+1]} \tag{4.10}$$

$$\varpi_2[n,m] \triangleq \frac{w[n,2m]}{s_1[n,2m]} - \frac{w[n,2m+1]}{s_1[n,2m+1]}. \tag{4.11}$$

With (4.7), we obtain

$$z_i[n,m] = H_i[n,2m]\ v_i[n,m] + \varpi_i[n,m]\ ,\ i=1,\ 2 \tag{4.12}$$

where

$$v_1[n,m] \triangleq \frac{s_1[n,2m]}{s_2[n,2m]} - \frac{s_1[n,2m+1]}{s_2[n,2m+1]} \tag{4.13}$$

$$v_2[n,m] \triangleq \frac{s_2[n,2m]}{s_1[n,2m]} - \frac{s_2[n,2m+1]}{s_1[n,2m+1]}. \tag{4.14}$$

From (4.12), it can be observed that the channel responses corresponding to different transmit antennas are decoupled. Hence, the channel estimation can be performed independently for each transmit-receive antenna pair by minimizing the following mean square error (MSE) cost function:

$$C\left(\{\tilde{h}_i[n,l] : i=1,\ 2\}\right) = \sum_{m=0}^{M-1} \left| z_i[n,m] - \sum_{l=0}^{K_0-1} \tilde{h}_i[n,l]\ W_M^{ml}\ v_i[n,m] \right|^2 \tag{4.15}$$

where $M = K/2$, and $\{\tilde{h}_i[n,l]\}$ are trial values for the minimum mean square error (MMSE) estimates of $\{h_i[n,l]\}$.

Solving the following

$$\frac{\partial C\left(\{\tilde{h}_i[n,l]\}\right)}{\partial \tilde{h}_i[n,l_0]} \triangleq \frac{1}{2}\left\{\frac{\partial C(\{\tilde{h}_i[n,l])}{\partial \Re(\tilde{h}_i[n,l_0])} - j\,\frac{\partial C(\{\tilde{h}_i[n,l])}{\partial \Im(\tilde{h}_i[n,l_0])}\right\} = 0 \tag{4.16}$$

where $\Re(*)$ and $\Im(*)$ denote the real and imaginary part of a complex number, respectively, and $l_0 = 0,\ 1,\ \ldots,\ K_0 - 1$, results in

$$\sum_{m=0}^{M-1}\left(z_i[n,m] - \sum_{l=0}^{K_0-1} \hat{h}_i[n,l]\ W_M^{ml}\ v_i[n,m]\right)\ v_i^*[n,m]\ W_M^{-ml_0} = 0 \tag{4.17}$$

where $\{\hat{h}_i[n,l]\}$ are the MMSE estimates.

Define

$$q_i[n,l] \triangleq \sum_{m=0}^{M-1} |v_i[n,m]|^2 \, W_M^{-ml} \tag{4.18}$$

$$p_i[n,l] \triangleq \sum_{m=0}^{M-1} z_i[n,m] \, v_i^*[n,m] \, W_M^{-ml}. \tag{4.19}$$

Then, (4.17) can be expressed as

$$\sum_{l=0}^{K_0-1} \hat{h}_i[n,l] \, q_i[n, l_0 - l] = p_i[n, l_0] \tag{4.20}$$

for $i = 1,\ 2$ and $l_0 = 0,\ 1,\ \ldots,\ K_0 - 1$. It can be expressed in matrix form as

$$\boldsymbol{Q}_i[n] \, \hat{\boldsymbol{h}}_i[n] = \boldsymbol{p}_i[n] \tag{4.21}$$

where

$$\boldsymbol{Q}_i[n] \triangleq \begin{pmatrix} q_i[n,0] & q_i[n,-1] & \ldots & q_i[n,-K_0+1] \\ q_i[n,1] & q_i[n,0] & \ldots & q_i[n,-K_0+2] \\ \vdots & \vdots & \ddots & \vdots \\ q_i[n,K_0-1] & q_i[n,K_0-2] & \ldots & q_i[n,0] \end{pmatrix} \tag{4.22}$$

$$\hat{\boldsymbol{h}}_i[n] \triangleq (\hat{h}_i[n,0],\ \hat{h}_i[n,1],\ \ldots,\ \hat{h}_i[n,K_0-1])^T \tag{4.23}$$

$$\boldsymbol{p}_i[n] \triangleq (p_i[n,0],\ p_i[n,1],\ \ldots,\ p_i[n,K_0-1])^T. \tag{4.24}$$

Hence, the channel impulse response can be estimated by

$$\hat{\boldsymbol{h}}_i[n] = \boldsymbol{Q}_i^{-1}[n] \, \boldsymbol{p}_i[n]. \tag{4.25}$$

Following [47], the complexity involved in $\boldsymbol{Q}^{-1}$ can be further reduced and the channel estimation performance can be further improved by using only J significant channel taps whose indexes are denoted by $\{l_m :\ m = 1,\ 2,\ \ldots,\ J;\ (0 \le l_1 < l_2 < \ldots < l_J \le K_0 - 1)\}$. Then, the simplified channel estimation is given by

$$\bar{\boldsymbol{h}}_i[n] = \bar{\boldsymbol{Q}}_i^{-1}[n] \, \bar{\boldsymbol{p}}_i[n] \tag{4.26}$$

where

$$\bar{\boldsymbol{h}}_j[n] \triangleq (\hat{h}_i[n,l_1],\ \hat{h}_i[n,l_2],\ \ldots,\ \hat{h}_i[n,l_J])^T \tag{4.27}$$

$$\bar{\boldsymbol{Q}}_i[n] \triangleq \begin{pmatrix} q_i[n,0] & q_i[n,l_1-l_2] & \ldots & q_i[n,l_1-l_J] \\ q_i[n,l_2-l_1] & q_i[n,0] & \ldots & q_i[n,l_2-l_J] \\ \vdots & \vdots & \ddots & \vdots \\ q_i[n,l_J-l_1] & q_i[n,l_J-l_2] & \ldots & q_i[n,0] \end{pmatrix} \tag{4.28}$$

$$\bar{\boldsymbol{p}}_i[n] \triangleq (p_i[n,l_1],\ p_i[n,l_2],\ \ldots,\ p_i[n,l_J])^T. \tag{4.29}$$

The value of J generally depends on the number of paths and the path delays, both of which are typically defined by the terrain environment. In [47], it is reported that the value of J typically ranges between 5 and 9 for 2-ray, TU, and HT channels. Due to the time-varying nature of the mobile wireless channel, the effective number of (sample-spaced) significant channel taps and/or their tap indexes can vary to some degree for different time instants. This prompts a question on the applicability of this significant tap catching approach in a fast time-varying channel. However, the results in [47] and also in this chapter show that even with a Doppler frequency of 200 Hz for the OFDM system with $200\mu s$ symbol interval and 10% training, the significant tap catching approach works well.

An alternative approach in the significant tap catching rather than using fixed value of J is described in the following. Suppose the maximum value of J for which the complexity can be afforded be J_m. Let $\{\hat{h}_{sort}[l]\}$ be the sorted version of $\{\hat{h}[l]\}$ in descending order, and J_i be the number of taps satisfying the following condition:

$$|\hat{h}[l]|^2 > \eta \cdot \frac{1}{\alpha} \sum_{l=0}^{\alpha-1} |\hat{h}_{sort}[l]|^2. \tag{4.30}$$

Then, the value of J is chosen as the minimum of J_i and J_m. In the above equation, η is a threshold value. Although $\alpha = 1$ is applicable, it was observed in our investigation that a little larger value (say, 3 or 4) gives more robustness to the noise. The threshold value η depends on the SNR value and is chosen according to

$$\eta_2 = \eta_1 \frac{SNR_1}{SNR_2} \tag{4.31}$$

where η_i is for SNR_i. We observed that the value of η about the range of 0.01 to 0.04 works well for a SNR value of 10 dB. This threshold value can be set according to

the designed received SNR or by means of the sync detection metric such as received power measurement. Due to the varying value of J at every training symbol, this approach will be denoted by "adaptive" in contrast to the fixed value of J. For channel environments where a suitable fixed value of J is unknown, this adaptive approach would be an alternative. It is noted that in the adaptive approach, the value of J need not be the same for the different transmit antennas.

4.3 Performance Analysis

4.3.1 MSE Performance

In the previous section, a reduced complexity channel estimation for OFDM systems with transmit diversity is proposed by assuming that (4.7) holds. In this section, the MSE performance of the proposed method in a multipath fading channel not satisfying (4.7) is analysed. For simplicity, the time index n is omitted in the following analysis. Define the following:

$$\begin{aligned} \Delta H_i[m] &\triangleq H_i[2m] - H_i[2m+1] \\ &= \sum_{l=0}^{K_0-1} h_i[l]\,(1 - W_K^l)\,W_K^{2ml} \end{aligned} \tag{4.32}$$

$$\Delta H_{e1}[m] \triangleq \Delta H_2[m] + \Delta H_1[m]\,\frac{s_1[2m+1]}{s_2[2m+1]}. \tag{4.33}$$

Then,

$$z_1[m] = \Delta H_{e1}[m] + H_1[2m]v_1[m] + \varpi_1[m] \tag{4.34}$$

$$p_1[l] = X_1[l] + \sum_{k=0}^{K_0-1} q_1[l-k]\,h_1[k] + \mathcal{W}_1[l] \tag{4.35}$$

where

$$X_1[l] \triangleq \sum_{m=0}^{M-1} \Delta H_{e1}[m]\,v_1^*[m]\,W_M^{-ml} \tag{4.36}$$

$$\mathcal{W}_1[l] \triangleq \sum_{m=0}^{M-1} \varpi_1[m]\,v_1^*[m]\,W_M^{-ml}. \tag{4.37}$$

In matrix form,

$$\boldsymbol{p}_1 = \boldsymbol{X}_1 + \boldsymbol{W}_1 + \boldsymbol{Q}_1\, \boldsymbol{h}_1 \tag{4.38}$$

where

$$\begin{aligned}
\boldsymbol{p}_1 &\triangleq (p_1[0],\ p_1[1],\ \ldots,\ p_1[K_0-1])^T \\
\boldsymbol{X}_1 &\triangleq (X_1[0],\ X_1[1],\ \ldots,\ X_1[K_0-1])^T \\
\boldsymbol{W}_1 &\triangleq (W_1[0],\ W_1[1],\ \ldots,\ W_1[K_0-1])^T \\
\boldsymbol{h}_1 &\triangleq (h_1[0],\ h_1[1],\ \ldots,\ h_1[K_0-1])^T .
\end{aligned}$$

The channel impulse response estimate corresponding to transmit antenna 1 is given by

$$\hat{\boldsymbol{h}}_1 \;=\; \boldsymbol{Q}_1^{-1}\, \boldsymbol{p}_1 = \boldsymbol{Q}_1{}^{-1}\, (\boldsymbol{X}_1 + \boldsymbol{W}_1) + \boldsymbol{h}_1. \tag{4.39}$$

The MSE of the channel impulse response estimate can be given by

$$\begin{aligned}
MSE \;&\triangleq\; E\left\{\left\|\hat{\boldsymbol{h}}_1 - \boldsymbol{h}_1\right\|^2\right\} \\
&=\; E\left\{[\boldsymbol{Q}_1^{-1}\, (\boldsymbol{X}_1 + \boldsymbol{W}_1)]^H \boldsymbol{Q}_1^{-1}\, (\boldsymbol{X}_1 + \boldsymbol{W}_1)\right\} \\
&=\; Trace\left\{\boldsymbol{Q}_1^{-1} E\{\boldsymbol{X}_1 \boldsymbol{X}_1^H\} \boldsymbol{Q}^{-1\,H}\right\} \\
&\quad + Trace\left\{\boldsymbol{Q}_1^{-1}\ E\{\boldsymbol{W}_1\, \boldsymbol{W}_1^H\}\ \boldsymbol{Q}^{-1\,H}\right\}.
\end{aligned} \tag{4.40}$$

The elements of $E\left\{\boldsymbol{X}_1\ \boldsymbol{X}_1^H\right\}$ are given by

$$\begin{aligned}
E\left\{X_1[l_0]\ X_1^*[l_1]\right\} \;=\; &\sum_{l=1}^{K_0-1} (1 - W_K^l) \sum_{k=1}^{K_0-1} (1 - W_K^{-k})\, (E\left\{h_1[l] h_1^*[k]\right\}\ \zeta_1[l_0 - l] \zeta_1^*[l_1 - k] \\
&+ E\left\{h_2[l] h_2^*[k]\right\}\ V_1[l_0 - l]\ V_1^*[l_1 - k])
\end{aligned} \tag{4.41}$$

with

$$V_1[k] \triangleq \sum_{m=0}^{M-1} v_1^*[m]\ W_M^{-mk}, \tag{4.42}$$

$$\zeta_1[k] \triangleq \sum_{m=0}^{M-1} v_1^*[m]\ \frac{s_1[2m+1]}{s_2[2m+1]}\ W_M^{-mk}. \tag{4.43}$$

The elements of $E\{\boldsymbol{W}_1\ \boldsymbol{W}_1^H\}$ are given by

$$E\{W_1[l_0]\ W_1^*[l_1]\} = \sigma_n^2\ \psi_1[l_0 - l_1] \tag{4.44}$$

where

$$\psi_1[l] \triangleq \sum_{m=0}^{M-1} \left(\frac{1}{|s_2[2m]|^2} + \frac{1}{|s_2[2m+1]|^2} \right) |v_1[m]|^2\ W_M^{-ml}. \tag{4.45}$$

By defining

$$\Psi_1 \triangleq \begin{pmatrix} \psi_1[0] & \psi_1[-1] & \dots & \psi_1[-K_0+1] \\ \psi_1[1] & \psi_1[0] & \dots & \psi_1[n,-K_0+2] \\ \vdots & \vdots & \ddots & \vdots \\ \psi_1[K_0-1] & \psi_1[K_0-2] & \dots & \psi_1[0] \end{pmatrix}, \tag{4.46}$$

we can express that

$$E\{\boldsymbol{W}_1\ \boldsymbol{W}_1^H\} = \sigma_n^2\ \Psi_1. \tag{4.47}$$

For constant modulus subcarrier symbols ($\{|s_i[m]|\}$ are constant), if $\{v_i[m]\}$ are constant, $E\{\boldsymbol{W}_1\ \boldsymbol{W}_1^H\}$ and $\boldsymbol{Q}_1$ become scaled identity matrixes and the diagonal elements of $E\{\boldsymbol{X}_1\ \boldsymbol{X}_1^H\}$ become $\{|1-W_K^l|^2\ K^2\ (P_1[l]+P_2[l]) : l = 0,\ 1,\ \dots,\ K_0-1.\}$ where $P_i[l] \triangleq E\{|h_i[l]|^2\}$ is the effective sample-spaced power delay profile of the channel corresponding to the transmit antenna i. One criterion that satisfies the above condition is given by $s_1[m] = (-1)^m\ s_2[m]$ which is the same as the optimal training design for [47]. Under this condition, the MSE (4.40) of the reduced complexity method becomes

$$MSE = \frac{1}{2} \sum_{l=1}^{K_0-1} \left|1 - W_K^l\right|^2\ P[l] + \frac{K_0\ \sigma_n^2}{K\ |s_i[m]|^2} \tag{4.48}$$

where the index i from $P[l]$ is omitted for simplicity since generally all channels have the same power delay profile.

Although the above MSE analysis is derived for $\boldsymbol{h}_1$, it also holds for other channels and hence, is the average MSE. The second term in (4.48) is the same as the MSE for [47] at the optimal condition. Hence, the reduced complexity method has a larger channel estimation MSE than [47] due to the assumption of (4.7). The extra term in

the MSE expression also indicates the dependence of the reduced complexity channel estimation MSE performance on the channel power delay profile. Particularly, the larger delay taps have more impact on the MSE. This fact is intuitively justified since the larger delay taps would cause more frequency selectivity of the channel.

It should be mentioned that the above MSE expressions for [47] and the reduced complexity method are derived assuming that the channel gains remain constant over one OFDM symbol, and all subchannels are used (i.e, without guard tones). If the channel gain varies during one OFDM symbol, there may be some degradation due to the inter-subchannel interference (ICI). If guard tones are used, $\boldsymbol{Q}_{ii}$ of [47] would not be exactly a diagonal matrix, and there may be some degradation, too.

From (4.48), the channel estimation MSE mainly depends on $\sigma_n^2/|s_i[m]|^2$ which in turn indicates that the channel estimation MSE performance evaluation by computer simulation depends on how to model $\{E\{|H_{ij}[n,k]|^2\}\}$. For a SNR value and fixed $E\{|s_i[m]|^2\}$, if $\{E\{|H_{ij}[n,k]|^2\}\}$ are modeled very small, σ_n^2 will be very small and consequently, the obtained channel estimation MSE will be very small. Hence, a suitable simulation model for channel estimation performance evaluation should be adopted. There are two possible approaches: the first one is to model $E\left\{\sum_{i=1}^{L}|H_{ij}[n,k]|^2\right\}=1$, and the second is to model $E\left\{|H_{ij}[n,k]|^2\right\}=1$. Due to the similar reasoning of the MSE's dependence on channel power gain and to be comparable with different number of diversity branches, the second approach of $E\left\{|H_{ij}[n,k]|^2\right\}=1$ is adopted in our simulation.

4.3.2 Channel Estimation Complexity

For channel estimation based on the training symbol, the required matrix inverse can be pre-computed. Hence, the discussion on the complexity will be focused on the channel estimation based on the decision-directed reference symbol. The number of complex multiplications will be used as a performance measure. Operations such as K-point FFT and $K_0 \times K_0$ matrix inversion have complexity order of $N\ log_2(N)$ and K_0^3, respectively. However, the exact complexity can vary depending on their implementation. Hence, we will use FFT_K and $[\cdot]^{-1}_{K_0\times K_0}$, respectively in the complexity expression rather than the number of complex multiplications for them. For a two transmit antenna space-time coded OFDM system with K total subcarriers and K_u

Table 4.1. *Channel Estimation Complexity*

# Rx. Ant.	Condition	Method	Complex Multiplications
1	Constant modulus	Li [47]	$3K + 4J^2 + 3J^3 + 3\ FFT_K + [\cdot]^{-1}_{J\times J}$
	with $K_u = K$	RC	$4.5K + 2J^2 + 3\ FFT_{K/2} + [\cdot]^{-1}_{J\times J}$
	Constant modulus	Li [47]	$3K_u + 4J^2 + 3\ FFT_K + [\cdot]^{-1}_{2J\times 2J}$
	with $K_u \neq K$	RC	$4.5K + 2J^2 + 3\ FFT_{K/2} + [\cdot]^{-1}_{J\times J}$
	Non-constant	Li [47]	$5K_u + 4J^2 + 5\ FFT_K + [\cdot]^{-1}_{2J\times 2J}$
	modulus	RC	$6K_u + 2J^2 + 4\ FFT_{K/2} + 2\ [\cdot]^{-1}_{J\times J}$
2	Constant modulus	Li [47]	$5K + 8J^2 + 6J^3 + 5\ FFT_K + 2\ [\cdot]^{-1}_{J\times J}$
	with $K_u = K$	RC	$7.5K + 4J^2 + 5\ FFT_{K/2} + 2\ [\cdot]^{-1}_{J\times J}$
	Constant modulus	Li [47]	$5K_u + 8J^2 + 5\ FFT_K + 2\ [\cdot]^{-1}_{2J\times 2J}$
	with $K_u \neq K$	RC	$7.5K_u + 4J^2 + 5\ FFT_{K/2} + 2\ [\cdot]^{-1}_{J\times J}$
	Non-constant	Li [47]	$7K_u + 8J^2 + 7\ FFT_K + 2\ [\cdot]^{-1}_{2J\times 2J}$
	modulus	RC	$9K_u + 4J^2 + 6\ FFT_{K/2} + 4\ [\cdot]^{-1}_{J\times J}$

used subcarriers, Table 4.1 lists the complexity measures of Li [47] and the reduced complexity method (denoted by RC), both using J significant taps. The significant tap catching is independently performed at each receive antenna and its complexity is not included in the complexity expression. It is noted that if the significant tap catching is performed by averaging over different receive antennas, the number of matrix inverse for the two receive antenna case will be halved for all methods.

For constant modulus subcarrier symbols with no guard tones, the $2J \times 2J$ matrix inversion required in Li [47] can be reduced to a $J \times J$ matrix inversion and some matrix multiplications (see Eq. 24a of [47]). Due to the spectrum requirement, OFDM

systems generally use some guard tones. In this case, the above simplification (Eq. 24a of [47]) does not hold. From Table 4.1, it can be observed that RC method achieves complexity reduction for all conditions. More complexity reduction is observed for the cases of non-const modulus subcarrier symbols and constant modulus subcarrier symbols with guard tones. It is also noted that the size of FFT for RC is $K/2$ while that for [47] is K for all conditions. Moreover, the matrix inverse size for RC is half of that for [47] for all conditions except constant modulus subcarrier symbols with no guard tones.

4.4 Further Improvement on Channel Estimation

In previous sections, the channel response is estimated based on the sample-spaced impulse response $[h[0],\ h[1],\ \ldots,\ h[K_0-1]]$. Generally, the channel path delays are not sample-spaced which causes the channel energy leakage to other sample-spaced taps besides the adjacent sample-spaced taps. In the following, the effect of non-sample-spaced path delay on the channel estimation is investigated.

By using (4.4), the sample-spaced channel tap gains can be given by

$$\begin{aligned} h[l] &= \frac{1}{K}\sum_{m=0}^{K-1}\sum_{k}\gamma_k\, e^{-j2\pi m\lambda_k/K}\, e^{j2\pi ml/K} \\ &= \sum_{k}\gamma_k\, g_k[l] \end{aligned} \tag{4.49}$$

where $\lambda_k \triangleq \tau_k K\,\Delta f$, $\{g_k[l]\}$ are the contribution of the unity gain channel path with delay τ_k over the sampled-spaced taps and given by

$$\begin{aligned} g_k[l] &\triangleq \frac{1}{K}\sum_{m=0}^{K-1} e^{j2\pi m(l-\lambda_k)/K} \\ &= \begin{cases} \delta[l-\lambda_k] & ,\ \text{if } \lambda_k = \text{integer} \\ \frac{\sin(\pi(l-\lambda_k))}{K\sin(\pi(l-\lambda_k)/K)}\, e^{j(K-1)\pi(l-\lambda_k)/K} & ,\ \text{otherwise.} \end{cases} \end{aligned} \tag{4.50}$$

The plots of $\{|g_k[l]| : l = 0,\ 1,\ \ldots,\ K-1\}$ for $0 < \lambda_k < 1$ and $4 < \lambda_k < 5$ are shown in Figs. 4.5 and 4.6, respectively. Firstly, the effect of different λ_k values on a sample-spaced tap will be discussed. Consider the range $(l' < \lambda_k < l'+1)$ with l' being an integer. As can be expected, the energy distribution to tap l' is larger if

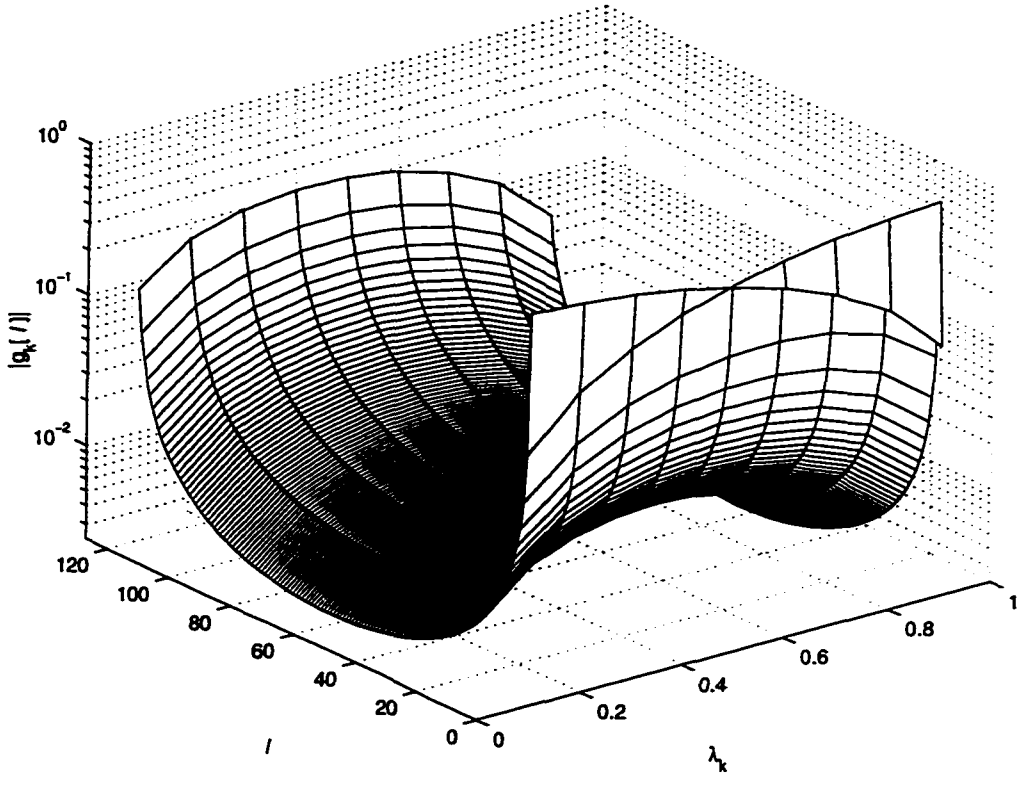

Figure 4.5. *The leakage of a unity gain channel path with non-sample-spaced path delay ($0 < \lambda_k < 1$). l is the index of sample-spaced channel taps, λ_k is the normalized delay of the k^{th} path.*

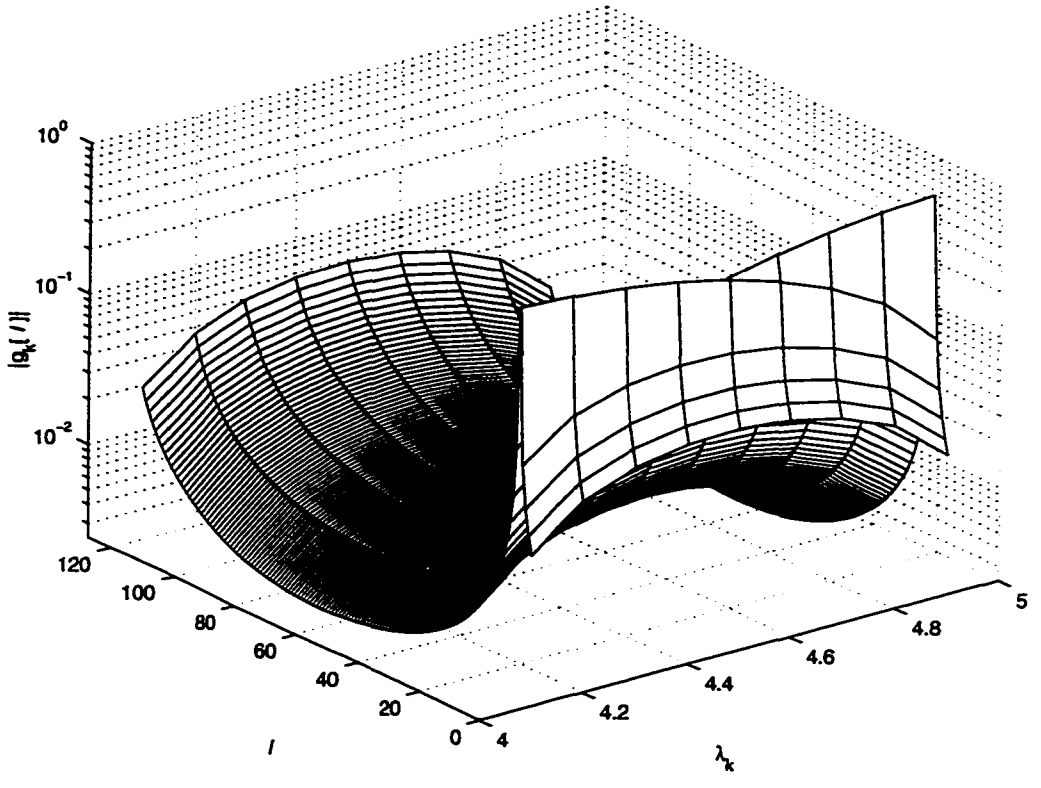

Figure 4.6. *The leakage of a unity gain channel path with non-sample-spaced path delay ($4 < \lambda_k < 5$). l is the index of sample-spaced channel taps, λ_k is the normalized delay of the k^{th} path.*

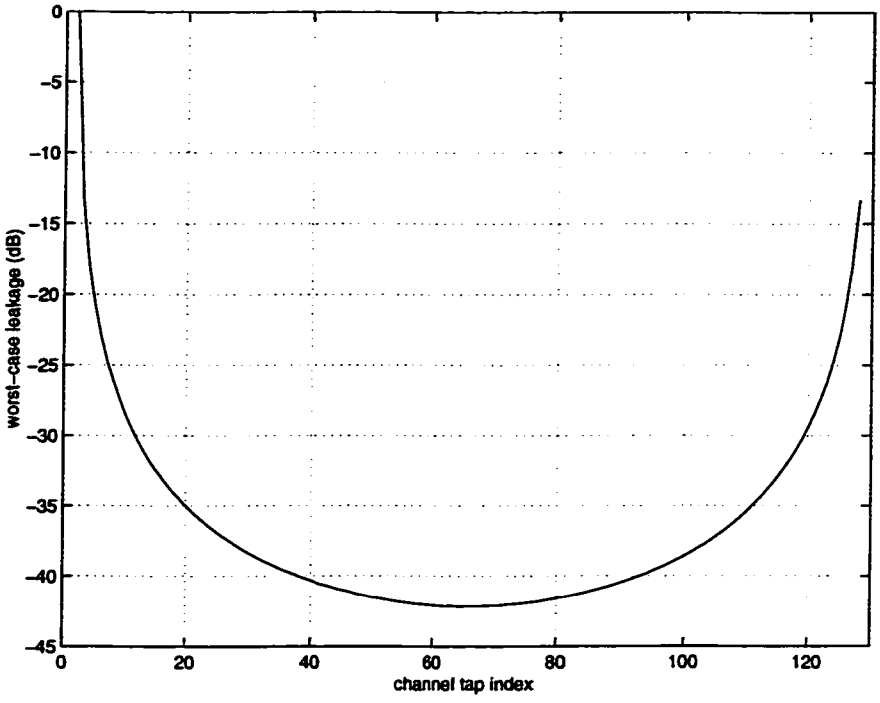

Figure 4.7. *The worst–case leakage of a unity gain channel path with non–sample–spaced path delay*

λ_k is closer to l'. The same holds for tap $l'+1$. To the other taps away from these two adjacent taps l' and $l'+1$, the largest energy distribution (energy leakage) occurs at $\lambda_k = l' + 0.5$. In other words, the energy leakage to not-nearby taps is maximum when $\lambda_k = l' + 0.5$.

Secondly, the energy distribution of a unity gain path with delay τ_k over the sample-spaced taps $\{l = 0,\ 1,\ \ldots,\ K-1\}$ is discussed. As can be expected, the larger energy is distributed to the nearer tap. However, since $g_k[l] = g_k[l-K]$, the path with λ_k near 0 will also cause leakage to the taps $(K-1,\ K-2,\ \ldots)$ where tap $K-1$ will get the largest leakage among them. Consequently, the channel estimation based on $[h[0],\ h[1],\ \ldots,\ h[K_0-1]]$ will lose some leakage energy especially from taps $(K-1,\ K-2,\ \ldots)$. From Figs. 4.5 and 4.6, it can be observed that if λ_k can be intentionally increased by some amount, the leakage to those taps $(K-1,\ K-2,\ \ldots)$ can be substantially reduced and the channel estimation can be improved. A simple way of establishing this is to use a pre-advancement of the timing point. A timing

pre-advancement of β samples will effectively increase λ_k to $(\tau_k K\ \Delta f + \beta)$. The value of β should not only be less than the ISI-free guard interval but also be small enough that most channel energy is contained in the $[h[0],\ h[1],\ \ldots,\ h[K_0 - 1]]$. If necessary, the value of K_0 may be increased in account for the timing pre-advancement. By using (6.35), a worst-case leakage may be found over $0 < \lambda_k < 1$. Fig. 4.7 shows this worst-case leakage for an OFDM system with $K = 128$ subcarriers. Based on this, β may be chosen for a designed SNR value. For example, the use of $\beta = 4$ will include all leakage down to approximately -23 dB of the total energy of the path with $0 < \lambda_k < 1$ in the channel estimation.

4.5 Simulation Results and Discussions

The OFDM system parameters used in the simulation are the same as [47]: 128 subchannels, 4 guard-subchannels on each end, $1/160\mu s$ subchannel spacing, and 40 μs guard interval. The channel models considered are two-ray and TU channel models with delay spread of $1.06\mu s$, two-ray and HT channel models with delay spread of $5.04\mu s$, and JTC channel model with delay spread of $34.8ns$. The classical Doppler spectrum with the maximum frequency of 40 Hz and 200 Hz are considered. The space-time codes used are of 16-state with 4-PSK and 16-QAM [60]. The signal constellations of 4-PSK and 16-QAM are given in Fig. 4.2. The trellis diagrams and the associated branch symbols of the space-time codes used are given in Figs. 4.3 and 4.4. The number of significant taps used is 7 for all channel estimation methods which use a fixed number of significant taps.

In the following, the performance degradation associated with the complexity reduction is investigated. For the channel estimation based on the training symbol, the method of [47] is also used in the reduced complexity method since a matrix inversion needs not be performed. The different methods are applied only for the channel estimation based on the decision directed reference symbols.

Figs. 4.8, 4.9, 4.10, 4.11, and 4.12 show the BER and MSE performance for 4-PSK, 16-state space-time code in different channel models with different delay spreads and Doppler frequencies. For the same delay spread, two-ray model shows a better performance due to the less channel energy leakage. The channels with larger delay

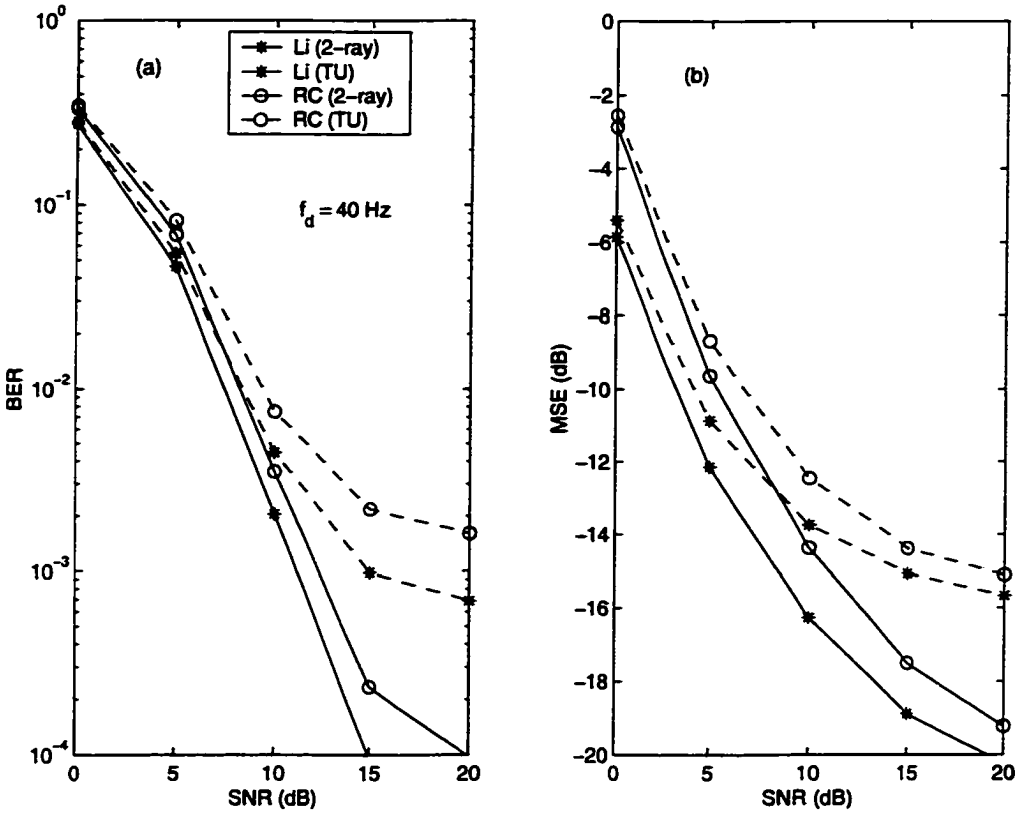

Figure 4.8. *Performance of the channel estimation methods in OFDM with 4-PSK, 16-state space-time code. The rms delay spread is* $1.06\mu s$*, the Doppler frequency is 40 Hz.*

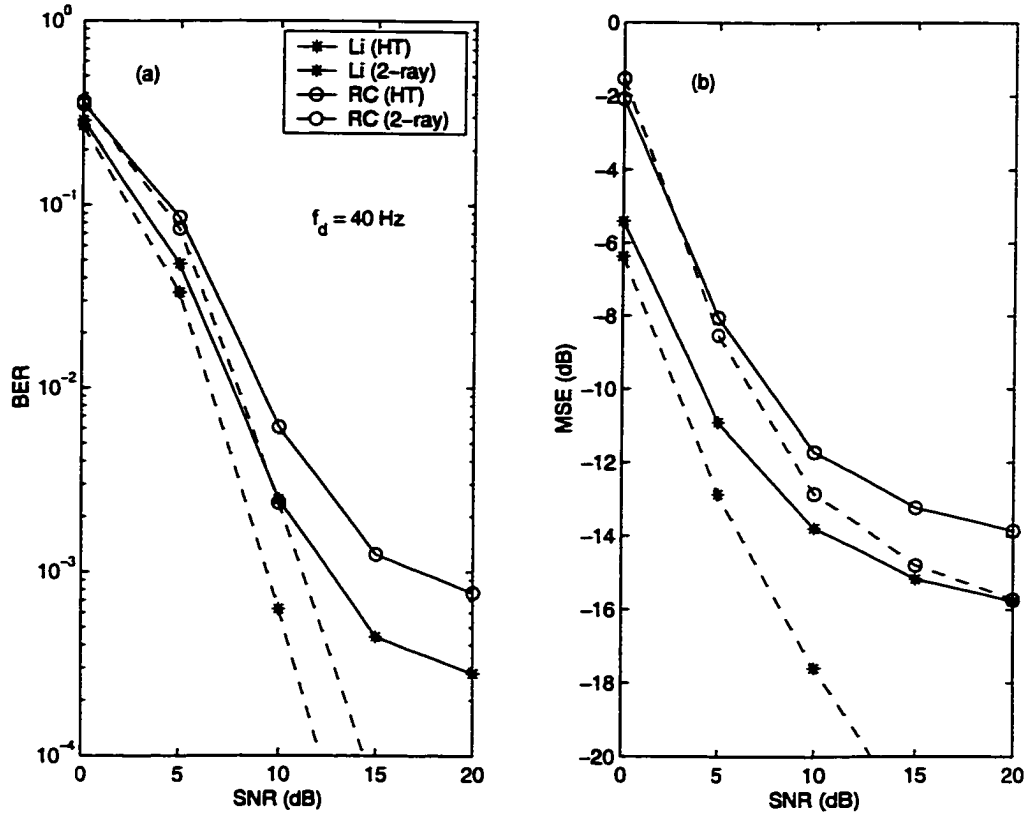

Figure 4.9. *Performance of the channel estimation methods in OFDM with 4-PSK, 16-state space-time code. The rms delay spread is* $5.04\mu s$*, the Doppler frequency is 40 Hz.*

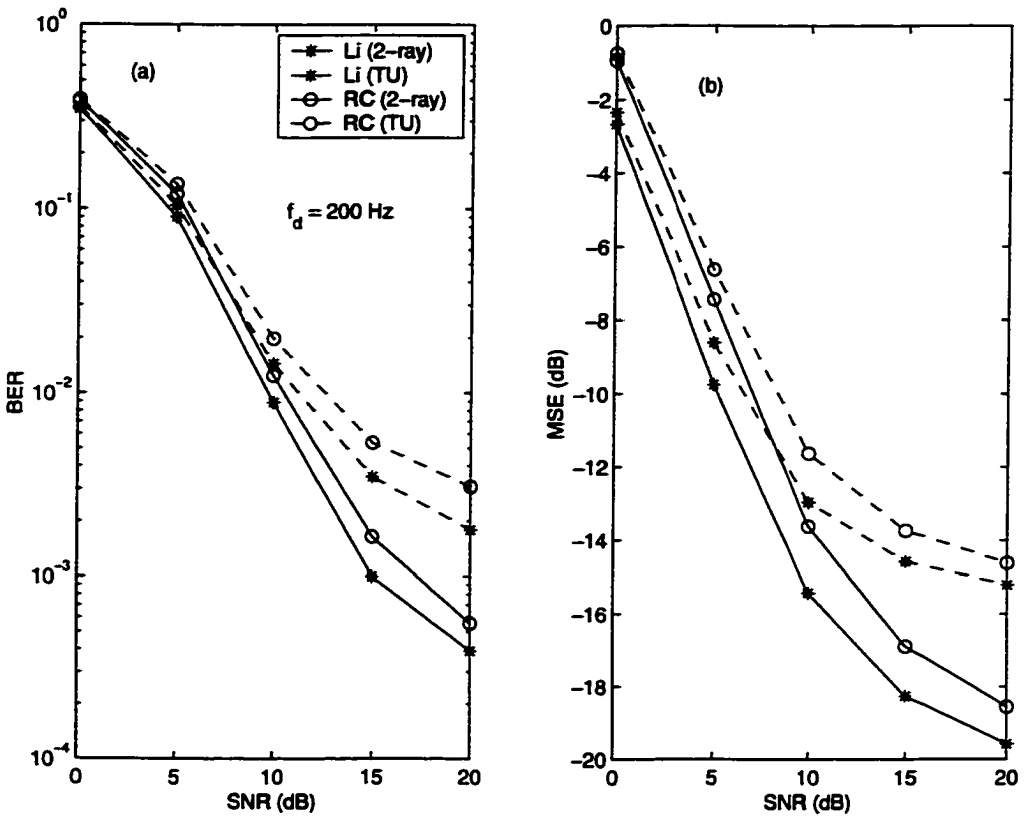

Figure 4.10. *Performance of the channel estimation methods in OFDM with 4-PSK, 16-state space-time code. The rms delay spread is* $1.06\mu s$*, the Doppler frequency is 200 Hz.*

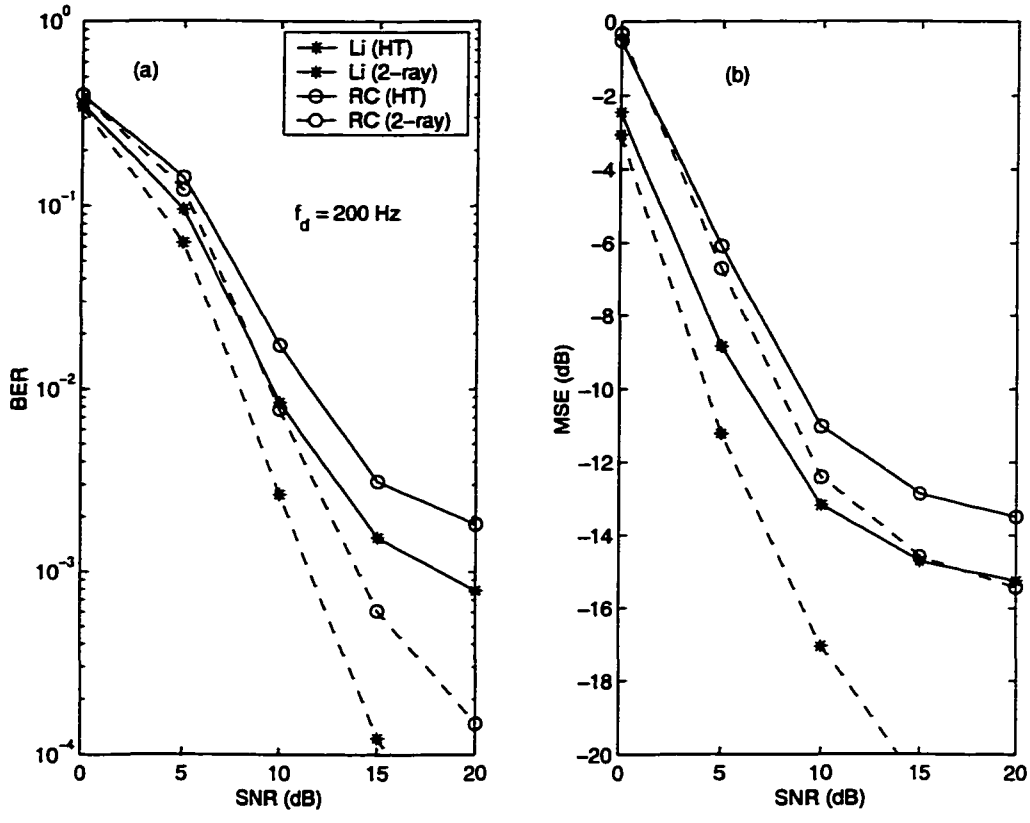

Figure 4.11. *Performance of the channel estimation methods in OFDM with 4-PSK, 16-state space-time code. The rms delay spread is* $5.04\mu s$*, the Doppler frequency is 200 Hz.*

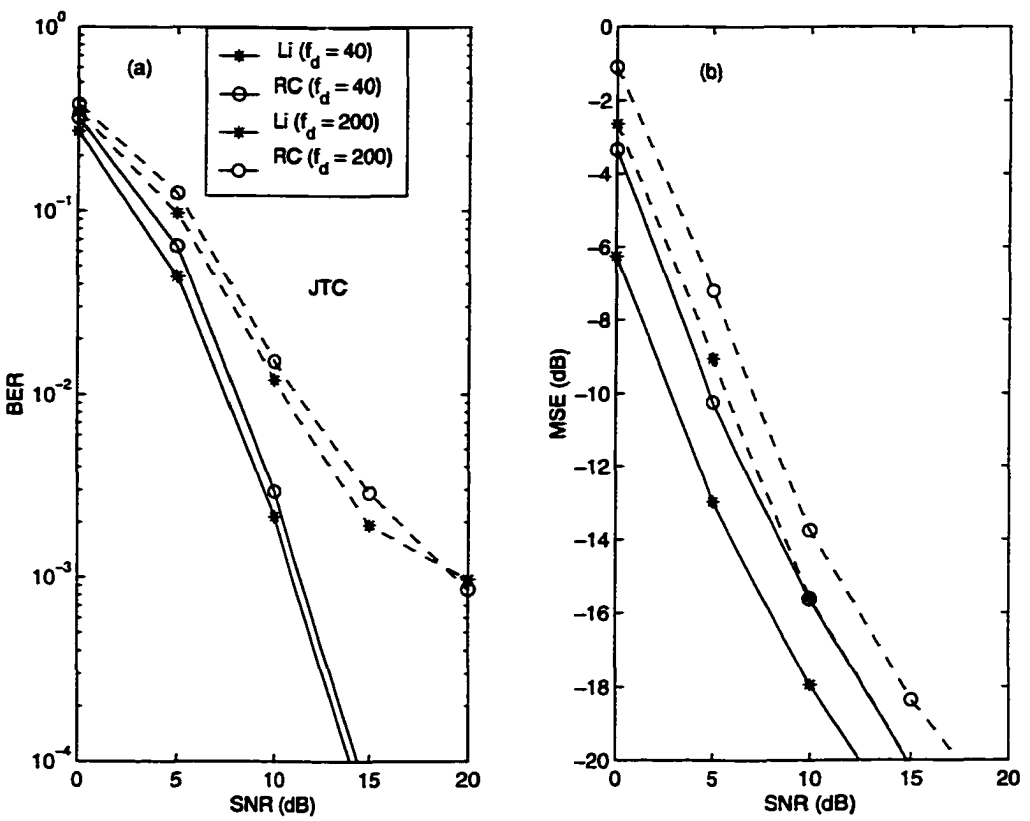

Figure 4.12. *Performance of the channel estimation methods in OFDM with 4-PSK, 16-state space-time code. The rms delay spread is* 34.8*ns.*

spread may not necessarily show a larger MSE. For example, the MSE of [47] for two-ray model with delay spread of $1.06\mu s$ is larger than that with delay spread of $5.04\mu s$. The reason can be ascribed to the much larger channel energy leakage of the former to the taps (K-1, K-2, ...) (see previous Section). By comparing the MSE in the JTC, TU and HT models, it is observed that at the same MSE level, RC method has more degradation in the channel with larger delay spread. This is due to the fact that the larger delay spread channel is more deviated from the assumption (4.7). For the same delay spread, RC method has more degradation in two-ray, especially if compared with HT model. The reason can be deduced from (4.48). Although the maximum delay spread of HT is larger than that of two-ray, the last path's power is larger in two-ray than HT. This causes a larger value of the first term in (4.48), hence, a larger MSE.

When comparing for different Doppler frequencies, (more or less) a larger MSE degradation for the higher Doppler frequency is observed at lower SNR values in all channel models. This may be ascribed to a larger reference symbol error caused by the larger time selectivity of the channel with a larger Doppler spread, in addition to the low SNR condition and ICI. However, on the contrary, a larger BER degradation is observed at higher SNR values. This indicates that the effect of the channel estimation errors on BER performance becomes more dominent at higher SNR values.

Another observation is that when comparing performance between JTC and other models, although JTC model has a larger MSE gap between [47] and RC than the other models at the same SNR value, it has a smaller BER gap between [47] and RC than the other models. This indicates that if the MSE is much smaller than the SNR value, (say, a difference of 6 dB or more), provided that the ICI is negiligible, then further reduction in MSE would not improve the BER performance very much.

From the above investigation, we can observe that the cost of RC method's complexity reduction is just a slight BER degradation for all SNR values in a channel with very small delay spread such as JTC model. For channels with larger delay spreads such as TU and HT, a small BER degradation is observed for low to moderate SNR values. Hence, if the complexity is affordable, [47] is a better solution. If the complexity is of concern, RC method can be an alternative.

In Fig. 4.13, the performances for 16-QAM, 16-state space-time coded OFDM

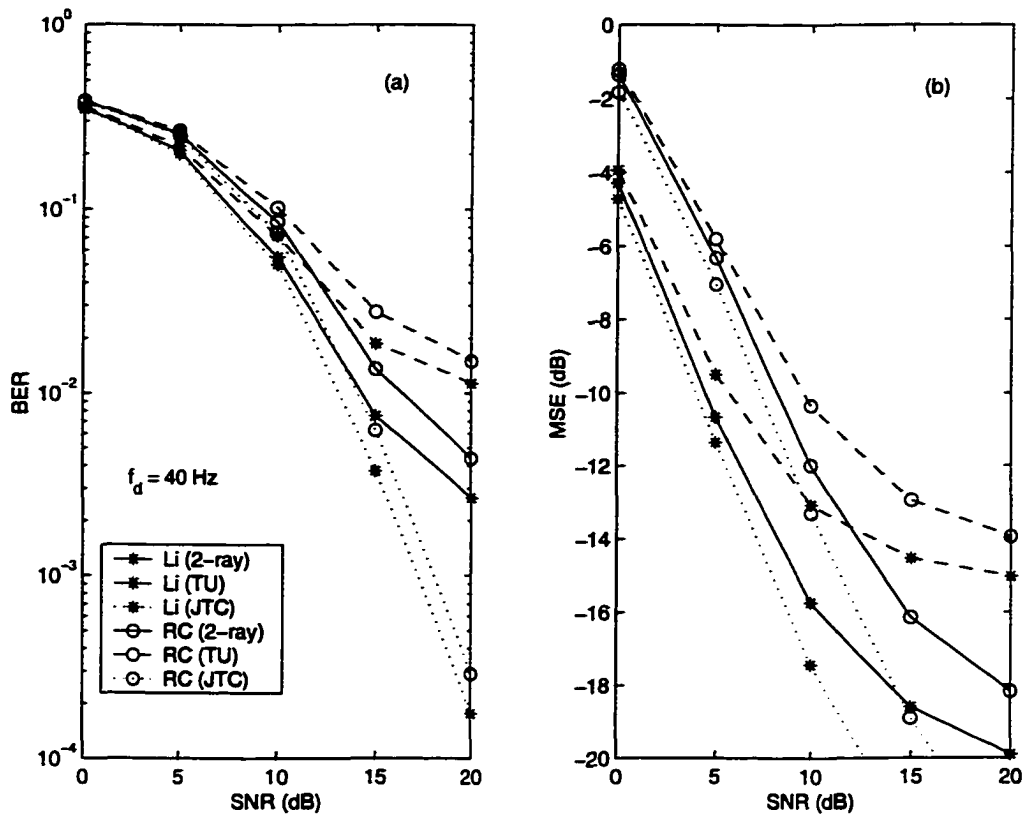

Figure 4.13. *Performance of the channel estimation methods in OFDM with 16-QAM, 16-state space-time code. The rms delay spread is* $1.06\mu s$ *for two-ray and TU,* $34.8ns$ *for JTC, the Doppler frequency is 40 Hz.*

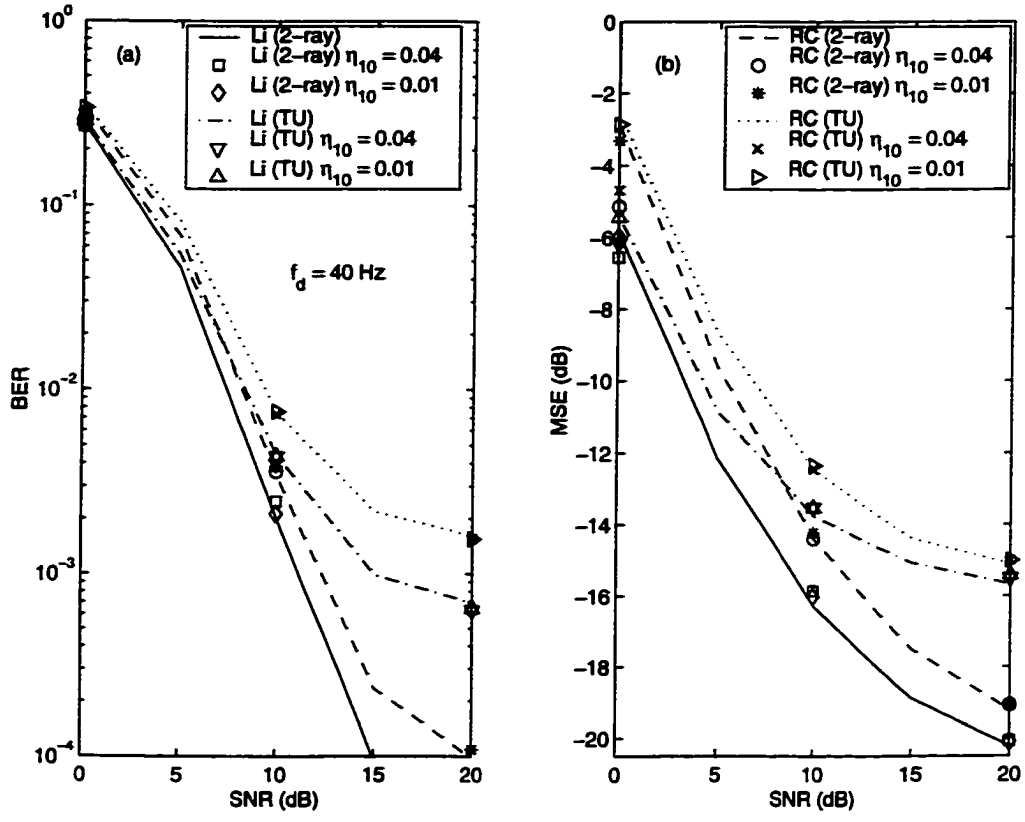

Figure 4.14. *Performance of the channel estimation methods with adaptive significant tap selection ($J_m = 7$, $\alpha = 4$) in two-ray and TU channels with delay spread of 1.06μs, and the Doppler frequency of 40 Hz for OFDM with 4-PSK, 16-state space-time code.*

system in two-ray, TU, and JTC channel models are presented. A higher MSE gap between [47] and RC is observed for 16-QAM than for 4-PSK case. The reason is that due to the non-constant modulus subcarrier symbols, the MMSE criterion in RC method loses its optimality in the maximum likelihood (ML) sense while [47] still holds the ML optimality. However, in terms of BER performance, only a small BER gap is observed. This indicates that RC method can be an alternative approach also for non-constant modulus subcarrier symbols when the complexity is an issue.

In Fig. 4.14, the performance of the adaptive selection of the number of significant taps is presented for two-ray and TU channel models with delay spread of 1.06μs, and the Doppler frequency of 40 Hz. The threshold values used at a SNR of 10 dB, denoted

by η_{10}, are 0.04 and 0.01. The other parameters are $J_m = 7$ and $\alpha = 4$. This adaptive approach has almost the same performance as the case with the knowledge of suitable fixed number of significant taps. For a low SNR value, the adaptive approach has a slight performance improvement. The reason is that the adaptive selection would quite often choose a smaller number of taps and hence, would suppress the effect of the dominant noise to a larger extent. The results also show that the threshold value around the range of 0.01 to 0.04 at a SNR of 10 dB works well. It is also noted that if J in the approach with fixed J value and J_m in the approach with adaptive J value are the same, the adaptive approach saves some complexity.

As discussed in the previous section, both [47] and RC methods can be modified by introducing some timing pre-advancement of β samples. The results of this modified approach with $\beta = 4$ as an example are presented in Fig. 4.15 for TU channel model with a Doppler frequency of 40 Hz. The results clearly show that for moderate to high SNR values, the modified approach achieves quite substantial improvement without any added complexity. This is a result of less unused leakage energy of the modified approach in the channel estimation.

4.6 Conclusions

In this chapter, we have investigated a reduced complexity channel estimation for an OFDM system with space-time coding in time-varying, dispersive multipath fading channels. In particular, the motivation was to reduce the complexity in the matrix inversion needed for every OFDM data symbols. The method is developed based on a channel with relatively small delay spread. By decoupling the channel responses from different transmit antennas, much complexity reduction is achieved. In particular, the sizes of the matrix inverse and the FFT's required in the channel estimation for every OFDM data symbol is reduced by half. The simulation results show that the price for the complexity reduction is just a slight BER degradation for channels with relatively small delay spreads. For cases where the complexity is of a major concern, the reduced complexity method can be considered as a good alternative. Adaptively finding the number of significant taps based on a threshold decision is also shown to have a comparable performance to the case where the suitable number of significant taps is

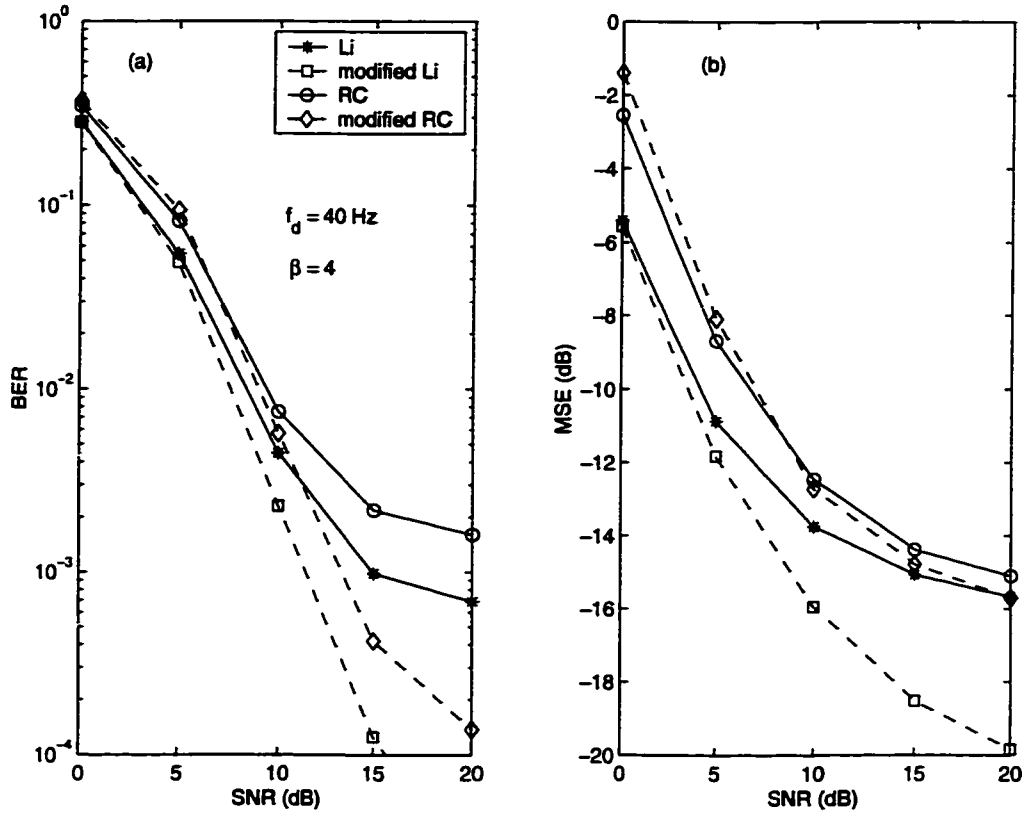

Figure 4.15. *Performance of the modified channel estimation methods in TU channel with the Doppler frequency of 40 Hz for OFDM with 4-PSK, 16-state space-time code.*

known. We have also investigated the effect of the channel path with non-sample-spaced delay on the channel estimation based on the sample-spaced channel taps. A simple modification by means of the timing pre-advancement is proposed in order to reduce the lost energy leakage of the paths with non-sample-spaced delays in the channel estimation. This modified approach brings about a substantial improvement without any added complexity.

Chapter 5

A Robust Timing and Frequency Synchronization for OFDM Systems

Due to the high sensitivity of OFDM system to the synchronization errors, synchronization in OFDM systems has achieved much research attention. Several approaches have been proposed for estimating the time and frequency offset either jointly [38]-[42] or individually. The interested reader is referred to [63]-[64] for further notes on frequency offset estimation and to [41]-[65] on timing estimation. In fact, there are numerous relevant contributions in the literature and a good discussion on them can be found in the recent paper of [66].

Most frequency and timing estimation methods exploit the periodic nature of the time-domain signal due to using the cyclic prefix [38] [41] [67] [42] or by designing the training symbol having repeated parts [63] [44] [64]. Regarding frequency estimation, in [44] a training symbol containing two identical halves is used and the frequency acquisition range is ± 1 subcarrier spacing. In order to increase the frequency capture range, a second training symbol is employed. A frequency estimation scheme improving the solution of [44] is proposed in [64], where only one training symbol having L identical parts is required and the frequency acquisition range is $\pm L/2$ subcarrier spacing.

Recently in [44] a robust timing synchronization scheme using a training symbol having two identical parts has been proposed. However, the timing metric plateau inherent in [44] results in a large timing offset estimation variance. This timing metric plateau can be eliminated and hence the timing offset estimation variance can be

reduced by designing the training symbol such that it gives a more pronounced timing metric trajectory [68]. For single carrier systems, in [69] the frame synchronization performance has been considerably improved by designing the training preambles to give a sharper peak timing metric trajectory.

All the above OFDM synchronization methods are associated with one or more of the following limitations or drawbacks: have a limited range of operation, address only one task, have a large estimation variance, lack robust sync detection capability, require extra overheads. To overcome these limitations, in this Chapter we investigate both timing and frequency synchronization for OFDM, particularly using only one training symbol (or one training block). The training symbol is designed to have a sharp timing metric trajectory. In choosing the timing metric, a robust sync detection capability has to be taken into consideration. We design the training symbol to be composed of repeated identical parts with possible sign inversions. Our choice of this type of training symbol is based on the following reasons. The periodicity or repetitive nature of the training symbol equips timing synchronization with robustness against frequency offsets. Having multiple identical parts gives the benefit of using the same training symbol for frequency synchronization, which can handle large frequency offset. By designing the signs of the identical parts to give the sharpest possible timing metric trajectory, the timing offset estimation can be improved. Both OFDM type training symbols, namely frequency domain (FD) training, and single carrier type training blocks, namely time domain (TD) training are investigated.

We present a synchronization scheme, which provides both timing and frequency estimation as well as channel estimates. A specifically designed training symbol is used for both timing and frequency synchronization. Channel estimation based on the designed training symbol is also incorporated in order to give fine timing and frequency offset estimates. The fine synchronization can be iteratively improved. The impact of using only one training symbol for both timing and frequency synchronization is discussed and a number of approaches are proposed for further performance improvement. The sync detection performance, timing synchronization performance, frequency synchronization performance and BER performance of the proposed method is evaluated by computer simulations.

Regarding our timing estimation performance measure in the context of OFDM,

the additional interference power caused by timing estimation might be considered, rather than the timing offset estimation variance, since the former reflects the actual impact of timing synchronization error on the system's performance. However, the interference power may also depend on the mean of the timing estimate. Hence, in this Chapter we introduce a more revealing performance measure for the timing characterization of OFDM systems.

This chapter is organized as follows. Section 5.1 describes the system considered. Section 5.2 briefly presents OFDM synchronization problem and the effects of the synchronization errors. In Section 5.3, the proposed synchronization scheme is presented. Performance evaluation, simulation results, and discussions are provided in Section 5.4. Finally, conclusions are provided in Section 5.5.

5.1 System Description

The samples of the transmitted baseband OFDM signal, assuming ideal Nyquist pulse shaping, can be expressed as:

$$s(k) = \frac{1}{\sqrt{N}} \sum_{n=0}^{N_u-1} c_n exp(j2\pi kn/N), \quad -N_g \leq k \leq N-1, \tag{5.1}$$

where c_n is the modulated data or sub-carrier symbol, N is the number of Inverse Fast Fourier Transform (IFFT) points, $N_u(\leq N)$ is the number of subcarriers, N_g is the number of guard samples, and $j = \sqrt{-1}$. Consider a frequency selective multipath fading channel with path gains $\{h_l : l = 0, 1, \ldots, K-1\}$ (including possible paths with a zero gain) and the corresponding path delays $\{\tau_l\}$. We assume that the path delays are sample-spaced (namely $\tau_l = l$). Hence, $\{h_l\}$ represents the discrete-time channel impulse response.

At the receiver there exist carrier frequency offset, sampling clock errors and symbol timing offset, which have to be estimated and compensated. Usually the frequency offset and timing errors are more dominant, than the sampling clock inaccuracy and we will consider the carrier frequency and symbol timing synchronization, assuming a perfect sampling clock. In this case, the received samples become

$$r(k) = exp(j\phi)exp(j2\pi kv/N) \sum_{l=0}^{K-1} h_l s(k-\tau_l) + n(k), \tag{5.2}$$

where $n(k)$ is the sample of zero mean complex Gaussian noise process with variance σ_n^2, v is the carrier frequency offset normalized by the subcarrier spacing and ϕ is an arbitrary carrier phase factor. The timing point of the start of the FFT window is determined by the timing synchronization scheme to be at the sample $r(\varepsilon)$ where ε is a timing offset in units of OFDM samples. We consider only integer timing offsets. If non-integer timing offsets and/or sampling clock errors need to be considered for a particular system, the method of [65] may be applied.

5.2 Synchronization

In OFDM systems, the main synchronization parameters to be estimated are a sync flag indicating the presence of the signal (especially for burst mode transmission), the starting time of the FFT window (timing synchronization), the frequency offset due to the inaccuracies of the transmitter and receiver oscillators and the Doppler shift of the mobile channel, as well as the channel estimates if coherent reception is adopted. The sync flag can be generated by automatic gain control (e.g., ramp-up indication via power measurement and threshold decision) or using a training symbol (which can also be used for timing synchronization and possibly frequency synchronization). For the latter case, the same metric used for timing synchronization may be used together with the threshold decision, in order to generate the sync flag. After detecting the presence of the signal, the other sync parameters are estimated. In the following, the effect of timing synchronization errors is briefly described for the later use.

5.2.1 Effect of Timing Offset and Carrier Frequency Offset

Let the sample indexes of a perfectly synchronized OFDM symbol be $\{-N_g, \ldots, -1, 0, 1, \ldots, N-1\}$, the timing offset be ε and the maximum channel delay spread be τ_{max}. Then, if $\varepsilon \in \{-N_g + \tau_{max}, -N_g + \tau_{max} + 1, \ldots, 0\}$, the orthogonality among the subcarriers will not be destroyed and the timing offset will only introduce a phase rotation in every subcarrier symbol, Y_m, at the FFT output as

$$Y_m = exp(j2\pi m\varepsilon/N)c_m H_m + n_m, \quad -N_g + \tau_{max} \leq \varepsilon < 0 \tag{5.3}$$

where m is the subcarrier index, H_m is the channel's frequency response for the m^{th} subchannel, i.e., $\{H_m\} = DFT_N(h_l)$, and n_m is a complex Gaussian noise term. For a coherent system, this phase rotation is compensated by the channel equalization scheme, which views it as a channel-induced phase shift. If the timing estimate is outside the above range, the orthogonality among the subcarriers will be destroyed by the resulting ISI and additional inter-subchannel interference (ICI) will be introduced as [70]:

$$Y_m = exp(j2\pi m\varepsilon/N)\ \alpha(\varepsilon)c_m H_m + I_m + n_m \tag{5.4}$$

where

$$\alpha(\varepsilon) \simeq \sum_l |h_l(t)|^2\ \frac{N - \Delta\varepsilon_l}{N} \tag{5.5}$$

and I_m constitutes both ISI and ICI terms. These terms can be modeled as Gaussian noise having a power of, (for unit signal power on each subcarrier),

$$\sigma_\varepsilon^2 = \sum_l |h_l(t)|^2 \left(2\frac{\Delta\varepsilon_l}{N} - (\frac{\Delta\varepsilon_l}{N})^2\right) \tag{5.6}$$

where for $\varepsilon > 0$

$$\Delta\varepsilon_l = \begin{cases} \varepsilon - \tau_l, & \varepsilon > \tau_l \\ \tau_l - N_g - \varepsilon, & 0 < \varepsilon < -(N_g - \tau_l) \\ 0, & \text{else.} \end{cases} \tag{5.7}$$

Similarly, for $\varepsilon < -N_g + \tau_{max}$, we can have

$$\Delta\varepsilon_l = \begin{cases} -N_g + \tau_l - \varepsilon, & \varepsilon < -N_g + \tau_l \\ 0, & \text{else.} \end{cases} \tag{5.8}$$

Hence, the guard interval should be long enough for the timing estimate to lie within the above range. In a loose sense, the smaller the variance of the timing estimator, the shorter the guard interval the system can have for the same performance, and hence the lower the overhead.

The effect of carrier frequency offset on the i^{th} OFDM symbol leads to a phase and amplitude distortion of the subcarrier symbols and results in additional ICI, which

can be described by [70]

$$Y_{i,m} = exp\left(j\pi v\frac{N-1}{N}\right) exp\left(j2\pi v\frac{i(N+N_g)+N_g}{N}\right) \frac{sin(\pi v)}{sin(\pi v/N)} c_{i,m} H_{i,m} + n_{i,m} + I_{i,m}(v) \quad (5.9)$$

where $I_{i,m}(v)$ is an additional ICI term. The phase distortion introduced by the frequency offset would not be completely compensated by channel equalization since it also depends on time. The amplitude distortion may cause total loss of subcarrier symbol at its location in FFT output at the frequency offsets of multiples of subcarrier spacing. Actually it causes shifting of the subcarrier symbols and can be detected if sufficiently large guard bands are used. Even with large guard bands, the amplitude distortion and additional ICI term introduced by fractional part of frequency offset cannot be neglected.

5.3 Proposed Synchronization Method

The scheme proposed for symbol timing and frequency synchronization of OFDM systems is shown in Fig. 5.1. A specifically designed training symbol is used. The sync flag is determined by the timing metric and an associated threshold decision. In the following, we assume that the presence of the signal has already been detected and hence the rest of the synchronization part will be presented. First, coarse timing estimation is performed based on the timing metric. It gives the estimate of the start position of the FFT window for the training symbol. The frequency offset is estimated based on the training symbol defined by the coarse timing estimation. Frequency offset compensation is then performed on the training symbol. Next, the channel impulse response is estimated based on the frequency offset compensated received training symbol. Given the channel estimation, the delay of the first channel path is found and added to the coarse timing estimate to give a fine timing estimate. The new training symbol defined by the fine timing estimate is used to estimate the fine frequency offset. Hence, the fine synchronization part contains frequency offset compensation, channel impulse response estimation, fine timing offset estimation, and fine frequency offset estimation. This fine synchronization procedure can be repeated in order to achieve further improvements. The channel impulse response

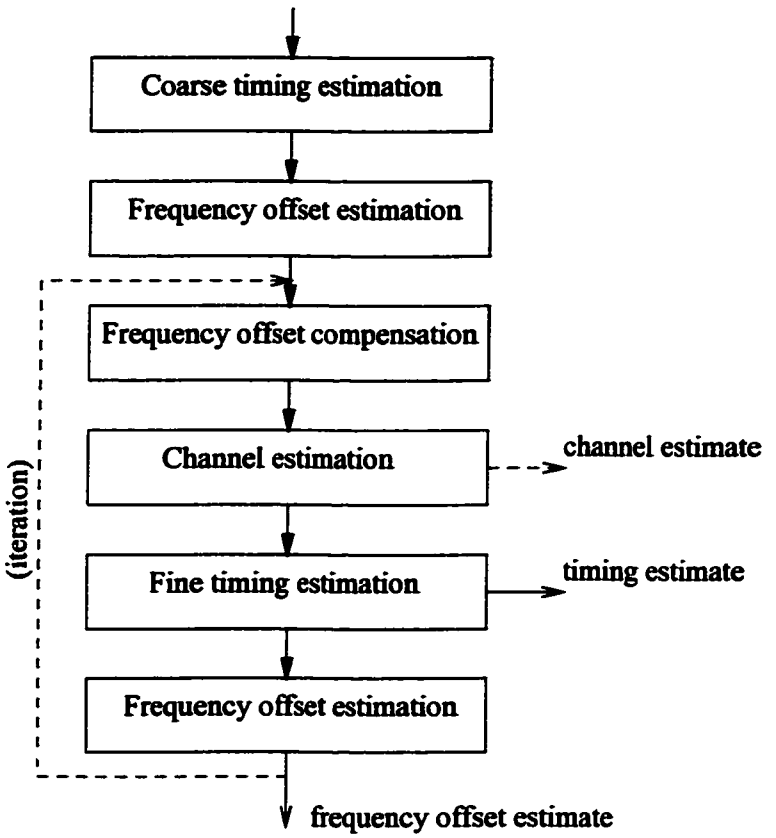

Figure 5.1. *Proposed synchronization scheme*

can then be estimated again after performing frequency offset compensation on the training symbol defined by the fine timing estimate. It may be directly used or further processed for employment in channel equalization, but further processing on the channel response estimate will not be considered in this Chapter.

The proposed synchronization method is applicable to both continuous mode transmission and burst mode transmission since it does not utilize any property specific to a particular transmission mode such as null interval in the burst mode transmission. In our simulations, we use a burst mode transmission where the training symbol is preceeded by noise samples and followed by data symbols.

5.3.1 Proposed Timing Metric

A desirable property of a timing estimation scheme is its robustness to the frequency offset. If the training symbol has a repetitive structure, a timing estimation scheme which is robust to the frequency offset can be obtained by means of correlation among the repetitive parts. Hence, we consider a repetitive training structure in this Chapter. Suppose that the training symbol is composed of two identical parts of M samples each. Then, this type of training symbol with two repeated parts can be efficiently searched by minimizing the metric which calculates the squared averaged distance between the two considered received signal parts of length M samples each as [71]-[72]:

$$\mathcal{V}(d) = \frac{E(d)}{M} - \frac{2}{M} \cdot |P(d)| \tag{5.10}$$

where

$$E(d) = \sum_{i=0}^{M-1} \left(|r(i+d+M)|^2 + |r(i+d)|^2 \right) \tag{5.11}$$

$$P(d) = \sum_{i=0}^{M-1} r(i+d+M) \cdot r^*(i+d). \tag{5.12}$$

It can be easily observed that the above metric is robust to any frequency offset. This minimum mean square error (MMSE) type metric of (5.10) shows almost the same timing estimation performance as the maximum likelihood estimate (For detailed timing performance comparison, one is referred to [73]). However, the above metric and those in [73], except the Schmidl & Cox (S&C) metric of [44], do not consider sync detection and are associated with a high false detection probability. This fact can be observed from (5.10) as follows. Under noiseless condition, $\mathcal{V}(d)$ will give a minimum metric value of zero when d is at the correct timing point and approximately a maximum metric value of $\frac{E(d)}{M}$ when d is such that $\{r(d+i) : i = 0, 1, \ldots, N-1\}$ do not correspond to the training symbol. When only noise is present, $\mathcal{V}(d)$ would give some value close to zero since the corresponding $\frac{E(d)}{M}$ would be very small, hence causing a false detection. Similar result will be obtained when the transmitted data symbols are in deep fade. This high false detection probability can be reduced using

the normalized metric:

$$\mathcal{V}_n(d) = \frac{E(d) - 2|P(d)|}{E(d)}. \tag{5.13}$$

Finding the minimum of $\mathcal{V}_n(d)$ is equivalent to finding the maximum of

$$\Lambda_n(d) = \frac{2}{E(d)} \cdot |P(d)|. \tag{5.14}$$

Now, under noiseless condition $\Lambda_n(d)$ will give a maximum value of 1 when d is at the correct timing point and approximately a minimum value of zero when d is such that $\{r(d+i) : i = 0, 1, \ldots, N-1\}$ do not correspond to the training symbol. When only noise is present, $|P(d)|$ would be approximately equal to zero and would be much less than $E(d)$, hence, $\Lambda_n(d)$ would give a value close to zero and a false detection would be avoided. Similar result will hold when the transmitted data symbols are in deep fade.

In practice, $\Lambda_n^2(d)$ instead of $\Lambda_n(d)$ can be considered. The timing metric of (5.14) which was introduced in the context of two identical parts can be further generalized for a training symbol containing L rather than two parts of M samples each. In this case, the timing metric to be maximized can be expressed as:

$$\Lambda_\varepsilon(d) = \left(\frac{L}{L-1}\frac{|P(d)|}{E(d)}\right)^2, \tag{5.15}$$

where

$$P(d) = \sum_{k=0}^{L-2} b(k) \cdot \sum_{m=0}^{M-1} r^*(d + kM + m)\, r(d + (k+1)M + m) \tag{5.16}$$

$$E(d) = \sum_{i=0}^{M-1} \sum_{k=0}^{L-1} |r(d + i + kM)|^2 \tag{5.17}$$

and $b(k) = p(k)\,p(k+1), k = 0, 1, \ldots, L-2$.

In the above equation, $\{p(k) : k = 0, 1, \ldots, L-1\}$ denote the signs of the repeated parts of the training symbol and will be called the training symbol pattern in the rest of this contribution. For $L = 2$ and for the training symbol pattern $p = [++]$, the timing metric of S&C is obtained if $E(d)$ is approximated by 2 $R(d)$ where $R(d) = \sum_{i=0}^{M-1} |r(i+d+M)|^2$. Hence, the S&C timing metric can be considered as an approximation of the proposed metric for the case of $L = 2$ and $p = [++]$.

5.3.2 Training Symbol

The training symbol can be designed either for an OFDM type frequency domain training (FD) or single carrier type time domain training (TD) [74]. The training symbol of S&C is of the FD type and gives a timing metric plateau which results in a high timing estimator variance. This can be avoided by designing the training symbol to have a steep roll-off timing metric trajectory. For example, the HiperLAN/2 type training symbol was designed for providing a steep roll-off timing metric trajectory [33]. On the other hand, it does not preserve the cyclic prefix structure of an OFDM system. In this Chapter, we will consider a training symbol that preserves the cyclic prefix structure. We design the training symbol such that it is composed of L identical parts to handle a frequency offset up to $\pm L/2$ subcarrier spacing and has a specific pattern (signs) of the L identical parts to give a timing metric having a steep roll-off trajectory. In our context, S&C uses a FD type training with $L = 2$ and the pattern of [++], while Morelli & Mengali (M&M) [64] uses a FD type training with ($L > 2$) and the pattern of all + signs.

In order to avoid nonlinear distortion at the transmitter, the training symbol should be designed to have a low peak-to-average power ratio (PAPR). Golay complementary sequences [75] are well known for having specific correlation properties which translate into a low PAPR value (3 dB) when they are mapped to the OFDM subcarriers [76]. Hence, a Golay complementary sequence is applied in our FD training symbol as follows. The repeated part has $M = N/L$ samples (for N point IFFT and L identical parts) and it is generated by the $M-$point IFFT of a length N_u/L Golay complementary sequence. By contrast, for TD training, a length M Golay complementary sequence is directly used in the time domain as the basic repeated part. In this case, it represents a constant amplitude training sequence. However, the cyclic prefix extention based structure is still maintained in the context of TD training.

As an example, let $N = N_u = 64$, $L = 4$, the bipolar representation of Golay complementary sequence of length 16 be $\boldsymbol{C}$ and the time-domain repeated part of length 16 be $\boldsymbol{A}$. Then, for TD training $\boldsymbol{A} = \boldsymbol{C}$ and for FD training $\boldsymbol{A} = FFT_{16}(\boldsymbol{C})$. In Fig. 5.2, the corresponding time-domain samples of the training symbol (excluding cyclic prefix) with the pattern [− + −−], which can be given by [$-\boldsymbol{A}\ \boldsymbol{A}\ -\boldsymbol{A}\ -\boldsymbol{A}$]

are presented. The repeated part boundaries are indicated by dash-lines.

5.3.2.1 Training Symbol Pattern

Suppose that the training symbol (excluding cyclic prefix) is composed of L identical parts as $[\pm\mathbf{A}, \pm\mathbf{A}, \ldots, \pm\mathbf{A}]$ where $\mathbf{A}$ represents the repeated part. If the timing metric given in (5.15)-(5.16) is used, then the best patterns (signs of the repeated parts) of the training symbol obtained by computer search are given in Table 5.1 for 10% cyclic prefix and $L = 4$, 8 and 16. These patterns were obtained by finding the patterns which give a minimum value of $\sum_{d=-N}^{N} |P(d)|^2$. In the computer search, $\{r(k) : -N_g \geq k \leq N-1\}$ correspond to the training symbol and the other $\{r(k)\}$ are simply set to zero. In Fig. 5.3, the plots of $|P(d)|^2$ for all possible patterns with $L = 4$ are shown. The patterns can be expressed as the bipolar form of the binary representation of the pattern sequence numbers shown on the subplots. From Fig. 5.3, it can be observed that the best pattern sequence numbers are 2, 7, 8 and 13. In Fig. 5.4, the corresponding values of $\sum_{d=-N}^{N} |P(d)|^2$ are shown for all pattern sequence numbers. The pattern sequence numbers 2, 7, 8 and 13 have the minimum value. It can be observed that the minimum values generally correspond to the best steepest roll-off correlation metric trajectories. Each L value has four patterns. The last two are the sign-inversion based variants of the first two.

The trajectories of the timing metrics used in coarse timing estimation for the training symbol patterns (the first one for each L value) given in Table 5.1 are shown in Fig. 5.5 under noiseless and no channel distortion condition. The timing metric trajectory of S&C is also included for comparison. Unlike S&C, there are no timing metric trajectory plateaus associated with the proposed method. A larger value of L gives a timing metric trajectory with a steeper roll-off.

5.3.3 Coarse Timing Estimation

Coarse timing estimation is based on the correlation among the L parts of size M samples each. The coarse timing estimator takes as the start of OFDM symbol (after cyclic prefix) the maximum point, d_{max}, of the timing metric given by (5.15)-(5.17) where d is a time index corresponding to the first sample in a window of N samples. In order to maintain orthogonality among subcarriers, the timing estimate should

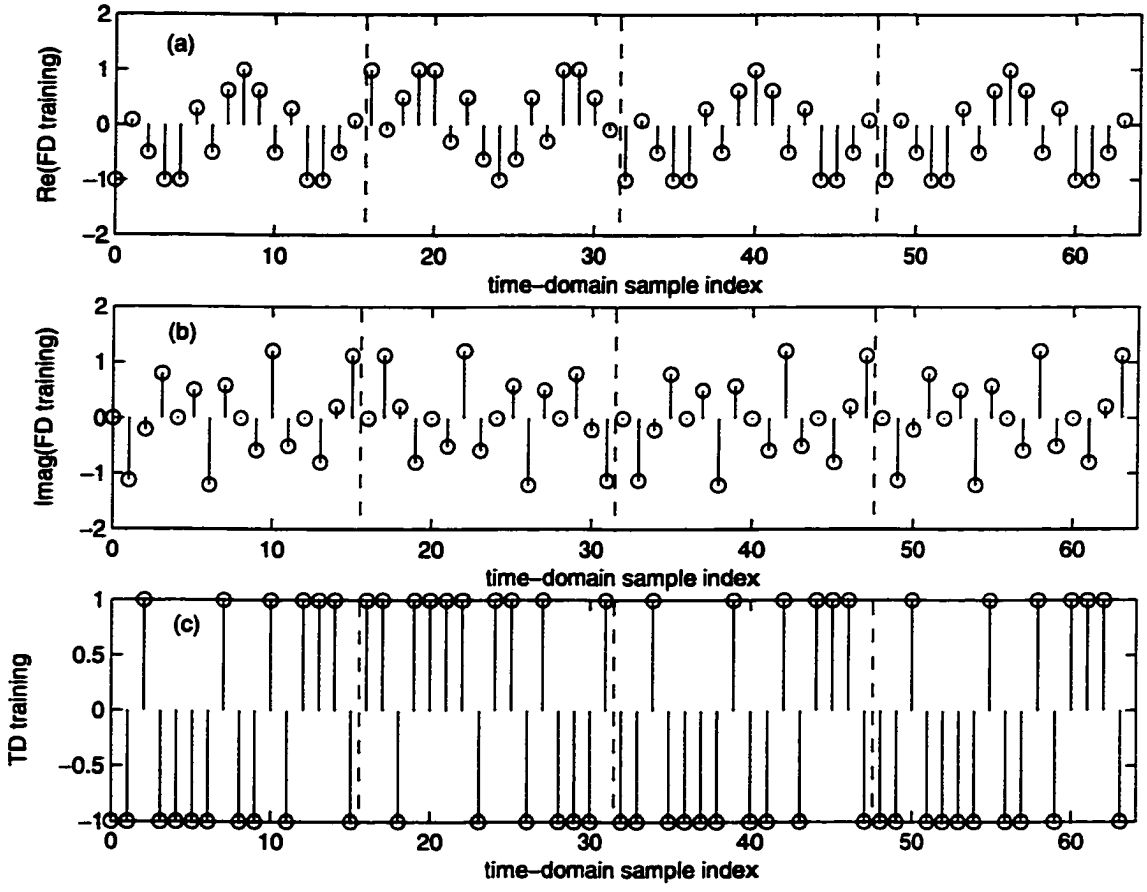

Figure 5.2. *An example of the time-domain samples of the 64-sample length training symbol defined by* $[-\boldsymbol{A}\ \boldsymbol{A}\ -\boldsymbol{A}\ -\boldsymbol{A}]$ *(The corresponding training symbol pattern is* $[-+--]$*. The cyclic prefix part is not shown.) : (a) Real part for FD training, (b) Imaginary part for FD training, (c) TD training*

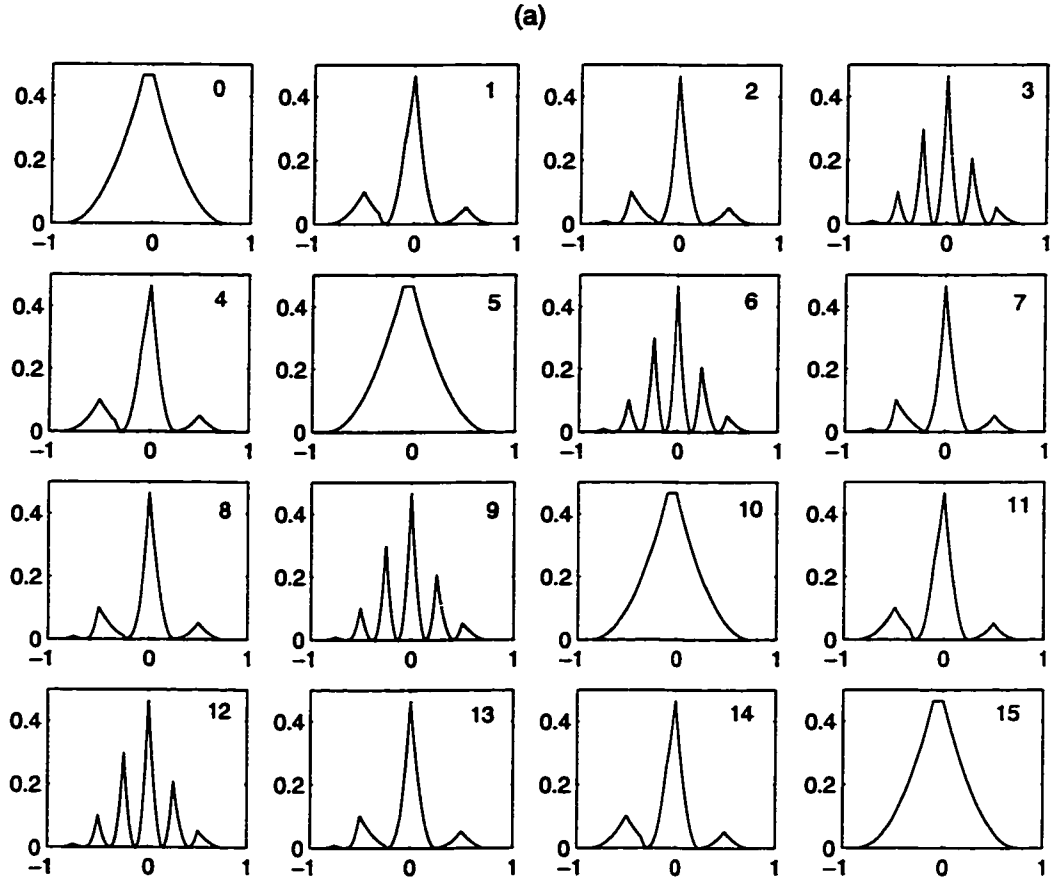

Figure 5.3. *Plot of* $|P(d)|^2$ *vs.* d/N *corresponding to all possible patterns for* $L = 4$. *The patterns can be expressed as the bipolar representation of the sequence number shown on the subplots.*

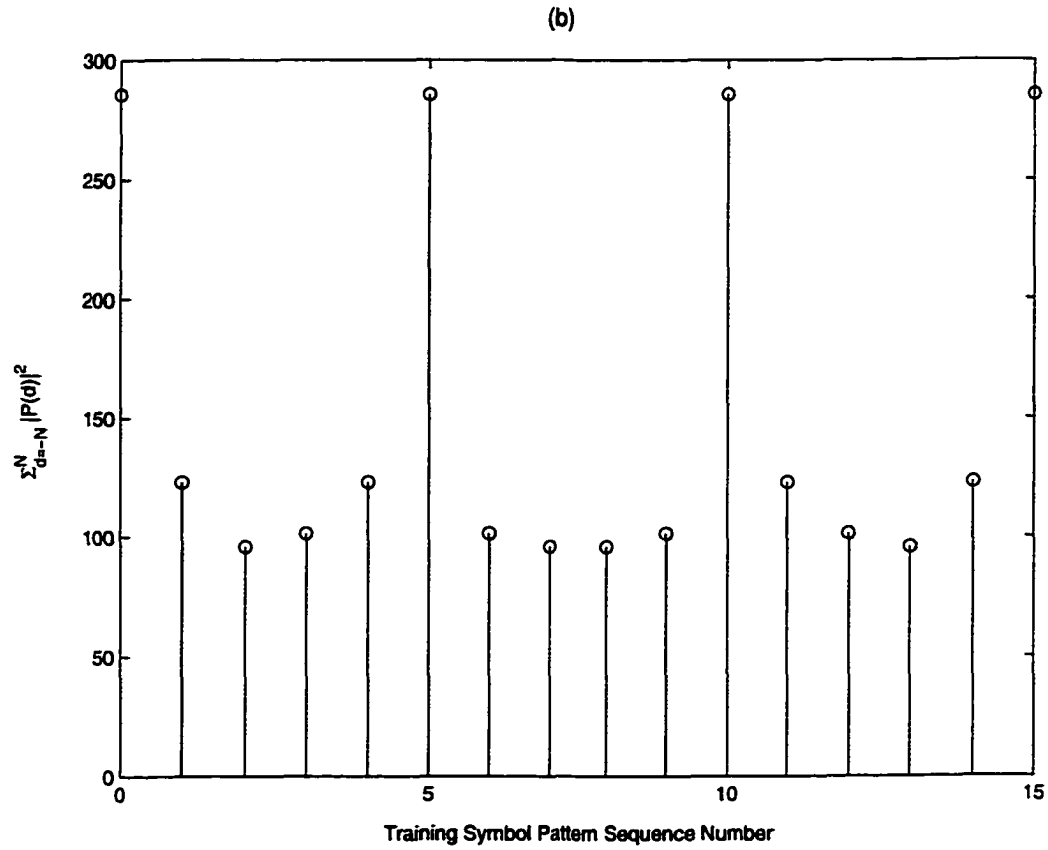

Figure 5.4. *The plot of* $\sum_{d=-N}^{N} |P(d)|^2$ *vs. all patterns denoted by the sequence numbers for* $L = 4$.

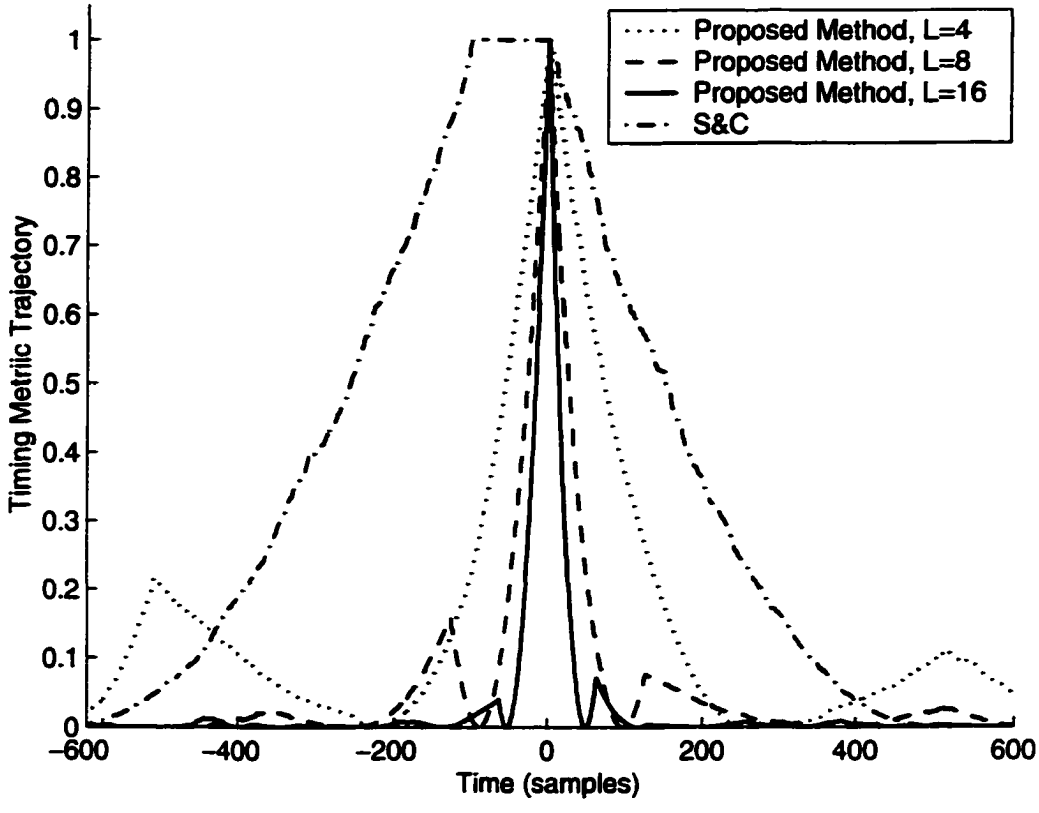

Figure 5.5. *Timing metric trajectory under noiseless and no channel distortion conditions. (Time index 0 corresponds to the exact timing point.)*

Table 5.1. *Training Symbol Pattern*

L	*Pattern*
4	$(-+--)$
	$(+++-)$
	$(+-++)$
	$(---+)$
8	$(++--+--)$
	$(-++---+-)$
	$(--++-++)$
	$(+--+++-+)$
16	$(+--+++--+-+++-+--)$
	$(--++-++----+++-)$
	$(-++---++-+--+-++)$
	$(++--+--++++----+)$

be in the ISI-free part of the cyclic prefix (i.e., the sample indexes $-N_g + \tau_{max}$, $-N_g + \tau_{max} + 1, \ldots, 0$). In an AWGN channel, the mean of the proposed timing metric trajectory peak is at the exact timing point, but in multipath channels it would be shifted (delayed) due to the channel dispersion. Hence, the coarse timing estimate, $\hat{\varepsilon}_c$, should be pre-advanced by some samples λ_c as

$$\hat{\varepsilon}_c = d_{max} - \lambda_c \tag{5.18}$$

where λ_c should be chosen to be higher than the (designed) mean shift of the timing point caused by the channel dispersion.

5.3.4 Coarse Carrier Frequency Offset Estimation

For coarse carrier frequency estimation, we follow the method of M&M [64] with appropriate modifications. Since the only difference in the training symbol structure is the sign pattern of L identical parts, the training symbol defined by the timing estimator is first modified to have the same structure as that proposed in M&M by multiplying the L parts with the sign pattern applied in the training symbol design. Then, the method of M&M is applied as follows. Let the modified training symbol defined by the coarse timing estimate be represented by $\{y(k) : k = 0, 1, \ldots, N-1\}$. Then the coarse frequency offset estimator is given by

$$\hat{v} = \frac{L}{2\pi} \sum_{m=1}^{H} w(m)\varphi(m) \tag{5.19}$$

where

$$w(m) = 3\frac{(L-m)(L-m+1) - H(L-H)}{H(4H^2 - 6LH + 3L^2 - 1)} \tag{5.20}$$

$$\varphi(m) = [arg\{R_y(m)\} - arg\{R_y(m-1)\}]_{2\pi},\ 1 \leq m \leq H \tag{5.21}$$

$$R_y(m) = \frac{1}{N - mM} \sum_{k=mM}^{N-1} y^*(k - mM)\, y(k),\ 0 \leq m \leq H \tag{5.22}$$

and $[x]_{2\pi}$ denotes modulo 2π operation (it reduces x to the interval $[-\pi, \pi)$), $arg\{R_y(m)\}$ is argument of $R_y(m)$ and H is a design parameter less than or equal to $L-1$. The optimal value for H is $L/2$ which will be used in our approach.

The frequency offset estimation range is $\pm L/2$ subcarrier spacing for a training symbol having L identical parts. However, the range is not limited by the length L of the sign pattern in our design. For example, by designing the repeated part having k identical subparts and using $H = L\ k/2$ and $M = N/(L\ k)$, the range becomes $\pm L\ k/2$. This is because the range depends on the spacing M between the correlating identical parts and is defined by $\pm N/(2M)$.

In a multipath dispersive channel, the repeated parts of the received training symbol will not be equal, even in the absence of noise, due to the sign conversion

in the transmitted training symbol. This effect perturbs the repetitive nature of the received training symbol. For frequency estimation, the received training symbol is multiplied with the sign pattern to restore the repetitive parts of all equal sign. But this sign flipping will not remedy the already channel-impaired repetitive parts. Hence, some interference is introduced to frequency estimation. Suppression of this interference will be addressed in fine frequency offset estimation.

5.3.5 Channel Impulse Response Estimation

Assume that the channel response remains constant over at least one OFDM symbol interval (quasi-static case) and let the instantaneous path gains be h_0, h_1, ... , ..., h_{K-1}. Let us define the following:

$$\begin{aligned}
\mathbf{r}(0) &\triangleq [r(0)\ r(1)\ \ldots\ r(N-1)]^T \\
\mathbf{h} &\triangleq [h_0\ h_1\ \ldots\ h_{K-1}]^T \\
\mathbf{W}(v) &\triangleq diag\{1,\ e^{j2\pi v/N},\ e^{j2\pi 2v/N},\ldots,\ e^{j2\pi(N-1)v/N}\} \\
\mathbf{n} &\triangleq [n(0)\ n(1)\ \ldots\ n(N-1)]^T \\
\mathbf{S} &\triangleq \begin{bmatrix} s(0) & s(-1) & \ldots & s(-K+1) \\ s(1) & s(0) & \ldots & s(-K+2) \\ \ddots & & & \\ s(N-1) & s(N-2) & \ldots & s(N-K) \end{bmatrix}
\end{aligned} \tag{5.23}$$

where $\{s(k) : k = -N_g, -N_g+1, \ldots, N-1\}$ are the samples of the transmitted training symbol (including the cyclic prefix part), $\{r(k) : k = 0, 1, \ldots, N-1\}$ the corresponding received samples (excluding the cyclic prefix part), $\{n(k) : k = 0, 1, \ldots, N-1\}$ the noise samples and v the normalized frequency offset. The received sample vector can then be expressed as:

$$\mathbf{r}(0) = e^{j\phi}\ \mathbf{W}(v) \cdot \mathbf{S} \cdot \mathbf{h} + \mathbf{n}. \tag{5.24}$$

Utilizing the frequency offset estimate $\hat{v}$ in place of v, the maximum likelihood (ML) channel response estimate [55] can be realized by

$$\hat{\mathbf{h}} = [\mathbf{S}^H \cdot \mathbf{S}]^{-1}\mathbf{S}^H \cdot \mathbf{W}^H(\hat{v}) \cdot \mathbf{r}(0), \tag{5.25}$$

where $(\cdot)^H$ represents a Hermitian transpose, $(\cdot)^{-1}$ represents a generalized matrix inverse and the phase factor has been absorbed in the channel estimate.

In the above channel estimation, the knowledge of the maximum channel delay spread is required. In practice, a design value K' has to be used. Moreover, due to the timing estimation error and the timing advance introduced in Section IV.C, the received training vector will be $\mathbf{r}(\varepsilon)$. The advancement of the timing offset estimate should be adjusted such that ε becomes negative most of the time. Otherwise, it will not only introduce ISI but also miss some channel taps in the channel estimation and cause large channel estimation errors. Consequently, the designed channel estimate length should be longer than the designed maximum channel delay spread plus the delay introduced by timing estimate advancement. Let the designed channel estimate length be $K^\dagger$ (which may be set to the guard interval length). By replacing K with $K^\dagger$ in (5.23), the channel response estimate is given by

$$\hat{\mathbf{h}} = [\mathbf{S}^H \cdot \mathbf{S}]^{-1}\mathbf{S}^H \cdot \mathbf{W}^H(\hat{v}) \cdot \mathbf{r}(\varepsilon), \tag{5.26}$$

where $\mathbf{W}^H(\hat{v})\cdot\mathbf{r}(\varepsilon)$ is the frequency offset compensated received training vector defined by the timing estimate ε.

If the length of the basic repeated training symbol part, M, is larger than the maximum channel delay spread, then the channel estimation complexity can be reduced by combining the basic repeated parts as follows. Let us consider $L = 4$ and let the repeated parts of the received training symbol, after frequency offset compensation, be $[\mathbf{Z_1}\ \mathbf{Z_2}\ \mathbf{Z_3}\ \mathbf{Z_4}]$. Then, from the training symbol pattern $[-+--]$, it can be observed that $\mathbf{Z_1}$ and $\mathbf{Z_4}$ are equivalently affected by the multipath fading environment. Similarly, $-\mathbf{Z_2}$ and $\mathbf{Z_3}$ are equivalently affected. Averaging over each set yields: $\mathbf{Z}_A = (\mathbf{Z_1} + \mathbf{Z_4})/2$ and $\mathbf{Z}_B = (-\mathbf{Z_2} + \mathbf{Z_3})/2$. Note that the separate use of $\mathbf{Z}_A$ and $\mathbf{Z}_B$ is an impact of the training symbol pattern. Define $\mathbf{S}_A$ composed of $\{s(-K^\dagger+1), \ldots, s(M-1)\}$ as

$$\mathbf{S}_A \triangleq \begin{bmatrix} s(0) & s(-1) & \ldots & s(-K^\dagger+1) \\ s(1) & s(0) & \ldots & s(-K^\dagger+2) \\ \ddots & & & \\ s(M-1) & s(M-2) & \ldots & s(M-K^\dagger) \end{bmatrix}. \tag{5.27}$$

Then, the channel estimate based on $\mathbf{Z}_A$ can be obtained as:

$$\hat{\mathbf{h}}_A = [\mathbf{S}_A{}^H \cdot \mathbf{S}_A]^{-1} \mathbf{S}_A{}^H \cdot \mathbf{Z}_A, \tag{5.28}$$

while $\hat{\mathbf{h}}_B$ based on $\mathbf{Z}_B$ can be obtained in a similar fashion using $\mathbf{S}_B$ composed of $\{s(2M-K^{\dagger}+1), \ldots, s(3M-1)\}$. The final channel estimate is taken as the average of $\hat{\mathbf{h}}_A$ and $\hat{\mathbf{h}}_B$ as:

$$\hat{\mathbf{h}} = (\hat{\mathbf{h}}_A + \hat{\mathbf{h}}_B)/2 = \{\hat{h}_i,\ i = 0, 1, \ldots, K^{\dagger}-1\}. \tag{5.29}$$

A similar approach can be applied to $L = 8$ and 16 cases, if the length of the repeated part is much larger than the maximum channel delay spread. Throughout our simulations, (5.26) will be used for channel estimation.

5.3.6 Fine Timing Estimation

The coarse timing estimate would be, most of the time, before the actual timing point due to the pre-advancement. However, even under noiseless condition, the timing estimate would be varying according to the time-varying nature of the channel response. Accordingly, at different snap-shots, the channel estimates would be delayed by different amounts due to different timing offset errors. If the delay in the channel estimate can be found, the effect of the time-varying channel response on the timing estimation can be removed by simply delaying the coarse timing estimate by the same amount of the channel estimate delay. In other words, the coarse timing estimate can be fine-tuned by adding the delay of the first actual channel tap from the channel estimate. A similar concept has been applied in [65] where some pilot tones are used throughout the burst (hence, frequency domain based channel estimation) and N_{av} consecutive channel impulse response estimates are averaged and the first channel tap is found by some criteria. In our considered system with one training symbol, the channel estimation is based on one snap-shot estimation in the time domain and a different criteria described in the following is used for the first channel tap selection.

One way of finding the delay of the first actual channel tap is described in the following. First, the strongest tap gain estimate, $\hat{h}_{max}$, is found as $\hat{h}_{max} = max\{\hat{h}_i : i = 0,\ 1,\ \ldots,\ K^{\dagger}-1\}$. Then, the delay estimate of the first actual channel tap, $\hat{\tau}_0$,

is given by

$$\hat{\tau}_0 = arg\ max_l\{E_h(l) : l = 0, 1, \ldots, K^\dagger - K'\} \tag{5.30}$$

where

$$E_h(l) = \begin{cases} \sum_{k=0}^{K'-1} |\hat{h}_{l+k}|^2 & \text{if } |\hat{h}_l| > \eta \cdot |\hat{h}_{max}|\} \\ 0 & \text{otherwise .} \end{cases} \tag{5.31}$$

$E_h(l)$ is the channel energy estimate contained in a length-K' window starting from the tap l with a condition that the channel energy estimate of tap l should be greater than some threshold. This condition reduces the probability of choosing a noise-only tap as the first actual channel tap. The delay estimate of the first actual channel tap given in (5.30) is essentially the starting tap index whose associated energy $E_h(l)$ is maximum. Due to the timing advancement λ_c in the coarse stage, the actual channel impulse response would be delayed by some amount. Since the channel estimate has $K^\dagger$ taps and the designed maximum channel delay spread is K', the range of the starting tap index of the energy window is $0 \leq l \leq K^\dagger - K'$ as described in (5.30). It should be noted that in order to keep the actual channel impulse response within the channel estimation length $K^\dagger$, $\lambda_c + K'$ should be smaller than $K^\dagger$.

In the above equation, η is a threshold factor for selecting the first channel tap. Note that η should be small if we do not want to miss the first tap. However, η should not be too small. Otherwise, the noise will increase the probability of wrongly picking up the channel tap before the first tap. One way for finding η for different SNR values is given by (see Appendix)

$$\eta_2 = \sqrt{\frac{SNR_1}{SNR_2}} \cdot \eta_1 \tag{5.32}$$

where η_1 is a known value obtained from the simulation at SNR_1 and η_2 is the threshold value for SNR_2.

The fine timing estimate is obtained by adding the delay estimate of the first actual channel tap to the coarse timing estimate as

$$\hat{\varepsilon} = \hat{\varepsilon}_c + \hat{\tau}_0 - \lambda_f \tag{5.33}$$

where λ_f is a designed pre-advancement to reduce the possible ISI. Without the pre-advancement of λ_f, the fine timing estimate would be, most of the time, at the exact

timing point. However, for the circumstances when the absolute gain ratio of the first tap to the strongest tap is smaller than η, the most likely chosen channel tap as the first tap would be the second channel tap. Hence, λ_f should be at least the delay difference between the first and the second taps.

The pre-advancement of fine timing estimate may introduce interference in the frequency offset estimation. The reason is that when the timing-advanced training symbol is multiplied by the training symbol pattern, the offset caused by the timing advancement would perturb the repeated structure of the training symbol and introduce some interference. Hence, a better choice of the received training symbol for frequency offset estimation should be defined by the fine timing estimate without pre-advancement; namely, $\hat{\varepsilon}_v = \hat{\varepsilon}_c + \hat{\tau}_0$ and the fine timing estimate is then advanced by λ_f as in (5.33). In this way, the timing offset error interference in the frequency offset estimation can be reduced and at the same time the ISI caused by the timing offset error can be reduced by means of pre-advancement.

5.3.7 Fine Frequency Estimation

As mentioned in the coarse frequency estimation section, the training symbol pattern can introduce some interference to frequency estimation. If this interference is not taken into consideration in the fine stage, the fine frequency estimation will inherit the performance degradation. To suppress this interference, the differently affected received samples can be excluded from the frequency estimation. For $L = 4$ and the training symbol pattern of $[- + --]$, it can be observed that after multiplying the received training symbol with the training symbol pattern, the first (K-1) received samples of the second and third repeated parts are different from those of the other repeated parts even in the absence of noise. Hence, they impair the repeated structure and introduce the interference. By excluding them, the interference can be suppressed. In practice, the first K' samples (designed maximum channel delay spread) of the second and third repeated parts may be excluded. The exclusion of those samples can easily be done by masking them with zeros. Then, the modified procedure becomes zero masking, sign flipping and applying M&M. This zero masking approach can be applied if the number of samples in the basis part is much larger than the maximum channel delay spread.

Another approach to avoid the interference is based on the ML principle. Since the fine timing synchronization will most of the time give a perfect timing, we will assume that perfect timing has been achieved. By replacing $\boldsymbol{h}$ by the ML channel estimate (5.25), the ML frequency estimation can be obtained by maximizing the following metric

$$\Lambda(\hat{\varepsilon}_v; \tilde{v}) = \boldsymbol{r}^H(\hat{\varepsilon}_v)\boldsymbol{W}(\tilde{v})\boldsymbol{B}\boldsymbol{W}^H(\tilde{v})\boldsymbol{r}(\hat{\varepsilon}_v) \tag{5.34}$$

where $\boldsymbol{B} = \boldsymbol{S}(\boldsymbol{S}^H\boldsymbol{S})^{-1}\boldsymbol{S}^H$ and $\boldsymbol{S}$ is an $N \times K'$ matrix. If $\hat{\varepsilon}_v = 0$ and $K' = K$, the above metric is exactly the same as that described in [77].

In the implementation of maximizing the metric, [77] used $N \cdot U$ point FFT in finding $\hat{v}$. Hence, the search space for $\hat{v}$ is approximately over the range of $(-N/2, N/2]$ and the resolution between trial frequency offset points is $1/U$ subcarrier spacing. In this Chapter, we make use of the information from the coarse frequency estimation. Since the coarse frequency offset estimate cannot be too far away from the actual frequency offset, we limit the search space for $\hat{v}$ around the coarse frequency offset estimate $\hat{v}_c$ as follows:

$$\hat{v} = arg\ max_{\tilde{v}}\{\Lambda(\hat{\varepsilon}_v; \tilde{v}) : \hat{v}_c - F \leq \tilde{v} \leq \hat{v}_c + F\}. \tag{5.35}$$

The trial points for $\tilde{v}$ are taken at a resolution of $\Delta = F/J$ subcarrier spacing within the search space; namely, $\{\tilde{v}(i) = \hat{v}_c + i\Delta : i = -J, -J+1, \ldots, J\}$, where J is the number of trial points at one side of $\hat{v}_c$. The value of F can be chosen according to the coarse frequency estimation performance. For example, if the error of the normalized coarse frequency offset estimate is expected to be less than 0.01 (which is usually the case for good coarse frequency estimation methods at moderate or high SNR values), F may be set to 0.01 or a little larger (say) 0.05. Finally, the final frequency offset estimate is given by

$$\hat{v}_f = \begin{cases} \hat{v} & \text{if } \hat{v} = \tilde{v}_{-J} \text{ or } \tilde{v}_J \\ v_q & \text{otherwise .} \end{cases} \tag{5.36}$$

where v_q is obtained by quadratic interpolation among the points $\hat{v}-\Delta$, $\hat{v}$, and $\hat{v}+\Delta$.

5.4 Performance Evaluation, Simulation Results and Discussion

5.4.1 Simulation Parameters

The performance of the proposed synchronization algorithm has been investigated by computer simulation. The OFDM system parameters used are 1024 subcarriers, 1024 point $IFFT/FFT$, and 10% guard interval (102 samples). The subcarrier modulation is QPSK and a carrier frequency offset of 6.2 subcarrier spacing is assumed. Unless stated otherwise, 10,000 simulation runs will be applied. For the training symbol pattern, the first one of the two patterns given in Table 5.1 is used for each L value.

The channels considered are described in the following. All channels except AWGN channel have 16 taps with equal tap spacing of 4 samples. The Rayleigh fading channel has an exponential power delay profile and the ratio of the first Rayleigh fading tap to the last Rayleigh fading tap is set to 20 dB. The Rician fading channel has a Rician factor of 4 and the first tap with delay zero is set as the direct path. The other taps are Rayleigh fading taps with exponential power delay profile and the ratio of the first Rayleigh fading tap to the last Rayleigh fading tap is set to 20 dB. The static ISI channel has fixed tap gains and the tap gain powers are the same as those of the Rayleigh fading channel.

The channel estimation length $K^{\dagger}$ is set to the guard interval length N_g. The actual maximum channel delay spread K for the considered multipath channels is 61. Since the designed maximum channel delay spread K' should be at least equal to or larger than K, we set $K' = 64$. In order to keep the channel impulse response within the channel estimation length $K^{\dagger}$, both $\lambda_c + K'$ and $\lambda_f + K'$ should be smaller than $K^{\dagger}$. Hence, we use $\lambda_c = 30$. Due to the better timing estimation in the fine stage, λ_f can be set to be smaller than λ_c. In choosing λ_f value, one can consult to our proposed timing performance measure which will be described in Subsection C of this Section. λ_f can be chosen from the interference-free interval which is shown in our proposed timing performance measure. Based on the above reasons, we set $\lambda_f = 20$. We estimate that the coarse normalized frequency offset error would be less than 0.01 for moderate and high SNR values. Hence, we set F to a little larger value 0.05. Since $2J + 1$ frequency offset trial points with a resolution of F/J subcarrier spacing

are evaluated in the fine stage, a larger value of J can give a slightly better frequency estimation performance but with a higher complexity. Since we also interpolate as in (5.36), we view that the frequency resolution of 0.005 is a reasonable value. Hence, we use the corresponding J value of 10. We evaluated several trial values 0.8, 0.4, 0.2, 0.05, 0.01 for η_{10}, the channel tap selection threshold at the SNR value of 10 dB. Since $\eta_{10} = 0.2$ gives the best fine timing estimation variance in the multipath Rayleigh fading channel, we use $\eta_{10} = 0.2$ for the SNR value of 10 dB throughout our simulations.

5.4.2 Missed Detection and False Detection Probabilities

The missed detection and false detection probabilities of the proposed approach and those associated with the MMSE approach in the 16-tap Rayleigh fading channel described above, obtained from 10^5 simulation runs, are presented in Fig.s 5.6 and 5.7, respectively. Since a burst mode transmission is considered in the simulations, the false detection probability is evaluated when noise only is present. Hence, the corresponding 1/SNR values for the false detection probability mean the variances of the noise. In evaluating the missed detection probability, the training symbol is preceeded by noise samples and followed by an OFDM data symbol. For the MMSE approach, the timing metric of $1 - \mathcal{V}(d)$, where $\mathcal{V}(d)$ was given in (5.10) is used for convenience.

The false detection probability curves of the proposed approach are the same for different values of the SNR, as seen in Fig. 5.6 and they are well separated from the missed detection probability curves in the figure. Hence, the proposed approach gives a very robust sync detection performance. On the other hand, the false detection probabilities of the MMSE approach depend on the value of the SNR. The higher the SNR, the worse the false detection performance of the MMSE approach. Furthermore, the MMSE approach does not have a timing metric threshold, where both the false detection and the missed detection probabilities are low. Hence, the MMSE approach is associated with a poor sync detection capability. Similarly, the unnormalized timing metrics from [73] are expected to have a poor sync detection capability due to the reason described in Section 5.3.1.

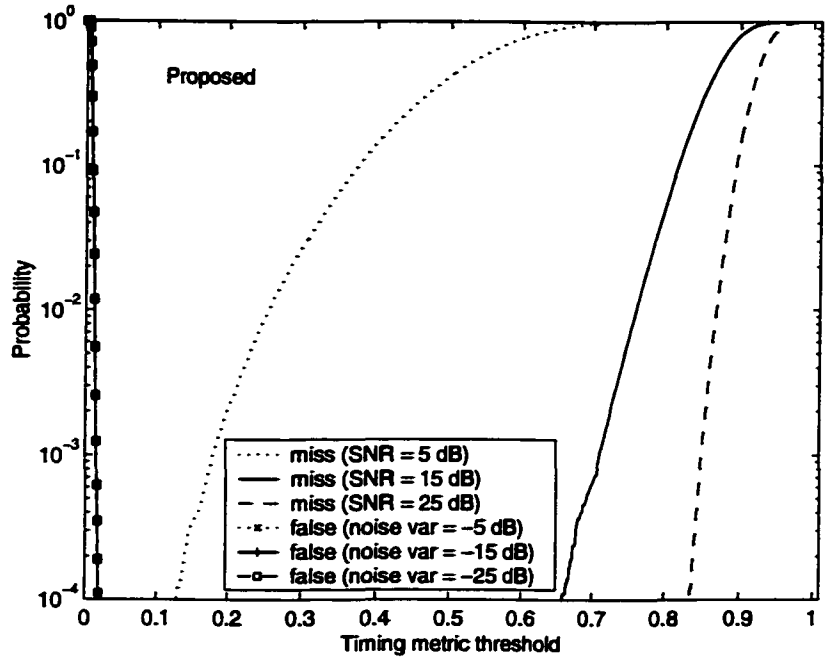

Figure 5.6. *Sync detection performance of the proposed method*

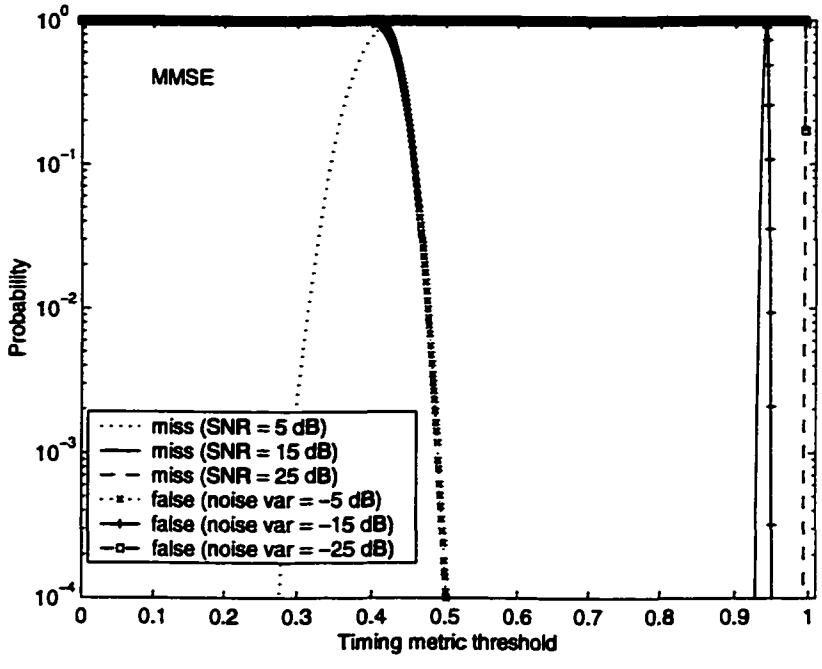

Figure 5.7. *Sync detection performance of the MMSE approach*

5.4.3 Timing Synchronization Performance

Timing estimation performance is often evaluated in terms of the estimator variance. Fig. 5.8 shows the timing offset variances of S&C (with 90 % maximum point averaging [1]) and the proposed approach (coarse timing only) for $L = 4$, 8 and 16. It shows the effect of the proposed training symbol pattern on the timing synchronization performance. For a Rician fading channel and AWGN channel, d_{max} from (5.18) of the proposed approach is observed to be always at the correct timing point while there are relatively substantial timing offset variations for S&C. For the static ISI channel, the proposed approach has some timing offset errors, but they are much smaller than S&C. From the Rician fading and static ISI channels results, it is noted that if the first channel tap is much larger than the other taps, the proposed approach's d_{max} can always lock to the first tap correctly. The scheme proposed by S&C also shows a better timing estimation performance in the Rician fading channel than the static ISI channel. For the Rayleigh fading channel, the proposed approach has better timing estimation variance at low SNR values but comparable variance at high SNR values if compared to S&C.

For AWGN, static ISI, and Rician channels, the timing estimation variance with reference to the first channel tap has some meaning since the first tap represents the desired timing point. However, for the Rayleigh fading channel, all channel tap gains are time-varying and missing the first tap with negligible gain may not result in a performance degradation. Hence, the timing estimation variance with reference to the first channel tap may not represent a good performance measure in this case. Moreover, for OFDM systems, as long as the timing estimate is within the ISI-free guard interval, the timing offset, regardless of its value, will not degrade the system performance. Only when the timing estimate falls outside the ISI-free guard interval, interference will be introduced. Hence, a more performance-oriented approach of evaluating the timing synchronization performance for a particular OFDM system would be the measure of interference power caused by the timing offsets. For each timing offset ε, the corresponding normalized interference power $I(\varepsilon)$, normalized by

[1] It means that the maximum timing metric point is first found and then on each side of the maximum metric point, a timing point having 90 % of the maximum metric is found. The timing estimate is given by the mid-point of the two 90 % maximum points.

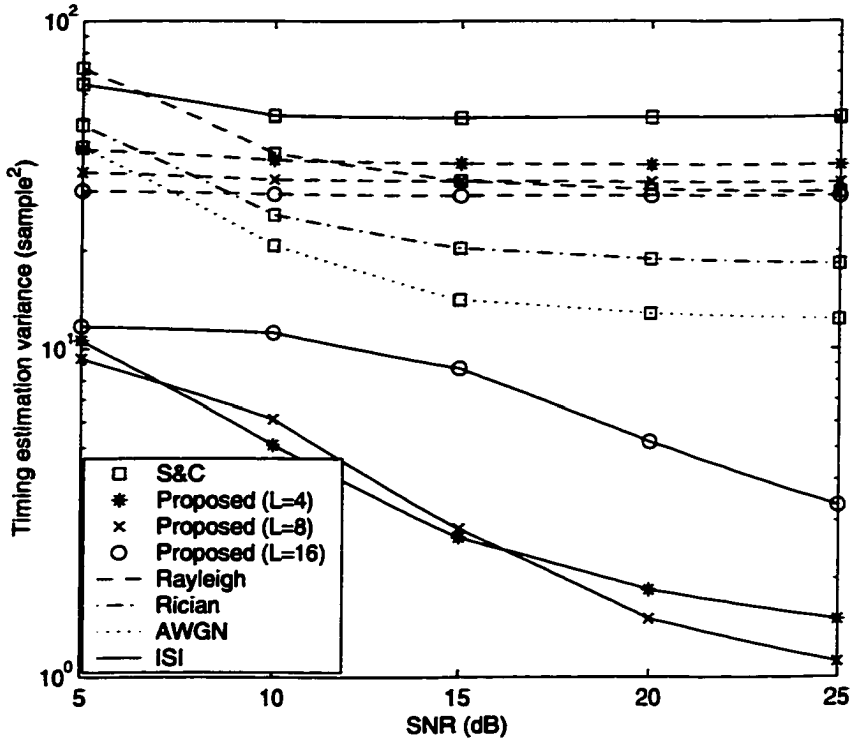

Figure 5.8. *Timing estimation variance in different channel environments. (No timing offset variations are observed for the proposed method in AWGN and in the multipath Rician fading channels considered, hence the corresponding results are not included in the figure.)*

the signal power, can be calculated as:

$$I(\varepsilon) = \frac{\sigma_\varepsilon^2}{\alpha^2(\varepsilon)} \tag{5.37}$$

where $\alpha(\varepsilon)$ and σ_ε^2 are given by (5.5) and (5.6), respectively.

Let the distribution of the timing offset estimates for the considered system and channel be $P(\varepsilon)$. The average normalized interference power caused by timing offset errors can then be given by

$$\mathcal{I}_\varepsilon = \sum_\varepsilon P(\varepsilon) I(\varepsilon). \tag{5.38}$$

The calculation of $I(\varepsilon)$ requires an instantaneous channel response (or instantaneous channel power gains) (see (5.37)(5.5) and (5.6)). Furthermore, the interference power can depend on the timing estimate shift λ (Note that $\lambda = -\lambda_c$ in (5.18).). Hence, it is not so easy to evaluate $\mathcal{I}_\varepsilon$ for different parameter settings of the timing estimator such as different timing estimate shifts (λ). One way to circumvent this is to approximate $I(\varepsilon)$ calculation by $\tilde{I}(\varepsilon)$ which uses the channel power delay profile instead of the instantaneous channel power gains.

By assuming that the timing estimate is independent of the instantaneous channel response [2], an approximation of $\mathcal{I}_\varepsilon(\lambda)$ for a timing estimate shift λ, denoted by $\tilde{\mathcal{I}}_\varepsilon(\lambda)$, can be calculated as

$$\tilde{\mathcal{I}}_\varepsilon(\lambda) = \sum_\varepsilon P(\varepsilon - \lambda) \cdot \tilde{I}(\varepsilon). \tag{5.39}$$

From the above equation, the optimum timing estimate shift for a considered system and channel can be obtained by

$$\lambda_{opt} = arg\ min_\lambda \left(\tilde{\mathcal{I}}_\varepsilon(\lambda) \right). \tag{5.40}$$

Let us define the average signal to timing-error-induced interference power ratio $SIR_\varepsilon = 1/\mathcal{I}_\varepsilon$ and its approximate version $\tilde{SIR}_\varepsilon = 1/\tilde{\mathcal{I}}_\varepsilon$. In Fig. 5.9, the $\tilde{SIR}_\varepsilon$ versus timing estimate shifts are plotted for S&C and the proposed method (L = 4, FD training) for the Rayleigh fading channel at the SNR value of 10 dB. Also included in the figure are the SIR_ε values for the timing estimate shifts of -50, -40, ... , 30

[2] Strictly speaking, this is not true.

samples. It can be observed that SIR_ϵ and $\tilde{SIR}_\epsilon$ are almost the same for S&C and the coarse timing stage of the proposed method, thus, indicating that the proposed approximate performance measure is a close approximation.

For the proposed fine timing stage with one iteration ("Fine[1]") and two iterations ("Fine[2]"), the actual values SIR_ϵ at the timing estimate shifts of -10 and 0 sample are greater than the approximate values $\tilde{SIR}_\epsilon$ by some amount. This can be explained as follows. The approximate expression $\tilde{SIR}_\epsilon$ is under the assumption that the timing estimate is independent of the instantaneous channel response. However, the proposed fine stage utilizes the information from the channel estimation. Hence, the above assumption is not justified. It can be observed that at these timing estimate shifts, the interference is caused by timing offsets greater than zero. For the proposed fine timing stage, this will most likely happen when the first channel tap gain is quite small. Consequently, the introduced interference which depends on the first channel tap gain would be smaller than the interference used in $\tilde{SIR}_\epsilon$ where the power delay profile is used. Despite some differences in values, the plots of SIR_ϵ and $\tilde{SIR}_\epsilon$ for the fine stage show the same trend. Hence, it still gives useful information on what timing estimate shift would be suitable.

Fig. 5.9 demonstrates the importance of proper timing shift setting. It can also be observed that comparing two timing estimators, each with a fixed timing estimate shift, will not give the general performance of the timing estimators. Each timing estimator has its own optimum timing estimate shift value(s). The optimum timing estimate shift for S&C in this case is at 14 samples which still introduces some interference. For the proposed coarse timing case, the optimum shift is at -40 samples where no interference is introduced. For the fine timing stage, the interference-free timing shift is within the interval from -42 to -16 samples.

It should be mentioned that although the timing estimation variance of L = 16 (coarse) case for the static ISI channel in Fig. 5.8 is larger than L = 4 and 8 cases, evaluating the $\tilde{SIR}_\epsilon$ versus timing estimate shifts plot at the SNR value of 10 dB gives an interference-free interval of 35 samples (-46 to -12) for both L = 16 and 8 cases, 28 samples (-45 to -18) for L = 4 case. Due to space limitation, this is not shown. From this fact, it can be stated that the timing estimation variance in OFDM system may not always result in a meaningful performance measure.

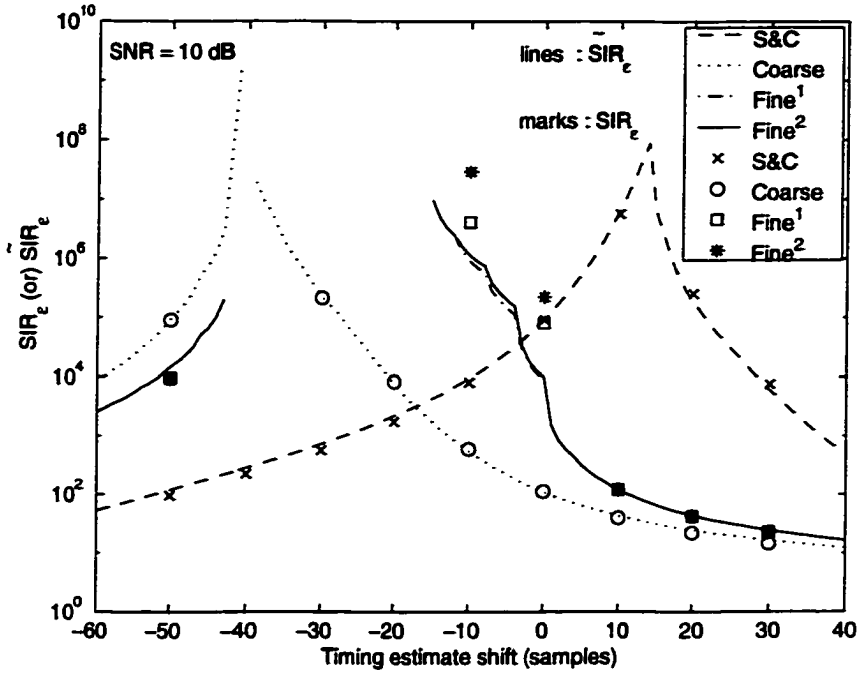

Figure 5.9. *Signal to timing-error-introduced average interference power ratio and its approximate version versus timing estimate shift in the 16 taps Rayleigh fading channel at an SNR value of 10 dB*

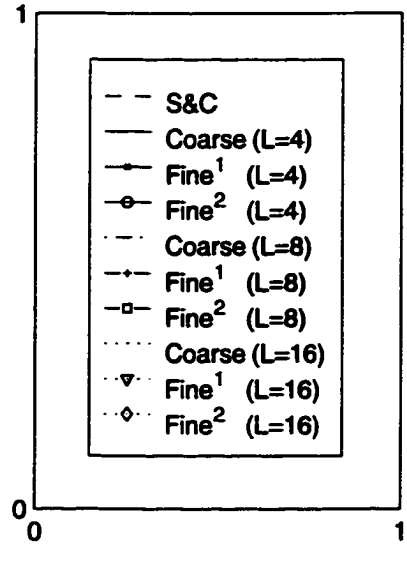

Legends for Figs. 5.10, 5.11 and 5.12

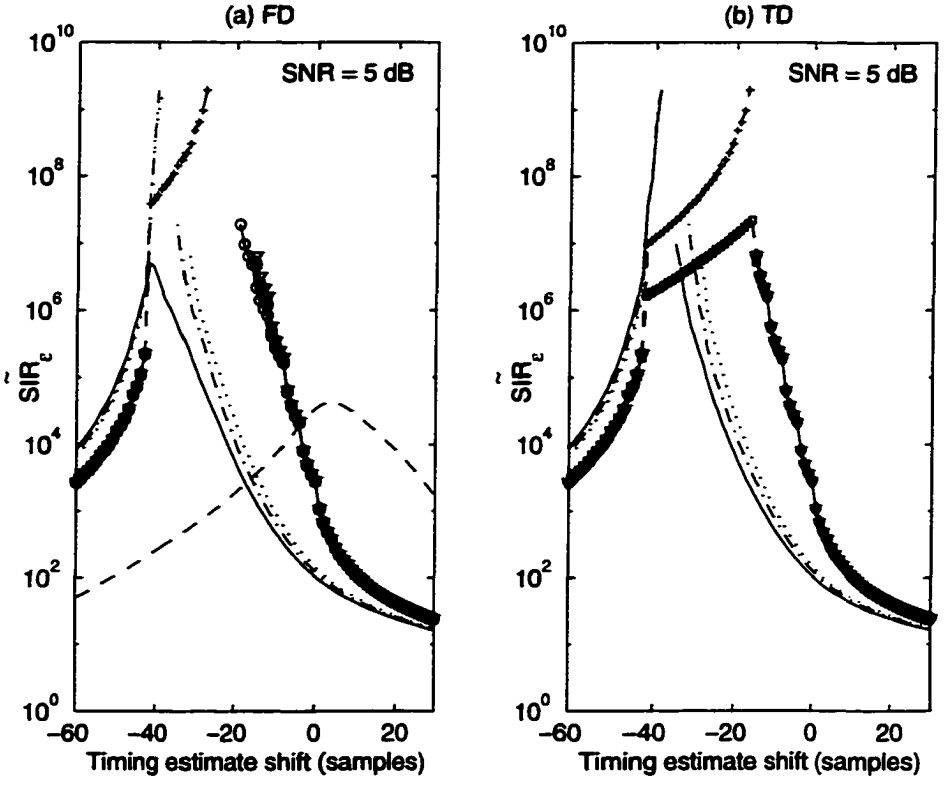

Figure 5.10. *Timing synchronization performance in terms of $\tilde{SIR}_\epsilon$ in the 16-tap Rayleigh fading channel at an SNR value of 5 dB*

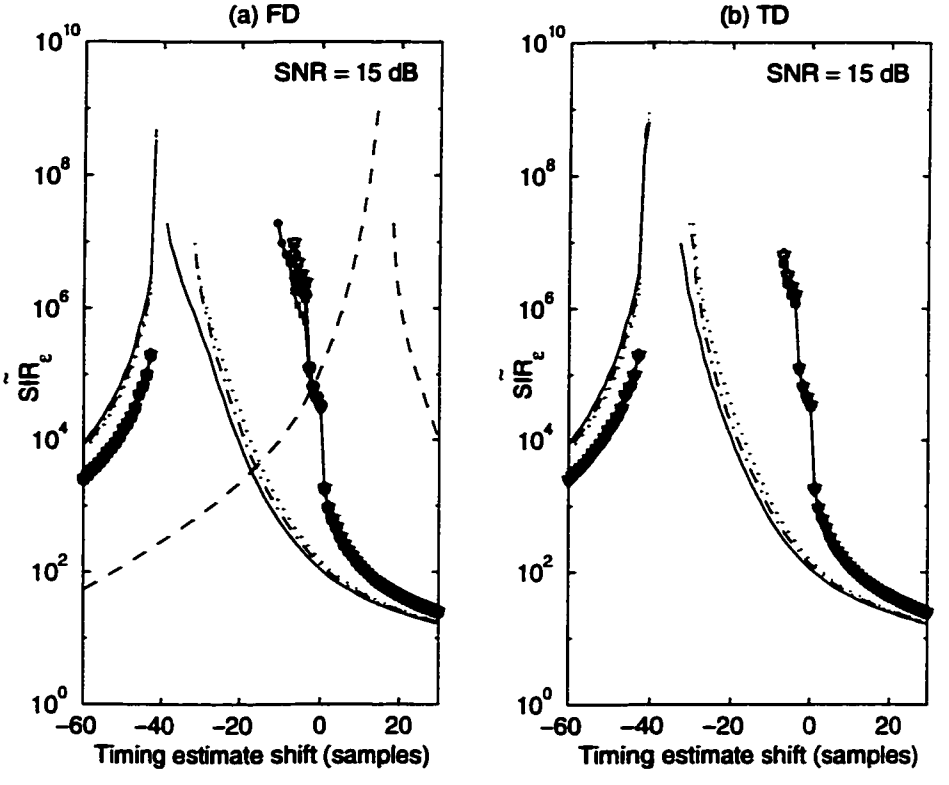

Figure 5.11. *Timing synchronization performance in terms of $S\tilde{I}R_\varepsilon$ in the 16-tap Rayleigh fading channel at an SNR value of 15 dB*

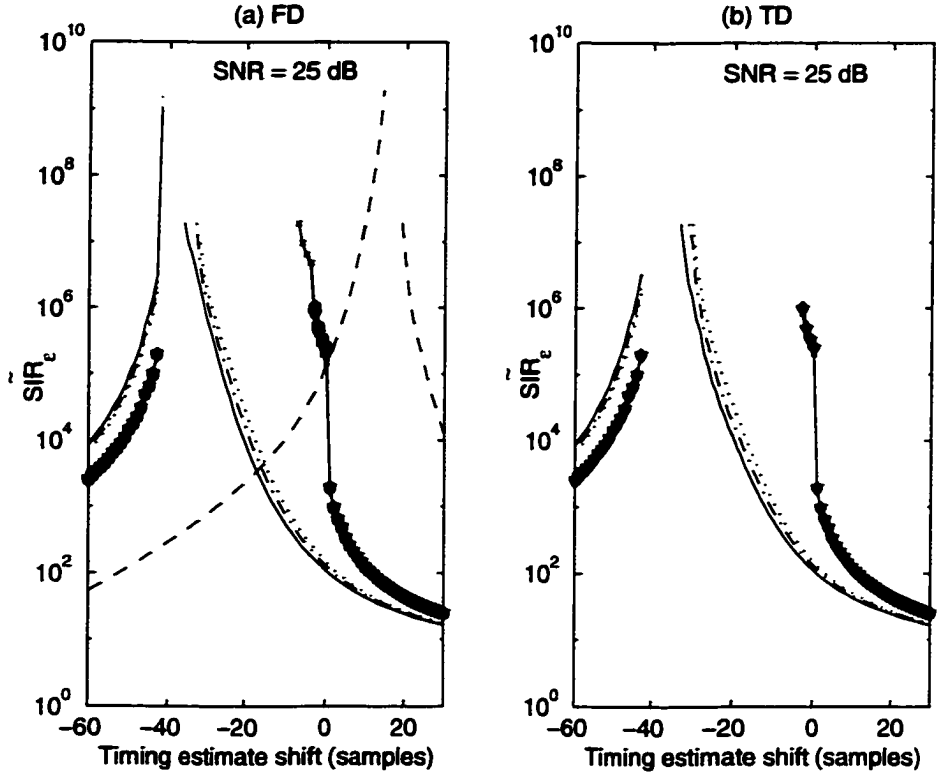

Figure 5.12. *Timing synchronization performance in terms of $\tilde{SIR}_\epsilon$ in the 16-tap Rayleigh fading channel at an SNR value of 25 dB*

In Figs. 5.10, 5.11 and 5.12, the timing estimation performance in the Rayleigh fading channel in terms of $\tilde{SIR}_\epsilon$ are presented for S&C and the proposed method. Both FD training and TD training are evaluated for the proposed method with L = 4, 8, and 16 cases. A close observation of these figures indicates that the proposed coarse timing stage has better performance than S&C particularly at low SNR values. At high SNR values, S&C has a comparable performance to the proposed coarse timing stage. For example, at an SNR value of 25 dB, S&C has an interference-free timing shift interval of 4 samples (15 to 18) and the proposed coarse timing stage has 5 samples (-41 to -37) for FD and 9 samples (-42 to -34) for TD. The coarse timing stage with a larger L value has a larger interference-free interval. It can be ascribed to the sharper timing metric trajectory for the larger L value. The fine timing stages ("Fine[1]" and "Fine[2]") are observed to give significant improvement over the coarse timing stage. Although "Fine[2]" case has generally a slight improvement over "Fine[1]" case, the performance gain is not significant and may not be justified for the associated complexity cost.

The fine stages with different L values have almost the same performance except at an SNR value of 5 dB where L = 8 case has some degradation. This fact indicates that the channel estimation at the fine timing stage depends on the L value or the training symbol pattern. Since the training symbol is of repetitive structure with some sign conversion, the channel estimate can be a quite different one, rather than a delayed version, in the presence of a large delay timing offset, hence, resulting in a wrong selection of the first channel tap and introducing some timing error at the fine stage. This occasional occurance is observed in the simulation of the L = 8 case at an SNR value of 5 dB. In particular,"Fine[1]" stage of L = 8 case with FD training shows such an occurance but "Fine[2]" stage is observed to be able to correct the corresponding timing error. However, "Fine[2]" stage of L = 8 case with TD training is unable to correct it. Nevertheless, all these cases still have better performance than S&C. It is also observed from Figs. 5.10, 5.11 and 5.12 that TD training has a slightly better performance than FD training for all cases except the fine stage of L = 8 case at an SNR value of 5 dB.

5.4.4 Performance of Frequency Synchronization

The frequency synchronization performance can be evaluated by the average normalized interference power $\mathcal{I}_v$ (normalized by the signal power) caused by frequency estimation errors. The normalized interference power $I_v(\Delta_v)$ caused by a normalized (by subcarrier spacing) frequency estimate error Δ_v can be approximated by [70]:

$$I_v(\Delta_v) \simeq \frac{\pi^2}{3} \cdot {\Delta_v}^2. \tag{5.41}$$

Hence, the $\mathcal{I}_v$ can be calculated from the mean square error (MSE) of the normalized frequency offset estimate, mse_v, as:

$$\mathcal{I}_v \simeq \frac{\pi^2}{3} \cdot mse_v. \tag{5.42}$$

It is noted that the frequency offset estimation MSE directly translates into the average interference power caused by the frequency estimation errors while the variance of the timing offset estimate does not directly translate into the interference power caused by timing estimation errors. In the following, the frequency estimation MSE will be used as the performance measure for the frequency synchronization.

Figs. 5.13 and 5.16 show the frequency estimation performance in the Rayleigh fading channel. The performance of M&M [64] using a training symbol with 16 identical parts (no sign flipping) under perfect timing synchronization is included as a reference. For the proposed scheme, the results are presented for the cases of coarse frequency estimation ("Coarse"), fine frequency estimation without zero masking ("Fine"), fine frequency estimation with zero masking ("zero mask"), and ML frequency estimation ("ML"). Only the results of the fine stage with one iteration are presented since no noticeable difference is observed between one iteration and two iterations.

All the fine stages have performance improvement over the corresponding coarse stages. However, all fine cases which do not consider the interference effect have some performance degradation if compared to M&M with perfect timing. An interesting observation from the results of "Fine" case with different L values is that the different training symbol patterns have different impacts on the frequency estimation performance. As previously mentioned, the training symbol pattern can introduce some interference in the frequency estimation in a dispersive channel. This interference

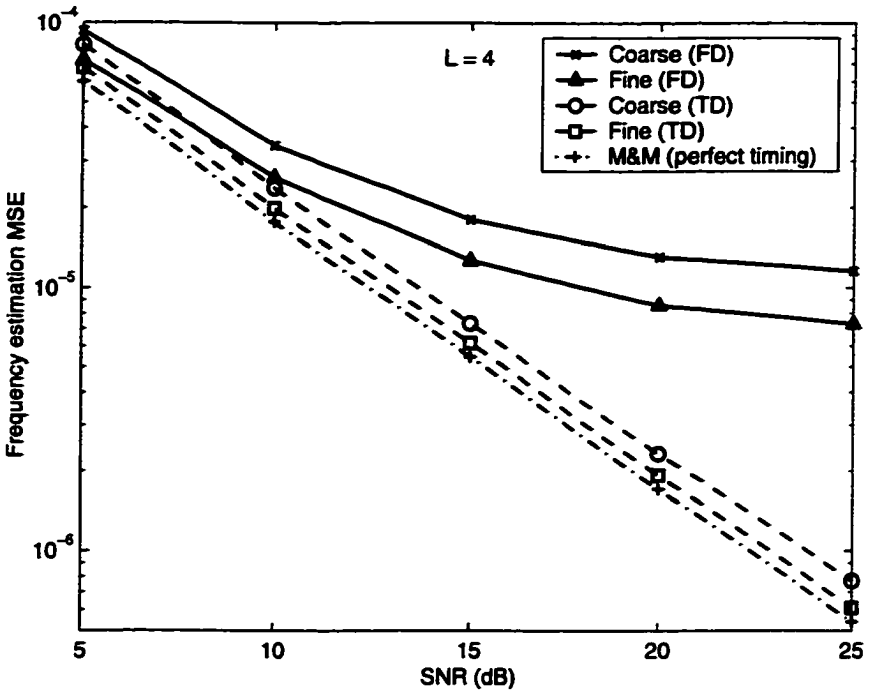

Figure 5.13. *Frequency estimation MSE performance of the proposed approaches with $L = 4$ that do not consider the interference effect in the 16-tap Rayleigh fading channel*

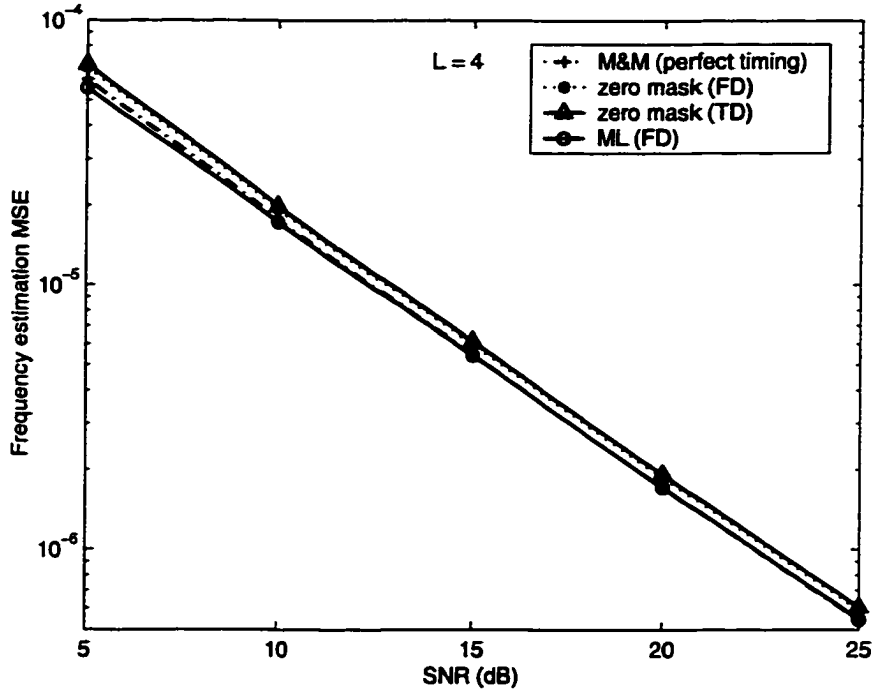

Figure 5.14. *Frequency estimation MSE performance of the proposed approaches with $L = 4$ that consider the interference effect in the 16-tap Rayleigh fading channel*

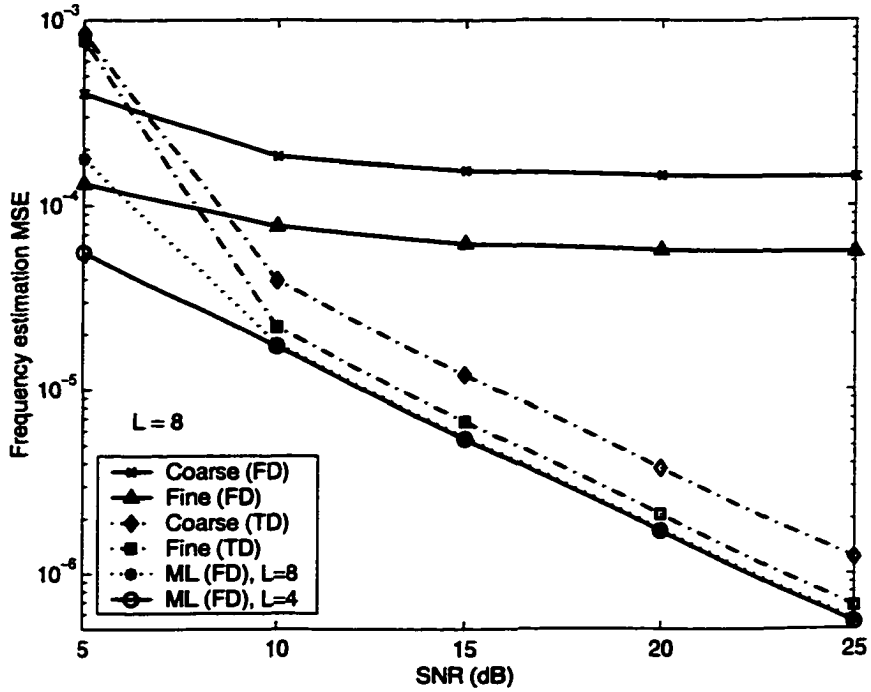

Figure 5.15. *Frequency estimation MSE performance of the proposed approaches with $L = 8$ in the 16 taps Rayleigh fading channel*

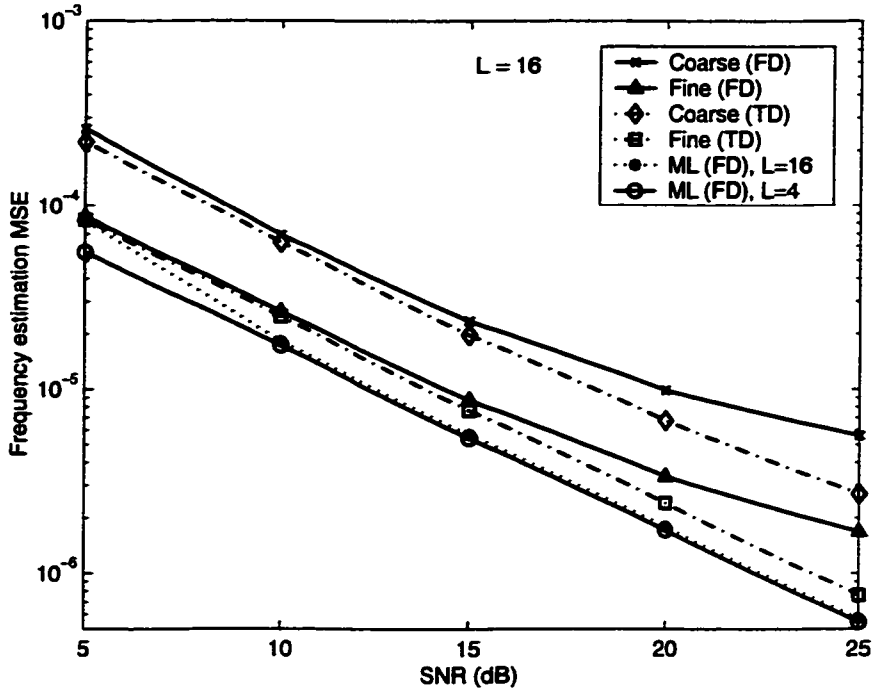

Figure 5.16. *Frequency estimation MSE performance of the proposed approaches with $L = 16$ in the 16 taps Rayleigh fading channel*

seems to be larger for the training symbol pattern of L = 8 case particularly with FD training as can be observed in Fig. 5.15. Interestingly, TD training is much more robust to this kind of interference than FD training except for L = 8 case at an SNR value of 5 dB. An intuitive reason for the better performance of TD training is that the TD training sample energies are distributed evenly and so do the average noise samples energies. Hence, the energy distribution of TD training is matched to that of the noise while FD training does not.

In Fig. 5.14, the performance of the fine frequency estimation approaches which consider the interference effect are presented. In fact, the ML approach does not suffer from the interference effect. Both zero masking approaches with FD and TD training have almost the same performance which is very close to the performance of M&M with perfect timing. Hence, zero masking appears to be an effective approach for the system which uses only one FD training (with possible sign flipping of the repetitive parts) for both timing and frequency synchronization and the length of one repetitive part is quite larger than the maximum channel delay spread. The ML approach has even a better performance than M&M particularly at low SNR values. However, in Figs. 5.15 and 5.16, the ML schemes with L = 8 and 16 cases show some performance degradation at an SNR value of 5 dB if compared to L = 4 case. In fact, this is due to the occasional occurrence of the coarse frequency offset estimates for which the search space $\hat{v}_c - F \leq \tilde{v} \leq \hat{v}_c + F$ is not close enough to the actual frequency offset where we note that F = 0.05 is used in the simulation. To confirm this fact, the ML approach for L = 8 and 16 cases at an SNR value of 5 dB are evaluated for F = 1.5, J = 10. The results obtained (not shown in the figure) are almost the same as that of ML with L = 4.

In general, TD training outperforms FD training. If only one training is used for both timing and frequency synchronization, the impact of the training symbol pattern can affect the frequency estimation performance. In this case, TD training or FD training with zero masking approach can be considered. If complexity is affordable, the ML approach can be considered. If two training symbols are applied, one with the proposed training symbol pattern can be considered for timing synchronization using the proposed timing metric and the other repetitive training without sign flipping can be considered for the frequency estimation using M&M. Also in this case, TD

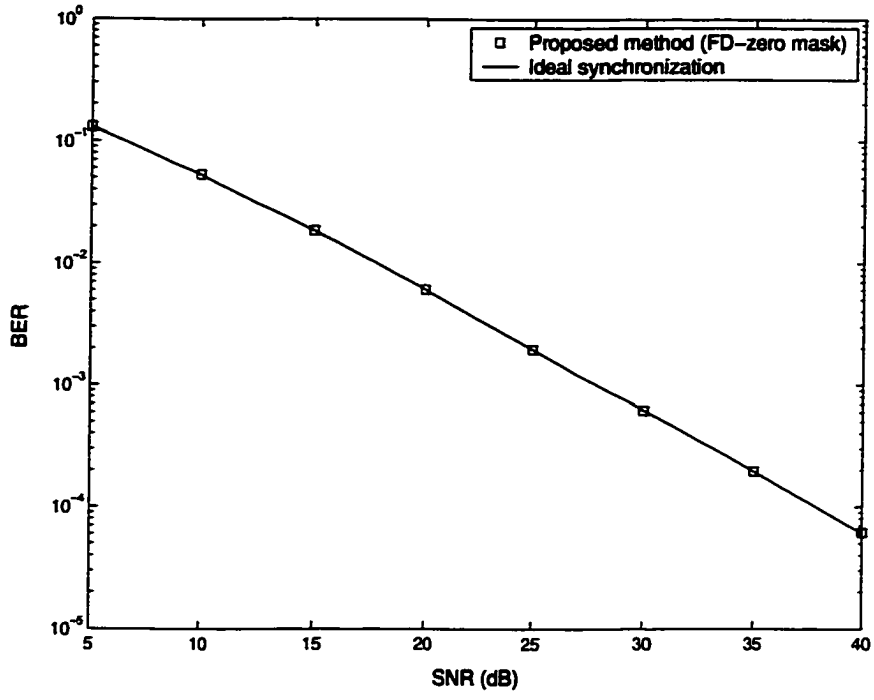

Figure 5.17. *BER performance comparison between the ideally synchronized system and the system using the proposed method (L=4, FD training, zero masking) in the 16-tap Rayleigh fading channel*

training is preferable over FD training.

5.4.5 BER Performance

Fig. 5.17 presents the BER performance comparison between the system using the proposed method and the system having ideal timing and frequency synchronization with the same channel estimation as in the proposed method. The considered system uses FD training followed by an OFDM data symbol and the channel is the multipath Rayleigh fading channel described previously. In the proposed method, zero masking approach is used for the fine frequency estimation. For SNR values of 25 dB and above, 100,000 simulation runs and for the other SNR values 10,000 simulation runs were used. It can be seen that for all SNR values, the proposed method has virtually the same BER performance as the perfectly synchronized system.

5.5 Conclusions

A robust symbol timing and carrier frequency synchronization method for OFDM systems in multipath fading environments is presented. The proposed method uses one specifically designed training symbol having a steep roll-off timing metric trajectory. This type of training symbol achieves some improvement in timing estimation for time-varying multipath Rayleigh fading channels and much more improvement in AWGN, Rician fading, and static dispersive channels. The channel estimation based on the designed training symbol is also incorporated to give further improvement in timing and frequency synchronization. This combined approach achieves considerable improvement by removing the time-varying multipath effect on timing synchronization. Using the training symbol of identical parts with different signs can introduce interference in the frequency estimation based on that training symbol. An approach of masking the interfered part with zeros is shown to be an effective way for suppressing the introduced interference in the frequency estimation. An ML frequency estimation which does not suffer from this interference is also described. From the simulation, using TD training is observed to be better than FD training.

For frequency estimation, MSE or frequency-error-introduced interference power reflects the frequency synchronization performance. However, for timing estimation, the plot of signal to timing-error-induced average interference power ratio SIR_ε vs. timing estimate shift for the considered system and channel appears to be a more revealing performance measure. A close approximation to this SIR_ε is also proposed using the channel power delay profile. This approximation yields a simple approach to find the optimum setting of the timing estimator.

Appendix

This Appendix outlines main steps in obtaining (5.32). Define two random variables D_n and D_h as

$$D_n \triangleq max\{[\hat{h}_{i_1-m}, \hat{h}_{i_1-m+1}, \cdots, \hat{h}_{i_1-1}]\} \tag{5.43}$$

i_1 corresponds to the first actual channel tap, m is integer > 0

$$D_h \triangleq max_i\{\hat{h}_i\} \tag{5.44}$$

D_n and D_h can be approximated as complex Gaussian variables with zero means and variances Ω_n and Ω_h where

$$\Omega_n = L_1 \frac{m}{N \cdot SNR}, \quad \Omega_h = L_2 \sum_l (\sigma_{h_l}^2 + \frac{1}{N \cdot SNR}) \simeq L_2 \sum_l \sigma_{h_l}^2 = L_2 \tag{5.45}$$

where $\sigma_{h_l}^2$ is the variance of l^{th} channel tap gain, $\sum_l \sigma_{h_l}^2 = 1$, L_1 and L_2 are some constants > 0.

Now, our interest is to find $Prob\{|D_n| \leq \eta \cdot |D_h|\}$, $\eta > 0$. By defining another random variable $Z \triangleq \frac{|D_n|}{|D_h|}$, we obtain

$$Prob\{|D_n| \leq \eta \cdot |D_h|\} = Prob\{Z \leq \eta\} = \frac{\eta^2}{\eta^2 + \Omega_n/\Omega_h}. \tag{5.46}$$

Using $\Omega_n/\Omega_h \propto \frac{1}{N \cdot SNR}$ in the above equation results in (5.32).

Chapter 6

A Maximum Likelihood-based Timing and Frequency Synchronization and Channel Estimation for OFDM

As the popularity of OFDM increases, synchronization and channel estimation in OFDM systems have recently received much research attention. Several approaches have been proposed for timing synchronization (e.g., [41] [43] [46] [65]) and frequency synchronization (e.g. [63]-[64], [78], [79]), separately. Those separate frequency synchronization methods assume perfect timing synchronization, which may not be always guaranteed, and timing estimation errors may affect frequency synchronization performance. In order to evaluate actual performance, joint timing and frequency synchronization approaches (e.g., [38] [44]) are desirable. In a coherent OFDM system, channel estimation becomes a necessity. Previous work on OFDM channel estimation (e.g. [51] [48] [54] [80]) assume perfect synchronization. However, this may not be guaranteed and synchronization errors can deteriorate the channel estimation performance [70]. Hence, a desirable approach which reflects a more accurate performance is to address synchronization and channel estimation tasks together.

In this chapter, we consider joint timing estimation, frequency offset estimation, and channel estimation for an OFDM system using a training sequence based approach. We resort to the ML principle and arrive at an unrealizable ML estimation for timing, frequency offset and channel response. In an attempt to realize the ML estimation, coarse and fine estimation are considered. At the coarse stage, the sync

detection performance is more emphasized than the coarse timing estimation. In fact, the sync detection metric is also used for the timing metric at the coarse timing estimation. Based on the repetitive structure of the training symbol mandated in the sync detection, an approximation to a minimum variance unbiased estimator (MVU) of the frequency offset is derived for the coarse frequency estimation. Then, using the repetitive training structure (not a necessity) and the coarse timing and frequency offset estimates, a channel estimation is developed. The resolution of the timing offset ambiguity involved in this channel estimation is also described. Finally, the ML realization of the fine timing and frequency offset estimation is performed.

The rest of the chapter is organized as follows. Section 6.1 describes the system considered and Section 6.2 details the proposed ML-based synchronization and channel estimation. Performance analyses of the frequency estimation and the channel estimation are presented in Section 6.3. Simulation results are discussed in Section 6.4, and conclusions are given in Section 6.5.

6.1 System Description

The complex baseband samples of an OFDM symbol, at the sampling rate of N times subcarrier spacing, can be given by

$$s(k) = \frac{1}{\sqrt{N}} \sum_{n=0}^{N-1} c_n \, exp(j2\pi kn/N), \quad -N_g \leq k \leq N-1 \tag{6.1}$$

where c_n is modulated data (zeros for null sub-carriers), N is the number of inverse Fast Fourier Transform (IFFT) points (same as the total number of sub-carriers), N_g is the number of guard samples and $j = \sqrt{-1}$. Consider a frequency selective multipath fading channel characterized by

$$h(k) = \sum_{l=0}^{K-1} h_l \, \delta(k - \tau_l) \tag{6.2}$$

where $\delta(k)$ represents the Dirac-Delta function, $\{h_l\}$ the complex path gains of the channel (including the filters' responses), $\{\tau_l\}$ the path time delays which are assumed in multiple of OFDM samples, and K the total number of paths. Here, we suppress the time dependence notation of the channel response for simplicity. Assuming perfect

sampling clock and no oscillator phase noise, the received sample in the presence of a carrier frequency offset can be given by

$$\begin{aligned} r(k) &= exp(j\phi)\, exp(j2\pi kv/N) \sum_{l=0}^{K-1} h_l s(k-\tau_l) + n(k) \\ &\triangleq exp(j\phi)\, exp(j2\pi kv/N)\; x(k) + n(k) \end{aligned} \tag{6.3}$$

where v is the carrier frequency offset normalized by the subcarrier spacing, ϕ is a carrier phase factor, and $\{n(k)\}$ are independent and identically distributed samples of zero mean complex white Gaussian noise process with variance σ_n^2.

Let us define the following for a training symbol with N_g samples of cyclic prefix part and $(\beta+1)$ samples of the useful part:

$$\begin{aligned} \boldsymbol{r}_\gamma(k) &\triangleq [r(k-\gamma)\; r(k-\gamma+1)\; \ldots\; r(k+\beta)]^T \\ \boldsymbol{h} &\triangleq [h(0)\; h(1)\; \ldots\; h(K-1)]^T \\ \boldsymbol{W}_\gamma(v,k) &\triangleq diag\{e^{j2\pi(k-\gamma)v/N}, e^{j2\pi(k-\gamma+1)v/N}, \ldots, e^{j2\pi(k+\beta)v/N}\} \\ &= e^{j2\pi kv/N}\, \boldsymbol{W}(v,0) \\ \boldsymbol{n}_\gamma(k) &\triangleq [n(k-\gamma)\; n(k-\gamma+1)\; \ldots\; n(k+\beta)]^T \\ \boldsymbol{S}_\gamma(k) &\triangleq \begin{bmatrix} s(k-\gamma) & s(k-\gamma-1) & \ldots & s(k-\gamma-K+1) \\ s(k-\gamma+1) & s(k-\gamma) & \ldots & s(k-\gamma-K+2) \\ \ddots & & & \\ s(k+\beta) & s(k+\beta-1) & \ldots & s(k+\beta-K+1) \end{bmatrix} \end{aligned} \tag{6.4}$$

where γ is an integer given by $0 \le \gamma \le N_g - K + 1$.

Then, the $(\gamma+\beta+1)$ length received samples vector, $\boldsymbol{r}_\gamma(k)$, can be given by

$$\boldsymbol{r}_\gamma(k) = e^{j\phi}\, e^{j2\pi kv/N} \boldsymbol{W}_\gamma(v) \cdot \boldsymbol{S}_\gamma(k) \cdot \boldsymbol{h} + \boldsymbol{n}_\gamma(k) \tag{6.5}$$

where $\boldsymbol{W}_\gamma(v) \triangleq \boldsymbol{W}_\gamma(v,0)$. In the following, $\gamma = N_g - K + 1$ (which corresponds to the maximum ISI-free received samples length of $(N_g - K + 2 + \beta)$ samples) will be used and the subscript γ will be omitted for notational simplicity but wherever the other value is used, the subscript will be included.

6.2 Maximum Likelihood-based Synchronization and Channel Estimation

In OFDM systems, the main synchronization parameters to be estimated are the sync flag indicating the presence of the signal (especially for burst mode transmission), the starting time of the FFT window (timing synchronization), the frequency offset due to the inaccuracies of the transmitter and receiver oscillators and the Dopplar shift of the mobile channel, and the channel estimates if coherent reception is adopted. The sync flag can be generated by automatic gain control (e.g., ramp-up indication via power measurement and threshold decision) [81] or using a training symbol (which can also be used for timing synchronization and possibly frequency synchronization). For the latter case, the same metric which will be used for timing synchronization may be used together with the threshold decision to indicate the sync flag. After detecting the presence of the signal, the rest of the sync parameters are estimated.

Assume that an OFDM training symbol, defined by $\boldsymbol{S} \triangleq \boldsymbol{S}(0)$, is used for synchronization. Then, for given parameters $(\boldsymbol{h}, \phi, v)$, the received vector $\boldsymbol{r}(0)$ is Gaussian with mean $e^{j\phi}\ \boldsymbol{W}(v) \cdot \boldsymbol{S} \cdot \boldsymbol{h}$ and covariance matrix $\sigma_n^2 \boldsymbol{I}_{N'}$ where $\boldsymbol{I}_{N'}$ is an $N' \times N'$ identity matrix with $N' = \gamma + \beta + 1$. Then the likelihood function for a received vector $\boldsymbol{r}(\varepsilon)$ and parameters $(\boldsymbol{h}, \phi, v)$, given that the training symbol defined by $\boldsymbol{S}$ is transmitted, is

$$\Lambda(\boldsymbol{r}(\tilde{\varepsilon}); \boldsymbol{h}, \phi, \tilde{\varepsilon}, \tilde{v}|\boldsymbol{S}) = \frac{1}{(\pi\sigma_n^2)^{N'}} \cdot exp\{-\frac{1}{\sigma_n^2}[\boldsymbol{r}(\tilde{\varepsilon}) - e^{j\phi}\ \boldsymbol{W}(\tilde{v})\boldsymbol{S}\boldsymbol{h}]^H[\boldsymbol{r}(\tilde{\varepsilon}) - e^{j\phi}\ \boldsymbol{W}(\tilde{v})\boldsymbol{S}\boldsymbol{h}]\} \tag{6.6}$$

where $\tilde{v}$ and $\tilde{\varepsilon}$ are trial values of v and ε and $(\ )^H$ represents Hermitian Transpose operation. For notational simplicity, the conditional expression, $|\boldsymbol{S}$, will be omitted in the following. Maximizing the above likelihood function is equivalent to minimizing the metric

$$\begin{aligned} \mathcal{V}(\boldsymbol{r}(\tilde{\varepsilon}); \boldsymbol{h}, \phi, \tilde{\varepsilon}, \tilde{v}) &= [\boldsymbol{r}(\tilde{\varepsilon}) - e^{j\phi}\ \boldsymbol{W}(\tilde{v})\boldsymbol{S}\boldsymbol{h}]^H[\boldsymbol{r}(\tilde{\varepsilon}) - e^{j\phi}\ \boldsymbol{W}(\tilde{v})\boldsymbol{S}\boldsymbol{h}] \\ &= \boldsymbol{r}^H(\tilde{\varepsilon})\boldsymbol{r}(\tilde{\varepsilon}) - 2 \cdot Re[\boldsymbol{r}^H(\tilde{\varepsilon})\boldsymbol{W}(\tilde{v})\boldsymbol{S}\boldsymbol{h}\ e^{j\phi}] + \boldsymbol{h}^H\boldsymbol{S}^H\boldsymbol{S}\boldsymbol{h} \end{aligned} \tag{6.7}$$

where $Re[\ ]$ indicates the real part.

The ML estimates of the timing point and the normalized carrier frequency offset, denoted by ε and $\hat{v}$ respectively, are then given by

$$(\varepsilon, \hat{v})_{ML} = argmin_{\tilde{\varepsilon},\tilde{v}} \mathcal{V}(\boldsymbol{r}(\tilde{\varepsilon}); \boldsymbol{h}, \phi, \tilde{\varepsilon}, \tilde{v}). \tag{6.8}$$

For a given set of parameters $(\boldsymbol{h}, \phi, \tilde{\varepsilon})$, and by removing the constant terms, the following metric to be minimized is obtained

$$\mathcal{V}_{|(\boldsymbol{h},\phi,\tilde{\varepsilon})}(\boldsymbol{r}(\tilde{\varepsilon}); \tilde{v}) \triangleq -2 \cdot Re[\boldsymbol{r}^H(\tilde{\varepsilon}) \boldsymbol{W}(\tilde{v}) \boldsymbol{S} \boldsymbol{h}\ e^{j\phi}]. \tag{6.9}$$

For a given $\tilde{\varepsilon}$, the metric to be minimized can be given by

$$\mathcal{V}_{|\tilde{\varepsilon}}(\boldsymbol{r}(\tilde{\varepsilon}); \boldsymbol{h}, \phi, \tilde{v}) \triangleq \mathcal{V}_{|(\boldsymbol{h},\phi,\tilde{\varepsilon})}(\boldsymbol{r}(\tilde{\varepsilon}); \tilde{v}) + \boldsymbol{h}^H \boldsymbol{S}^H \boldsymbol{S} \boldsymbol{h}. \tag{6.10}$$

Similarly, for a given pair $(\boldsymbol{h}, \phi)$, the metric to be minimized can be given by

$$\mathcal{V}_{|(\boldsymbol{h},\phi)}(\boldsymbol{r}(\tilde{\varepsilon}); \tilde{\varepsilon}, \tilde{v}) \triangleq \boldsymbol{r}^H(\tilde{\varepsilon})\ \boldsymbol{r}(\tilde{\varepsilon}) + \mathcal{V}_{|(\boldsymbol{h},\phi,\tilde{\varepsilon})}(\boldsymbol{r}(\tilde{\varepsilon}); \tilde{v}). \tag{6.11}$$

Hence, (6.7) can be expressed as

$$\mathcal{V}(\boldsymbol{r}(\tilde{\varepsilon}); \boldsymbol{h}, \phi, \tilde{\varepsilon}, \tilde{v}) = \mathcal{V}_{|(\boldsymbol{h},\phi)}(\boldsymbol{r}(\tilde{\varepsilon}); \tilde{\varepsilon}, \tilde{v}) + \boldsymbol{h}^H \boldsymbol{S}^H \boldsymbol{S} \boldsymbol{h}. \tag{6.12}$$

The above ML estimator is unfortunately unrealizable since $\boldsymbol{h}$ and ϕ are unknown. Hence, we consider to replace $\boldsymbol{h}$ and ϕ in (6.7) with their estimates. In order to get the estimate of $\boldsymbol{h}\ e^{j\phi}$, we first perform coarse timing and frequency estimation. In fact, the coarse timing point can be obtained from the sync detection stage and the coarse frequency estimation is then performed based on the received vector defined by the coarse timing estimate. In the following, we describe the sync detection and the coarse timing and frequency estimation which facilitate the ML realization in the fine stage.

6.2.1 Sync Detection

The first synchronization task is to detect the presence of the training symbol, especially for the burst transmission. The sync detection metric value for the training symbol should be quite distinct from the value of the noise or other data symbols. From (6.5), it is noted that the observation vector is Gaussian with mean $\boldsymbol{W}(v) \cdot \boldsymbol{S} \cdot \boldsymbol{h}\ e^{j\phi}$

and covariance matrix $\sigma_n^2 \boldsymbol{I}_{N'}$ for the training symbol, with zero mean and covariance matrix $\sigma_n^2 \boldsymbol{I}_{N'}$ for the noise, and with zero mean and covariance matrix $(\sigma_s^2 + \sigma_n^2)\boldsymbol{I}_{N'}$ (approximately) for data symbols where $\sigma_s^2 \triangleq \frac{1}{N}\sum_{k=0}^{N-1} |s(k)|^2$, (here, {s(k)} represent data samples). However, since $\boldsymbol{h}$, ϕ, and v are unknown, the mean or covariance of the observation vector cannot be used for the metric. Hence, we look into another property of the observation vector which is well distinctive between the training symbol and the other cases. Let us define the following normalized autocorrelation function

$$C(\boldsymbol{r}(k), d) \triangleq \frac{N'}{(N'-d)\ \boldsymbol{r}^H(k) \cdot \boldsymbol{r}(k)} \left| \sum_{i=-\gamma}^{\beta-d} r^*(k+i) \cdot r(k+d+i) \right|. \tag{6.13}$$

It can be observed that (6.13) is independent of v due to the absolute value operation, independent of ϕ due to the conjugate correlation, and quite robust against the channel (i.e., regardless of whether in deep fade or not) due to the normalization. The mean of $C(\boldsymbol{r}(k), d)$ would be approximately close to zero for the noise or the data symbol due to the uncorrelation among the samples. On the other hand, we can design the training symbol to maximize the mean of $C(\boldsymbol{r}(k), d)$. If the received training samples under no noise condition are such that $[r(-\gamma), r(-\gamma+1), \ldots, r(\beta-d)] = [r(-\gamma+d), r(-\gamma+d+1), \ldots, r(\beta)]$, then $C(\boldsymbol{r}(k), d)$ would be maximum with unity value. This condition requires that $[s(-N_g), s(-N_g+1), \ldots, s(\beta-d)] = [s(-N_g+d), s(-N_g+d+1), \ldots, s(\beta)]$. It can be obtained if the training symbol contains multiple identical parts and d is set to the length of one part. Because of this repetitive structure of the training symbol, (6.13) gives a well distinctive metric between the training symbol and the other cases, and hence, can now be used as the sync detection metric. If the metric value reaches above a threshold, the sync flag is declared. The threshold value is usually set by the required sync detection performance, namely the missed detection probability and the false detection probability. In practice, $C^2(\boldsymbol{r}(k), d)$ instead of $C(\boldsymbol{r}(k), d)$ may be considered.

6.2.2 Coarse timing and frequency estimation

After detecting the sync flag, the coarse timing point may be taken as the sync detected point (the point that has triggered the sync flag). Alternatively, the coarse timing point can be taken as the one that has maximum sync detection metric within

a time window starting from the sync detected point. The latter approach would give a more accurate coarse timing point due to the more reliable metric value. In a multipath channel environment, due to dispersion, the coarse timing point may be at some delay with respect to the actual point and can cause ISI in the synchronization tasks to be performed afterwards. In order to prevent this, the coarse timing point can be advanced by some amount λ_c (> 0) . After obtaining the coarse timing point ε_c, coarse normalized frequency offset estimation is pursued as follows.

Since there will be some timing offset, the coarse frequency offset estimation should be robust against the timing offset. Moreover, its robustness against the channel is also desirable. The repetitive training structure used in the sync detection inherently provides these robustness properties. Assume that the training symbol has $P+1$ identical parts with M samples in each part; the first one with the time indexes $[-M, -M+1, \ldots, -1]$ might be thought of as the cyclic prefix part for the training symbol. Suppose the coarse timing point is within $[-M+K-1, -M+K, \ldots, 0]$. Define a new observation variable:

$$\begin{aligned} u(k) &\triangleq \sum_{p=0}^{P-2} r^*(k+p\cdot M)\cdot r(k+p\cdot M+M) \\ &= e^{j2\pi vM/N}\ (P-1)\ |x(k)|^2 + w(k) \end{aligned} \tag{6.14}$$

where $w(k)$ is a zero mean noise term with variance $\sigma_u^2(k)$, and the mean and variance of $u(k)$ are given by

$$\mu_u(k) = e^{j2\pi vM/N}\ (P-1)|x(k)|^2 \tag{6.15}$$

$$\sigma_u^2(k) = (P-1)(2|x(k)|^2\sigma_n^2 + \sigma_n^4). \tag{6.16}$$

Then, we have a new observation vector

$$\boldsymbol{u} = |\boldsymbol{\mu}|\ \theta + \boldsymbol{w} \tag{6.17}$$

where

$$\begin{aligned} \boldsymbol{u} &= [u(0), u(1), \ldots, u(M-1)]^T \\ \boldsymbol{\mu} &= [\mu_u(0), \mu_u(1), \ldots, \mu_u(M-1)]^T \\ \boldsymbol{w} &= [w(0), w(1), \ldots, w(M-1)]^T \\ \theta &= e^{j2\pi vM/N}. \end{aligned} \tag{6.18}$$

The vector $\boldsymbol{u}$ can be approximated as Gaussian with mean $\boldsymbol{\mu}$ and covariance matrix $\boldsymbol{C_u} \triangleq diag\{\sigma_u^2(0), \sigma_u^2(1), \ldots, \sigma_u^2(M-1)\}$. Then, the minimum variance unbiased estimator (MVU) of θ can be given by [55],

$$\hat{\theta} = (|\boldsymbol{\mu}|^H \boldsymbol{C_u^{-1}} |\boldsymbol{\mu}|)^{-1} (|\boldsymbol{\mu}|^H \boldsymbol{C_u^{-1}} \boldsymbol{u}) \tag{6.19}$$

and the estimate of v is obtained by

$$\begin{aligned} \hat{v} &= \frac{N}{2\pi M} arg\{ \hat{\theta} \} \\ &= \frac{N}{2\pi M} arg\{ \sum_{k=0}^{M-1} \frac{|x(k)|^2}{2\,|x(k)|^2 + \sigma_n^2} u(k) \}. \end{aligned} \tag{6.20}$$

At this point, since we do not have any knowledge of $x(k)$ and σ_n^2, resorting to a high SNR approximation gives rise to the following estimator

$$\hat{v}_c = \frac{N}{2\pi M} arg\{ \sum_{k=0}^{M-1} u(k) \} \tag{6.21}$$

which will be used as a coarse normalized frequency offset estimation. From (6.21), the acquisition range of the frequency estimation is $-\frac{N}{2M} < \hat{v}_c \leq \frac{N}{2M}$. Depending on the oscillator behavior and the channel environment, M can be designed to handle the possible maximum frequency offset.

6.2.3 Fine timing and frequency estimation

After obtaining a coarse timing estimate ε_c and a coarse normalized frequency offset estimate $\hat{v}_c$, the ML estimates $(\varepsilon, \hat{v})_{|(\varepsilon_c, \hat{v}_c)}$ which is based on $(\varepsilon_c, \hat{v}_c)$ can be obtained from (6.8) as

$$\begin{aligned} (\varepsilon, \hat{v})_{|(\varepsilon_c, \hat{v}_c)} &= argmin_{(\tilde{\varepsilon}, \tilde{v})} \{ \mathcal{V}(\boldsymbol{r}(\tilde{\varepsilon}); \boldsymbol{h}, \phi, \tilde{\varepsilon}, \tilde{v}) \\ &\quad : \varepsilon_c - T_1 \leq \tilde{\varepsilon} \leq \varepsilon_c + T_2,\ \hat{v}_c - F_1 \leq \tilde{v} \leq \hat{v}_c + F_2 \}. \end{aligned} \tag{6.22}$$

Here, the search space is limited to $\varepsilon_c - T_1 \leq \tilde{\varepsilon} \leq \varepsilon_c + T_2$ and $\hat{v}_c - F_1 \leq \tilde{v} \leq \hat{v}_c + F_2$ since ε_c and $\hat{v}_c$ cannot be too much far away from the correct values 0 and v. It also reduces the algorithm's complexity.

A simple implementation of (6.22) is to first find $\tilde{v}$ that minimizes the metric for each $\tilde{\varepsilon}$, denoted by $\hat{v}_{|\tilde{\varepsilon}}$, and then choose the pair $(\tilde{\varepsilon}, \hat{v}_{|\tilde{\varepsilon}})$ that has minimum metric,

which is denoted by $\mathcal{V}_{(\varepsilon_c,\hat{v}_c)}$. The details are given below. Using (6.9), an ML estimate of v for a trial timing point $\tilde{\varepsilon}$ is obtained as

$$\hat{v}_{|\tilde{\varepsilon}} = argmin_{\tilde{v}}\{\mathcal{V}_{|(\boldsymbol{h},\phi,\tilde{\varepsilon})}(\boldsymbol{r}(\tilde{\varepsilon});\tilde{v}) \ : \hat{v}_c - F_1 \leq \tilde{v} \leq \hat{v}_c + F_2\} \tag{6.23}$$

with the corresponding minimum metric $\mathcal{V}_{|(\boldsymbol{h},\phi,\tilde{\varepsilon})}(\boldsymbol{r}(\tilde{\varepsilon});\hat{v}_{|\tilde{\varepsilon}})$. Then, using (6.11), an ML estimate of the timing point is obtained as

$$\varepsilon_f = argmin_{\tilde{\varepsilon}}\{\mathcal{V}_{|(\boldsymbol{h},\phi)}(\boldsymbol{r}(\tilde{\varepsilon});\tilde{\varepsilon},\hat{v}_{|\tilde{\varepsilon}}) \ : \varepsilon_c - T_1 \leq \tilde{\varepsilon} \leq \varepsilon_c + T_2\} \tag{6.24}$$

and hence, the fine estimates are given by $(\varepsilon_f, \hat{v}_f)$ with $\hat{v}_f = \hat{v}_{|\varepsilon_f}$. In the following, the required estimation of both the channel impulse response and the carrier phase factor for ML realization is pursued.

At the correct sync parameters $\varepsilon = 0$ and v, the received vector $\boldsymbol{r}(0)$ is Gaussian with mean $\boldsymbol{W}(v)\boldsymbol{S}\boldsymbol{h}\ e^{j\phi}$ and covariance matrix $\sigma_n^2\boldsymbol{I}_{N'}$. Let us consider that the channel response includes the carrier phase factor. Define $\hbar \triangleq \boldsymbol{h}\ e^{j\phi}$. The ML estimator (also MVU, [55]) of $\hbar$ is then given by

$$\hat{\hbar}_{ML} = (\boldsymbol{S}^H\boldsymbol{S})^{-1}\boldsymbol{S}^H\boldsymbol{W}^H(v)\boldsymbol{r}(0). \tag{6.25}$$

Since v and $\boldsymbol{r}(0)$ are unknown, one possible approach for a realizable ML estimator of (6.22) is to estimate $\hbar$ by (6.25) with $\boldsymbol{r}(0)$ and v replaced by a received vector $\boldsymbol{r}(\varepsilon)$ and a frequency estimate $\hat{v}$, respectively, which are obtained in the coarse synchronization stage. In this case, in order to avoid the inclusion of non-training samples in the observed received vector $\boldsymbol{r}_\gamma(\varepsilon)$, $\gamma = 0$ would be used since it allows some timing offset. Then,

$$\begin{aligned}\hat{\hbar} &= (\boldsymbol{S}_0^H\boldsymbol{S}_0)^{-1}\boldsymbol{S}_0^H\boldsymbol{W}_0^H(\hat{v})\boldsymbol{r}_0(\varepsilon) \\ &= (\boldsymbol{S}_0^H\boldsymbol{S}_0)^{-1}\boldsymbol{S}_0^H\boldsymbol{W}_0^H(\hat{v})e^{j2\pi\varepsilon v/N}\boldsymbol{W}_0(v)\boldsymbol{S}_0(\varepsilon)\hbar + \boldsymbol{n}_h\end{aligned} \tag{6.26}$$

where $\boldsymbol{n}_h = (\boldsymbol{S}_0^H\boldsymbol{S}_0)^{-1}\boldsymbol{S}_0^H\boldsymbol{W}_0^H(\hat{v})\boldsymbol{n}_0$. Observing the above equation reveals that even if $\hat{v} = v$, the mean of $\hat{\hbar}$ turns out to be

$$E[\hat{\hbar}] = e^{j2\pi\varepsilon\hat{v}/N}(\boldsymbol{S}_0^H\boldsymbol{S}_0)^{-1}\boldsymbol{S}_0^H\boldsymbol{S}_0(\varepsilon)\hbar \tag{6.27}$$

which is not unbiased unless $\varepsilon = 0$. To circumvent this, we propose the following channel estimation. First, define the following

$$\boldsymbol{S}(k) \triangleq \begin{bmatrix} s(k) & s(k-1) & \dots & s(k-K+1-K_1) \\ s(k+1) & s(k) & \dots & s(k-K+2-K_1) \\ \ddots & & & \\ s(k+N-1) & s(k+N-2) & \dots & s(k+N-K-K_1) \end{bmatrix} \tag{6.28}$$

$$\boldsymbol{g} \triangleq [\hbar^T, \mathbf{0}_{1\times K_1}]^T \tag{6.29}$$

where $\mathbf{0}_{1\times K_1}$ is an all zero row vector of length K_1 and $N = \beta + 1$. Then, we can observe that $\boldsymbol{S}_0(\varepsilon)\hbar = \boldsymbol{S}(\varepsilon)\boldsymbol{g}$. Consequently, $\boldsymbol{r}_0(\varepsilon)$ can now be expressed as

$$\boldsymbol{r}_0(\varepsilon) = e^{j2\pi\varepsilon v/N}\boldsymbol{W}_0(v)\cdot\boldsymbol{S}(\varepsilon)\cdot\boldsymbol{g} + \boldsymbol{n}_0(\varepsilon). \tag{6.30}$$

From the definitions of (6.28) and (6.29), the following equality is observed, for $-K_1 \le \varepsilon \le 0$,

$$\boldsymbol{S}(\varepsilon)\boldsymbol{g} = \boldsymbol{S}(0)\ \mathcal{I}(\varepsilon)\ \boldsymbol{g} \tag{6.31}$$

where $\mathcal{I}(\varepsilon)$ is a $(K+K_1)\times(K+K_1)$ unitary matrix whose elements are given by $[\mathcal{I}(\varepsilon)]_{i,j} = [\boldsymbol{I}]_{(i+\varepsilon)mod\ N,j}$ with $\boldsymbol{I}$ being an $(K+K_1)\times(K+K_1)$ identity matrix. In the following, $\boldsymbol{S}(0)$ will be denoted by $\boldsymbol{S}$. It is noted that $\mathcal{I}(\varepsilon)\boldsymbol{g}$ is just a cyclically shifted version of $\boldsymbol{g}$. Substituting (6.31) into $\boldsymbol{r}_0$ and applying the ML principle, at the correct sync parameters ($\varepsilon = 0, \hat{v} = v$), result in

$$\hat{\boldsymbol{g}}(0,v) = (\boldsymbol{S}^H\boldsymbol{S})^{-1}\boldsymbol{S}^H\boldsymbol{W}_0^H(v)\boldsymbol{r}_0(0). \tag{6.32}$$

Applying (6.32) for $\boldsymbol{r}_0(\varepsilon_c)$ with v replaced by $\hat{v}_c$ gives

$$\hat{\boldsymbol{g}}(\varepsilon_c,\hat{v}_c) = (\boldsymbol{S}^H\boldsymbol{S})^{-1}\boldsymbol{S}^H\boldsymbol{W}_0^H(\hat{v}_c)\boldsymbol{r}_0(\varepsilon_c). \tag{6.33}$$

The mean of the above estimator, if $\hat{v}_c = v$, is

$$E[\hat{\boldsymbol{g}}(\varepsilon_c,\hat{v}_c)] = e^{j2\pi\varepsilon_c\hat{v}_c/N}\ \mathcal{I}(\varepsilon_c)\ \boldsymbol{g}. \tag{6.34}$$

From the above equation, we can observe that $\boldsymbol{g}$ can be estimated if ε_c and $\hat{v}_c$ are known. Since we have $\hat{v}_c$ from the coarse synchronization stage, using an estimate $\hat{\varepsilon}_c$ for ε_c results in an estimate of $\boldsymbol{g}$ based on the pair $(\varepsilon_c, \hat{v}_c)$ as follows:

$$\hat{\boldsymbol{g}}_{|(\varepsilon_c,\hat{v}_c)} = e^{-j2\pi\hat{\varepsilon}_c\hat{v}_c/N}\boldsymbol{\mathcal{I}}^H(\hat{\varepsilon}_c)\hat{\boldsymbol{g}}(\varepsilon_c, \hat{v}_c). \tag{6.35}$$

Let $\{\hat{g}(i) : i = 0, 1, \ldots, K+K_1-1\}$ and $\{\hat{g}_c(i) : i = 0, 1, \ldots, K+K_1-1\}$ denote the elements of $\hat{\boldsymbol{g}}_{|(\varepsilon_c,\hat{v}_c)}$ and $\hat{\boldsymbol{g}}(\varepsilon_c, \hat{v}_c)$, respectively. Then, from (6.29), we obtain a channel response estimate together with the carrier phase factor based on the pair $(\varepsilon_c, \hat{v}_c)$ as

$$\hat{\boldsymbol{h}}(\varepsilon_c, \hat{v}_c) = [\hat{g}(0), \hat{g}(1), \ldots, \hat{g}(K-1)]^T. \tag{6.36}$$

The estimate $\hat{\varepsilon}_c$ required in (6.35) can be obtained as

$$\hat{\varepsilon}_c = argmax_l\{E_h(l, \varepsilon_c) : \ l = 0, -1, \ldots, -K_1\} \tag{6.37}$$

where

$$E_h(l, \varepsilon_c) = \begin{cases} \sum_{k=0}^{K-1} |\hat{g}_c((-l+k)_{mod\ (K+K_1)})|^2 & \text{if } |\hat{g}_c(-l)| > \eta \cdot max_i\{|\hat{g}_c(i)|\} \\ 0 & \text{otherwise .} \end{cases} \tag{6.38}$$

Here, η is a threshold parameter for selecting the first tap of the channel impulse response. This first channel tap selection assumes that the absolute ratio of the first channel tap gain to the maximum channel tap gain is greater than η. If the first channel tap gain is very small, it will not be included in the estimated channel impulse response and there will be no significant impact on the receiver performance since this tap will not be distinct from the noise. Larger value of η will increase the probability of missing the first (and possibly more) channel tap(s) in the channel estimate. On the other hand, smaller value of η will increase the probability of wrongly picking up one of the noise samples preceeding the actual first channel tap as the estimated first channel tap. Details on the setting of η value is described in the Appendix A.

The above channel estimation is valid for $-K_1 \leq \varepsilon \leq 0$ since (6.31) is only valid for this range. From (6.28), the valid maximum value for K_1 is $N_g - K + 1$, or the allowable timing offset is $-Ng + K - 1 \leq \varepsilon \leq 0$, provided that $(\boldsymbol{\mathcal{S}}^H\boldsymbol{\mathcal{S}})$ is

invertible. Strictly speaking, this allowable timing offset range can be extended to $-N_g + K - 1 - a \leq \varepsilon \leq 0$ by using a received vector of accordingly reduced length $\beta+1-a$ and the $(\beta+1-a)\times(N_g+1+a)$ matrix $\boldsymbol{\mathcal{S}}$ in the place of length $(\beta+1)$ received vector and $(\beta+1)\times(N_g+1)$ size matrix $\boldsymbol{\mathcal{S}}$, provided that $(\boldsymbol{\mathcal{S}}^H\boldsymbol{\mathcal{S}})$ is invertible. This will be violated if the samples $\{s(k)\}$ are composed of identical parts and repeated within $N_g - K + 1 + a$ length.

In wireless LAN standards such as IEEE 802.11(a), HiperLAN 2, or MMAC, where OFDM is adopted, training preambles with repetitive parts are used and hence, for this type of training preamble the above extension is not possible and the allowable timing offset for the channel estimation is reduced to $-Ng + K \leq \varepsilon \leq 0$. Since the repetitive structure provides a robust sync detection and facilitates simple coarse timing and frequency synchronization, we also use the training symbol with repetitive parts. Particularly, we consider a training preamble consisting of $(P + 1)$ identical parts; each part contains N_g samples (i.e., $\beta = P \cdot N_g - 1$). The first part can be considered as the cyclic prefix part and the rest as the useful part of the training symbol, in analogy to a normal OFDM data symbol. Now, with $K_1 = N_g - K$ and the repetitive parts in mind, we have

$$\boldsymbol{\mathcal{S}}(\varepsilon) = \boldsymbol{\mathcal{S}}\boldsymbol{\mathcal{I}}(\varepsilon) \tag{6.39}$$

and hence, (6.33) and (6.34) still hold exactly for $-N_g + K - 1 \leq \varepsilon \leq 0$ and approximately for $-N_g + K - 1 - K_2 \leq \varepsilon \leq -N_g + K - 2$ and $1 \leq \varepsilon \leq K_3$, for small $K_2, K_3 > 0$. The approximity is due to the inclusion of non-training samples in the vector $\boldsymbol{r}_0(\varepsilon)$. Note that in (6.31), the equality (6.39) does not hold.

Let $-N_g+K-1-K_2 \triangleq -K_4$. Since (6.33) produces a cyclically shifted version of a length N_g vector $\hat{\boldsymbol{g}}$, the allowable timing offset for the channel estimation is limited to $-K_4 \leq \varepsilon \leq K_3$ where $K_3 + K_4 + 1 = N_g$. (6.37) now becomes

$$\hat{\varepsilon}_c = \begin{cases} l_{max} & \text{if } l_{max} \geq -K_4 \\ N_g + l_{max} & \text{otherwise} \end{cases} \tag{6.40}$$

where

$$l_{max} \triangleq argmax_l\{E_h(l, \varepsilon_c) \ : l = 0, -1, \ldots, -N_g + 1\} \tag{6.41}$$

and together with (6.35), (6.36), (6.23) and (6.24), ML estimation (6.22) can now be realized for $-K_4 \leq \varepsilon_c \leq K_3$.

If $\varepsilon_c < -K_4$, the required channel estimate $\hat{\boldsymbol{h}}_{req}(\varepsilon_c, \hat{v}_c)$ for the realization of (6.22) is given by (6.36) and (6.35) with $\hat{\varepsilon}_c$ replaced by l_{max}. However, due to the ambiguity, $\hat{\varepsilon}_c$ will be $N_g + l_{max}$ and consequently the estimated channel response would be $\hat{\boldsymbol{h}}(\varepsilon_c, \hat{v}_c) = \hat{\boldsymbol{h}}_{req}(\varepsilon_c, \hat{v}_c)\, e^{-j2\pi N_g \hat{v}_c/N}$ under no noise condition. Then, (6.22) would quite likely give a timing point around $-N_g$ due to the extra factor $e^{-j2\pi N_g \hat{v}_c/N}$ contained in the channel estimate. Similarly, if $\varepsilon > K_3$, (6.22) would quite likely give a timing point around N_g.

To solve this ambiguity problem, we consider three candidates for coarse timing estimation, namely, $\{\varepsilon_i \ : i = -1, 0, 1\}$ with $\varepsilon_i = \varepsilon_c + i \cdot N_g$. If $\varepsilon_c < -K_4$, although $\hat{\boldsymbol{h}}(\varepsilon_0, \hat{v}_c)$ would not be the proper estimate required for (6.22), $\hat{\boldsymbol{h}}(\varepsilon_1, \hat{v}_c)$ would be the proper one since ε_1 is within the allowable range. Similarly, if $\varepsilon_c > K_3$, $\hat{\boldsymbol{h}}(\varepsilon_{-1}, \hat{v}_c)$ would be the proper one. For each set $(\varepsilon_i, \hat{v}_c)$, realizing (6.22) results in a candidate set of fine estimates $(\varepsilon_f, \hat{v}_f)_i$ together with the corresponding minimum metric $\mathcal{V}_{(\varepsilon_i, \hat{v}_c)}$. The fine estimates are then obtained as

$$(\varepsilon_f, \hat{v}_f) = argmin_{(\varepsilon_f, \hat{v}_f)_i} \{\mathcal{V}_{(\varepsilon_i, \hat{v}_c)} : i = -1, 0, 1\}. \tag{6.42}$$

Since each candidate ε_i can produce a proper channel estimate if it is within the allowable range, the search window of $\tilde{\varepsilon}$ can be set such that $T_1 = K_3$ and $T_2 = K_4$. By this ambiguity resolution, the allowable coarse timing offset range for realization of (6.22) is extended to $-N_g - K_4 \leq \varepsilon \leq N_g + K_3$ which is usually more than sufficient for the SNR of interest.

After obtaining ε_f and $\hat{v}_f$, fine estimation stage can be iterated for further improvement. At this time, ambiguity resolution will no longer be required. And in those equations used, ε_c and $\hat{v}_c$ will be replaced by ε_f and $\hat{v}_f$ obtained in the previous iteration. The final estimates can be taken from the last iteration or from the iteration with minimum metric among the implemented iterations.

In the following, we describe the fine frequency offset estimation or the implementation of (6.23). Define $\hat{\boldsymbol{r}}_{ref} \triangleq \boldsymbol{S}\hat{\boldsymbol{h}}$ whose elements are denoted as $\{\hat{r}_{ref}(k)\}$, where $\hat{\boldsymbol{h}}$ is obtained from (6.36) used in the chosen set among $\{\varepsilon_i, \hat{v}_c\}$ (or, if at further iteration of the fine synchronization, it is obtained from (6.36) with previous ε_f and $\hat{v}_f$). Then,

(6.9) can be realized as

$$\mathcal{V}_{|(\tilde{h},\tilde{\varepsilon})}(\boldsymbol{r}(\tilde{\varepsilon});\tilde{v}) = -2 \cdot Re[\sum_{k=-\gamma}^{\beta} q(k)\ e^{-j2\pi\tilde{v}k/N}] \tag{6.43}$$

where $q(k) \triangleq \hat{r}^*_{ref}(k)\ r(\tilde{\varepsilon}+k)$.

After obtaining $\{q(k)\}$ for a trial point $\tilde{\varepsilon}$, (6.23) is implemented in an iterative way using (6.43) as follows.

$$\begin{aligned}
&F_1 = F_2;\ \hat{v}_0 = \hat{v}_c;\ \Delta_0 = F_1/J_1 \\
&\text{for } i = 1:1:J_2 \\
&\qquad \tilde{v}_k = \hat{v}_{i-1} + k \cdot \Delta_{i-1} \\
&\qquad \hat{v}_i = argmin_{\tilde{v}_k}\{\mathcal{V}_{|(\tilde{h},\tilde{\varepsilon})}(\boldsymbol{r}(\tilde{\varepsilon});\tilde{v}_k)\ \ : k = -J_1:1:J_1\} \\
&\qquad \Delta_i = \xi \cdot \Delta_{i-1}/J_1 \\
&\text{end} \\
&\hat{v}_{|\tilde{\varepsilon}} = \hat{v}_{J_2}.
\end{aligned} \tag{6.44}$$

Depending on the coarse frequency offset estimation performance, the choice of the parameter F_1 can appropriately be set for complexity reduction. For example, if the error of $\hat{v}_c$ is much smaller than 1, which is usually the case, F_1 may be set to 0.5 or even less. The parameters (J_1, J_2, ξ) give a trade-off between the accuracy and the complexity of the estimation.

It is noted from (6.43) that (6.23) can also be implemented using FFT. In this case, a $[N \cdot \kappa]$ point FFT would give the resolution grid of $\frac{1}{\kappa}$ for $\hat{v}$. The complexity may be reduced by calculating the appropriate number of FFT output points around the point nearest to $\hat{v}_c$. In this paper, (6.44) will be used.

6.2.4 Estimation of channel frequency response

After obtaining fine estimates $(\varepsilon_f, \hat{v}_f)$, the fine timing point will be most of the time at the correct point and hence, the channel estimation performed then can be based on the $(\beta + N_g - K + 2)$ length received vector $\boldsymbol{r}$, (i.e., $\gamma = N_g - K + 1$), as follows:

$$\hat{\boldsymbol{h}}_f = (\boldsymbol{S}^H\boldsymbol{S})^{-1}\boldsymbol{S}^H\boldsymbol{W}^H(\hat{v}_f)\boldsymbol{r}(\varepsilon_f). \tag{6.45}$$

At this stage, if we have knowledge of the number of non-trivial channel taps (the taps with non-negligible energy) among the estimated K taps, the channel estimation can further be improved as follows, by using a similar approach of [48]. Let this number be $\mathcal{K}$. Then, by using the $\mathcal{K}$ largest energy taps out of K estimated taps and suppressing the other taps by setting them to zero, the noise contamination from those trivial taps can be removed.

To account for the occasional occurance of $\varepsilon_f > 0$ case, one might design the OFDM data symbol with cyclic suffix, in addition to cyclic prefix, in order to prevent ISI. Alternatively, if no cyclic suffix is used, the fine timing estimate can be advanced by some amount λ_f (> 0). In this case, $\hat{h}_f$ which is obtained above with no timing advancement can be modified as

$$\hat{h}_f(\lambda_f) = e^{-j2\pi\hat{v}_f\lambda_f/N}\,[\mathbf{0}_{1\times\lambda_f},\ \hat{h}_f^T]^T. \tag{6.46}$$

Finally, applying FFT to $\hat{h}_f(\lambda_f)$ gives the channel frequency response estimates of the subchannels.

6.2.5 Practical Considerations

In the derivation of the proposed method, perfect sampling clock is assumed. In practice, it will not be guaranteed. If the sampling clock specification is 10 parts per million (ppm), for burst mode transmission such as HiperLAN 2 where the sampling rate is 20 MHz, the symbol timing drift can be about 0.4 sample per a frame of 2 ms. However, one frame consists of many uplink and downlink user bursts, control channels, and random access channels. Hence, the sampling clock error effect can be neglected in this case. For applications where the sampling clock error effect needs to be considered, a delay-locked loop (DLL) approach of [65] can be incorporated.

The total number of channel taps K (some tap gains may be zero), which represents the maximum channel delay spread, is assumed known in the proposed method. In practice, K is replaced by a design value K' which should not be smaller than K. In OFDM systems, the guard interval is usually designed to be longer than the maximum channel delay spread. The extra part beyond the maximum channel delay spread accounts for the possible timing errors. Hence, K' can be designed based on the knowledge of the maximum channel delay spread or if such knowledge is not

available, it can be set to a value a little smaller than the guard interval. The number of most significant taps $\mathcal{K}$ used in the channel estimation is also a design value which should be chosen depending on the application environment. Most wireless mobile environments have a small number of significant channel paths. Broadcasting environment such as single frequency network can have more significant channel paths. If complexity is affordable, the number of significant paths can be estimated by the method of [80]. For instance, base station can detect it using [80] and inform it to the mobile through a broadcast or control channel.

The timing ambiguity resolution of the proposed method imposes more complexity. One way to avoid this is to use a longer training preamble so that the coarse timing point is within the ambiguity-free range and the ambiguity resolution is no longer required. Another way is to apply an adaptive ambiguity resolution where the ambiguity resolution is carried out only when the SNR of the received signal is below some threshold. As can be seen from Fig. 6.9, an indication of the received signal SNR can be obtained from the sync detection metric. Details will be discussed in Section 6.4.

6.3 Performance Analysis

In this section, the performances of the (fine) frequency estimation (6.43) and the channel estimation (6.45) are investigated.

6.3.1 Frequency estimation performance

The frequency estimation metric can be equivalently expressed as the one to maximize

$$\Lambda_{|\ (\tilde{h},\varepsilon)}(\tilde{v}) = \boldsymbol{r}^H(\varepsilon)\ \boldsymbol{W}(\tilde{v})\ \boldsymbol{S}\ \tilde{h} + \tilde{h}^H\ \boldsymbol{S}^H\ \boldsymbol{W}^H(\tilde{v})\ \boldsymbol{r}(\varepsilon). \tag{6.47}$$

The mean square error (MSE) of the frequency estimation can be expressed as

$$\mathrm{MSE}\{\hat{v}\} = \sum_k P_\varepsilon(k)\ \mathrm{MSE}\{\hat{v}_{|\ \varepsilon=k}\}\ \geq \mathrm{MSE}\{\hat{v}_{|\ \varepsilon=0}\} \tag{6.48}$$

where $P_\varepsilon(k)$ is the probability distribution of the timing offset. For moderate and high SNR, the timing estimates at the fine stage are most of the time at the correct

point (i.e., $P_\varepsilon(0) \simeq 1$) and hence, MSE$\{\hat{v}_{|\ \varepsilon=0}\}$ well-approximates MSE$\{\ \hat{v}\ \}$ and will be investigated in the following. For simplicity, $\Lambda_{|\ (\tilde{h},\varepsilon=0)}(\tilde{v})$ will be denoted by $\Lambda(\tilde{v})$.

The mean and variance of the frequency estimation can be found by the method from [82] [77] as

$$E[\hat{v}] \ \cong\ v - \frac{E[\dot{\Lambda}(v)]}{E[\ddot{\Lambda}(v)]} \tag{6.49}$$

$$var[\hat{v}] \ \cong\ \frac{E[(\dot{\Lambda}(v))^2]}{(E[\ddot{\Lambda}(v)])^2} \tag{6.50}$$

where $\dot{\Lambda}(v)$ and $\ddot{\Lambda}(v)$ are the first and second derivatives of $\Lambda(\tilde{v})$ at $\tilde{v} = v$. Let $\Delta\hbar = \hat{\hbar} - \hbar$. Using (6.50) and assuming that $E[\Delta\hbar(k)] = 0$ and $var[\Delta\hbar(k)] = \sigma^2_{\Delta h}$ for $k = 0, 1, \ldots, K-1$, the following results are obtained (details are given in Appendix B).

$$E[\hat{v}] = v \tag{6.51}$$

$$var[\hat{v}] \simeq \frac{1}{2}\left\{\frac{\boldsymbol{s}^H\ \boldsymbol{s}}{N\ \mathrm{SNR}\ (\boldsymbol{y}^H\ \boldsymbol{y})} + \frac{\sigma^2_{\Delta h}[\boldsymbol{y}^H \boldsymbol{S}\boldsymbol{S}^H \boldsymbol{y} + \frac{4\pi^2}{N^2}\ \frac{\boldsymbol{s}^H\ \boldsymbol{s}}{N\ \mathrm{SNR}}\ trace\{\boldsymbol{W}\boldsymbol{S}\boldsymbol{S}^H\boldsymbol{W}\}]}{(\boldsymbol{y}^H\boldsymbol{y})^2}\right\} \tag{6.52}$$

where

$$\boldsymbol{y} \ \triangleq\ \frac{2\pi}{N}\,\boldsymbol{W}\boldsymbol{S}\boldsymbol{h} \tag{6.53}$$

$$\boldsymbol{W} \ \triangleq\ diag\{-N_g + K - 1, -N_g + K, \ldots, \beta\} \tag{6.54}$$

$$\boldsymbol{s} \ \triangleq\ [s(0), s(1), \ldots, s(N-1)]^T \tag{6.55}$$

and the SNR $\triangleq \frac{\sigma_{\hbar}^2}{\sigma_n^2}$ is for the training symbol with the assumption of unity channel power transfer gain. (6.51) indicates the unbiasedness of the estimator and the frequency estimation MSE is now given by (6.52).

From (6.52), it can be observed that the frequency estimation accuracy is independent of the carrier phase factor ϕ, but depends on the channel response through $\boldsymbol{y}$, the training symbol through $(\boldsymbol{y}^H\ \boldsymbol{y})$ and $(\boldsymbol{y}^H\boldsymbol{S}\boldsymbol{S}^H\boldsymbol{y})$, and the channel estimation error through $\sigma^2_{\Delta h}$. Note that if $\sigma^2_{\Delta h} = 0$, the second term will vanish and hence, the first term represents the ideal performance obtained with the perfect knowledge of the channel response.

6.3.2 Channel estimation performance

Similar to the frequency estimation performance, the channel estimation MSE can be given by

$$\mathrm{MSE}[\hat{\hbar}] = \sum_{k} P_{\epsilon}(k)\ \mathrm{MSE}[\hat{\hbar}_{|\ \epsilon=k}]\ \geq \mathrm{MSE}[\hat{\hbar}_{|\ \epsilon=0}]. \tag{6.56}$$

For moderate and high SNR, $P_{\epsilon}(0) \simeq 1$ and the lower bound becomes close to equality. Hence, $\mathrm{MSE}[\hat{\hbar}_{|\ \epsilon=0}]$ can be used to approximate $\mathrm{MSE}[\hat{\hbar}]$. Then, from Appendix C, the channel estimation MSE of the k^{th} channel tap for a channel response $\boldsymbol{h}$, a carrier phase factor ϕ, and a frequency estimate error Δv is given by

$$\begin{aligned}\mathrm{MSE}[\hat{h}(k)] \simeq \Bigg[\frac{\boldsymbol{s}^H\boldsymbol{s}\ (\boldsymbol{S}^H\boldsymbol{S})^{-1}}{N\ \mathrm{SNR}} \ &+\ \{\boldsymbol{h}\boldsymbol{h}^H - (\boldsymbol{S}^H\boldsymbol{S})^{-1}\boldsymbol{S}^H\boldsymbol{W}^H(\Delta v)\ \boldsymbol{S}\boldsymbol{h}\boldsymbol{h}^H\} \\ &\cdot\ \{\boldsymbol{I} - \boldsymbol{S}^H\boldsymbol{W}(\Delta v)\boldsymbol{S}(\boldsymbol{S}^H\boldsymbol{S})^{-1}\}\Bigg]_{k,k}\end{aligned} \tag{6.57}$$

where $\Delta v \triangleq \hat{v} - v$ and $[\boldsymbol{Y}]_{k,k}$ is the k^{th} row, k^{th} column element of the matrix $\boldsymbol{Y}$.

(6.57) indicates that the channel estimation accuracy is independent of the carrier phase factor, but depends on the frequency estimation accuracy. The second term, which is caused by the frequency estimation error, also depends on the channel response and the training symbol. If $\Delta v = 0$, the second term will vanish and hence, $\frac{\boldsymbol{s}^H\boldsymbol{s}}{N\ \mathrm{SNR}}\ [(\boldsymbol{S}^H\boldsymbol{S})^{-1}]_{k,k}$ represents the ideal performance obtained with perfect frequency recovery.

From (6.52) and (6.57), it is clear that in order to get the average MSE's for the frequency estimation and the channel estimation, the statistics of $\boldsymbol{h}$, $\Delta\boldsymbol{h}$ and Δv are required. Consequently, it is an intractable task to derive the analytical expressions for the average MSE's of the frequency estimation and the channel estimation in a frequency selective multipath fading channel in the presence of the synchronization and channel estimation errors. Hence, in the next section, we resort to computer simulation for the performance evaluation.

6.4 Performance Evaluation, Simulation Results, and Discussion

The performance of the proposed synchronization and channel estimation scheme has been investigated by computer simulation in a frequency selective multipath fading channel. Regarding the sync detection performance, the probabilities of missed detection and false detection are evaluated. The behavior of the timing estimation is evaluated by the timing offset variance and the average normalized interference power P_N, (normalized by the signal power), caused by the timing offsets.

For each timing offset ε, the corresponding normalized interference power $P_N(\varepsilon)$ can be calculated as:

$$P_N(\varepsilon) = \frac{\sigma_\varepsilon^2}{\alpha^2(\varepsilon)} \tag{6.58}$$

where $\alpha(\varepsilon)$ and σ_ε^2 are given by [70]:

$$\alpha(\varepsilon) \simeq \sum_l |h(l)|^2 \frac{N - \Delta\varepsilon_l}{N} \tag{6.59}$$

$$\sigma_\varepsilon^2 = \sum_l |h(l)|^2 \left(2\frac{\Delta\varepsilon_l}{N} - (\frac{\Delta\varepsilon_l}{N})^2\right). \tag{6.60}$$

and for $\varepsilon > 0$,

$$\Delta\varepsilon_l = \begin{cases} \varepsilon - \tau_l, & \varepsilon > \tau_l \\ \tau_l - N_g - \varepsilon, & 0 < \varepsilon < -(N_g - \tau_l) \\ 0, & \text{else.} \end{cases} \tag{6.61}$$

Similarly, for $\varepsilon < -N_g + \tau_{max}$, we can have

$$\Delta\varepsilon_l = \begin{cases} -N_g + \tau_l - \varepsilon, & \varepsilon < -N_g + \tau_l \\ 0, & \text{else.} \end{cases} \tag{6.62}$$

For the frequency offset estimation performance, the mean square error (MSE) is evaluated. Regarding the channel estimation MSE evaluation, the effective channel impulse response with respect to the timing estimate is taken as the correct one. The channel estimation MSE is defined by $E\{\Delta\hbar^H \cdot \Delta\hbar\}$ where $\Delta\hbar = \hat{\hbar}_{eff} - \hbar_{eff}$. If the

timing offset ε is negative, the effective channel impulse response and the effective channel impulse response estimate are, respectively, given by

$$\hbar_{eff} = [\mathbf{0}_{1\times|\varepsilon|}\ ,\ \hbar^T]^T\ e^{j2\pi\varepsilon v/N} \tag{6.63}$$

$$\hat{\hbar}_{eff} = [\hat{\hbar}^T\ ,\ \mathbf{0}_{1\times|\varepsilon|}]^T \tag{6.64}$$

and for a positive value of ε, they are, (the effective channel impulse response becomes non-causal),

$$\hbar_{eff} = [\hbar^T\ ,\ \mathbf{0}_{1\times\varepsilon}]^T\ e^{j2\pi\varepsilon v/N} \tag{6.65}$$

$$\hat{\hbar}_{eff} = [\mathbf{0}_{1\times\varepsilon}\ ,\ \hat{\hbar}^T]^T. \tag{6.66}$$

Finally, as an overall performance, the bit error rate (BER) is evaluated.

6.4.1 Simulation Parameters

OFDM system parameters are $N = 64$ point IFFT/FFT, (i.e., 64 subcarriers, including null subcarriers), 52 used-subcarriers (their indexes are according to the HiperLAN 2 specification, [33]), $N_g = 16$ cyclic prefix samples, and no cyclic suffix sample is used. The subcarrier modulation is QPSK. The training symbol is composed of $P + 1 = 5$ identical parts with each part having 16 samples. In order to avoid nonlinear distortion of the training symbol at the transmitter, the 16 samples identical part of the training symbol are generated by 16 point IFFT of length 16 Golay complementary sequence [75] which has a very low peak-to-average power ratio of 3 dB [76].

The multipath fading channel is modelled by (6.2) where $\{h_l\}$ are complex Gaussian channel tap gains representing a frequency selective Rayleigh fading environment. The number of sample-spaced channel taps used is $K = 8$ and the corresponding power delay profile is with 3 dB per tap decaying factor. The quasi-static case, where the channel tap gains remain unchanged over the packet interval, is assumed. The average total channel power transfer gain is set to unity and hence, the signal-to-noise ratio is defined as SNR $= \sigma_s^2/\sigma_n^2$.

In the coarse timing estimation, the timing estimate is advanced by $\lambda_c = 4$ samples. The last fine timing estimate is advanced by $\lambda_f = 2$ samples. The normalized

carrier frequency offset is set to $v = 1.6$. At the fine synchronization stage, the parameters for fine tuning of the frequency offset estimate (6.44) are: the search window $F_1 = 0.1$, the number of grid points at each side $J_1 = 10$, the iteration loop $J_2 = 5$, and $\xi = 2$. The search window parameters for the fine timing offset in (6.24) are $T_1 = K_3 = 4$ and $T_2 = K_4 = 11$. With the coarse timing advancement of $\lambda_c = 4$ samples, K_3 and K_4 would approximately give the search window centered around the correct point $\varepsilon = 0$ for (6.24). The designed maximum channel delay spread $K' = K = 8$ and the number of most significant channel taps $\mathcal{K} = 8$ will be used unless stated otherwise. One packet is assumed to be composed of one training symbol and 5 data symbols and the results are obtained from 100,000 simulation runs.

6.4.2 Results and Discussions

Using $\mathcal{C}^2(\boldsymbol{r}(k), N_g)$ as a sync detection metric, Figs. 6.1 and 6.2 show the probabilities of missed detection and false detection, denoted by "Prob{ Miss }" and "Prob{ False }", respectively, versus the sync detection metric threshold. For example, at SNR of 10 dB, the sync detection metric threshold of 0.2 would approximately give the missed detection and false detection probabilities of 10^{-4}. Better sync detection performance can be achieved by boosting the transmit power for the training symbol or by using a longer training symbol.

Fig. 6.3 (a) presents the timing offset variances of the coarse synchronization stage (denoted by "Coarse"), of the first iteration at the fine synchronization stage (denoted by "Fine^1"), and of the second iteration at the fine synchronization stage (denoted by "Fine^2"). The estimation performance is much improved in the fine synchronization stage but more iteration in the fine synchronization stage does not bring about further timing estimation improvement. Since in realizing the ML estimation (6.22), the channel estimate has to be used, it would be interesting to see how much performance gap is there between the realizable ML estimate and the ML estimate with ideal channel estimation (i.e., the exact channel response is used in (6.22)). In this regard, Fig. 6.3 (a) also includes the timing offset variance of the fine synchronization stage (first iteration) with ideal channel estimation (denoted by "Fine (ideal ch)"). The variance for SNR of 15 dB and above are not present in the figure for no timing offset is observed in the simulation.

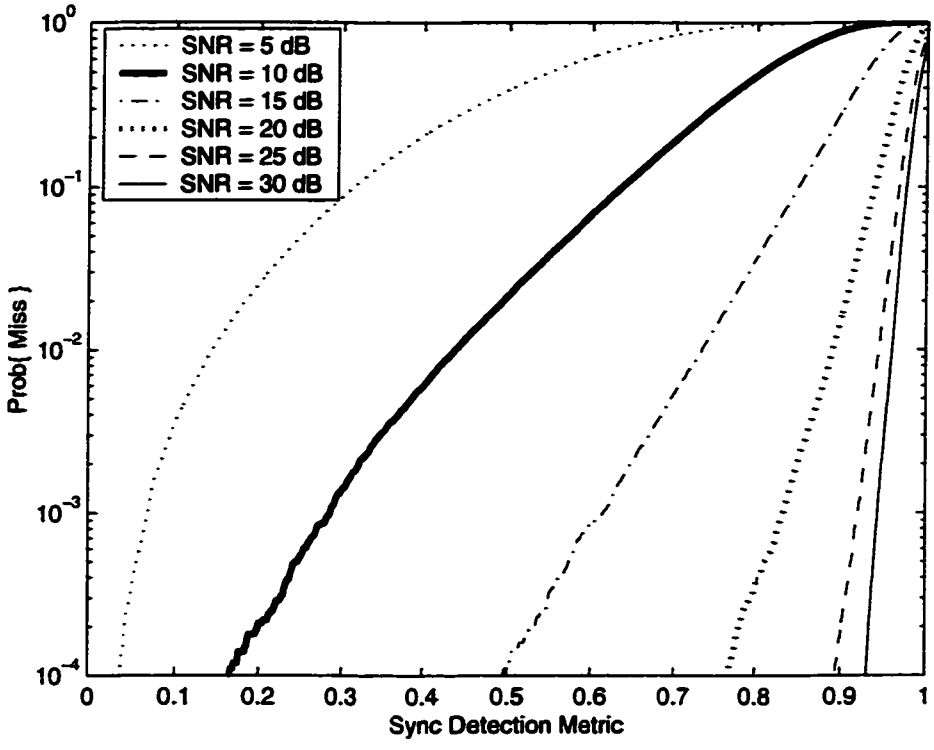

Figure 6.1. *Probability of missed detection versus sync detection metric threshold*

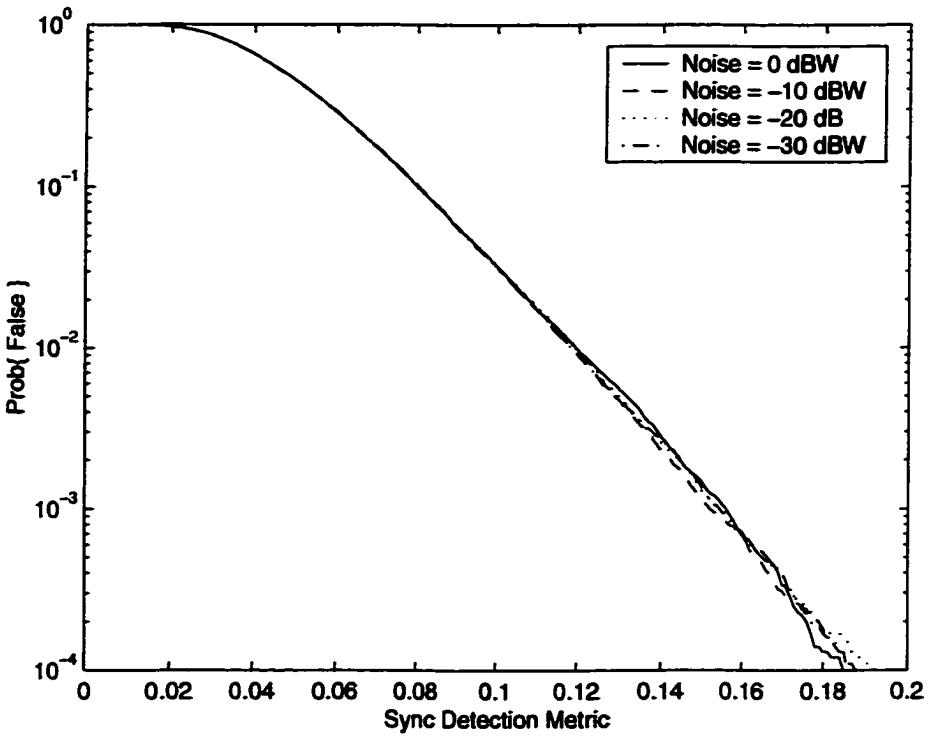

Figure 6.2. *Probability of false detection versus sync detection metric threshold*

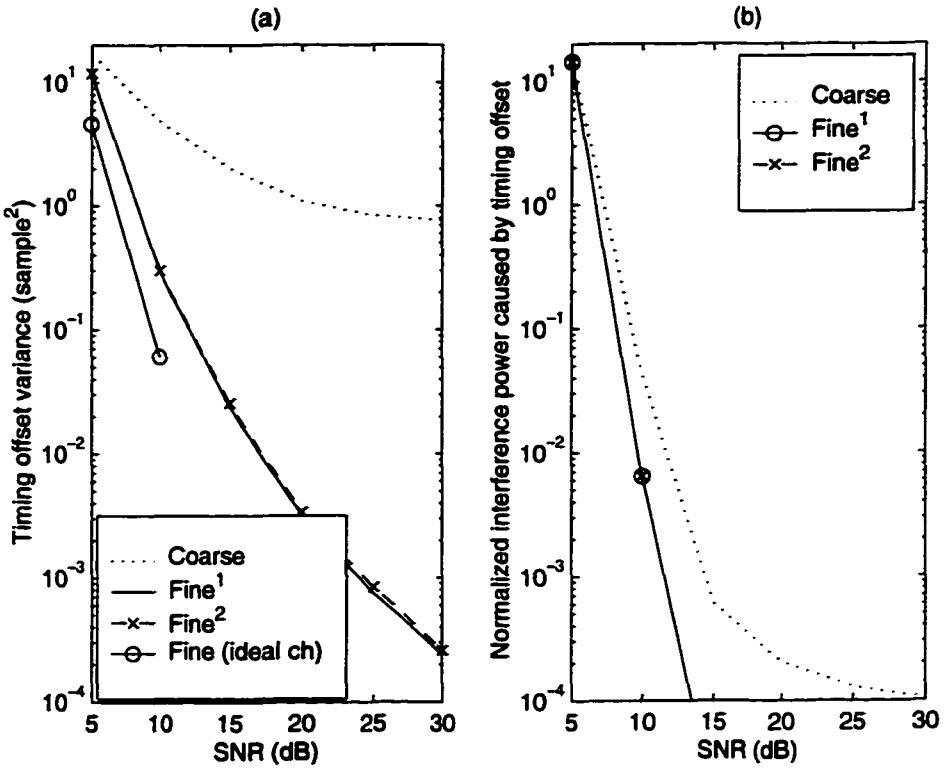

Figure 6.3. *Timing Estimation Performance*

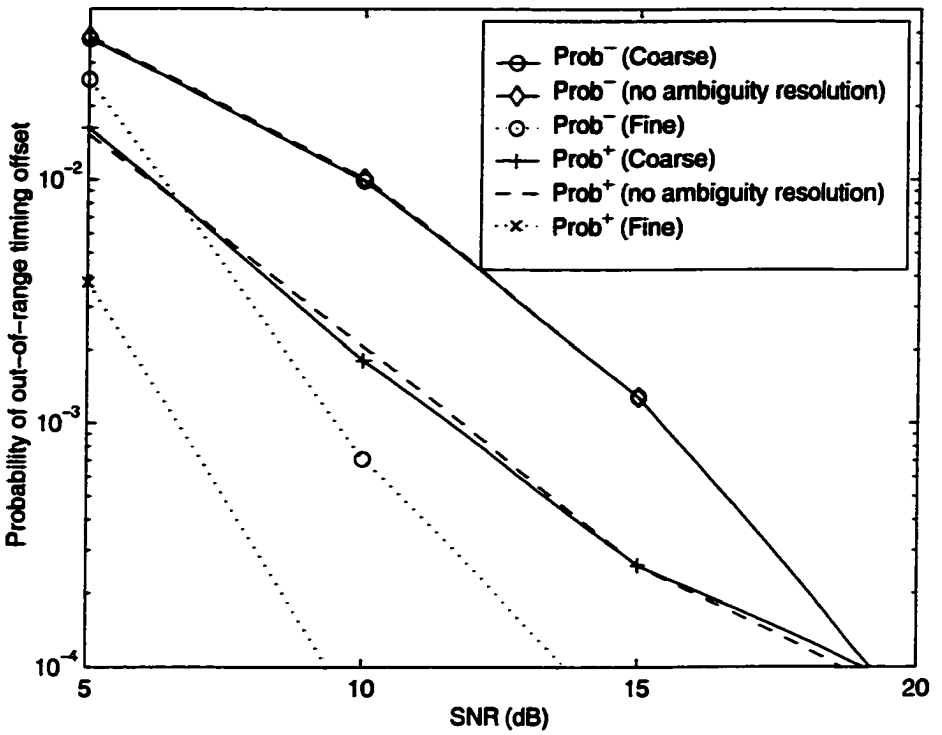

Figure 6.4. *Performance of timing offset ambiguity resolution for the channel estimation*

For the timing offsets within the ISI-free cyclic prefix part, the system performance may not be affected. Hence, one may consider another performance measure which is more oriented to the system performance rather than the estimation performance. In this light, the average normalized interference power caused by the timing estimation is presented in Fig. 6.3 (b). Similar to variance performance, the fine synchronization stages have less interference power than the coarse stage, and more iterations in the fine synchronization stage do not reduce the interference power caused by the timing offsets.

In Fig. 6.4, the performance of the ambiguity resolution of the timing offset at the fine synchronization stage is presented. Since the ambiguity-free timing offset range is $-K_4 \leq \varepsilon \leq K_3$, we evaluate the probability of out-of-range (i.e., out of the ambiguity-free range) timing offset in terms of the probability of timing offset less than $-K_4$ and the probability of timing offset greater than K_3, denoted by "Prob$^-$" and "Prob$^+$", respectively. These probabilities for the coarse timing and the fine

timing without ambiguity resolution are essentially the same since no timing offset ambiguity is resolved. On the other hand, with the ambiguity resolution, the fine timing stage has well reduced these probabilities and improved the performance.

Regarding frequency synchronization, the MSE's of the normalized frequency offset estimation in the coarse and fine stages are plotted in Fig. 6.5. Also included in the performance comparison is a near optimal frequency estimator of Morelli & Mengali (M&M) [64]. M&M has a better MSE performance than the coarse frequency estimation stage. Fine frequency estimation stages have better MSE performance than M&M for all considered SNR except at 5 dB where the fine frequency estimation at the first iteration has a slightly larger MSE than M&M, the second iteration has almost the same MSE as M&M and the fifth iteration has a slightly better MSE than M&M. The results also show that more iteration of the fine synchronization can improve the frequency estimation performance although it does not improve the timing estimation. This also suggests that, if more than one iteration is used, the fine timing estimation part can be skipped after the first iteration. To be more specific, the fine tuning can be performed by using $\mathcal{V}_{|\ \varepsilon_f}(\boldsymbol{r}(\varepsilon_f);\ \hat{h}, \tilde{v})$, $\mathcal{V}_{|\ (\hat{h},\ \varepsilon_f)}(\boldsymbol{r}(\varepsilon_f);\ \tilde{v})$ and $\hat{h}(\varepsilon_f, \hat{v}_f)$ from (6.10), (6.9) and (6.36) where ε_f and $\hat{v}_f$ are the fine sync parameters obtained in the previous iteration.

Since M&M has a better performance than the coarse frequency estimation, we also evaluate the performance of the fine frequency estimation with M&M as a coarse estimation, and further improvement is observed. The proposed method at fifth iteration has almost the same frequency estimation MSE as at the second iteration of the proposed method using M&M as a coarse estimation. Also shown in the figure is the result denoted by "Fine (selected)" which is obtained from the iteration with the minimum metric among the 5 iterations. It has a slight improvement over "Fine^5" case without requiring any considerable complexity. The ideal performance of the fine frequency estimation with the ideal channel estimation is also included as a lower bound. The performance gap can be viewed as the sensitivity of the fine synchronization to the channel estimation errors.

Fig. 6.6 presents the channel estimation MSE's for the cases of the coarse synchronization only, up to the first, second and fifth iteration of the fine synchronization stage. In the case of the coarse synchronization only, in order to account for some

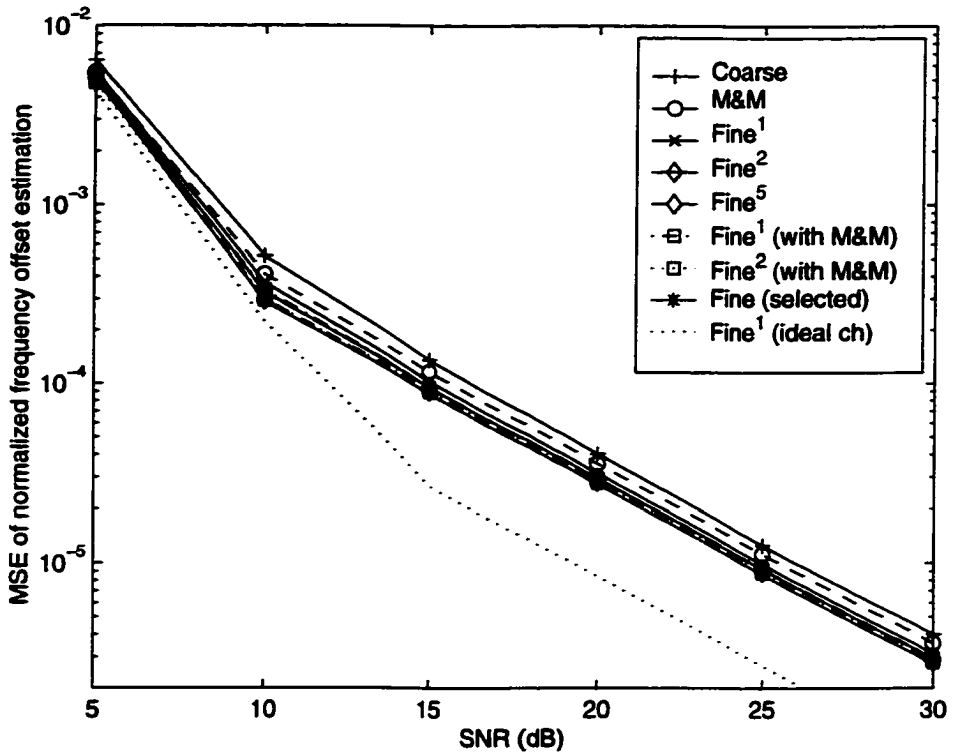

Figure 6.5. *Mean square error (MSE) of the normalized frequency offset estimation (normalized by the subcarrier spacing)*

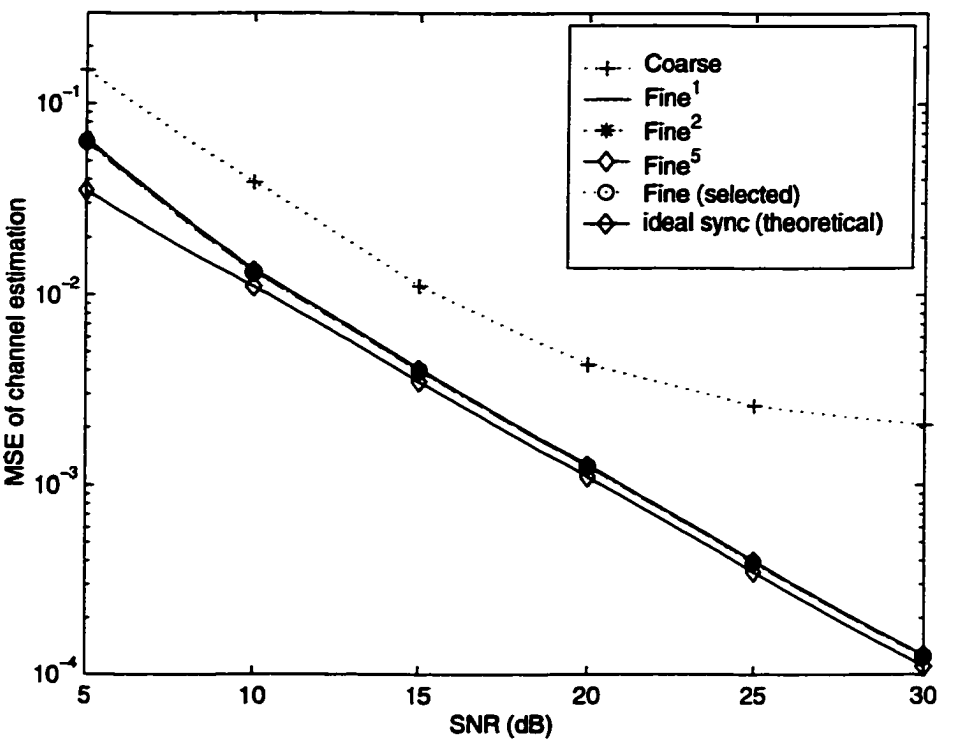

Figure 6.6. *Mean square error (MSE) of the channel estimation*

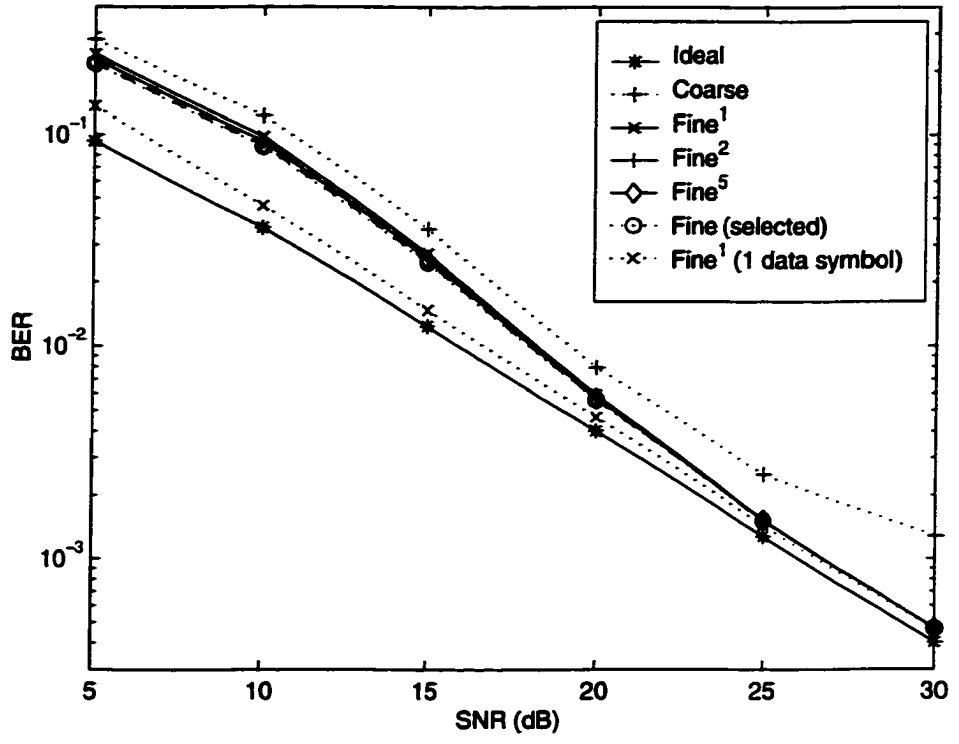

Figure 6.7. *BER performance*

timing offsets and not to miss some channel taps, $K' = N_g$ is used. Clearly, all cases of the fine stage have much better performance than the coarse synchronization only case. Due to the better frequency estimation, more iterations at the fine stage have slightly improved channel estimation and "Fine (selected)" case has the best performance (not so visible in the figure). Also included in the figure is the theoretical channel estimation MSE obtained with ideal timing and frequency synchronization, i.e., the trace of the first term in (6.57). As can be observed in the figure, the channel estimation performance in the proposed method is quite close to the ideal performance obtained with ideal synchronization. The larger performance gap at low SNR values can be ascribed to the more synchronization errors at low SNR values.

In Fig. 6.7, as an overall performance measure, BER performance curves are presented. As an ideal reference, the BER performance with ideal synchronization and ideal channel estimation is included. The coarse synchronization stage has a relatively high BER due to the high channel estimation and frequency estimation

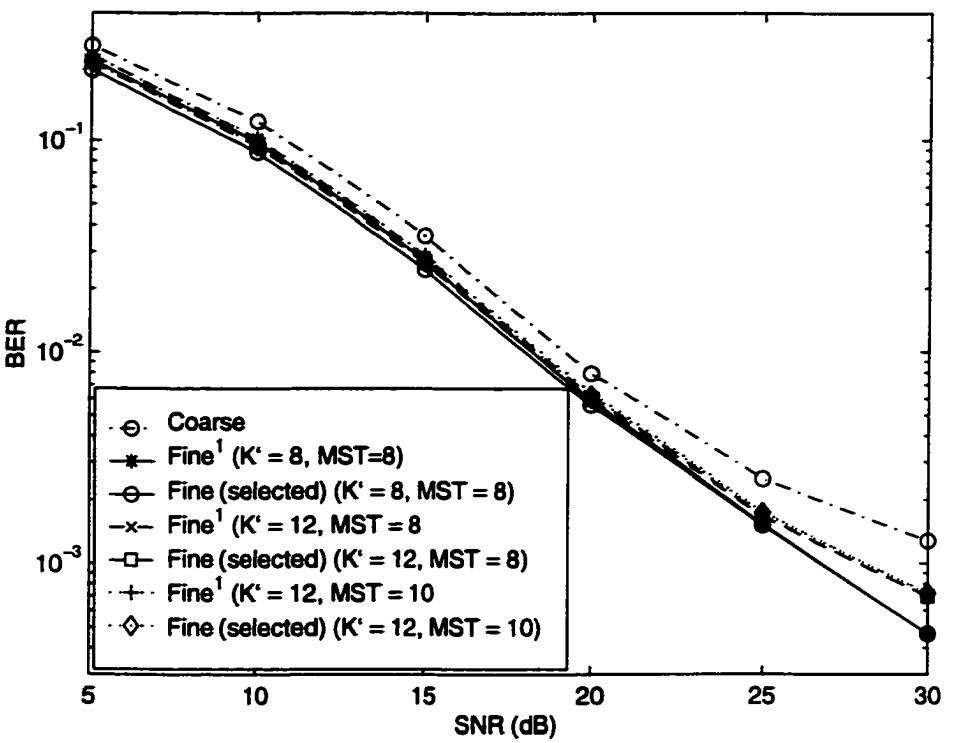

Figure 6.8. *BER performance with different parameter values*

errors. The fine stages have much better BER performance than the coarse stage due to the better synchronization and channel estimation. More iteration in the fine stage slightly improves the BER performance especially at moderate and low SNR values. In this SNR region, the synchronization and channel estimation errors have more impact on the BER performance than the noise has. Hence, the improvement in synchronization and channel estimation achieved by means of more iterations brings about a slight BER improvement. In high SNR region, since the synchronization and channel estimation errors become so small and the noise effect on BER becomes more dominant, the slight improvement of more iterations in synchronization and channel estimation does not give rise to a noticeable BER improvement. A larger BER performance gap between the fine stages and the ideal case at a lower SNR value also indicates that the synchronization and channel estimation errors have more impact on BER at lower SNR values. Due to the slight improvement in the frequency estimation and the channel estimation, "Fine (selected)" case achieves a slightly better BER performance than other non-ideal cases.

In Fig. 6.7, the BER performance at the first iteration of the fine synchronization stage for a packet containing one training symbol and one data symbol is listed. By this, the accumulative phase error caused by the frequency estimation error (which becomes significant as the packet length increases) can be removed and the resultant performance reflects more about the snap-shot synchronization and channel estimation errors effect rather than the accumulative synchronization and channel estimation errors effect. The results indicate that the proposed scheme performance is quite close to the ideal case. On the other hand, the noticeable performance gap between the snap-shot and the accumulative performance reminds the importance of the frequency estimation accuracy.

In practice, the knowledge of the maximum channel delay spread and the number of most significant channel taps may not be available. Hence, we evaluate the proposed method with the designed maximum channel delay spread K' and the designed number of the most significant channel taps $\mathcal{K}$ (which is denoted by "MST" in the figure) different from their actual values. The BER curves are given in Fig. 6.8. Due to the noise contamination from the extra taps, a slight performance loss is observed. The performance loss is larger at SNR value of 30 dB than at smaller SNR values.

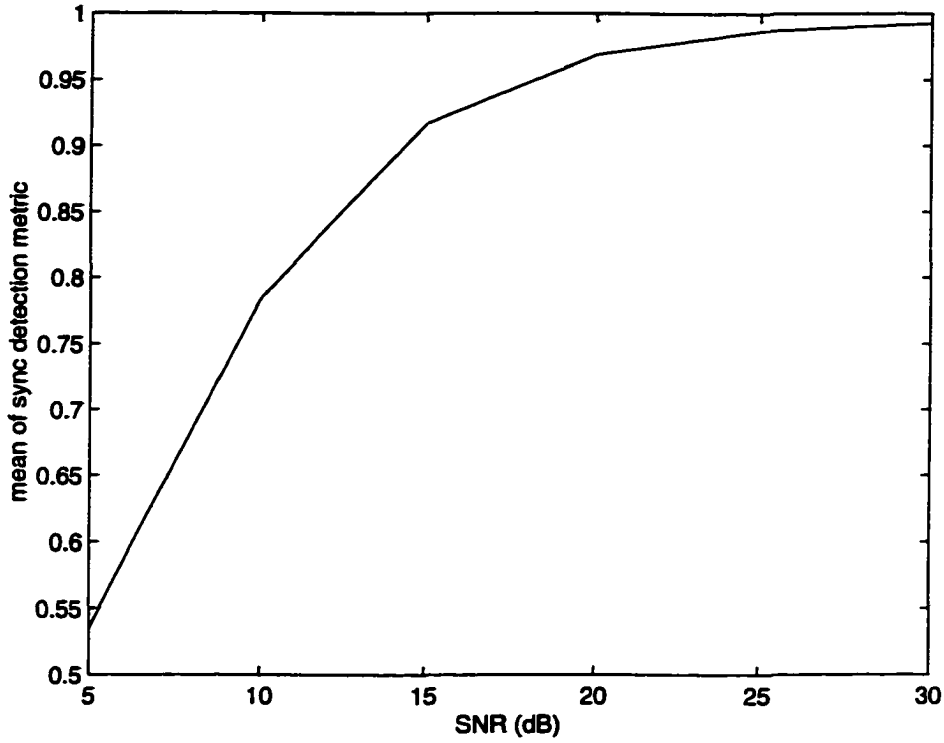

Figure 6.9. *Mean of the sync detection metric* $C^2(\boldsymbol{r}(\varepsilon_c), N_g)$

The reason is that at high SNR value, the additional noise effect on BER becomes dominant and consequently the noise contamination from the extra taps brings about more impact. However, a substantial performance improvement over the coarse stage is still achieved.

As a means of complexity reduction, adaptive ambiguity resolution approach is also evaluated. From Fig. 6.9, it can be seen that the sync detection metric gives an indication of the received signal's SNR. From Fig. 6.4, it can be observed that the occurance of the out-of-range timing offsets is very small for SNR values of 10 dB and higher. Hence, the mean of the sync detection metric at SNR value of 10 dB is used as a threshold for the adaptive ambiguity resoultion scheme. If the sync detection metric is higher than this threshold, no ambiguity resolution is carried out. Fig. 6.10(a) shows the BER performance of the proposed method with (nonadaptive) ambiguity resolution and with adaptive ambiguity resolution. Almost the same BER performance is observed. Fig. 6.10(b) shows the complexity gain of the adaptive

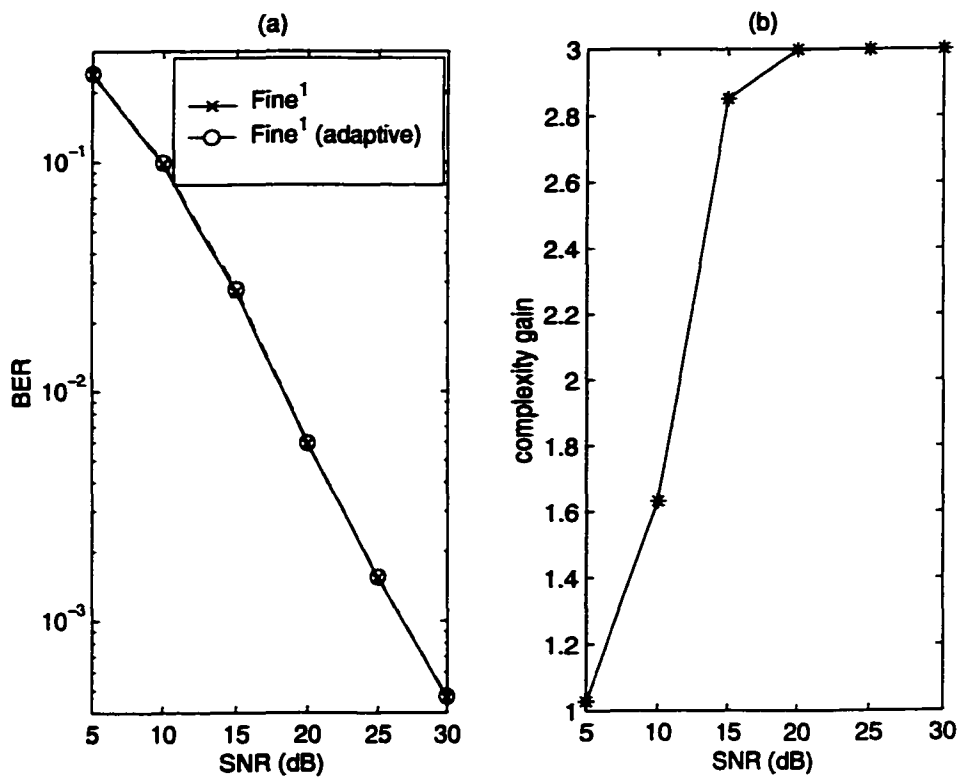

Figure 6.10. *BER performance and complexity gain of the adaptive ambiguity resolution scheme*

ambiguity resolution approach over non-adaptive ambiguity resolution approach defined by the ambiguity resolution complexity ratio of the nonadaptive to adaptive approach. Substantial complexity gain is observed particularly at higher SNR values.

6.5 Conclusions

In this chapter, joint timing and frequency synchronization and channel estimation are discussed. A realizable ML-based synchronization and channel estimation is performed in two stages. At the first stage, robust sync detection and simple coarse synchronization tasks are accomplished by using the repetitive structure of the training symbol. At the second stage, the ML estimation is realized by using the coarse estimates of the sync parameters obtained in the first stage. This two stage approach not only yields the ML realization of timing, frequency, and channel estimation but also reduces the complexity. The fine stage ML-based algorithm can also be applied to non-repetitive training structure since it only requires coarse timing and frequency estimates. The simulation results show that the performance improvement of the proposed scheme is quite promising. A means of complexity reduction by an adaptive scheme is also presented which achieves almost the same BER performance and much complexity reduction. The proposed scheme can be applied not only in OFDM-like systems but also in other single carrier systems.

Appendix A

In this appendix, we describe how to find the first channel tap selection threshold η used in (6.38). Since the operation in (6.35) does not affect the first channel tap selection, we just need to observe $\hat{\boldsymbol{g}}(\varepsilon_c, \hat{v}_c)$ in (6.33). After perfect frequency recovery, the minimum variance of $\hat{g}_c(i)$ for a given channel response is given by [55]

$$var(\hat{g}_c(i))_{|\boldsymbol{h}} = [(\boldsymbol{S}^H \boldsymbol{C}_n^{-1} \boldsymbol{S})^{-1}]_{ii} = \sigma_n^2 [(\boldsymbol{S}^H \boldsymbol{S})^{-1}]_{ii} \tag{6.67}$$

where $\boldsymbol{C}_n$ is the covariance matrix of *iid* complex Gausian samples with variance σ_n^2 and hence $\boldsymbol{C}_n^{-1} = \frac{1}{\sigma_n^2} \boldsymbol{I}$. Suppose $(\beta + 1)$ received samples are used in (6.33), (in our considered system, the length $(\beta + 1)$ of P identical training parts is N). Since

$\boldsymbol{S}^H \boldsymbol{S}$ used in our system is almost a diagonal matrix (the off-diagonal elements are two or more order smaller than the diagonal elements), it can be well-approximated as a diagonal matrix by neglecting the off-diagonal elements. The diagonal elements are of the same value due to the cyclic prefix repetition of the training symbol. Then the minimum variance for a given channel response is given by

$$var(\hat{g}_c(i))_{|\boldsymbol{h}} = \frac{\sigma_n^2}{(\beta+1)\,\sigma_s^2} = \frac{1}{(\beta+1)\;SNR} \tag{6.68}$$

where $\sum_l \sigma_{h_l}^2 = 1$ is assumed. Including the off-diagonal elements will introduce to the above equation a scaling factor which is just slightly greater than unity but this scaling factor will not affect the final result and hence is omitted. Including the variations of the channel tap gains, the variance $var(\hat{g}_c(i))$ becomes as follows:

$$var(\hat{g}_c(i)) = \begin{cases} \frac{1}{(\beta+1)\;SNR} + \sigma_{h_l}^2 & \text{if } i \text{ corresponds to } \{h_l, l = 0, 1, \ldots, K-1\} \\ \frac{1}{(\beta+1)\;SNR} & \text{otherwise.} \end{cases} \tag{6.69}$$

Define two random variables D_n and D_h as

$$D_n \triangleq max\{[\hat{g}_c(i_1 - m), \hat{g}_c(i_1 - m + 1), \ldots, \hat{g}_c(i_1 - 1)]\} \tag{6.70}$$

i_1 corresponds to the first actual channel tap, m is integer > 0

$$D_h \triangleq max_i\{\hat{g}_c(i)\}. \tag{6.71}$$

$\{\hat{g}_c(i)\}$ are *iid* complex Gaussian with zero mean and variance given by (6.69). At this stage, we approximate D_n and D_h as complex Gaussian variables with zero means and variances Ω_n and Ω_h where

$$\Omega_n = L_1 \frac{m}{(\beta+1)\cdot SNR} \tag{6.72}$$

$$\Omega_h = L_2 \sum_l (\sigma_{h_l}^2 + \frac{1}{(\beta+1)\cdot SNR}) \simeq L_2 \sum_l \sigma_{h_l}^2 = L_2 \tag{6.73}$$

where L_1 and L_2 are some constants > 0.

Now, our interest is to find $Prob\{|D_n| \leq \eta \cdot |D_h|\}$, $\eta > 0$. By defining another random variable $Z \triangleq \frac{|D_n|}{|D_h|}$, and keeping in mind that both $|D_n|$ and $|D_h|$ have Rayleigh distributions, the probability density function of Z can be obtained as

$$f_Z(z) = \frac{2\,\Omega_n\, z}{\Omega_h\,(z^2 + \Omega_n/\Omega_h)^2}\, U(z) \tag{6.74}$$

where $U(z)$ is a unit step function. Then

$$Prob\{|D_n| \leq \eta \cdot |D_h|\} = Prob\{Z \leq \eta\} = \frac{\eta^2}{\eta^2 + \Omega_n/\Omega_h}. \tag{6.75}$$

Not to pick up a wrong tap as the first channel tap, the above probability should be maximized (i.e., $\eta >>$). On the other hand, not to miss the first channel tap, η should be smaller. Hence, the optimum value of $Prob\{|D_n| \leq \eta \cdot |D_h|\}$ is unclear. To this end, we adopt a quasi-analytical, quasi-simulation approach. We find the best η value for a particular SNR value by means of simulations with trial η values. The BER can be used as a performance measure for selecting the best η value. Alternatively, the timing offset variance can be used. From our simulation results, we found that both gave the same best η value and the timing offset variance was more sensitive to η than BER was. The η value for other SNR value can then be obtained from (6.75), with $\Omega_n/\Omega_h \propto \frac{1}{(\beta+1)\cdot SNR}$ in mind, as

$$\eta_2 = \sqrt{\frac{SNR_1}{SNR_2}} \cdot \eta_1 \tag{6.76}$$

where η_1 is a known value obtained from simulation at SNR_1 and η_2 is the threshold value for SNR_2 and the same training symbol is assumed in both SNR's.

In our simulation, we find that the best value at SNR = 10 dB among the trial values of $1/3, 1/5, 1/7, 1/10$ is $\eta = 1/5$. In Fig. 6.11, the timing offset variance at the first iteration of the fine synchronization is shown for the threshold values obtained from (6.76), i.e., η, and the threshold values of $\eta/2$ and $3\eta/2$. The results show that the adopted quasi-analytical, quasi-simulation approach for the threshold value selection works well for all considered SNR's.

Appendix B

In this appendix, the main steps leading to the frequency estimation performance expressions (6.51) and (6.52) are presented. The first and second derivatives of $\Lambda(\tilde{v})$ in (6.47) at $\tilde{v} = v$ are given by

$$\dot{\Lambda}(v) = \frac{j2\pi}{N}\{\boldsymbol{r}^H \boldsymbol{W}(v)\, \boldsymbol{W}\boldsymbol{S}\hat{\boldsymbol{h}} - \hat{\boldsymbol{h}}^H \boldsymbol{S}^H \boldsymbol{W}^H(v)\, \boldsymbol{W}\boldsymbol{r}\} \tag{6.77}$$

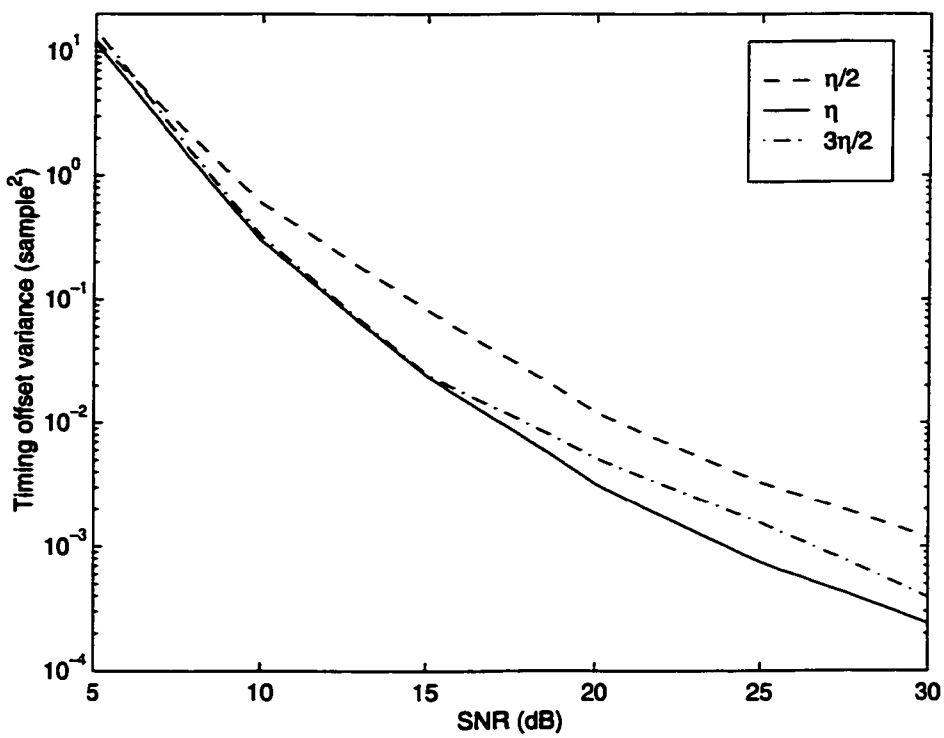

Figure 6.11. *Performance with different threshold values for the first channel tap selection*

$$\ddot{\Lambda}(v) = \frac{-4\pi^2}{N^2} \{\boldsymbol{r}^H \boldsymbol{W}(v)\, \boldsymbol{\mathcal{W}}^2 \boldsymbol{S}\hat{\boldsymbol{h}} - \hat{\boldsymbol{h}}^H \boldsymbol{S}^H \boldsymbol{W}^H(v)\, \boldsymbol{\mathcal{W}}^2 \boldsymbol{r}\} \tag{6.78}$$

where $\boldsymbol{\mathcal{W}} \triangleq diag\{-N_g+K-1, -N_g+K, \ldots, \beta\}$, and the correct timing is assumed.

Substituting $\boldsymbol{r} = \boldsymbol{W}(v)\, \boldsymbol{S}\hbar + \boldsymbol{n}$ into (6.77) and replacing $\hat{\hbar}$ with $\hbar + \Delta\hbar$ result in

$$\dot{\Lambda}(v) = \frac{j2\pi}{N} \left\{\boldsymbol{n}^H \boldsymbol{W}(v)\, \boldsymbol{\mathcal{W}}\boldsymbol{S}\hat{\hbar} + \hbar^H \boldsymbol{S}^H \boldsymbol{\mathcal{W}}\boldsymbol{S}\Delta\hbar - \Delta\hbar^H \boldsymbol{S}^H \boldsymbol{\mathcal{W}}\boldsymbol{S}\hbar - \hat{\hbar}^H \boldsymbol{S}^H \boldsymbol{W}^H(v)\, \boldsymbol{\mathcal{W}}\boldsymbol{n}\right\} \tag{6.79}$$

where $\Delta\hbar$ is the channel estimation error vector which will be assumed to have zero mean and to be uncorrelated among themselves and also from the AWGN noise $\boldsymbol{n}$, for analytical tracibility. Then we have $E[\dot{\Lambda}(v)] = 0$ and from (6.50), we arrive at

$$E[\hat{v}] = v. \tag{6.80}$$

By using the same approach, we have

$$E[\ddot{\Lambda}(v)] = \frac{-8\pi^2}{N^2}\, \boldsymbol{h}^H \boldsymbol{S}^H \boldsymbol{\mathcal{W}}^2 \boldsymbol{S}\boldsymbol{h}. \tag{6.81}$$

Next, from (6.79) together with

$$E[\boldsymbol{n}\boldsymbol{n}^H] = \sigma_n^2 \boldsymbol{I} \tag{6.82}$$

$$E[\Delta\hbar\, \Delta\hbar^H] = \sigma_{\Delta h}^2\, \boldsymbol{I} \tag{6.83}$$

$$E[\Delta\hbar^H \boldsymbol{S}^H \boldsymbol{\mathcal{W}}^2 \boldsymbol{S}\Delta\hbar] = \sigma_{\Delta h}^2\, trace(\boldsymbol{\mathcal{W}}\boldsymbol{S}\boldsymbol{S}^H\boldsymbol{\mathcal{W}}), \tag{6.84}$$

we get

$$E[(\dot{\Lambda}(v))^2] = \frac{8\pi^2}{N^2} \{\sigma_{\Delta h}^2\, \boldsymbol{h}^H \boldsymbol{S}^H \boldsymbol{\mathcal{W}}\boldsymbol{S}\boldsymbol{S}^H \boldsymbol{\mathcal{W}}\boldsymbol{S}\boldsymbol{h} + \sigma_n^2\, \boldsymbol{h}^H \boldsymbol{S}^H \boldsymbol{\mathcal{W}}^2 \boldsymbol{S}\boldsymbol{h} + \sigma_n^2\, \sigma_{\Delta h}^2\, trace(\boldsymbol{\mathcal{W}}\boldsymbol{S}\boldsymbol{S}^H\boldsymbol{\mathcal{W}})\}. \tag{6.85}$$

Let $\boldsymbol{y} \triangleq \frac{2\pi}{N}\, \boldsymbol{\mathcal{W}}\boldsymbol{S}\boldsymbol{h}$. Then, from (6.50), we obtain

$$var[\hat{v}] = \frac{1}{2} \left\{ \frac{\sigma_n^2}{\boldsymbol{y}^H\boldsymbol{y}} + \frac{\sigma_{\Delta h}^2 \left[\boldsymbol{y}^H \boldsymbol{S}\boldsymbol{S}^H \boldsymbol{y} + \frac{4\pi^2}{N^2}\, \sigma_n^2\, trace(\boldsymbol{\mathcal{W}}\boldsymbol{S}\boldsymbol{S}^H\boldsymbol{\mathcal{W}})\right]}{(\boldsymbol{y}^H\boldsymbol{y})^2} \right\}. \tag{6.86}$$

Using the definition of SNR $= \sigma_s^2/\sigma_n^2$ based on the unity channel power transfer gain, the above equation leads to the equation (6.52).

Appendix C

This appendix presents the calculation of the channel estimation MSE expression in (6.57). From (6.45) with $\varepsilon_f = 0$ and $\hat{v}_f = v + \Delta v$, the channel response estimate can be expressed as

$$\hat{\hbar} = \hbar - (\boldsymbol{S}^H \boldsymbol{S})^{-1} \boldsymbol{S}^H (\boldsymbol{I} - \boldsymbol{W}(\Delta v))^H \boldsymbol{S}\hbar + \boldsymbol{n}_h \tag{6.87}$$

where $\boldsymbol{n}_h \triangleq (\boldsymbol{S}^H \boldsymbol{S})^{-1} \boldsymbol{S}^H \boldsymbol{W}^H(\hat{v})\boldsymbol{n}$.

With $E[\boldsymbol{n}_h \boldsymbol{n}_h^H] = \sigma_n^2 (\boldsymbol{S}^H \boldsymbol{S})^{-1}$, and assuming that Δv is uncorrelated from AWGN noise $\boldsymbol{n}$, the MSE of the k^{th} channel tap estimate for a channel response $\hbar$ and a frequency estimate error Δv can be given by

$$\begin{aligned} \mathrm{MSE}[\hat{h}(k)] = \big[\sigma_n^2 (\boldsymbol{S}^H \boldsymbol{S})^{-1} \; + \; & \boldsymbol{h}\boldsymbol{h}^H - (\boldsymbol{S}^H \boldsymbol{S})^{-1} \boldsymbol{S}^H \boldsymbol{W}^H(\Delta v)\, \boldsymbol{S}\boldsymbol{h}\boldsymbol{h}^H) \\ & (\boldsymbol{I} - \boldsymbol{S}^H \boldsymbol{W}(\Delta v)\, \boldsymbol{S}(\boldsymbol{S}^H \boldsymbol{S})^{-1})\big]_{k,k} \end{aligned} \tag{6.88}$$

which leads to (6.57) if the definition of SNR is used for σ_n^2.

Chapter 7

On the Peak Factors of Sampled and Continuous Signals

In peak-to-average power ratio (PAPR) reduction techniques for OFDM, the PAPR of a continuous analog signal (denoted by PF_c) is approximately evaluated from that of the signal's samples (denoted by PF_s). In [83], it is shown that reducing PF_s does not necessarily result in a similar reduction of PF_c. Recently, Wulich [84] constructed a bandlimited function from a series (of samples) and showed that PF_s is finite but PF_c is infinite. At first sight, the example appears to be wrong because the variations of a bandlimited function must be bounded (i.e., such a function cannot take infinite values between two finite samples). This example therefore raises a number of fundamental questions. Firstly, "under what conditions, if any, can a bandlimited function take infinite values between finite samples?" To answer this, we present several bounds for a function $x(t)$, its first derivative $x'(t)$ and its variation $|x(t) - x(t+\tau)|$ in terms of bandwidth and signal energy or power. These bounds follow readily from the use of the Cauchy-Schwarz inequality and are instructive in their own right. Secondly, "does an arbitrary sequence $\{x_n\}$ represent the samples of a bandlimited function?" We show that Wulich's sequence does not satisfy the necessary conditions. The rest of this chapter is organized as follows. In Section 7.1, we analyze Wulich's sequence. In Section 7.2, various bounds of bandlimited periodic and non-periodic functions are presented. Some aspects on the sampling theorem and sampling series are discussed in Section 7.3 and conclusions are given in Section 7.4.

7.1 Wulich's Example

In OFDM, we are dealing with periodic signals which have infinite energy. Hence, the average power is used for normalization purposes. The example in [84] deals with a non-periodic function. While the peak of such a function can still be found, it is not meaningful to define the PAPR because the average power in this case would be zero for a finite energy function. Thus, Definition (2) in [84] appears to be ill-advised but the example worked only because the function used is of infinite energy. On the other hand, the PAPR for an OFDM signal is upper bounded as $PF_c \leq N$, where N is the number of subcarriers. This means Wulich's example is clearly not relevant for normal OFDM. Let us consider Wulich's example, [84, Eqn. (5)], which can be expressed as

$$x[n] = e^{j\pi n} + 2\delta[n] - 2u[n]e^{j\pi n} \tag{7.1}$$

where $\delta[n]$ is the discrete-time Dirac Delta function and $u[n]$ is the discrete-time unit step function. Applying $\mathcal{F}\{e^{j\theta_o n}\ y[n]\} = Y_d(e^{j(\theta-\theta_o)})$ where $\mathcal{F}\{\ \}$ indicates Fourier transform and $Y_d(e^{j\theta}) = \mathcal{F}\{y[n]\}$, the Fourier transform of $x[n]$ is given by [85]

$$X_d(e^{j\theta}) = \frac{2}{1+e^{j\theta}}. \tag{7.2}$$

Consequently, the Fourier transform of $x(t)$, denoted by $X(f)$, is given by

$$X(f) = \frac{1}{f_s}\ rect\left(\frac{f}{f_s}\right)\frac{2}{(1+e^{j2\pi f/f_s})}. \tag{7.3}$$

Wulich's example can be explained qualitatively as follows. In time domain, $x(t)$, [84, Eqn. (1)], is an infinite sum of *sinc* functions. $sinc(t) \triangleq \frac{\sin(\pi t)}{\pi t}$ varies as $1/t$ and changes sign as t crosses integer values. We know that the infinite series

$$S = \sum_{n=1}^{n=\infty} \frac{1}{n} \tag{7.4}$$

diverges to infinity. It can be shown that Wulich's function behaves approximately as this series and hence has an infinite amplitude for any time instant that is not a sampling instant. Mathematically, for a time instant t with $|t| < K/f_s$ but $t \neq n/f_s$, (n an integer), the function value is given by

$$x(t) = \sum_{|n|=0}^{K-1} x[n]sinc(f_s t - n) + \sum_{|n|=K}^{\infty} x[n]sinc(f_s t - n). \tag{7.5}$$

If $x[n]$ for $|n| \geq K$ are alternating signs with equal amplitude and $x[n] = x[-n]$, then the second summation in the above equation will behave as in Eqn. (4) while the first summation has a finite amplitude, hence resulting in an infinite amplitude for that time instant. Wulich's samples are exactly of the type described above. Hence, except at sampling instants (where the contributions from all other samples are all zeros), the function has infinite amplitude for all other time instants, excluding $t = \pm\infty$.

7.2 Bounds for a Bandlimited Function

The bandwidth is a measure of how fast a function varies; consequently, the variations of a bandlimited function between its two adjacent samples will be finite and bounded, due to the finite bandwidth. This is provided that the function is either of a nonperiodic, finite energy type or of a periodic, finite power type. So, in general, the function cannot take infinite values if the two samples are finite. In the following, we explore the bounds for a bandlimited function.

7.2.1 Periodic Function

Let us consider a bandlimited periodic function $x(t)$, whose power spectral density is zero for $|f| > Lf_o$. It can be expressed by a Fourier series as:

$$x(t) = \sum_{n=-L}^{L} c_n e^{j2n\pi f_o t} \tag{7.6}$$

where $\{c_n\}$ are Fourier series coefficients for $x(t)$. Applying the following Cauchy-Schwarz inequality

$$\left|\sum a_n\, b_n\right|^2 \leq \sum |a_n|^2 \sum |b_n|^2, \tag{7.7}$$

to (7.6), we obtain

$$|x(t)| \leq \sqrt{(2L+1)\sum_{n=-L}^{L} |c_n|^2}. \tag{7.8}$$

From Parseval's theorem we know $\sum_{n=-L}^{L} |c_n|^2 = P$, the total average power of $x(t)$. Hence, we obtain

$$|x(t)| \leq \sqrt{(2L+1)\ P}. \tag{7.9}$$

Similarly, we can proceed for the derivative of $x(t)$ and obtain the following:

$$|x'(t)| \leq 2\pi f_o \sqrt{\frac{PL(L+1)(2L+1)}{3}}. \tag{7.10}$$

Alternatively, we can find $|x(t+\tau) - x(t)|$ as follows:

$$\begin{aligned} x(t+\tau) - x(t) &= \int_{-Lf_o}^{Lf_o} X(f)(e^{j2\pi f\tau} - 1)e^{j2\pi ft} df \\ |x(t+\tau) - x(t)| &\leq \sqrt{\sum_{k=-L}^{L} |c_k|^2 4 \sum_{n=-L}^{L} \sin^2(n\pi f_o \tau)}. \end{aligned}$$

Using $\sin^2(\phi) \leq \phi^2$ and Parseval's theorem, we get

$$|x(t+\tau) - x(t)| \leq 2\pi\ f_o\tau \sqrt{P\,\frac{L(L+1)(2L+1)}{3}}. \tag{7.11}$$

Hence, for an OFDM signal $x(t)$ with N subcarriers, similar to (7.9), we see that

$$|x(t)| \leq \sqrt{NP} \tag{7.12}$$

and consequently, $PF_c \leq N$ if signal constellations that have constant amplitude, such as quadrature phase shift keying (QPSK), are used. We are also aware that

$$|x'(t)| \leq 2\pi f_o \sqrt{P(N-1)N(2N-1)/6} \tag{7.13}$$

$$|x(t+\tau) - x(t)| \leq 2\pi f_o\tau \sqrt{P(N-1)N(2N-1)/6} \tag{7.14}$$

where f_o is the subcarrier spacing of an OFDM signal. It is noted that the signal amplitude $|x(t)|$ does not depend on the absolute bandwidth, but only on the number of subcarriers N, regardless of f_o. But the variations of the signal, which can be given by $|x'(t)|$ and $|x(t+\tau) - x(t)|$, depend on both N and f_o.

7.2.2 Non-periodic Function

For a non-periodic function $x(t)$ with energy E and Fourier transform $X(f)$ where $X(f) = 0$ for $|f| > f_c$, using Cauchy-Schwarz inequality and Parseval's theorem would lead to the following bounds [86]:

$$|x(t)| \leq \sqrt{2f_cE}. \tag{7.15}$$

$$|x'(t)| \leq \sqrt{8\pi^2 f_c^3 E/3}. \tag{7.16}$$

$$|x(t+\tau) - x(t)| \leq \sqrt{E \cdot \{4f_c - \frac{2}{\pi\tau}\sin(2\pi f_c\tau)\}}. \tag{7.17}$$

Thus, both the function and its variations are bounded in terms of its energy and bandwidth. For $|f_c\tau| < 1$, we have the following expression:

$$x(\tau/2) - x(-\tau/2) = 2j \int_{-f_c}^{f_c} X(f)\,\mathrm{sgn}(f)\frac{\tau}{|\tau|}|\sin(\pi f\tau)|\,df. \tag{7.18}$$

Using the mean value theorem, we can obtain

$$\begin{aligned} x(\tau/2) - x(-\tau/2) &\geq m2j\int_{-f_c}^{f_c} |\sin(\pi f\tau)|\,df \\ &\geq \frac{4jm}{\pi\tau}[1 - \cos(\pi f_c\tau)] \end{aligned} \tag{7.19}$$

where $\min\{X(f)\ \mathrm{sgn}(f)\ \frac{\tau}{|\tau|}\} \leq m \leq \max\{X(f)\ \mathrm{sgn}(f)\ \frac{\tau}{|\tau|}\}$. The energy of Wulich's function is given by

$$E = \int_{-\infty}^{\infty} |x(t)|^2\,dt = \int_{-\infty}^{\infty} |X(f)|^2 df = \infty. \tag{7.20}$$

Hence, (7.15) indicates that Wulich's function $x(t)$ can have infinite amplitudes, while (7.16) and (7.17) suggest that the variations of $x(t)$ can be infinite. Alternatively, (7.19) suggests that the variations of Wulich's function can be infinite since $X(f = \pm f_s/2)$ has an infinite amplitude.

7.3 Sampling Series

In [84], Wulich uses a function defined in (7.1) as a sampling series and constructs a bandlimited function. In what follows, we present related aspects on sampling. From [87] we know that the following sampling expansion

$$x(t+\tau) = \sum_{n=-\infty}^{\infty} x(t+nT)\,\frac{\sin(2\pi f_c[\tau - nT])}{2\pi f_c[\tau - nT]} \tag{7.21}$$

where $T = 1/(2f_c)$, does not hold, in general, for finite power signals. In fact, we can observe from (7.6) that it requires $2L+1$ coefficients of orthogonal kernels in order to completely define $x(t)$. From this fact, we can deduce that within one period (which is enough to represent the periodic signal) it requires $2L+1$ orthogonal samples (we consider only equally spaced samples) to completely define the signal without any additional knowledge of the signal or restrictions on the sampling. However, if we sample over more than one period, it is not necessary to do so at a frequency of $(2L+1)f_o$. It is sufficient to sample at a frequency that gives $2L+1$ samples in only one of the considered periods. If we sample over an infinite period of time, i.e., $-\infty < t < \infty$, then it is sufficient to use a sampling frequency f_s just greater than $2Lf_o$.

Consider a signal with $X(f) = 0$ for $|f| > f_c$. In this case, the support of $X(f)$ or bandwidth can be given by a closed interval, $[-f_c,\ f_c]$. For such a bandlimited signal of finite energy, the sampling theorems of Shannon [88], Whittakers and Kotel'nikov [89] state that the required sampling frequency is $f_s \geq 2f_c$. Later, Campbell [90] extended the sampling theorem by considering a rather general scope, namely, distribution with bounded support beyond the originally considered case, which was of a bandlimited finite energy signal. This scope encompassed bandlimited periodic signals. It was emphasized that it is a requirement that the support of $X(f \pm nf_s)$ for the integer $n \neq 0$ be disjoint from the support of the Fourier transform of interpolating function (in our case, an ideal low pass filter). From [90], we can see that by means of disjoint supports, it avoids the case with a sampling frequency f_s and $X(|f| > f_s/2) = 0$ where $X(f = \pm f_s/2) \neq 0$ when extending the bounded support finite energy function to the bounded support distribution.

Let us consider an interpolating function $p(t) = \frac{\sin(\pi f_s t)}{\pi f_s t}$ whose Fourier transform

is given by

$$P(f) = \begin{cases} 1/f_s, & |f| < f_s/2 \\ 1/(2f_s), & |f| = f_s/2 \\ 0, & |f| > f_s/2. \end{cases} \tag{7.22}$$

For a bandlimited finite energy signal $x(t)$ where $X(|f| > f_s/2) = 0$ but $X(f = \pm f_s/2) \neq 0$, the reconstruction of the signal from its sampling series will result in a frequency spectrum that is exactly the same as the original one if the original frequency spectrum has the same value at $|f| = f_s/2$ (i.e., $X(-f_s/2) = X(f_s/2)$); $X(f)$ need not be symmetric. Even if this condition is not satisfied, the only difference between the original frequency spectrum and the reconstructed frequency spectrum will be at $|f| = f_s/2$. For a finite energy signal, the ratio of the energy content at $|f| = f_s/2$ to the total energy of the signal is zero. Hence, the reconstructed signal is essentially the same as the original one, justifying the use of the sampling theorems of Shannon, Whittakers and Kotel'nikov [88]-[89].

For a bandlimited periodic signal with a maximum frequency content of Lf_o, if the frequency spectra are the same at $|f| = f_s/2$, the reconstructed signal is exactly the same as the original one. An example of this type is $x(t) = \cos(2\pi L f_o t)$. If the frequency spectra are not the same at $|f| = f_s/2$, the reconstructed spectrum will not be exactly the same as the original one. The reconstruction error would depend on the ratio of the error power at $|f| = f_s/2$ to the total power of the original signal. For an extreme case where $x(t) = \sin(2\pi L f_o t)$, whose spectrum at $|f| = f_s/2$ are exactly opposite and the above power ratio is unity, there would be a total loss of the original signal. This fact can also be recognized from the signal's sampling series, which is a set of zeros. Hence, in general, for any bandlimited signal (regardless of finite energy signal or periodic signal) whose frequency spectrum $X(f) = 0$ for $|f| > f_c$, the sufficient sampling frequency is $f_s > 2f_c$. This reflects the requirement of disjoint supports, as stated in [90]. This disjoint support requirement can also be observed in another treatment on sampling series for bandlimited generalized functions (see Lemma 1 of [91]). The above statement, however, does not mean that any function with bandwidth $[-f_c, f_c]$ requires $f_s > 2f_c$ but simply means that there are some functions with bandwidth $[-f_s, f_c]$ that require $f_s > 2f_c$, while the other functions require $f_s \geq 2f_c$.

Another interesting point, made by Jerri in [92], is that a sampling series $\{x(nT)\}$ given by an arbitrary sequence $\{x_n\}$, lacking the assertion of $\sum_{n=-\infty}^{\infty} |x_n| < \infty$, does not necessarily imply that the series represents a bandlimited function. The sequence used in [84] is not a periodic signal and does not satisfy this assertion. Moreover, from its Fourier transform we can observe that it does not have a disjoint support as required in [90] [91]. Hence, this sequence and its corresponding function may not fall inside the scope of previous sampling theorems.

Next, we discuss on how much the PF_c and PF_s can differ. For a periodic function, from (7.12), we have $PF_c \leq N$. Since the possible minimum PF_s is unity, the ratio of PF_c to PF_s is upperbounded by

$$PF_c/PF_s \leq N. \tag{7.23}$$

For a non-periodic function, if the average power over some finite observation time T_o is considered, we have $PF_c \leq 2f_cT_o$. Since $PF_s \geq 1$, the ratio PF_c to PF_s is upperbounded by

$$PF_c/PF_s \leq 2f_cT_o. \tag{7.24}$$

The above bound suggests that for a case with infinite $f_c\,T_o$, it is possible to have an infinite difference between PF_c and PF_s. Wulich's sequence is an example of this case. A closer look at the time domain function in Section 7.1 reveals that except at the sampling points where the function has values given by [84, Eqn. (5)], the function has an infinite amplitude for all other time instants (excluding $t = \pm\infty$). Hence, it does not represent a practical signal in communication systems. We may also conclude that arbitrarily chosen series may not necessarily represent a bandlimited signal that is continuous or has finite jumps.

7.4 Conclusions

In this chapter, we discuss some aspects on the sampling theorem and sampling series which are beyond the scope of the Shannon's sampling theorem. We describe several bounds on the band-limited function which leads to the PAPR bounds of the continuous signal and the bound of the peak factor ratio of the continuous signal to the

sampled signal. For a bandlimited periodic signal, the amplitude is bounded by the total power and the number of constituent harmonic tones. The signal variation is bounded by the total power and the bandwidth. For a bandlimited non-periodic signal, the amplitude and variation are bounded by the total energy and the bandwidth. For an OFDM signal, the peak factor ratio of the continuous signal to the sampled signal is upperbounded by the number of tones. Analogously, for a single-carrier signal, this peak factor ratio is upperbounded by the number of samples. Using an arbitrarily chosen data sequence for the sampling series may not necessarily result in a bandlimited signal of interest for communications systems.

Chapter 8

Peak-to-Average Power Ratio Behavior of Some Reed-Muller Codes in OFDM System

OFDM has been of major interest for future wireless and wireline applications. However, it is also accompanied by many practical issues and high peak-to-average power ratio (PAPR) is one of the major issues. Several approaches have been proposed to alleviate the PAPR problem. The easiest way is digital hard limiting of the signal [93]-[94] with the expense of some performance degradation. Another way is to introduce redundancy in some form [95]-[96] to control the PAPR but it is neither general nor practical for a large number of carriers. Some approaches [97]-[98] choose the one with minimum PAPR from a set of signals all representing the same information or use similar concept. Other approaches [99]-[100] use some forms of online optimization to modify the signal to get minimum possible PAPR under some optimization criteria. These approaches using optimization are rather general at the expense of added complexity and some redundancy but there is no guarantee for a fixed PAPR limit.

However, the methods mentioned above do not address the error control part. Concept of coding for both PAPR reduction and error control was introduced in [101]. In reference [76] [102], Golay complementary sequences have been used for both PAPR reduction and error correction and have received much attention (for example, see [103]). Reference [102] and [104] recognize the connection between Golay complementary sequences and second-order cosets of the first order Reed-Muller code and hence, resulting in the efficient encoding and decoding. It has been extended

to q-ary alphabet case (q even) in [105] where Graph interpretation for the second-order cosets is also presented. This approach of using cosets of RM code for both PAPR reduction and error correction enjoys both tight PAPR control and good error correction capability. However, for an OFDM system with a large number of carriers, the code rate of this approach becomes too small. Hence, we consider higher order cosets of RM(1,m) codes beyond its original constraint to second-order cosets.

In this chapter, we study some PAPR behavior of second-order cosets for $m = 4$ and 5, and third-order cosets for $m = 4$ of RM(1,m) codes in OFDM system in order to explore the possibility of including third-order cosets. The organization of this chapter is as follows. In Section 8.1, the connection between Golay complementary sets and second-order cosets of first order RM codes and Graph interpretation of the second-order cosets [102]-[105] are briefly discussed. Section 8.2 describes PAPR behavior of second-order cosets of RM(1,m) codes for $m = 4$ and 5 in an alternative form. Section 8.3 discusses PAPR behavior of third-order cosets of RM(1,m) code for $m = 4$. Finally, conclusions are given in Section 8.4.

8.1 PAPR, Second-Order Cosets of First-Order Reed-Muller Code and Graph Interpretation

The simplified OFDM signal in baseband can be expressed as

$$s(t) = \sum_{k=0}^{N-1} c[k]\, e^{j2\pi k\Delta f t} \tag{8.1}$$

where $\{c[k] : k = 0, 1, \ldots, N-1\}$ form an information bearing sequence called an OFDM codeword, N is the number of sub-carriers, $\Delta f \triangleq 1/T_s$ is the subcarrier spacing and T_s is the OFDM symbol period without including the cyclic prefix. The peak-to-average power ratio (PAPR) of an OFDM signal $s(t)$ is defined as

$$PAPR = \frac{\max_{0\le t<T_s} |s(t)|^2}{E[|s(t)|^2]} \tag{8.2}$$

where $E[\,]$ denotes the expectation. The PAPR for an OFDM system is defined as the maximum PAPR among all possible codewords $\{c[k] : k = 0, 1, \ldots, N-1\}$. In calculation of PAPR of the OFDM signal, we use $8N$ point IFFT.

In this chapter, only binary alphabet is considered. The generator matrix of an r^{th} order Reed-Muller code RM(r,m) can be expressed as

$$\boldsymbol{G} = [\boldsymbol{G}_0,\ \boldsymbol{G}_1,\ \boldsymbol{G}_2,\ \ldots,\ \boldsymbol{G}_r]^T \tag{8.3}$$

where $[\ ]^T$ is the transpose operation and

$$\boldsymbol{G}_0 = \mathbf{1} \tag{8.4}$$

$$\boldsymbol{G}_1 = [\boldsymbol{x}_1,\ \boldsymbol{x}_2,\ \boldsymbol{x}_m]^T \tag{8.5}$$

$$\boldsymbol{G}_2 = [\boldsymbol{x}_1\boldsymbol{x}_2,\ \boldsymbol{x}_1\boldsymbol{x}_3,\ \ldots,\ \boldsymbol{x}_1\boldsymbol{x}_m,\ \boldsymbol{x}_2\boldsymbol{x}_3,\ \boldsymbol{x}_2\boldsymbol{x}_4,\ \ldots,\ \boldsymbol{x}_{m-1}\boldsymbol{x}_m]^T. \tag{8.6}$$

$\{\boldsymbol{G}_k : 2 < k \leq r\}$ can be deducted from the above equations. The vector $\boldsymbol{x}_k\boldsymbol{x}_l$ represents the element by element product of the two vectors $\boldsymbol{x}_k$ and $\boldsymbol{x}_l$. For $m = 4$ case, we have

$$\begin{aligned}
\mathbf{1} &= [1\,1\,1\,1\,1\,1\,1\,1\,1\,1\,1\,1\,1\,1\,1\,1] \\
\boldsymbol{x}_1 &= [0\,0\,0\,0\,0\,0\,0\,0\,1\,1\,1\,1\,1\,1\,1\,1] \\
\boldsymbol{x}_2 &= [0\,0\,0\,0\,1\,1\,1\,1\,0\,0\,0\,0\,1\,1\,1\,1] \\
\boldsymbol{x}_3 &= [0\,0\,1\,1\,0\,0\,1\,1\,0\,0\,1\,1\,0\,0\,1\,1] \\
\boldsymbol{x}_4 &= [0\,1\,0\,1\,0\,1\,0\,1\,0\,1\,0\,1\,0\,1\,0\,1].
\end{aligned} \tag{8.7}$$

The RM(r,m) code is gven by

$$\boldsymbol{c} = [\boldsymbol{M}_0,\ \boldsymbol{M}_1,\ \ldots,\ \boldsymbol{M}_r]\ [\boldsymbol{G}_0,\ \boldsymbol{G}_1,\ \ldots,\ \boldsymbol{G}_r]^T \tag{8.8}$$

where $\{\boldsymbol{M}_i\}$ are the respective message vectors corresponding to $\{\boldsymbol{G}_i\}$. Then $\boldsymbol{M}_2\boldsymbol{G}_2$ can be considered as the coset representatives for the cosets of RM(1,m) codes in RM(2,m) codes and will be called the second order coset representatives of RM(1,m). It can be expressed in terms of the row vectors of $\boldsymbol{G}_1$ as

$$\boldsymbol{M}_2\boldsymbol{G}_2 = \sum_{1 \leq i < j \leq m} b_{ij}\ \boldsymbol{x}_i\boldsymbol{x}_j = Q(\boldsymbol{x}_1,\ \boldsymbol{x}_2,\ \ldots,\ \boldsymbol{x}_m),\ b_{ij} \in \mathbb{Z}_2 \tag{8.9}$$

where Q can be regarded as a quadratic form in m variables, $(\boldsymbol{x}_1,\ \boldsymbol{x}_2,\ \ldots,\ \boldsymbol{x}_m)$, over $\mathbb{Z}_2$.

We can form a graph $G(Q)$ on m vertices with Q as follows. The vertices of $G(Q)$ are labeled by 1, 2, ..., m and if $b_{ij} \neq 0$, the vertices i and j are joined by an edge.

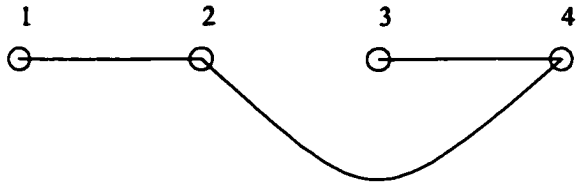

Figure 8.1. *Graph representation of* $x_1x_2 + x_2x_4 + x_3x_4$ *: A path on the vertices (1, 2, 3, 4) or the path 1243.*

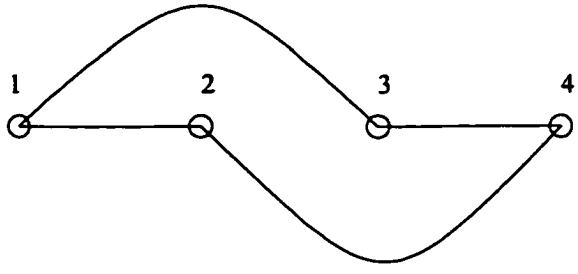

Figure 8.2. *Graph representation of* $x_1x_2 + x_2x_4 + x_3x_4 + x_1x_3$ *: A circle on the vertices (1, 2, 3, 4)*

$G(Q)$ is defined as a path if either $G(Q)$ contains a single vertex and no edges (i.e., $m = 1$ case), or $G(Q)$ contains exactly m -1 edges which form a Hamiltonian path in G (i.e., $m \geq 2$ case). For $m \geq 2$ case, a path on m vertices corresponds to a quadratic form of the type

$$\sum_{j=1}^{m-1} \boldsymbol{x}_{\pi(j)}\ \boldsymbol{x}_{\pi(j+1)} \tag{8.10}$$

where π is a permutation of $\{1, 2, ..., m\}$.

$G(Q)$ is defined as a circle if its m -1 edges form a path and the m^{th} edge joins the start and end vertices of the path. We say for the expression

$$\sum_{j=1}^{k-1} y_j\ y_{j+1} \tag{8.11}$$

that $y_1y_2,\ y_2y_3,\ \ldots,\ y_{k-1}y_k$ form a path $(123 \ldots k)$, and for the expression

$$\sum_{j=1}^{k-1} y_{\pi(j)}\ y_{\pi(j+1)} \tag{8.12}$$

that $y_{\pi(1)}y_{\pi(2)},\ y_{\pi(2)}y_{\pi(3)},\ \ldots,\ y_{\pi(k-1)}y_{\pi(k)}$ form a path on the vertices $(1,\ 2,\ 3,\ \ldots,\ k)$. Similarly, for the expression

$$\sum_{j=1}^{k-1} y_{\pi(j)}\ y_{\pi(j+1)} + y_{\pi(1)}\ y_{\pi(k)} \tag{8.13}$$

we say that $y_{\pi(1)}y_{\pi(2)},\ y_{\pi(2)}y_{\pi(3)},\ \ldots,\ y_{\pi(k-1)}y_{\pi(k)}, y_{\pi(1)}\ y_{\pi(k)}$ form a circle on the vertices $(1,\ 2,\ 3, \ldots,\ k)$.

In the following, some results of [105] are briefly summarized for the binary case. For details, one is referred to [105]. Suppose $Q : \{0,1\}^m \rightarrow \mathbb{Z}_2$ is a quadratic form in variables $\boldsymbol{x}_1,\ \boldsymbol{x}_2,\ \ldots,\ \boldsymbol{x}_m$. Suppose further that $G(Q)$ contains a set of k distinct vertices labeled $j_1,\ j_2,\ \ldots,\ j_k$ with $(0 \leq k < m)$ and has the property that deleting these k vertices and their edges results in a path. Let e be the label of either end vertex in this path (or the single vertex of the graph when $k = m - 1$). Then, for any choice of $g',\ g_i \in \mathbb{Z}_2$,

$$\left\{ Q + \sum_{i=1}^{m} g_i\, \boldsymbol{x}_i\ +\ g'\ + \sum_{\alpha=1}^{k} d_\alpha\, \boldsymbol{x}_{j_\alpha}\ + d\, \boldsymbol{x}_e\ :\ d,\ d_\alpha\ \in \{0,1\} \right\} \tag{8.14}$$

is a Golay complementary set of size 2^{k+1}. All the codewords of the Golay complementary set identified above are contained in the same coset Q + RM(1,m) and have PAPR at most 2^{k+1}. And Q can be expressed as

$$Q = \sum_{i=1}^{m-k-1} x_{\pi(i)}\, x_{\pi(i+1)} + \sum_{i=1}^{m-k} \sum_{j=1}^{k} a_{ij}\, x_{\pi(i)}\, x_{\pi(m-k+j)} + \sum_{1\le i<j\le k} c_{ij}\, x_{\pi(m-k+i)}\, x_{\pi(m-k+j)} \;:\; a_{ij},\, c_{ij} \in \{0,1\}. \tag{8.15}$$

The above expression of Q does not cover three second-order cosets of RM(1,4) which are of the form $Q_1 = x_0x_1 + x_2x_3$, $Q_2 = x_0x_2 + x_1x_3$, $Q_3 = x_0x_3 + x_1x_2$. In order to include them, [105] extended the description of Q by allowing $G(Q)$ to contain a set of k distinct vertices labeled $j_1, j_2, \ldots, j_k$ with the property that deleting those k vertices and their edges results in a path on $m-k-1$ vertices and a single vertex of degree zero. However, there are still quadratic forms in 5 variables which the extension does not cover (e.g., $x_0x_1 + x_0x_4 + x_1x_4 + x_2x_4 + x_3x_4$ where deletion of the vertex 4 gives a graph with a single edge and two degree zero vertices) and [105] commented that it is tempting to conjecture that the more general form of describing Q may be with the property that a deletion of k vertices gives a Hamiltonian path and any number of degree zero vertices. That description of Q for $m-1 \ge k \ge 1$ can be expressed as

$$\sum_{i=1}^{p-1} x_{\pi(i)}\, x_{\pi(i+1)} + \sum_{i=1}^{p} \sum_{j=1}^{k} a_{ij}\, x_{\pi(i)}\, x_{\pi(m-k+j)} + \sum_{1\le i<j\le k} c_{ij}\, x_{\pi(m-k+i)}\, x_{\pi(m-k+j)} + \sum_{j=1}^{m-p-k} \left(x_{\pi(p+j)}\, x_{\pi(l_j)} + d_j\, x_{\pi(p+j)}\, x_{\pi(\beta_j)} \right) \;:\; a_{ij},\, c_{ij},\, d_j \in \{0,1\} \tag{8.16}$$

where $x_{\pi(l_j)}, x_{\pi(\beta_j)} \in \{x_{\pi(m-k+1)}, x_{\pi(m-k+2)}, \ldots, x_{\pi(m)}\}$, $x_{\pi(l_j)} \neq x_{\pi(\beta_j)}$, and $2 \le p \le m-k$.

For the cases of $m = 4$, 5 and $k = 1$, we have tested the above description of Q and found that all cosets of RM(1,m) produced by the coset representatives Q have PAPR at most 4, hence, that general form of Q holds for $m = 4$ and 5, and $k = 1$ cases. This Section indicates, by means of Graph interpretation approach, the PAPR behaviour of second-order cosets of RM(1,m) codes; particularly, it states that cosets

corresponding to certain quadratic form Q have PAPR at most 2^{k+1}. For higher order cosets, Graph interpretation may not be feasible. In the next section, alternative observation of PAPR behaviour of second and higher order cosets of RM(1,m) codes will be discussed.

8.2 PAPR Behavior of Second-Order Cosets

Three notations, $\mathcal{S}$, $\mathcal{C}$ and $\mathcal{O}$ defined below are used to describe the pattern of the message vector $\boldsymbol{M}_2$ corresponding to $\boldsymbol{G}_2$, in orther words, the pattern of row vectors from $\boldsymbol{G}_2$ corresponding to 1's in $\boldsymbol{M}_2$, which generates second-order cosets with PAPR at most 4, for $m = 4$ and 5. Each row in $\boldsymbol{G}_2$ can be expressed as a path with 2 vertices and the label of the vertices are hereforth referred as the indexes of the corresponding vector. For example, $\boldsymbol{x}_1\boldsymbol{x}_2$ is a row vector from $\boldsymbol{G}_2$ and the corresponding indexes are 1 and 2.

The meanings of the notations are as follows. The number associated with each notation indicates the number of vectors for the corresponding notation. $\mathcal{S}$ means "having one *same* index". 2 $\mathcal{S}$ means any 2 row vectors from $\boldsymbol{G}_2$ which have one same index. We say that they are from the same class of that same index. However, 1 $\mathcal{S}$ can be any vector from $\boldsymbol{G}_2$. $\mathcal{C}$ means "not from the same class of $\mathcal{S}$ and having one (*complementary*) index which is not included in all indexes of $\mathcal{S}$ ". $\mathcal{O}$ means " any *other* vector not from the same class of $\mathcal{S}$.

Example : For $m = 4$, the pattern (2 $\mathcal{S}$, 1 $\mathcal{C}$, 1 $\mathcal{O}$) has the following interpretation.

For $m = 4$, 2 $\mathcal{S}$ can be any of ($\boldsymbol{x}_1\boldsymbol{x}_2$, $\boldsymbol{x}_1$ $\boldsymbol{x}_3$), ($\boldsymbol{x}_1\boldsymbol{x}_2$, $\boldsymbol{x}_1\boldsymbol{x}_4$), ($\boldsymbol{x}_1\boldsymbol{x}_3$, $\boldsymbol{x}_1\boldsymbol{x}_4$), ($\boldsymbol{x}_1\boldsymbol{x}_2$, $\boldsymbol{x}_2\boldsymbol{x}_3$), ($\boldsymbol{x}_1\boldsymbol{x}_2$, $\boldsymbol{x}_2\boldsymbol{x}_4$), ($\boldsymbol{x}_2\boldsymbol{x}_3$, $\boldsymbol{x}_2\boldsymbol{x}_4$), ($\boldsymbol{x}_1\boldsymbol{x}_3$, $\boldsymbol{x}_2\boldsymbol{x}_3$), ($\boldsymbol{x}_1\boldsymbol{x}_3$, $\boldsymbol{x}_3\boldsymbol{x}_4$), ($\boldsymbol{x}_2\boldsymbol{x}_3$, $\boldsymbol{x}_3\boldsymbol{x}_4$), ($\boldsymbol{x}_1\boldsymbol{x}_4$, $\boldsymbol{x}_2\boldsymbol{x}_4$), ($\boldsymbol{x}_1\boldsymbol{x}_4$, $\boldsymbol{x}_3\boldsymbol{x}_4$) or ($\boldsymbol{x}_2\boldsymbol{x}_4$, $\boldsymbol{x}_3\boldsymbol{x}_4$). If 2 $\mathcal{S}$ = ($\boldsymbol{x}_1\boldsymbol{x}_2$, $\boldsymbol{x}_1\boldsymbol{x}_3$), then 1 $\mathcal{C}$ can be $\boldsymbol{x}_2\boldsymbol{x}_4$ or $\boldsymbol{x}_3\boldsymbol{x}_4$. If 2 $\mathcal{S}$ = ($\boldsymbol{x}_1\boldsymbol{x}_2$, $\boldsymbol{x}_1\boldsymbol{x}_3$) and 1 $\mathcal{C}$ = $\boldsymbol{x}_2\boldsymbol{x}_4$, then 1 $\mathcal{O}$ can be $\boldsymbol{x}_2\boldsymbol{x}_3$ or $\boldsymbol{x}_3\boldsymbol{x}_4$.

In Table 8.1, the patterns of $\boldsymbol{M}_2$ corresponding to the second-order cosets of RM(1,m) codes with PAPR at most 4, for $m = 4$ and 5 are tabulated. $W_H(\ )$ refers to the Hamming weight. For m=4 and $W_H(\boldsymbol{M}_2)$=2, since 1 $\mathcal{S}$ indicates any $\boldsymbol{G}_2$ vector and does not impose any restriction of the same class, 1 $\mathcal{C}$ can be any other $\boldsymbol{G}_2$ vector. Hence, the pattern 1 $\mathcal{S}$, 1 $\mathcal{C}$ means any two vectors out of the total 6

Table 8.1. *Pattern corresponding to second-order coset representatives of RM(1,m) codes with PAPR* ≤ 4

m	$W_H(M_2)$	Pattern	Example (x_1x_2, x_1x_3, x_1x_4, x_2x_3, x_2x_4, x_3x_4)	No. of coset representatives
4	2	1 $\mathcal{S}$, 1 $\mathcal{C}$	1 0 0 0 0 1	15
	3	3 $\mathcal{S}$	1 1 1 0 0 0	4
		path on 4 vertices / (2 $\mathcal{S}$, 1 $\mathcal{C}$)	1 1 0 0 0 1	12
	4	2 $\mathcal{S}$, 1 $\mathcal{C}$, 1 $\mathcal{O}$	1 0 1 1 1 0	15
	5	3 $\mathcal{S}$, 2 $\mathcal{O}$	1 1 1 1 1 0	6
			(x_1x_2, x_1x_3, x_1x_4, x_1x_5, x_2x_3, x_2x_4, x_2x_5, x_3x_4, x_3x_5, x_4x_5)	
5	3	2 $\mathcal{S}$, 1 $\mathcal{C}$	1 0 1 0 1 0 0 0 0 0	90
	4	3 $\mathcal{S}$, 1 $\mathcal{C}$	1 0 1 1 1 0 0 0 0 0	60
		path on 5 vertices	1 1 0 0 0 0 0 1 0 1	60
	5	2 $\mathcal{S}$, 2 $\mathcal{C}$, 1 $\mathcal{O}$	0 1 0 1 1 0 1 1 0 0	222
	6	Zeros: (i) 3 $\mathcal{S}$, 1 $\mathcal{O}$	1 1 1 1 0 1 1 0 0 0	120
		Zeros: (ii) path on 5 vertices	1 0 1 0 0 0 1 1 1 1	60
	7	Zeros: path on 4 vertices	1 1 1 1 1 0 1 1 0 0	60
	8	Zeros: 2 $\mathcal{S}$	1 1 1 1 1 1 1 1 0 0	30

vectors of $\boldsymbol{G}_2$ which constitute 15 coset representatives.

For m=4 and $W_H(\boldsymbol{M}_2)$= 3, the pattern which forms a path on m vertices are the $m!/2$ coset representatives with PAPR at most 2 obtained from Q in (8.15) with $k = 0$ (see [104] [105] for details). They can alternatively be covered by the pattern 2 $\mathcal{S}$, 1 $\mathcal{C}$. The pattern 3 $\mathcal{S}$ for m=4 and $W_H(\boldsymbol{M}_2)$= 3 indicates 4 coset representatives namely $(\boldsymbol{x}_1\boldsymbol{x}_2, \boldsymbol{x}_1\boldsymbol{x}_3, \boldsymbol{x}_1\boldsymbol{x}_4)$, $(\boldsymbol{x}_1\boldsymbol{x}_2, \boldsymbol{x}_2\boldsymbol{x}_3, \boldsymbol{x}_2\boldsymbol{x}_4)$, $(\boldsymbol{x}_1\boldsymbol{x}_3, \boldsymbol{x}_2\boldsymbol{x}_3, \boldsymbol{x}_3\boldsymbol{x}_4)$ and $(\boldsymbol{x}_1\boldsymbol{x}_4, \boldsymbol{x}_2\boldsymbol{x}_4, \boldsymbol{x}_3\boldsymbol{x}_4)$. The 15 coset representatives covered by the pattern 2 $\mathcal{S}$, 1 $\mathcal{C}$, 1 $\mathcal{O}$ for m=4 and $W_H(\boldsymbol{M}_2)$= 4 are in fact obtained by the complements of the $\boldsymbol{M}_2$ vectors covered in m=4 and $W_H(\boldsymbol{M}_2)$= 2. Hence, the $\boldsymbol{M}_2$ vector [0 1 1 1 1 0], which is the complement of an $\boldsymbol{M}_2$ vector [1 0 0 0 0 1] shown in Table 8.1, is covered by the pattern 2 $\mathcal{S}$, 1 $\mathcal{C}$, 1 $\mathcal{O}$. The vectors covered by 3 $\mathcal{S}$, 2 $\mathcal{O}$ for $m = 4$ and $W_H(\boldsymbol{M}_2)$= 5 indicate that they are any five vectors out of the total 6 vectors of $\boldsymbol{G}_2$.

Similarly, for m=5 and $W_H(\boldsymbol{M}_2)$= 4, the pattern which forms a path on m vertices are the $m!/2$ coset representatives with PAPR at most 2 obtained from Q in (8.15) with $k = 0$. For $m = 5$ and $W_H(\boldsymbol{M}_2) = 6$, 7, 8 cases, the patterns mentioned correspond to zero positions in $\boldsymbol{M}_2$. In the case of m=6 and $W_H(\boldsymbol{M}_2)$= 6, the pattern 3 $\mathcal{S}$, 1 $\mathcal{O}$ for zero positions indicates that 4 zeros can be, for example, corresponding to $\boldsymbol{x}_2\boldsymbol{x}_3$, $\boldsymbol{x}_3\boldsymbol{x}_4$, $\boldsymbol{x}_3\boldsymbol{x}_5$ and $\boldsymbol{x}_4\boldsymbol{x}_5$ and hence, the corresponding $\boldsymbol{M}_2$ vector would be [1 1 1 1 0 1 1 0 0 0].

In the case of m=5 and $W_H(\boldsymbol{M}_2) = 6$, the zero positions of the $\boldsymbol{M}_2$ vectors form a path on 5 vertices. In fact, these $\boldsymbol{M}_2$ vectors are the complements of the $\boldsymbol{M}_2$ vectors corresponding to m=5 and $W_H(\boldsymbol{M}_2) = 4$ case which form a path on 5 vertices. For example, consider an $\boldsymbol{M}_2$ vector [0 1 0 1 1 1 0 0 0 0] which corresponds to the vectors $\boldsymbol{x}_{13}$, $\boldsymbol{x}_{15}$, $\boldsymbol{x}_2\boldsymbol{x}_3$ and $\boldsymbol{x}_2\boldsymbol{x}_4$ from $\boldsymbol{G}_2$ and can be characterized by a path on the vertices (1, 2, 3, 4, 5). This vector is one of the $m!/2$ coset representatives with PAPR at most 2. Its complement vector [1 0 1 0 0 0 1 1 1 1] is an $\boldsymbol{M}_2$ vector for m=5 and $W_H(\boldsymbol{M}_2)$= 6.

For m=5 and $W_H(\boldsymbol{M}_2)$= 7, the zero positions form a path on 4 vertices. For example, an $\boldsymbol{M}_2$ vector [1 1 1 1 1 0 1 1 0 0] has zero positions corresponding to the vectors $\boldsymbol{x}_2\boldsymbol{x}_4$, $\boldsymbol{x}_3\boldsymbol{x}_5$ and $\boldsymbol{x}_4\boldsymbol{x}_5$ which form a path on the 4 vertices of (2, 3, 4, 5). For m=5 and $W_H(\boldsymbol{M}_2)$= 8, the two $\boldsymbol{G}_2$ vectors for the zero positions have one same index. For example, an $\boldsymbol{M}_2$ vector [1 1 1 1 1 1 1 1 0 0] has zero positions for the

G_2 vectors x_3x_5 and x_4x_5 which have one same index of 5. From Table 8.1, we can see that all the second-order coset representatives with PAPR at most 4 follow some regular patterns.

For $k = 1$ in (8.15) which corresponds to PAPR at most 4, [105]'s approach covers second-order coset representatives with $W_H(M_2)$ from $(m-2)$ to $(2m-3)$. For $m = 5$, it covers for $W_H(M_2)$ from 3 to 7. But there are 30 coset representatives with $W_H(M_2) = 8$ in Table 8.1 which are not covered in [105]. The corresponding M_2 vectors for those 30 coset representatives are given in Table 8.2. Hence, there can be more coset representatives than those covered by [105].

8.3 PAPR Behavior of Third-Order Cosets

In the following, the patterns of row vectors from G_2 and G_3 which generate cosets of RM(1,4) code with PAPR at most 4 are discussed by some examples. By vectors corresponding to M_2, we mean the vectors from G_2 which correspond to 1's in M_2. The approach is such that for a given pattern of M_3, the pattern of M_2 is described.

8.3.1 Case 1: $W_H(M_3) = 2$, $W_H([M_2, M_3]) = 4$ to 7.

Let M_3 = 1 1 0 0 which includes two row vectors $(x_1x_2x_3)$ and $(x_1x_2x_4)$, and excludes the other two vectors $(x_1x_3x_4)$ and $(x_2x_3x_4)$ from G_3.

(a) $W_H(M_2) = 2$

One of the two vectors corresponding to M_2 is found to be x_3x_4 whose indexes are contained in the indexes of both excluded vectors of G_3 (i.e., the common indexes in both excluded vectors of G_3). And the other vector for M_2 forms a path with the first vector x_3x_4 and the three vertices of the path are the indexes of either excluded vector, (i.e., vertices are (1,3,4) or (2,3,4), and the vectors are $(x_3x_4,\ x_1x_3)$ or $(x_3x_4,\ x_1x_4)$ if the vertices are (1,3,4)). This pattern of M_2 holds for any M_3 with $W_H(M_3) = 2$, which corresponds to $4\binom{4}{2} = 24$ third-order coset representatives. The M_2 and M_3 vectors for these coset representatives are given in Table 8.3.

Table 8.2. *M_2 vectors corresponding to second-order coset representatives of RM(1,m) code with PAPR $\leq$ 4 for m=5 and $W_H(M_2)$=8 which have the pattern 2 S for zero positions*

$(x_1x_2,\ x_1x_3,\ x_1x_4,\ x_1x_5,\ x_2x_3,\ x_2x_4,\ x_2x_5,\ x_3x_4,\ x_3x_5,\ x_4x_5)$
1 1 1 1 1 1 1 1 0 0
1 1 1 1 1 1 1 0 1 0
1 1 1 1 1 1 0 1 1 0
1 1 1 1 1 0 1 1 1 0
1 1 1 0 1 1 1 1 1 0
1 1 0 1 1 1 1 1 1 0
1 1 1 1 1 1 1 0 0 1
1 1 1 1 1 1 0 1 0 1
1 1 1 1 0 1 1 1 0 1
1 1 1 0 1 1 1 1 0 1
1 0 1 1 1 1 1 1 0 1
1 1 1 1 1 0 1 0 1 1
1 1 1 1 0 1 1 0 1 1
1 1 0 1 1 1 1 0 1 1
1 0 1 1 1 1 1 0 1 1
1 1 1 1 1 0 0 1 1 1
1 1 1 1 0 1 0 1 1 1
1 1 1 0 1 1 0 1 1 1
0 1 1 1 1 1 0 1 1 1
1 1 1 1 0 0 1 1 1 1
1 1 0 1 1 0 1 1 1 1
0 1 1 1 1 0 1 1 1 1
1 0 1 1 0 1 1 1 1 1
0 1 1 1 0 1 1 1 1 1
1 1 0 0 1 1 1 1 1 1
1 0 1 0 1 1 1 1 1 1
0 1 1 0 1 1 1 1 1 1
1 0 0 1 1 1 1 1 1 1
0 1 0 1 1 1 1 1 1 1
0 0 1 1 1 1 1 1 1 1

(b) $W_H(\boldsymbol{M}_2) = 3$

One of the three vectors corresponding to $\boldsymbol{M}_2$ is found to be $\boldsymbol{x}_3\boldsymbol{x}_4$ whose indexes are the common indexes of both excluded vectors of $\boldsymbol{G}_3$. And the other two vectors are found to be of the two forms:

(i) They form a path on the vertices which are the indexes of either included vector of $\boldsymbol{G}_3$ (e.g., $\boldsymbol{x}_1\boldsymbol{x}_2$ and $\boldsymbol{x}_1\boldsymbol{x}_3$ which form a path on (1, 2, 3)). This pattern of $\boldsymbol{M}_2$ holds for any $\boldsymbol{M}_3$ with $W_H(\boldsymbol{M}_3) = 2$, which corresponds to $6\binom{4}{2} = 36$ third-order coset representatives.

(ii) Their four indexes constitute (1, 2, 3, 4) (e.g., $\boldsymbol{x}_1\boldsymbol{x}_4$ and $\boldsymbol{x}_2\boldsymbol{x}_3$). This pattern of $\boldsymbol{M}_2$ holds for any $\boldsymbol{M}_3$ with $W_H(\boldsymbol{M}_3) = 2$, which corresponds to $2\binom{4}{2} = 12$ third-order coset representatives. The $\boldsymbol{M}_2$ and $\boldsymbol{M}_3$ vectors for these coset representatives of both forms are given in Table 8.4.

(c) $W_H(\boldsymbol{M}_2) = 4$

$\boldsymbol{x}_3\boldsymbol{x}_4$, whose indexes are the common ones of both excluded vectors of $\boldsymbol{G}_3$, is again one of the four vectors. And the other three vectors are found to be the complements of the two vectors for $W_H(\boldsymbol{M}_2) = 3$ case, (e.g., $\boldsymbol{x}_1\boldsymbol{x}_4$, $\boldsymbol{x}_2\boldsymbol{x}_3$ and $\boldsymbol{x}_2\boldsymbol{x}_4$ if two vectors for $W_H(\boldsymbol{M}_2) = 3$ case are $\boldsymbol{x}_1\boldsymbol{x}_2$ and $\boldsymbol{x}_1\boldsymbol{x}_3$). This pattern of $\boldsymbol{M}_2$ also holds for any $\boldsymbol{M}_3$ with $W_H(\boldsymbol{M}_3) = 2$, which corresponds to $8\binom{4}{2} = 48$ third-order coset representatives. The $\boldsymbol{M}_2$ and $\boldsymbol{M}_3$ vectors for these coset representatives are given in Table 8.5.

(d) $W_H(\boldsymbol{M}_2) = 5$

Again, the vector $\boldsymbol{x}_3\boldsymbol{x}_4$, which has the common indexes of both excluded vectors of $\boldsymbol{G}_3$, is one of the five vectors. And the other four vectors are found to be the complements of the second vector for $W_H(\boldsymbol{M}_2) = 2$ case, (e.g., $\boldsymbol{x}_1\boldsymbol{x}_2$, $\boldsymbol{x}_1\boldsymbol{x}_3$, $\boldsymbol{x}_2\boldsymbol{x}_3$ and $\boldsymbol{x}_2\boldsymbol{x}_4$ if the second vector for $W_H(\boldsymbol{M}_2) = 2$ case is $\boldsymbol{x}_1\boldsymbol{x}_4$). This pattern constitutes $4\binom{4}{2} = 24$ third-order coset representatives, holding for any $\boldsymbol{M}_3$ with $W_H(\boldsymbol{M}_3) = 2$. The $\boldsymbol{M}_2$ and $\boldsymbol{M}_3$ vectors for these coset representatives are given in Table 8.6.

8.3.2 Case 2: $W_H(M_3) = 3$, $W_H([M_2, M_3]) = 4$ to 7.

Let $M_3 = 1\ 1\ 1\ 0$ which includes three row vectors $(x_1x_2x_3)$, $(x_1x_2x_4)$ and $(x_1x_3x_4)$, and excludes the other vector $(x_2x_3x_4)$ from G_3.

(a) $W_H(M_2) = 1$

The vector corresponding to M_2 is found to be any vector whose indexes are contained in the indexes of excluded vector of G_3, (e.g., x_2x_3 or x_2x_4 or x_3x_4 if the excluded vector is $x_2x_3x_4$). This pattern holds for any M_3 with $W_H(M_3) = 3$ and constitutes $3\binom{4}{3} = 12$ third-order coset representatives. The M_2 and M_3 vectors for these coset representatives are given in Table 8.7.

(b) $W_H(M_2) = 2$

The two vectors corresponding to M_2 form a path on the vertices of the indexes of the excluded vector of G_3, (e.g., $(x_2x_3,\ x_2x_4)$ or $(x_2x_3,\ x_3x_4)$ or $(x_2x_4,\ x_3x_4)$ if the excluded vector is $x_2x_3x_4$). This pattern holds for any M_3 with $W_H(M_3) = 3$ and constitutes $3\binom{4}{3} = 12$ third-order coset representatives. The M_2 and M_3 vectors for these coset representatives are given in Table 8.8.

(c) $W_H(M_2) = 3$

The three vectors corresponding to M_2 are of the following two forms:

(i) They form a circle on the vertices of the indexes of any included vector of G_3, (e.g., $(x_1x_2,\ x_1x_3,\ x_2x_3)$ for an included vector $x_1x_2x_3$). This pattern holds for any M_3 with $W_H(M_3) = 3$ and constitutes $3\binom{4}{3} = 12$ third-order coset representatives.

(ii) They form a path $(v_1v_2v_3v_4)$, where $(v_1v_2v_3v_4) = \pi(x_1, x_2, x_3, x_4)$ and v_1, v_4 are not equal to the index common in all three included vectors of G_3, (e.g., if the included vectors of G_3 are $(x_1x_2x_3)$, $(x_1x_2x_4)$ and $(x_1x_3x_4)$, the path can be 4123, 4132, 4213, 3142, 4312 or 3412. And the vectors are $(x_1x_2,\ x_1x_4,\ x_2x_3)$ if the path is 4123). This pattern holds for any M_3 with $W_H(M_3) = 3$ and constitutes

$6\binom{4}{3} = 24$ third-order coset representatives. The $\boldsymbol{M}_2$ and $\boldsymbol{M}_3$ vectors for these coset representatives of both forms are given in Table 8.9.

(d) $W_H(\boldsymbol{M}_2) = 4$

The four vectors corresponding to $\boldsymbol{M}_2$ are of the following two forms:

(i) They form a circle on the vertices (1, 2, 3, 4), (e.g., $\boldsymbol{x}_1\boldsymbol{x}_3$, $\boldsymbol{x}_1\boldsymbol{x}_4$, $\boldsymbol{x}_2\boldsymbol{x}_3$, $\boldsymbol{x}_2\boldsymbol{x}_4$). This pattern holds for any $\boldsymbol{M}_3$ with $W_H(\boldsymbol{M}_3) = 3$ and constitutes $3\binom{4}{3} = 12$ third-order coset representatives.

(ii) The first three vectors are from the same class which is not the same class of the index common in all three included vectors of $\boldsymbol{G}_3$. The fourth one contains the index common in all three included vectors of $\boldsymbol{G}_3$, (e.g., index 1 is common in all three included vectors of $\boldsymbol{G}_3$ in our example, so the first three vectors can be from same class of index 2, ($\boldsymbol{x}_1\boldsymbol{x}_2$, $\boldsymbol{x}_2\boldsymbol{x}_3$, $\boldsymbol{x}_2\boldsymbol{x}_4$), or of index 3, ($\boldsymbol{x}_1\boldsymbol{x}_3$, $\boldsymbol{x}_2\boldsymbol{x}_3$, $\boldsymbol{x}_3\boldsymbol{x}_4$), or of index 4, ($\boldsymbol{x}_1\boldsymbol{x}_4$, $\boldsymbol{x}_2\boldsymbol{x}_4$, $\boldsymbol{x}_3\boldsymbol{x}_4$). The fourth one can be $\boldsymbol{x}_1\boldsymbol{x}_3$, or $\boldsymbol{x}_1\boldsymbol{x}_4$ if the first three are ($\boldsymbol{x}_1\boldsymbol{x}_2$, $\boldsymbol{x}_2\boldsymbol{x}_3$, $\boldsymbol{x}_2\boldsymbol{x}_4$). This pattern holds for any $\boldsymbol{M}_3$ with $W_H(\boldsymbol{M}_3) = 3$ and constitutes $6\binom{4}{3} = 24$ third-order coset representatives. The $\boldsymbol{M}_2$ and $\boldsymbol{M}_3$ vectors for these coset representatives of both forms are given in Table 8.10.

We have observed that 240 third-order coset representatives out of 265 which have PAPR at most 4 follow some regular patterns. But there are 12 coset representatives corresponding to $W_H(\boldsymbol{M}_3) = 1$ and 13 coset representatives corresponding to $W_H(\boldsymbol{M}_3) = 4$ for which no regular patterns have been observed.

It is also observed that in the 4^{th} order cosets of RM(1,4) code, those with coset representatives corresponding to $W_H(\boldsymbol{M}_3) = 1$, $\boldsymbol{M}_4 = 1$, and pattern of $\boldsymbol{M}_2$ being a path on 4 vertices (i.e., the $m!/2$ second-order coset representatives with PAPR at most 2) have PAPR at most 4. We have tested for $m \leq 6$ and found that those codes with the coset representatives corresponding to $W_H(\boldsymbol{M}_{m-1}) = 1$, $\boldsymbol{M}_m = 1$, and pattern of $\boldsymbol{M}_2$ being a path on m vertices have PAPR at most 4. Actually these m^{th} order coset representatives have Hamming distance of 1 from the corresponding second-order coset representatives with PAPR at most 2.

Table 8.3. *M_2 and M_3 vectors corresponding to third-order coset representatives of RM(1,m) code with PAPR ≤ 4 for m=4, $W_H(M_2)=2$ and $W_H(M_3)=2$*

$(x_1x_2,\ x_1x_3,\ x_1x_4,\ x_2x_3,\ x_2x_4,\ x_3x_4)$	$(x_1x_2x_3,\ x_1x_2x_4,\ x_1x_3x_4,\ x_2x_3x_4)$
0 1 0 0 0 1	1 1 0 0
0 0 1 0 0 1	1 1 0 0
0 0 0 1 0 1	1 1 0 0
0 0 0 0 1 1	1 1 0 0
1 0 0 0 1 0	1 0 1 0
0 0 1 0 1 0	1 0 1 0
0 0 0 1 1 0	1 0 1 0
0 0 0 0 1 1	1 0 1 0
1 0 0 1 0 0	0 1 1 0
0 1 0 1 0 0	0 1 1 0
0 0 0 1 1 0	0 1 1 0
0 0 0 1 0 1	0 1 1 0
1 0 1 0 0 0	1 0 0 1
0 1 1 0 0 0	1 0 0 1
0 0 1 0 1 0	1 0 0 1
0 0 1 0 0 1	1 0 0 1
1 1 0 0 0 0	0 1 0 1
0 1 1 0 0 0	0 1 0 1
0 1 0 1 0 0	0 1 0 1
0 1 0 0 0 1	0 1 0 1
1 1 0 0 0 0	0 0 1 1
1 0 1 0 0 0	0 0 1 1
1 0 0 1 0 0	0 0 1 1
1 0 0 0 1 0	0 0 1 1

Table 8.4. *M_2 and M_3 vectors corresponding to third-order coset representatives of RM(1,m) code with PAPR ≤ 4 for $m=4$, $W_H(M_2)=3$ and $W_H(M_3)=2$*

form	$(x_1x_2,\ x_1x_3,\ x_1x_4,\ x_2x_3, x_2x_4,\ x_3x_4)$		$(x_1x_2x_3,\ x_1x_2x_4,\ x_1x_3x_4,\ x_2x_3x_4)$	
(i)	1 1 0 0 0 1	1 1 0 0	1 1 1 0 0 0	1 0 0 1
	1 0 1 0 0 1	1 1 0 0	1 0 1 1 0 0	1 0 0 1
	1 0 0 1 0 1	1 1 0 0	0 1 1 1 0 0	1 0 0 1
	0 1 0 1 0 1	1 1 0 0	0 0 1 1 1 0	1 0 0 1
	1 0 0 0 1 1	1 1 0 0	0 0 1 1 0 1	1 0 0 1
	0 0 1 0 1 1	1 1 0 0	0 0 1 0 1 1	1 0 0 1
(ii)	0 0 1 1 0 1	1 1 0 0	1 0 1 0 0 1	1 0 0 1
	0 1 0 0 1 1	1 1 0 0	0 1 1 0 1 0	1 0 0 1
(i)	1 1 0 0 1 0	1 0 1 0	1 1 1 0 0 0	0 1 0 1
	0 1 1 0 1 0	1 0 1 0	1 1 0 0 1 0	0 1 0 1
	1 0 0 1 1 0	1 0 1 0	0 1 1 0 1 0	0 1 0 1
	0 1 0 1 1 0	1 0 1 0	0 1 0 1 1 0	0 1 0 1
	0 1 0 0 1 1	1 0 1 0	0 1 0 1 0 1	0 1 0 1
	0 0 1 0 1 1	1 0 1 0	0 1 0 0 1 1	0 1 0 1
(ii)	1 0 0 0 1 1	1 0 1 0	1 1 0 0 0 1	0 1 0 1
	0 0 1 1 1 0	1 0 1 0	0 1 1 1 0 0	0 1 0 1
(i)	1 0 1 1 0 0	0 1 1 0	1 1 1 0 0 0	0 0 1 1
	0 1 1 1 0 0	0 1 1 0	1 0 0 1 1 0	0 0 1 1
	1 0 0 1 1 0	0 1 1 0	1 1 0 0 0 1	0 0 1 1
	0 0 1 1 1 0	0 1 1 0	1 0 1 0 0 1	0 0 1 1
	0 1 0 1 0 1	0 1 1 0	1 0 0 1 0 1	0 0 1 1
	0 0 1 1 0 1	0 1 1 0	1 0 0 0 1 1	0 0 1 1
(ii)	1 0 0 1 0 1	0 1 1 0	1 1 0 0 1 0	0 0 1 1
	0 1 0 1 1 0	0 1 1 0	1 0 1 1 0 0	0 0 1 1

Table 8.5. *M_2 and M_3 vectors corresponding to third-order coset representatives of RM(1,m) code with PAPR ≤ 4 for $m=4$, $W_H(M_2)=4$ and $W_H(M_3)=2$*

$(x_1x_2,\ x_1x_3,\ x_1x_4,\ x_2x_3,\ x_2x_4,\ x_3x_4)$		$(x_1x_2x_3,\ x_1x_2x_4,\ x_1x_3x_4,\ x_2x_3x_4)$	
110101	1100	111100	1001
101101	1100	111010	1001
011101	1100	011110	1001
110011	1100	111001	1001
101011	1100	101101	1001
011011	1100	101011	1001
010111	1100	011011	1001
001111	1100	001111	1001
110110	1010	111100	0101
101110	1010	111010	0101
011110	1010	011110	0101
110011	1010	111001	0101
101011	1010	110101	0101
011011	1010	011101	0101
100111	1010	110011	0101
001111	1010	010111	0101
110110	0110	111100	0011
101110	0110	111010	0011
011110	0110	110110	0011
110101	0110	101110	0011
101101	0110	111001	0011
011101	0110	101101	0011
100111	0110	110011	0011
010111	0110	100111	0011

Table 8.6. *M_2 and M_3 vectors corresponding to third-order coset representatives of RM(1,m) code with PAPR ≤ 4 for m=4, $W_H(M_2)=5$ and $W_H(M_3)=2$*

$(x_1x_2,\ x_1x_3,\ x_1x_4,\ x_2x_3,\ x_2x_4,\ x_3x_4)$	$(x_1x_2x_3,\ x_1x_2x_4,\ x_1x_3x_4,\ x_2x_3x_4)$
1 1 1 1 0 1	1 1 0 0
1 1 1 0 1 1	1 1 0 0
1 1 0 1 1 1	1 1 0 0
1 0 1 1 1 1	1 1 0 0
1 1 1 1 1 0	1 0 1 0
1 1 1 0 1 1	1 0 1 0
1 1 0 1 1 1	1 0 1 0
0 1 1 1 1 1	1 0 1 0
1 1 1 1 1 0	0 1 1 0
1 1 1 1 0 1	0 1 1 0
1 0 1 1 1 1	0 1 1 0
0 1 1 1 1 1	0 1 1 0
1 1 1 1 1 0	1 0 0 1
1 1 1 1 0 1	1 0 0 1
1 0 1 1 1 1	1 0 0 1
0 1 1 1 1 1	1 0 0 1
1 1 1 1 1 0	0 1 0 1
1 1 1 0 1 1	0 1 0 1
1 1 0 1 1 1	0 1 0 1
0 1 1 1 1 1	0 1 0 1
1 1 1 1 0 1	0 0 1 1
1 1 1 0 1 1	0 0 1 1
1 1 0 1 1 1	0 0 1 1
1 0 1 1 1 1	0 0 1 1

Table 8.7. *M_2 and M_3 vectors corresponding to third-order coset representatives of RM(1,m) code with PAPR ≤ 4 for m=4, $W_H(M_2)=1$ and $W_H(M_3)=3$*

$(x_1x_2,\ x_1x_3,\ x_1x_4,\ x_2x_3,\ x_2x_4,\ x_3x_4)$	$(x_1x_2x_3,\ x_1x_2x_4,\ x_1x_3x_4,\ x_2x_3x_4)$
0 0 0 1 0 0	1 1 1 0
0 0 0 0 1 0	1 1 1 0
0 0 0 0 0 1	1 1 1 0
0 1 0 0 0 0	1 1 0 1
0 0 1 0 0 0	1 1 0 1
0 0 0 0 0 1	1 1 0 1
1 0 0 0 0 0	1 0 1 1
0 0 1 0 0 0	1 0 1 1
0 0 0 0 1 0	1 0 1 1
1 0 0 0 0 0	0 1 1 1
0 1 0 0 0 0	0 1 1 1
0 0 0 1 0 0	0 1 1 1

Table 8.8. *M_2 and M_3 vectors corresponding to third-order coset representatives of RM(1,m) code with PAPR ≤ 4 for $m=4$, $W_H(M_2)=2$ and $W_H(M_3)=3$*

$(x_1x_2,\ x_1x_3,\ x_1x_4,\ x_2x_3,\ x_2x_4,\ x_3x_4)$	$(x_1x_2x_3,\ x_1x_2x_4,\ x_1x_3x_4,\ x_2x_3x_4)$
0 0 0 1 1 0	1 1 1 0
0 0 0 1 0 1	1 1 1 0
0 0 0 0 1 1	1 1 1 0
0 1 1 0 0 0	1 1 0 1
0 1 0 0 0 1	1 1 0 1
0 0 1 0 0 1	1 1 0 1
1 0 1 0 0 0	1 0 1 1
1 0 0 0 1 0	1 0 1 1
0 0 1 0 1 0	1 0 1 1
1 1 0 0 0 0	0 1 1 1
1 0 0 1 0 0	0 1 1 1
0 1 0 1 0 0	0 1 1 1

Table 8.9. *M_2 and M_3 vectors corresponding to third-order coset representatives of RM(1,m) code with PAPR ≤ 4 for m=4, $W_H(M_2)$=3 and $W_H(M_3)$=3*

$(x_1x_2,\ x_1x_3,\ x_1x_4,\ x_2x_3,\ x_2x_4,\ x_3x_4)$		$(x_1x_2x_3,\ x_1x_2x_4,\ x_1x_3x_4,\ x_2x_3x_4)$	
form (i)		form (ii)	
110100	1110	101100	1110
101010	1110	011100	1110
011001	1110	110010	1110
110100	1101	011010	1110
101010	1101	110001	1110
000111	1101	101001	1110
110100	1011	101100	1101
011001	1011	110010	1101
000111	1011	010110	1101
101010	0111	001110	1101
011001	0111	100101	1101
000111	0111	100011	1101
		011100	1011
		010110	1011
		110001	1011
		100101	1011
		001101	1011
		010011	1011
		011010	0111
		001110	0111
		101001	0111
		001101	0111
		100011	0111
		010011	0111

Table 8.10. *M_2 and M_3 vectors corresponding to third-order coset representatives of RM(1,m) code with PAPR ≤ 4 for m=4, $W_H(M_2)=4$ and $W_H(M_3)=3$*

$(x_1x_2,\ x_1x_3,\ x_1x_4,\ x_2x_3,\ x_2x_4,\ x_3x_4)$		$(x_1x_2x_3,\ x_1x_2x_4,\ x_1x_3x_4,\ x_2x_3x_4)$	
form (i)		form (ii)	
011110	1110	110110	1110
101101	1110	101110	1110
110011	1110	110101	1110
011110	1101	011101	1110
101101	1101	101011	1110
110011	1101	011011	1110
011110	1011	111100	1101
101101	1011	111010	1101
110011	1011	010111	1101
011110	0111	110101	1101
101101	0111	101011	1101
110011	0111	001111	1101
		111100	1011
		111001	1011
		110110	1011
		100111	1011
		011011	1011
		001111	1011
		111010	0111
		111001	0111
		100111	0111
		101110	0111
		011101	0111
		010111	0111

8.4 Conclusions

High peak-to-average power ratio (PAPR) is one of the main obstacles for a wider acceptance of OFDM technology. Several approaches have been proposed to alleviate the PAPR problem. Recently, coding approach for both PAPR reduction and error correction has emerged as one of the promising techniques. Based on the recognition of the connection between Golay complementary sequences and second-order cosets of RM(1,m) codes, this approach enjoys both tight PAPR control and good error correction capability. However, for an OFDM system with a large number of carriers, the code rate of this approach becomes too small. Hence, we have considered higher order cosets of RM(1,m) codes beyond its original constraint to second-order cosets. We have studied PAPR behavior of second-order cosets for $m = 4$ and 5, and third-order cosets for $m = 4$ of RM(1,m) codes in OFDM system in order to explore the possibility of including third-order cosets. We have observed that for PAPR at most 4, all 52 second-order coset representatives for $m = 4$, all 702 second-order coset representatives for $m = 5$, and 240 third-order coset representatives out of 265 for $m = 4$ follow some regular patterns. Although our results could not provide a general pattern covering all cases, the regularities in the observed PAPR behavior suggest that in order to increase the code rate, it is possible to include the third-order cosets of RM(1,m) codes in the approach using RM codes in OFDM systems.

Chapter 9

An Efficient ARQ Protocol for Adaptive Error Control over Time-Varying Channels

For communications services where very high system performance is of primary requirement and delay is not a major concern, ARQ and hybrid ARQ error control strategies are usually incorporated in system design to achieve the high system reliability. However, the inherent disadvantage of these schemes is that its throughput declines rapidly as channel error rate increases. In mobile wireless communications, radio channels induce a time-varying response with bursty errors due to multipath fading and shadowing effects. During the fades the channel becomes too noisy and at the other times it well-behaves. For such a time-varying channel, it is clear that the use of a single error control strategy will not yield the optimal throughput. Therefore, in order to provide a reliable packet data transmission, the use of different error control strategies for different channel conditions are highly desired, since it can provide high throughput under a wide range of error rate conditions.

Recently, there has been considerable interest in adaptive ARQ schemes [106]-[107]. The basic idea is by dynamically changing the protocol operation mode according to channel state information, the higher throughput is realized over a wide range of channel conditions. For real-time implementation, the channel state information needs to be estimated reliably and effectively. That means in order to track channel variations closely, reliable estimation of the channel state information should be carried out within short enough intervals (which may involve accurate estimation of the signal strength via signal power measurement or with pilot tone transmission,

and in turn give rise to high implementation complexity).

Several indirect methods have recently been proposed in order to address this issue [106]-[107]. Since the frequency of the retransmission requests provide a natural source of CSI, no additional circuitry is required for estimating the channel state condition. In most of the indirect methods, the channel is monitored typically by counting the number of retransmissions during a fixed observation interval and comparing that number with a set of threshold to determine the channel condition. However, the fixed sample size method usually requires a large observation interval to obtain a reliable CSI decision. This will cause the delay in reacting to a change in the channel and thus result in a reduction in the efficiency of the system.

In [108], a simple channel state estimator (CSE) based on the count of contiguous ACKs and/or NAKs messages is proposed. This method can be treated as a variable observation interval method with weighted success or error events. This ensures that the influence of the most recent errors is the largest. In the performance analysis of [108], the adaptive GBN-ARQ scheme was modeled using a simple two-state Markov chain. However, this representation becomes void if the design variables (see Figs. 9.1 and 9.2) are selected to be larger than unity because now the present state probabilities will be dependent on a specified number of previous state values. In this chapter, we refine the analytical model in [108] and derive an exact expression for the throughput efficiency. By using the proposed method, we will investigate the performance of an efficient and simple SW-ARQ protocol with adaptive error control strategies. In our system, the variable observation interval method with weighted success or error events is employed for channel state estimation.

This chapter is organized as follows. Section 9.1 details the operation of the proposed mixed-mode SW-ARQ protocol. In Section 9.2, an accurate throughput efficiency expression for the adaptive SW-ARQ scheme is derived for a stationary channel. Subsequently, the optimal design of the adaptive system is discussed in Section 9.3 and the computational results of the suboptimal design parameters are discussed in Section 9.4. Then the throughput performance of the proposed scheme in a time-varying mobile radio channel is investigated by computer simulation in Section 9.5. Finally, the conclusions are drawn in Section 9.6.

9.1 System Description

For the sake of illustration, let us consider a stop-and-wait ARQ scheme which can operate in one of its three operation modes, namely mode L, mode M and mode H. The difference of the three operation modes is that different error control strategies are used. The decision regarding the transitions between different operation modes is made based on the received acknowledgment messages as illustrated in Fig. 9.1. The system assumes that the channel is transiting from the low error rate to the medium error rate condition upon receiving α contiguous NAKs while in mode L, and consequently will change its operation mode to mode M. Likewise, if the system which is operating in mode M receives γ contiguous NAKs, then the system would consider that the channel is further deteriorated to the high channel error rate condition, and correspondingly a switching to mode H will be executed. On other hand, if the system receives β contiguous ACKs at operation mode M, the system will switch back to mode L. When the system is operating in mode H, an operation switch to mode M will be executed only when λ contiguous ACKs have been received, since in this case the system would consider that the channel condition is getting better.

Clearly, we can characterize the adaptive mixed-mode ARQ system by an $(\alpha + \beta + \gamma - 1 + \lambda)$-state Markov chain as shown in Fig. 9.2. The state space of the Markov chain can be partitioned into three groups of α, $\beta + \gamma - 1$ and λ states which correspond to the three different operation modes respectively. Based on this Markov chain representation, we will analyze the throughput efficiency of the adaptive system in the following section.

9.2 Throughput Analysis

The performance of an ARQ scheme is generally measured in terms of its throughput efficiency and its delay characteristics. In this section, we focus on the throughput efficiency, which is defined as the ratio of the number of information bits delivered to the total number of bits that transmitter could have transmitted. For simplicity, we made the following assumptions in the evaluation of the throughput.

1). All acknowledgment messages (ACK/NAK) are received error-free at the transmitter, i.e., the feedback channel of the system is noiseless;

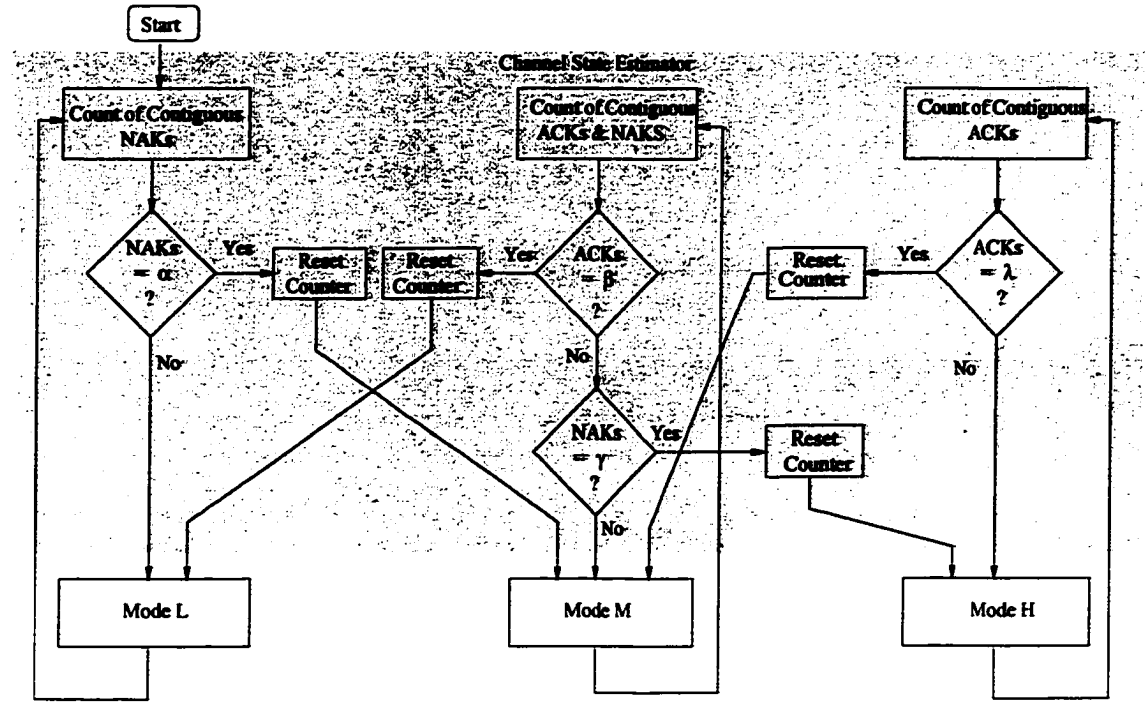

Figure 9.1. *System description of an adaptive SW ARQ protocol with sliding observation interval and three operation modes.*

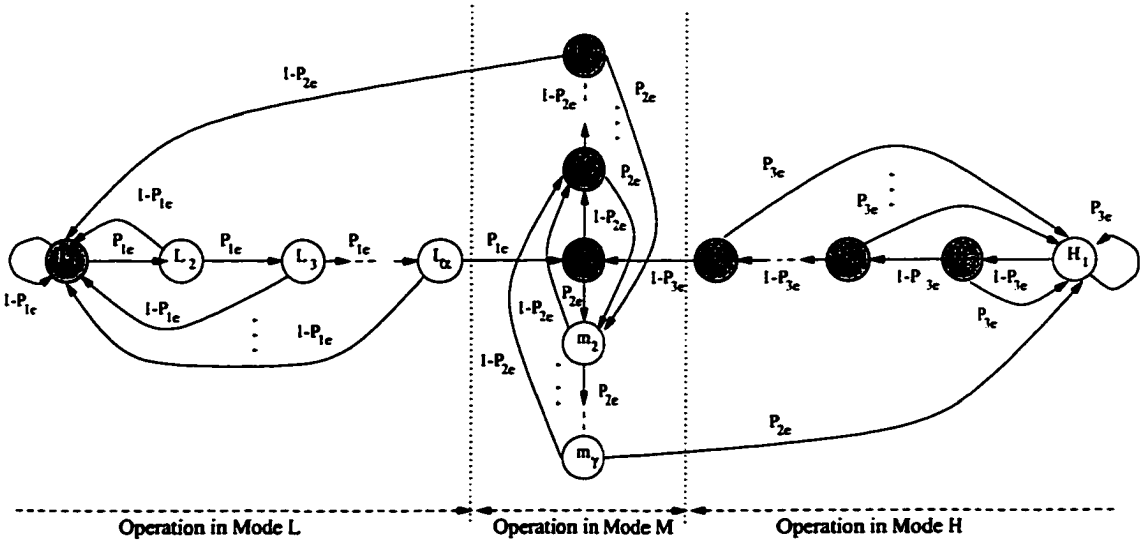

Figure 9.2. *Markov chain representation for the proposed adaptive SW-ARQ protocol with three operation modes*

2). Transmission errors in consecutive packets occur independently.

We conduct our study of the ARQ scheme introduced in the previous sections under assumption of a stationary channel. The analytical results can provide fundamental insights into how the system parameters interact and determine the performance, and also enable us to design the system for time-varying channels.

9.2.1 Steady-state Probabilities

When we assume the channel is stationary, the transition probabilities in Fig. 9.2 do not vary with the time. Thus, the Markov chain is stationary and the steady-state probabilities exist. Since these steady-state probabilities are required to estimate the throughput of the investigated adaptive ARQ system, we will derive them in the following.

From Fig. 9.2, it is straightforward to construct the $(\alpha+\beta+\gamma-1+\lambda)$-state transition matrix. Thus, the steady-state probabilities must satisfy the following equations.

$$
\begin{aligned}
&P_{L_1} = (1-P_{2e})P_{M_\beta} + (1-P_{1e})\textstyle\sum_{k=1}^{\alpha} P_{L_k} \\
&P_{L_i} = P_{1e}^{i-1}P_{L_1}, \qquad i=2,\ldots,\alpha; \\
&P_{M_1} = P_{1e}^{\alpha}P_{L_1} + (1-P_{3e})^{\lambda}P_{H_1}; \\
&P_{M_2} = (1-P_{2e})(P_{M_1} + P_{m_2} + P_{m_3} + \ldots + P_{m_\gamma}) \\
&P_{M_i} = (1-P_{2e})^{i-2}P_{M_2}, \qquad i=3,\ldots,\beta; \\
&P_{m_2} = P_{2e}(P_{M_1} + P_{M_2} + \ldots + P_{M_\beta}) \\
&P_{m_i} = P_{2e}^{i-2}P_{m_2}, \qquad i=3,\ldots,\gamma; \\
&P_{H_1} = P_{2e}P_{m_\gamma} + P_{3e}(P_{H_1} + \ldots + P_{H_\lambda}); \\
&P_{H_i} = (1-P_{3e})^{i-1}P_{H_1}, \qquad i=2,\ldots,\lambda; \\
&\textstyle\sum_{k=1}^{\alpha} P_{L_k} + \sum_{k=1}^{\beta} P_{M_k} + \sum_{k=2}^{\gamma} P_{m_k} + \sum_{k=1}^{\lambda} P_{H_k} = 1.
\end{aligned}
\tag{9.1}
$$

where P_{1e}, P_{2e} and P_{3e} denote the message packet error probabilities of operation modes L, M and H, respectively. After some mathematical manipulations, we can obtain the steady-state probabilities as follows.

$$
\begin{aligned}
P_{L_i} &= CP_{1e}^{i-1}P_{2e}(1-P_{2e})^{\beta-1}(1-P_{2e}^{\gamma})(1-P_{3e})^{\lambda};\ i=1,2,\ldots,\alpha;\\
P_{M_1} &= CP_{1e}^{\alpha}[P_{2e}^{\gamma}-P_{2e}^{\gamma}(1-P_{2e})^{\beta-1}+P_{2e}(1-P_{2e})^{\beta-1}](1-P_{3e})^{\lambda};\\
P_{M_i} &= CP_{1e}^{\alpha}P_{2e}(1-P_{2e})^{i-2}(1-P_{2e}^{\gamma})(1-P_{3e})^{\lambda};\ i=2,3,\ldots,\beta;\\
P_{m_i} &= CP_{1e}^{\alpha}P_{2e}^{i-1}(1-(1-P_{2e})^{\beta})(1-P_{3e})^{\lambda};\ i=2,3,\ldots,\gamma;\\
P_{H_i} &= CP_{1e}^{\alpha}P_{2e}^{\gamma}(1-(1-P_{2e})^{\beta})(1-P_{3e})^{i-1};\ i=1,2,\ldots,\lambda.
\end{aligned}
\tag{9.2}
$$

where C is a constant.

9.2.2 Throughput Estimation

In SW-ARQ schemes, the transmitter sends out a packet and waits for an acknowledgment. Once the receiver has processed the packet, it responds by sending a positive acknowledgment (ACK) if the packet can be successfully decoded, otherwise, it sends a retransmission request. Therefore, a new packet will be transmitted only after a positive acknowledgment for the previous packet has been received. This means that, in the Markov chain representation as shown in Fig. 9.2, the first transmission of a new packet can only start from the states which can be reached in one-step with an ACK, i.e., states L_1, M_i, $i = 1,2,\ldots,\beta$, H_j, $j = 2,3,\ldots,\lambda$. For convenience of presentation, we define a state variable X, which denotes a state where a new packet is oriented. We denote f as the number of transmissions (including the original transmission and retransmissions) required for a successful packet. Then, for a packet oriented from state X to be successfully accepted by the receiver, the average number of bits that the transmitter could have transmitted can be calculated as follows.

a). When the packet is oriented from state L_1, it can be seen from Fig. 9.2 that if the number of (re)transmissions is less than α, all the transmissions are sent in mode L. However, after more than α and less than $\alpha+\gamma$ consecutive failures in transmission attempts for that packet, the transmitter will operate in mode M during the following possible retransmissions. When the number of transmission failures for the packet is larger than $\alpha+\gamma$, the transmitter will finally operate in mode H. Therefore, the

conditional probability of $P(f = k|X = L_1)$ can be calculated as

$$P(f = k|X = L_1) = \begin{cases} P_{1e}^{k-1}(1 - P_{1e}); & k \leq \alpha \\ P_{1e}^{\alpha} P_{2e}^{\gamma} P_{3e}^{k-\alpha-\gamma-1}(1 - P_{3e}); & k > \alpha + \gamma \\ P_{1e}^{\alpha} P_{2e}^{k-\alpha-1}(1 - P_{2e}); & otherwise. \end{cases} \tag{9.3}$$

Consequently, the average number of bits that the transmitter could have transmitted for the packet to be successfully received and acknowledged is

$$\begin{aligned} T_{L_1} &= \sum_{k \leq \alpha} k(n_1 + R\tau)\ P(f = k|L_1) \\ &\quad + \sum_{\alpha < k \leq \alpha+\gamma} [\alpha(n_1 + R\tau) + k(n_2 + R\tau)]\ P(f = k|L_1) \\ &\quad + \sum_{k > \alpha+\gamma} [\alpha(n_1 + R\tau) + \gamma(n_2 + R\tau) + k(n_3 + R\tau)]\ P(f = k|L_1) \\ &= (1 - P_{1e}^{\alpha})\ \frac{n_1 + R\tau}{1 - P_{1e}} + P_{1e}^{\alpha}\ (1 - P_{2e}^{\gamma})\ \frac{n_2 + R\tau}{1 - P_{2e}} + P_{1e}^{\alpha}\ P_{2e}^{\gamma}\ \frac{n_3 + R\tau}{1 - P_{3e}} \end{aligned} \tag{9.4}$$

where n_1, n_2 and n_3 are the numbers of bits in a packet transmitted in mode L, mode M and mode H respectively, τ is the idle time from the end of transmission of one packet to the beginning of transmission of the next, and R is the transmission rate in bits per second.

b). When the packet is oriented from state M_i, $i = 1, 2, \ldots, \beta$, the first γ transmissions, if necessary, are in mode M. However, if the number of retransmissions is larger than γ, then all possible retransmissions after γ retransmissions will be in mode H. Similar to the case of $X = L_1$, we have

$$P(f = k|X = M_i) = \begin{cases} P_{2e}^{k-1}(1 - P_{2e}); & k \leq \gamma \\ P_{2e}^{\gamma} P_{3e}^{k-\gamma-1}(1 - P_{3e}); & k > \gamma \end{cases} \tag{9.5}$$

and the average number of bits that the transmitter could have transmitted is

$$\begin{aligned} T_{M_i} &= \sum_{k \leq \gamma} k(n_2 + R\tau)P(f = k|M_i) + \sum_{k > \gamma} [\gamma(n_2 + R\tau) + k(n_3 + R\tau)]P(f = k|M_i) \\ &= (1 - P_{2e}^{\gamma})\ \frac{n_2 + R\tau}{1 - P_{2e}} + P_{2e}^{\gamma}\ \frac{n_3 + R\tau}{1 - P_{3e}}. \end{aligned} \tag{9.6}$$

c). When the packet is oriented from state H_i, $i = 2, \ldots, \lambda$, all the (re)transmissions will be operated in mode H. Therefore, we simply have

$$T_{H_i} = \frac{n_3 + R\tau}{1 - P_{3e}}. \tag{9.7}$$

It is useful to define a new parameter p_X, which dictates the conditional probability that when there is a new packet to be transmitted, the packet is transmitted at state X. From the steady-state probabilities of the adaptive system, we can obtain the probability that there is a new packet to be transmitted as

$$P_{new} = P_{L_1} + P_{M_{1H}} + \sum_{i=2}^{\beta} P_{M_i} + \sum_{j=2}^{\lambda} P_{H_j} \tag{9.8}$$

where $P_{M_{1H}} = P_{2e}^{\gamma-1} P_{m_2}$. Then the conditional probability p_X can be calculated as

$$p_X = \frac{P_X}{P_{new}}, \tag{9.9}$$

where $X = L_1$, M_{1H}, M_i, $(i = 2, \ldots, \beta)$ or H_j, $(j = 2, 3, \ldots, \lambda)$.

Therefore, the average number of bits required for a packet of k information bits to be successfully received and acknowledged is

$$\bar{T} = T_{L_1}\, p_{L_1} + T_{M_1}\, p_{M_{1H}} + \sum_{i=2}^{\beta} T_{M_i}\, p_{M_i} + \sum_{j=2}^{\lambda} T_{H_j}\, p_{H_j}, \tag{9.10}$$

and the throughput efficiency of this adaptive scheme can be obtained by

$$\eta = \frac{k}{\bar{T}}\,. \tag{9.11}$$

9.3 Throughput Optimization

As illustrated in Section III, the throughput efficiency of the adaptive system depends on the parameters $(\alpha, \beta, \gamma, \lambda)$. Thus, it requires a careful selection of these parameters to optimize the system performance. In the following, we discuss the optimal design of the investigated adaptive system in terms of throughput efficiency. First, we start with an investigation on some properties of the system.

Proposition I: Upper bound of the throughput efficiency

The throughput efficiency of the adaptive mixed-mode ARQ system is upper bounded by η^*, which is defined as

$$\eta^* = \begin{cases} \eta_L & 0 < P_S \le P_{co}^{(1)} \\ \eta_M & P_{co}^{(1)} < P_S \le P_{co}^{(2)} \\ \eta_H & P_{co}^{(2)} < P_S < 1 \end{cases} \tag{9.12}$$

where $P_{co}^{(1)}$ is the throughput crossover probability of the systems operating in single mode L and mode M, $P_{co}^{(2)}$ is the throughput crossover probability of the systems operating in single mode M and mode H, and P_S is the symbol error probability.

From *Proposition I*, it can be seen that the throughput performance of the proposed adaptive system can be upper bounded by one of its operation modes in different ranges of symbol error probability. Furthermore, we can obtain the asymptotic properties of the system as follows.

Proposition II: The asymptotic properties of the throughput efficiency

1). If $\lim_{\alpha,\beta\to\infty} \frac{\alpha}{\beta-1} > \frac{\ln(1-P_{2e})}{\ln(P_{1e})}$ and $\lim_{\gamma,\lambda\to\infty} \frac{\gamma-1}{\lambda-1} > \frac{\ln(1-P_{3e})}{\ln(P_{2e})}$ then

$$\lim_{\alpha,\beta,\gamma,\lambda\to\infty} \eta = \eta_L.$$

2). If $\lim_{\alpha,\beta\to\infty} \frac{\alpha}{\beta-1} < \frac{\ln(1-P_{2e})}{\ln(P_{1e})}$ and $\lim_{\gamma,\lambda\to\infty} \frac{\gamma-1}{\lambda-1} < \frac{\ln(1-P_{3e})}{\ln(P_{2e})}$ then

$$\lim_{\alpha,\beta,\gamma,\lambda\to\infty} \eta = \eta_H.$$

3). If $\lim_{\alpha,\beta\to\infty} \frac{\alpha}{\beta-1} < \frac{\ln(1-P_{2e})}{\ln(P_{1e})}$ and $\lim_{\gamma,\lambda\to\infty} \frac{\gamma-1}{\lambda-1} > \frac{\ln(1-P_{3e})}{\ln(P_{2e})}$ then

$$\lim_{\alpha,\beta,\gamma,\lambda\to\infty} \eta = \eta_M. \tag{9.13}$$

By choosing set of $(\alpha, \beta, \gamma, \lambda)$ to satisfy that

$$\begin{aligned} \frac{\alpha}{\beta-1} &= \frac{\ln(1-P_{2e}(P_{co}^{(1)}))}{\ln P_{1e}(P_{co}^{(1)})}, \\ \text{and} \quad \frac{\gamma-1}{\lambda-1} &= \frac{\ln(1-P_{3e}(P_{co}^{(2)}))}{\ln P_{2e}(P_{co}^{(2)})}; \end{aligned} \tag{9.14}$$

it can be easily verified that the conditions in (1), (2) and (3) will be satisfied when the symbol error probability P_S takes value from the intervals $(0, P_{co}^{(1)})$, $(P_{co}^{(1)}, P_{co}^{(2)})$ and $(P_{co}^{(2)}, 1)$, respectively. Therefore, *Proposition II* shows that the throughput of the proposed system has an optimum in $\alpha \times \beta \times \gamma \times \lambda$ space, which is the upper limit η^* imposed by *Proposition I*. It also implies that the optimum $(\alpha^*, \beta^*, \gamma^*, \lambda^*)$ lies in the infinite space. However, in practical applications, we may prefer to smaller α, β, γ and λ since this will reduce the delay in reacting to a change in the channel and thus improve the adaptability of the system.

By using *Proposition I* and *II*, we can now formulate an objective function to determine the suboptimal design parameters such that the throughput of the adaptive ARQ scheme, η best approximates η^* in the sense that the mean square error (MSE) is minimized, i.e.,

$$\begin{aligned} E(\alpha,\beta,\gamma,\lambda) &= \int_0^1 w[\eta(P_S)-\eta^*(P_S)]^2 dP_S \\ &= \Delta\sum_{k=1}^{L} w_k[\eta(P_S^{(k)})-\eta^*(P_S^{(k)})]^2 \\ \text{subject to:} \quad & d_{min} < (\alpha,\beta,\gamma,\lambda) < d_{max} \end{aligned} \tag{9.15}$$

where L and $P_S^{(k)}$ denote the sample size and symbol error probability of the kth sample, respectively. w_k is a pre-defined weight sequence that provides additional flexibility in matching different data points with varying accuracy, and the optimization variables can assume any values from set $\mathbb{Z}$, which consists of positive integers.

Discrete determination of the MSE $E(\alpha,\beta,\gamma,\lambda)$ is valid if the step size Δ between the consecutive data points is selected to be relatively small. In addition, the boundary constraints to the design parameters (which will be specified by the channel behavior) are introduced to achieve a good compromise between the ability to react to channel fluctuation rate (in a time-varying channel) and the switching reliability criterion (i.e., the MSE value). In the minimization problem (9.15), the boundary constraints can be eliminated via transformation $y = \tanh(z)$ or alternatively $y = 2\arctan(z)/\pi$.

9.4 Computational Results and Remarks

In this subsection, we present a few examples to illustrate the system design and the parameter optimization for the CSE algorithm. In our examples, we assume that one data packet contains only one codeword. All the codes of differernt modes contain the same length of information bits. In mode L, which corresponds to low error rate mode, only CRC is used for error detection. Besides CRC, in mode H and M, which correspond to high error rate mode and moderate error rate mode, a Reed-Solomon code RS(31,15) and a punctured RS code (21,15) are used for error

Table 9.1. *Suboptimal Design Parameters ($d_{min} = 1$)*

d_{max}	$(\alpha^*, \beta^*, \gamma^*, \lambda^*)$	MSE
5	(1,5,2,5)	4.20×10^{-4}
10	(2,10,3,10)	1.75×10^{-4}
15	(2,15,3,15)	1.10×10^{-4}
20	(2,20,3,20)	9.55×10^{-5}
25	(2,21,3,25)	9.50×10^{-5}
30	(3,30,4,30)	7.40×10^{-5}

correction, respectively. The round-trip delay of 2 RS symbol intervals is assumed. In throughput evaluation, perfect error detection of CRC is assumed and the CRC parity bits are not included in throughput calculation.

Table 9.1 depicts the suboptimal design parameters (obtained via quasi-Newton method) and their corresponding switching reliability criterion for the proposed adaptive SW-ARQ system. The weight sequence w_k in (9.15) can be defined according to the fading channel statistics and SNR operation point of the system. However, in order to observe the generality and robustness of the adaptive system parameters, no specific weight sequence is applied in our optimization, i.e., $w_k = 1$ for all k. In other words, no channel statistics and no particular SNR operation point of the system are assumed in our optimization. From this table, we found that for the suboptimal points, the parameters β and λ are always much larger than α and γ as predicted by our Proposition II in Section 9.3. It is also seen that the MSE decreases as the ratio of suboptimal design variables β^*/α^* or λ^*/γ^* increases.

Fig. 9.3 illustrates the throughput performance of a mixed-mode SW-ARQ scheme for three different sets of suboptimal design parameters. It is clear that the adaptive scheme yields much higher throughput than other comparable nonadaptive ARQ schemes over a wide range of error rates. Moreover, it is seen that with the design parameters $(\alpha, \beta, \gamma, \lambda)$=(2,20,3,20), which has the largest ratios of β^*/α^* and λ^*/γ^* among the three sets, its actual throughput efficiency is the closest to the desired

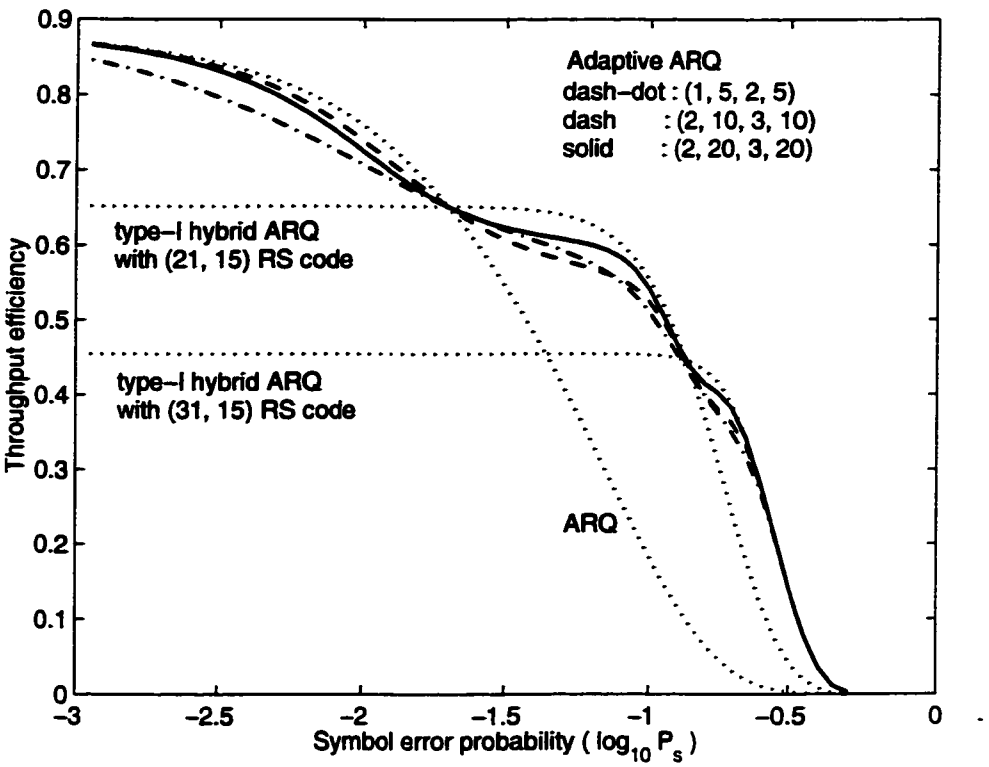

Figure 9.3. *Performance comparison of the proposed adaptive ARQ system with different sets of design parameters* $(\alpha, \beta, \gamma, \lambda)$

performance curve among the three sets, as discussed previously. This trend holds for stationary channels, but in practical applications in time-varying channels, we may prefer to smaller α, β, γ and λ since this will reduce the delay in reacting to a change in the channel and thus improve the adaptability of the system.

The throughput of adaptive ARQ scheme is conventionally calculated as a simple average of the throughput values of each distinct operation modes, namely, $\eta = \sum P_i \eta_i$. However, it should be noted that this conventional throughput calculation is not exact. For the adaptive system investigated in this chapter, comparisons between throughput performance obtained by the conventional approach and that developed in this chapter are shown in Fig. 9.4 for an adaptive SW-ARQ scheme with $(\alpha, \beta, \gamma, \lambda) = (1, 5, 2, 5)$. We found that the curve obtained by (9.11) is in good agreement with the throughput values obtained by computer simulations whereas that of the conventional approach shows some small discrepency against simulation results. This observation validates the accuracy of our analytical model.

9.5 Simulation of the Adaptive ARQ Scheme over Time-varying Channels

In previous section, the throughput performance of adaptive ARQ scheme is analysed, assuming a static channel case. However, a practical mobile radio channel is a time-varying environment and consequently the adaptive system becomes a nonstationary Markov process. Furthermore, transmission errors in consecutive packets no longer occur independently due to the time-correlation characteristics of the mobile radio channel. Thus, an exact throughput analysis of an adaptive ARQ scheme in a time-varying mobile radio channel becomes intractable. Hence, simulation approach is adopted here to evaluate the adaptive ARQ scheme performance in a typical mobil radio channel. Particularly, the suboptimal CSE design parameters obtained for stationary channel will be used for time-varying channel and the applicability of these parameters in a practical time-varying channel will be investigated.

9.5.1 Channel Model

Mobile radio channel is typically characterized by multipath fading and shadowing. In our simulation, multipath fading is modeled with Rayleigh distribution. Doppler spread induced by the motion of a mobile terminal, which corresponds to the time correlation of the fading gain samples, is also included. Jake's Doppler spectrum is assumed and the correlated Rayleigh fading gain samples are generated by using the method of [109]. The shadowing effect which causes slower variation of the short term median strength of the received signal is usually modeled with lognormal distribution, i.e., the short term median strength $\gamma(t)$ of the received signal can be expressed as

$$\gamma(t) = 10^{-\xi(t)/10}, \tag{9.16}$$

where $\xi(t)$ is a time-correlated Gaussian random variable. In our simulation, the method of [110] is used for lognormal shadowing where the lognormal shadowing is modeled as a Gaussian white noise process which is filtered with first order lowpass filter. With this model,

$$\xi_{k+1} = \varepsilon \cdot \xi_k + (1 - \varepsilon) \cdot \nu_k, \tag{9.17}$$

where ν_k is a zero mean white Gaussian random variable with variance Ω_ν^2, ε is a parameter that controls the spatial correlation of the shadowing and given by

$$\varepsilon = \varepsilon_D^{vT_s/d}. \tag{9.18}$$

The parameter ε_D is the correlation between two points separated by a spatial distance of D, v is the velocity of the mobile terminal, T_s is the sampling period. For typical suburban propagation at 900 MHz, it has been suggested in [110] that $\Omega_\xi \approx 7.5$ dB with a correlation $\varepsilon_D \approx 0.82$ and D = 100.

9.5.2 Simulation Results and Discussions

In this subsection, the simulation results of the throughput performances of the proposed adaptive ARQ scheme and non-adaptive ARQ schemes in a typical time-varying mobile radio channel for different mobile speeds are presented. The system parameters used in Section 9.4 are also applied in the simulation and BPSK modulation with coherent detection is considered. The adaptive ARQ parameters of

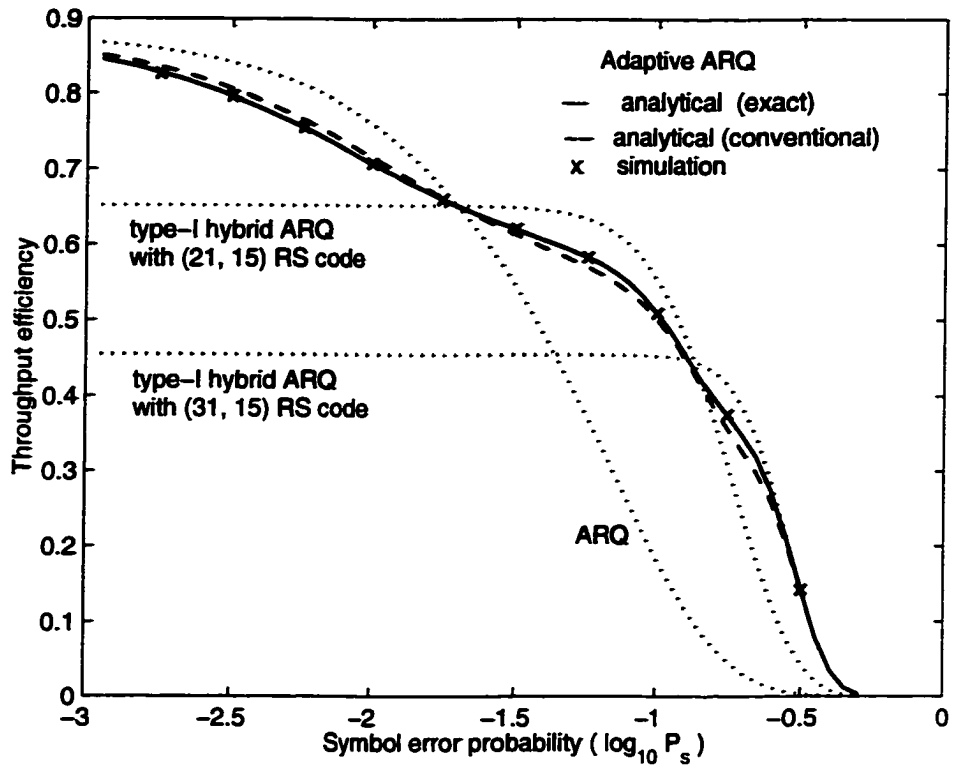

Figure 9.4. *Throughput versus symbol error probability. Adaptive ARQ parameters:* $(\alpha = 1, \beta = 5, \gamma = 2, \lambda = 5)$

$(\alpha, \beta, \gamma, \lambda) = (1, 5, 2, 5)$ is used in our simulation. The carrier frequency of 900 MHz and the data rate of 14.4 kbps are assumed.

Figs. 9.5, 9.6 and 9.7 show, as a function of time, short-term average throughput of the proposed adaptive SW-ARQ scheme and conventional SW-ARQ schemes applying the codes used in adaptive scheme for the mobile speeds of 50 km/hr, 10 km/hr and 1 km/hr, respectively. The short-term throughput is obtained by averaging over every 0.1 second interval. From the figures, it is observed that for very slow fading case of v = 1km/hr, the short-term throughput is mainly determined by the multipath fading effect. On the other hand, for faster fading cases of v=10 km/hr and 50 km/hr, the effects of shadowing on throughput performance become prominent. Regarding the tracking capability to channel conditions, it is observed that the adaptive system can track the channel variations quite well for all fading rates considered, especially for

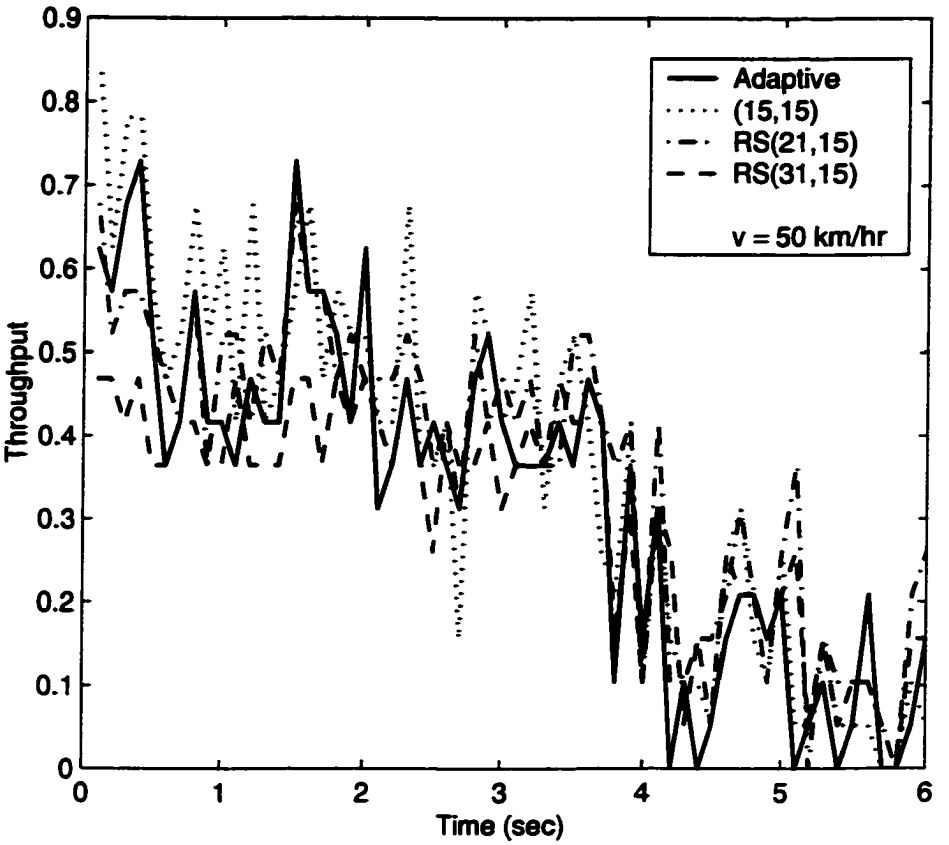

Figure 9.5. *Short-term throughput of the adaptive and nonadaptive ARQ schemes for mobile speed of 50 km/hr and long term SNR of 5 dB*

slower fading cases. As expected, it can adapt to multipath fading more closely for very slow fading case than faster fading cases. The tracking trends for faster fading cases cannot follow multipath fading quite closely but they follow the shadowing effect.

In Figs. 9.8, 9.9 and 9.10, the throughput performance of the proposed adaptive SW-ARQ scheme and conventional SW-ARQ schemes which use the codes applied in adaptive system are shown as a function of long term SNR values for the mobile speeds of v = 50 km/hr, 10 km/hr and 1 km/hr, respectively. First of all, the throughput performances of ARQ schemes for faster fading rates are observed to be smaller than those for slower fading rates. It is expected since faster fading causes more random channel errors and hence, more retransmission and less throughput.

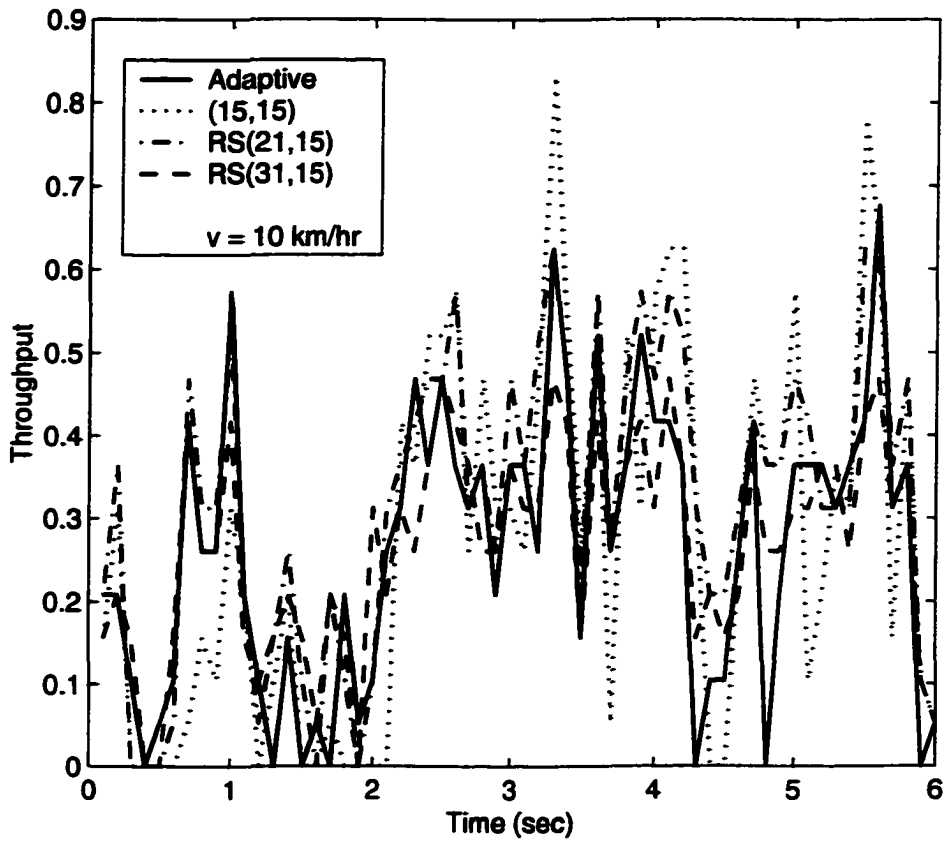

Figure 9.6. *Short-term throughput of the adaptive and nonadaptive ARQ schemes for mobile speed of 10 km/hr and long term SNR of 5 dB*

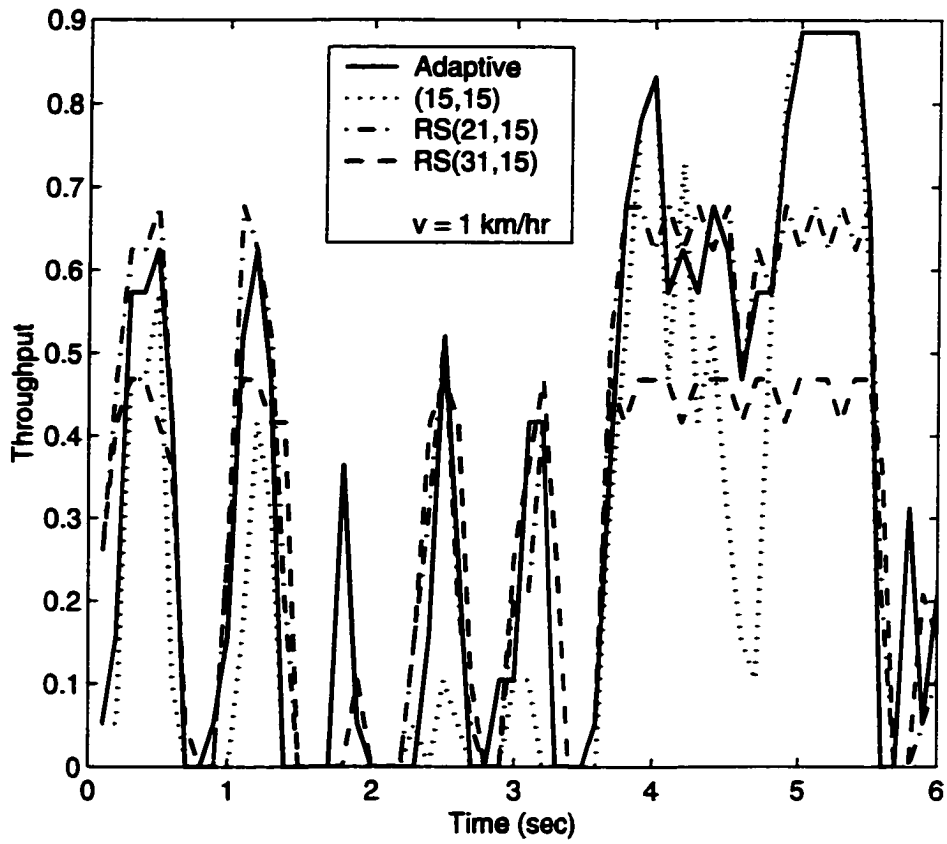

Figure 9.7. *Short-term throughput of the adaptive and nonadaptive ARQ schemes for mobile speed of 1 km/hr and long term SNR of 5 dB*

The greater throughput performance improvement of adaptive system is observed for slower fading case. As discussed previously, the adaptive system can track multipath fading more closely for slower fading rate case and hence, this brings about the greater improvement. For the cases with mobile speeds of 10 km/hr and 1 km/hr, the adaptive system throughput is higher than any of the conventional SW-ARQ schemes for almost all SNR values considered. The exceptions are at the very high SNR value of 30 dB and the very low SNR value of 0 dB. For very high SNR value, all the packets are received correctly almost all the time. However, occasional packet errors cause the adaptive system to switch the operation mode unnecessarily and because of this unnecessary mode switching, the adaptive system has a slightly lower throughput than the conventional one at the very high SNR value. At the very low SNR value, noise is the main contributor to packet errors and the better error correction capability of the mode H code over mode M code becomes less effective under very noisy condition and hence, cannot give the throughput gain. As a result, the adaptive system does not achieve throughput improvement for very low SNR value.

For the case with 50 km/hr, the adaptive system does not achieve the same kind of improvement as 10 km/hr and 1 km/hr cases due to its less tracking capability to time-varying channel with a faster fading rate. However, the adaptive system throughput still follows the trend it should. In other words, for the SNR region where the throughput of conventional scheme with mode L's code is higher than the other two conventional cases, the throughput of adaptive system follows that of conventional scheme with mode L's code. Similarly, it follows that of mode M's code for the corresponding SNR region of mode M code's.

In brief, the simulation study of the throughput performance in a time-varying mobile radio channel shows that the proposed adaptive ARQ system can adapt to the channel variations quite closely, especially for slow fading case, and hence achieve significant throughput improvement over nonadaptive schemes. Moreover, the results also confirm the applicability of the adaptive system parameters, so-obtained by analysis and optimization in the stationary channel case, to the time-varying fading channel case.

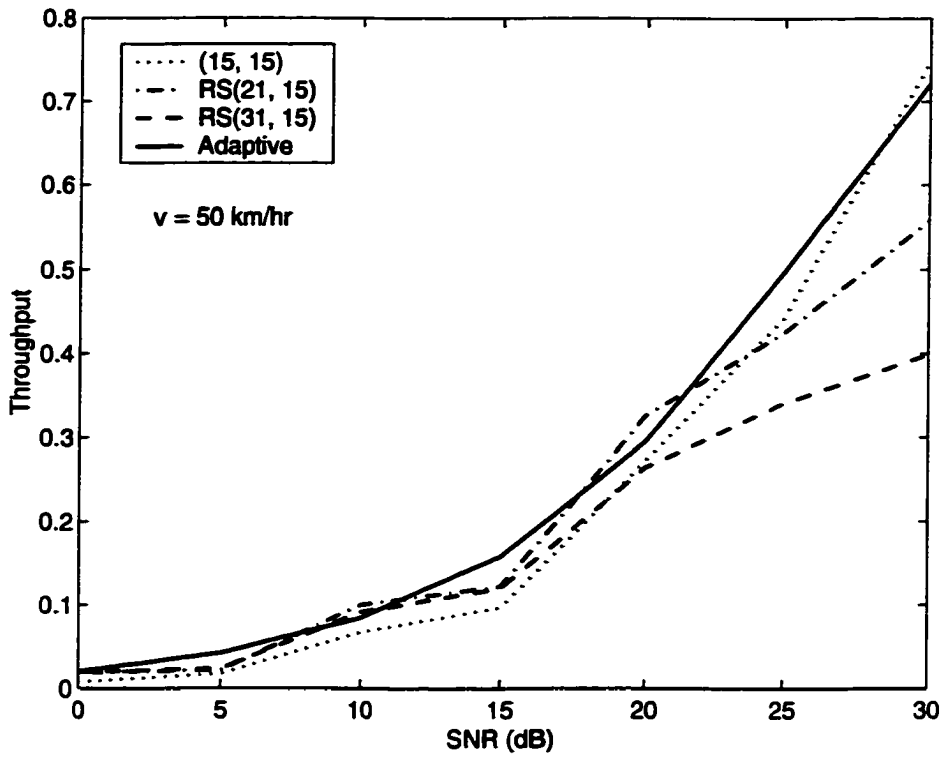

Figure 9.8. *Throughput of the adaptive and nonadaptive ARQ schemes for mobile speed of 50 km/hr*

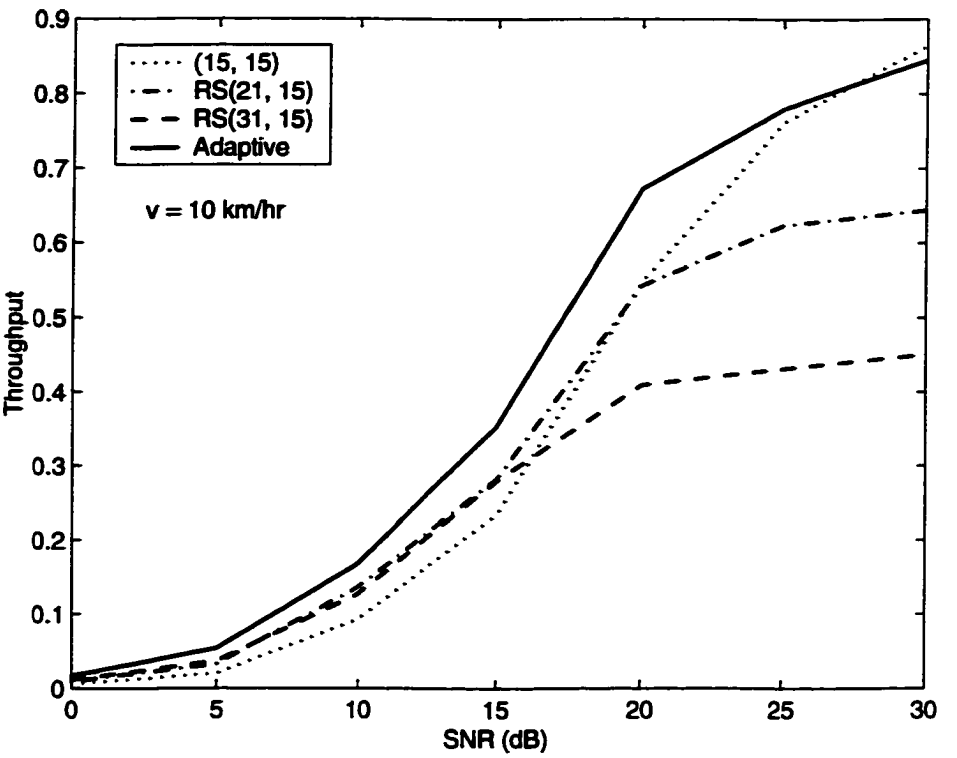

Figure 9.9. *Throughput of the adaptive and nonadaptive ARQ schemes for mobile speed of 10 km/hr*

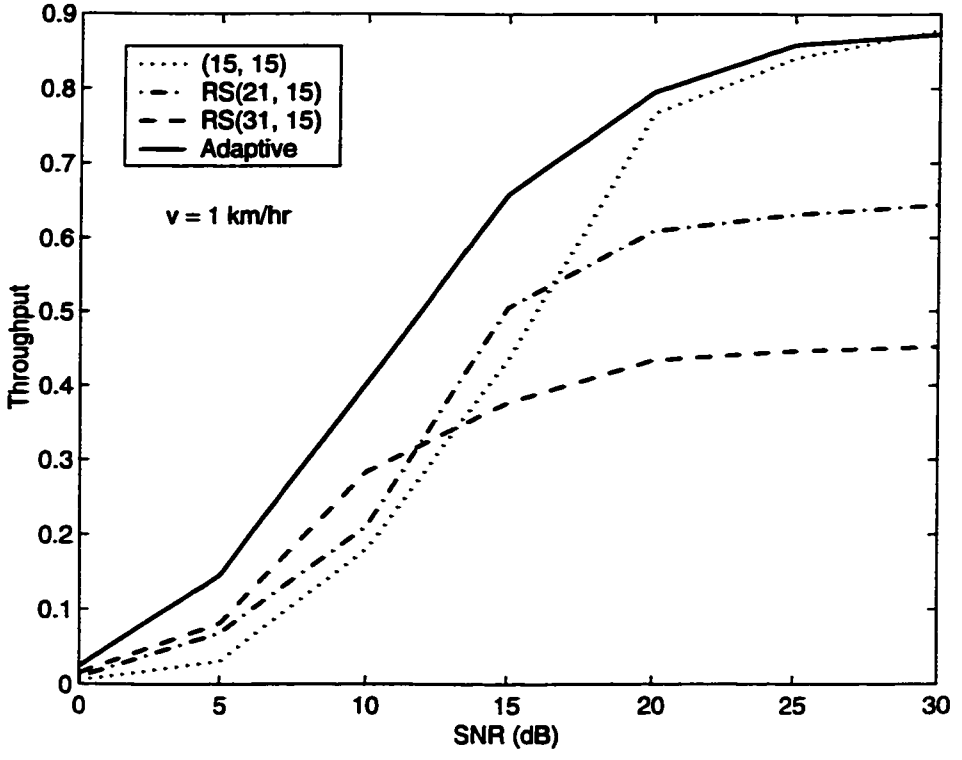

Figure 9.10. *Throughput of the adaptive and nonadaptive ARQ schemes for mobile speed of 1 km/hr*

9.6 Conclusions

In this chapter, a simple and efficient stop-and-wait (SW) automatic repeat-request (ARQ) scheme with adaptive error control is investigated. In this scheme, the channel state information (CSI) is extracted by monitoring the contiguous positive acknowledgment (ACK) or negative acknowledgment (NAK) messages. Exploiting this CSI, we adapt the coding strategy to the changes in the channel condition, and thus, improve the throughput efficiency.

In order to facilitate the throughput analysis and parameters optimization, we model the adaptive system by a Markov chain. Using this analytical model and assuming a static channel, an exact throughput expression for the adaptive ARQ protocol is derived and suboptimal adaptive system parameters are obtained. These design parameters are applied for the adaptive system in a typical time-varying mobile radio channel characterized by Rayleigh multipath fading on top of lognormal shadowing. The throughput performance of the proposed adaptive SW-ARQ scheme in such a time-varying fading channel is evaluated by computer simulation. For slow fading channels, the proposed adaptive system can track the channel variations very well, hence, much throughput improvement is achieved over conventional nonadaptive SW-ARQ schemes for almost all SNR values considered. The simulation results also confirm the applicability of the adaptive system parameters so-obtained by the throughput analysis in a static channel, to a time-varying mobile radio channel. It is noted that the analysis and optimization methods presented in this chapter are applicable to a more general class of adaptive systems (e.g., modulation or packet length) which employ the proposed channel sensing algorithm for link adaptation. Similarly, the performance of an adaptive system with more than three operation modes can be evaluated by using the methodology outlined in Section 9.2.

Chapter 10

On ARQ Scheme with Adaptive Error Control

ARQ and hybrid ARQ error control strategies are usually incorporated in the system design for non-delay-sensitive communications services with very high system performance requirement. If those services are provided through mobile wireless radio channel, the nature of the time-varying multipath fading channel has to be taken into consideration in the system design. Practical mobile radio channel induces a time-varying response with bursty errors due to multipath fading and shadowing effects. During the fades the channel becomes too noisy and at the other times it well-behaves. For such a time-varying channel, it is clear that the use of a single error control strategy will not yield the optimal throughput. Therefore, in order to counteract the fading channel conditions, adaptive schemes need to be incorporated into ARQ schemes, e.g., the use of different error control strategies for different channel conditions needs to be established for an ARQ system with adaptive error correcting codes. Generally, adaptive scheme can be performed not only on error control code, but also on packet length, modulation format, etc.

For real-time implementation of adaptive ARQ schemes, the channel state information needs to be estimated reliably and effectively. That means in order to track channel variations closely, reliable estimation of the channel state information should be carried out within short enough intervals. The channel state information may be directly estimated by means of signal power measurement which gives rise to some extra complexity. Recently, indirect approaches ([111]-[112], [108], [113]-[114]) for channel state estimation have been proposed in the literature.

In [111], S. Hara et. al. estimated the packet error rate by using the count of

NACK packets in a fixed observation interval. However, the choice of observation interval for reliable estimation highly depends on the fading/shadowing condition. If the observation interval is small relative to channel fading rate, reliable estimate of channel state information cannot be achieved. Consequently, the mode change decision based on the unreliable channel estimate may lose significant potential throughput gain achievable by adaptive scheme. On the other hand, if the observation interval is large relative to the channel fading rate, the potential throughput gain may be lost significantly due to the delay in responding to the channel state changes. Moreover, the channel states at different modes of the adaptive system would not be the same and hence, the use of one fixed observation interval may not be of wise choice. Using a fixed observation interval for channel state estimation in an unknown fading environment gives an estimate averaged over the interval but does not give much information on how likely the next packet(s) will encounter similar channel conditions.

In [115], packet error rate was estimated using count of NACK packets in different observation intervals for different modes of the adaptive scheme. The Markov channel model with known state transition probabilities and known channel transition probabilities within each state is assumed. Based on the assumed channel model and channel statistics, the observation intervals are found. However, this approach might not be applicable to an unknown fading environment. The applicability of the design parameters obtained with the assumed channel model and channel statistics to the practical time-varying fading channel needs further investigation. Using different observation intervals for different modes of the adaptive scheme may be conceptually viewed as a way to achieve different channel state estimates in different modes with same estimation reliability. It tries to avoid unnecessarily long observation intervals for some modes and insufficient observation intervals for others. For the known channel, the fading rate information is incorporated in the design by the known channel statistics. However, in an unknown fading environment, it does not give much information on how likely the next packet(s) will experience similar channel conditions.

In [112], a sequential scheme for channel state estimation was proposed where each transmitted packet is scored based on the outcome of the decoding process (i.e., ACK or NACK). When the cumulative score crosses a decision threshold, the coding strategy (mode) is changed and the sequential inspection scheme is restored using the

same scoring routine with different weighting and decision threshold constants. The Markov channel model with known state transition probabilities and known channel transition probabilities within each state is assumed. Based on the known channel statistics, the weighting and decision threshold constants for each mode is found by optimizing the throughput using reliability as a constraint. For an unknown fading environment, the approach might not be applicable. The applicability of the design parameters obtained with the assumed channel model and channel statistics to the practical time-varying fading channel needs further investigation.

In [116], XOR-ing of the two consecutive erroneous copies is used to estimate the channel BER for an adaptive ARQ scheme with no error correction in a stationary channel. As originally stated, XOR-ing was first used by Sindhu in [117] to locate the errors. But how to deal with the case when there is no consecutive unsuccessful packets was not considered by [116]. Although [116] states that their channel BER estimation can be applied to any adaptive scheme, we notice that for ARQ schemes with adaptive error correction codes, the channel BER may not be estimated properly due to error correction of FEC. Specifically, their method gives channel BER estimation for one direction only (i.e., from good channel state to bad channel state direction). In this chapter, how to estimate channel error rate for the other direction (i.e., from bad channel state to good channel state) is also addressed.

In [108], count of successive ACK or NACK is used for mode change decision in a two mode adaptive system in a stationary channel. If α successive ACKs are received in mode-H (high error rate mode), the adaptive system assumes that the channel is returning to good state and changes its mode to mode-L (low error rate mode). If β successive NACKs are received in mode-L, the adaptive system assumes that the channel is deteriorating into a bad state and changes its mode to mode-H. The values of the design parameters α and β are found by trials. A way of finding adaptive system parameters is proposed in [113]-[114] where the parameters of the adaptive ARQ system with three modes are found by optimization of the throughput assuming a stationary channel.

The use of successive ACKs or NACKs gives some information on how likely the next packet(s) will experience similar channel conditions. However, finding the optimum parameter values of successive ACKs or NACKs in a time varying fading

channel is an infeasible task. Finding the adaptive system parameters by optimization of the throughput assuming a stationary channel is one way to get suitable design parameters. Although the designed adaptive system parameters do not represent as optimal ones for the practical time-varying fading channel due to the stationary channel assumption, their applicability to a practical time-varying fading channel has been confirmed by simulation studies in [114]. However, for an adaptive system with more than 3 modes, the task involved in this approach becomes tedious. In this chapter we present an alternative approach for ARQ scheme with adaptive error control codes, particularly using the codes with known error correction capability such as Reed-Solomon codes. The proposed approach avoids the throughput calculation and optimization in finding the adaptive system design parameters used in [113]-[114]. It uses the count of consecutive ACKs or NACKs just to determine whether the selection of the most suitable mode should be performed or not; the operation mode may not necessarily be changed, in contrast to previous use of consecutive ACKs or NACKs count to definitely change the adaptive system mode. Based on the proposed channel error estimate together with the error correction capabilities of the FEC codes used, the decision on in which mode the system should operate is made. The mode change may not be necessary for some channel conditions.

For circumstances of deep fades in slow fading environment, even stronger FEC code may not be helpful in achieving throughput gain. For such situation, some other dimension diversity schemes such as frequency dimension may be incorporated to improve the system performance. In this chapter, an adaptive ARQ scheme incorporated with frequency hopping concept is also investigated.

This chapter is organized as follows: In Section 10.1, the adaptive ARQ scheme based on the throughput optimization with stationary channel assumption [113]-[114] is briefly described. In Section 10.2, an ARQ scheme with adaptive error control is introduced, and a robust channel sensing algorithm is also proposed for the link adaptation. In Section 10.3, the introduction of frequency hopping concept into adaptive ARQ scheme is discussed. The simulation study of the proposed adaptive ARQ schemes are presented in Section 10.4. The results of [114] and random non-adaptive FH system are also included for comparison. Finally, conclusions are given in Section 10.5.

10.1 Adaptive ARQ scheme

The general description of adaptive ARQ scheme with J modes is given in Fig. 10.1. Based on the channel estimation in each mode, the most suitable mode for the next transmission is chosen and the system is switched to the chosen mode. As an example, the adaptive ARQ scheme proposed in [113]-[114] is briefly described in the following where mode change is allowed only to adjacent modes and channel estimation is based on the count of consecutive ACKs or consecutive NACKs. The corresponding Markov chain representation of the adaptive ARQ system with 3 modes (namely, mode L, M and H) is shown in Fig. 10.2. While operating in mode L, if α consecutive NACKs are received, the adaptive system is switched to mode M. While in mode M, if β consecutive ACKs are received, the adaptive system is switched back to mode L; on the other hand if γ consecutive NACKs are received, the adaptive system is switched to mode H. If λ consecutive ACKs are received while operating in mode H, the adaptive system is switched back to mode M. Assuming a stationary channel, the adaptive system parameters $(\alpha, \beta, \gamma, \lambda)$ are found by optimization of the throughput efficiency over a range of symbol error probabilities. The throughput efficiency of the adaptive ARQ scheme is given by

$$\eta = \frac{K}{T} \tag{10.1}$$

where T is the average number of bits that would have been transmitted for a successful reception of a packet of K information bits and given by

$$T = p_{L_1} T_{L_1} + p_{M_1 H} T_{M_1} + \sum_{i=2}^{\beta} p_{M_i} T_{M_i} + \sum_{j=2}^{\lambda} p_{H_j} T_{H_j} \tag{10.2}$$

where

$$p_X = \frac{P_X}{P_{new}} \tag{10.3}$$

$$P_{new} = P_{L_1} + P_{M_1 H} + \sum_{i=2}^{\beta} P_{M_i} + \sum_{j=2}^{\lambda} P_{H_j} \tag{10.4}$$

and

$$P_{M_1 H} = P_{M_1} - P_{L_1} P_{1e}^{\alpha}. \tag{10.5}$$

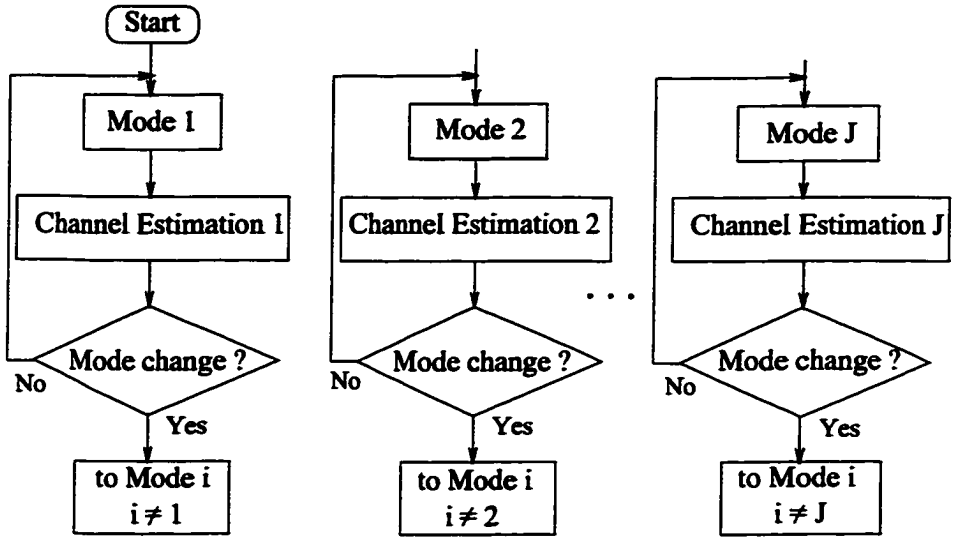

Figure 10.1. *General description of adaptive ARQ scheme with J modes*

In the above equation, T_x stands for the average number of bits that would have been transmitted for a successful reception of a packet of K information bits whose first transmission is initiated in state x, P_x is the steady state probability of state x, P_{new} is the steady state probability of a new packet to be transmitted, p_x is the conditional probability of a new packet initiated in state x given that a new packet is to be transmitted.

10.2 Proposed Adaptive ARQ Scheme

10.2.1 Channel error rate estimation

In [116], XOR-ing (originally used by [117]) of the two consecutive errorneous copies is used to estimate the channel BER for an adaptive ARQ scheme with no error correction in a stationary channel. The work in [116] did not address for the case with error correcting code in a typical time-varying mobile channel environment. If the method of [116] is directly applied to the case with error correcting code in time-varying mobile channel, the channel BER may not be estimated properly due to error correction of FEC. Specifically, their method gives channel BER estimation for one

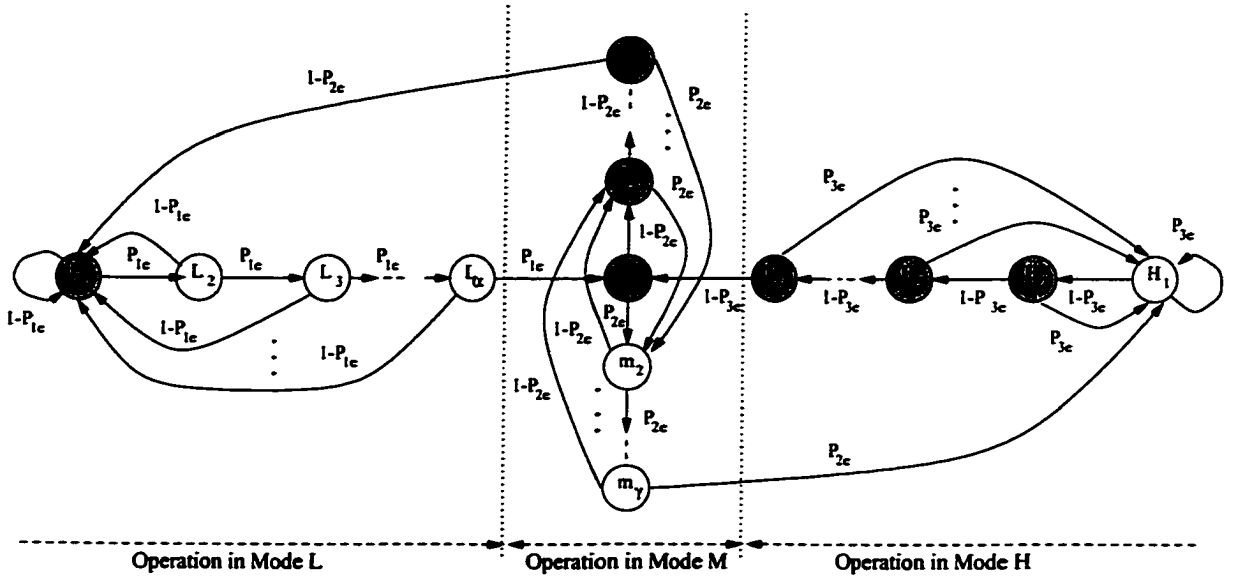

Figure 10.2. *Markov chain representation of adaptive ARQ scheme with 3 modes based on stationary channel assumption*

direction only (i.e., from good channel state to bad channel state direction). In this chapter, we address channel error rate estimation in a typical time-varying mobile channel with error correcting code of nonbinary alphabet (binary alphabet case is just a simplified case of nonbinary one). We describe how to estimate channel error rate for both directions (i.e., from bad channel state to good channel state and vice versa).

The proposed channel error rate estimation scheme is given in Fig. 10.3. Error correcting codes with nonbinary symbols are considered. Mode 1 uses the code with the least error correction capability (usually no error correction capability), the larger mode number indicates the code with stronger error correcting capability and Mode J uses the code with the strongest error correcting capability among all J modes. While operating in mode i, the count of successive NACKs is stored in M_{iu}, and the count of successive ACKs is stored in M_{id}. Although FEC can do error detection, for simplicity we assume, without loss of generality, there is CRC (Cyclic Redundancy Check) for error detection on top of FEC for error correction. Suppose that after FEC decoding a packet error be detected by CRC . If the previous packet is received successfully (then $M_{iu} = 1$), the HD (Hard Decisions) of the current erroneous packet

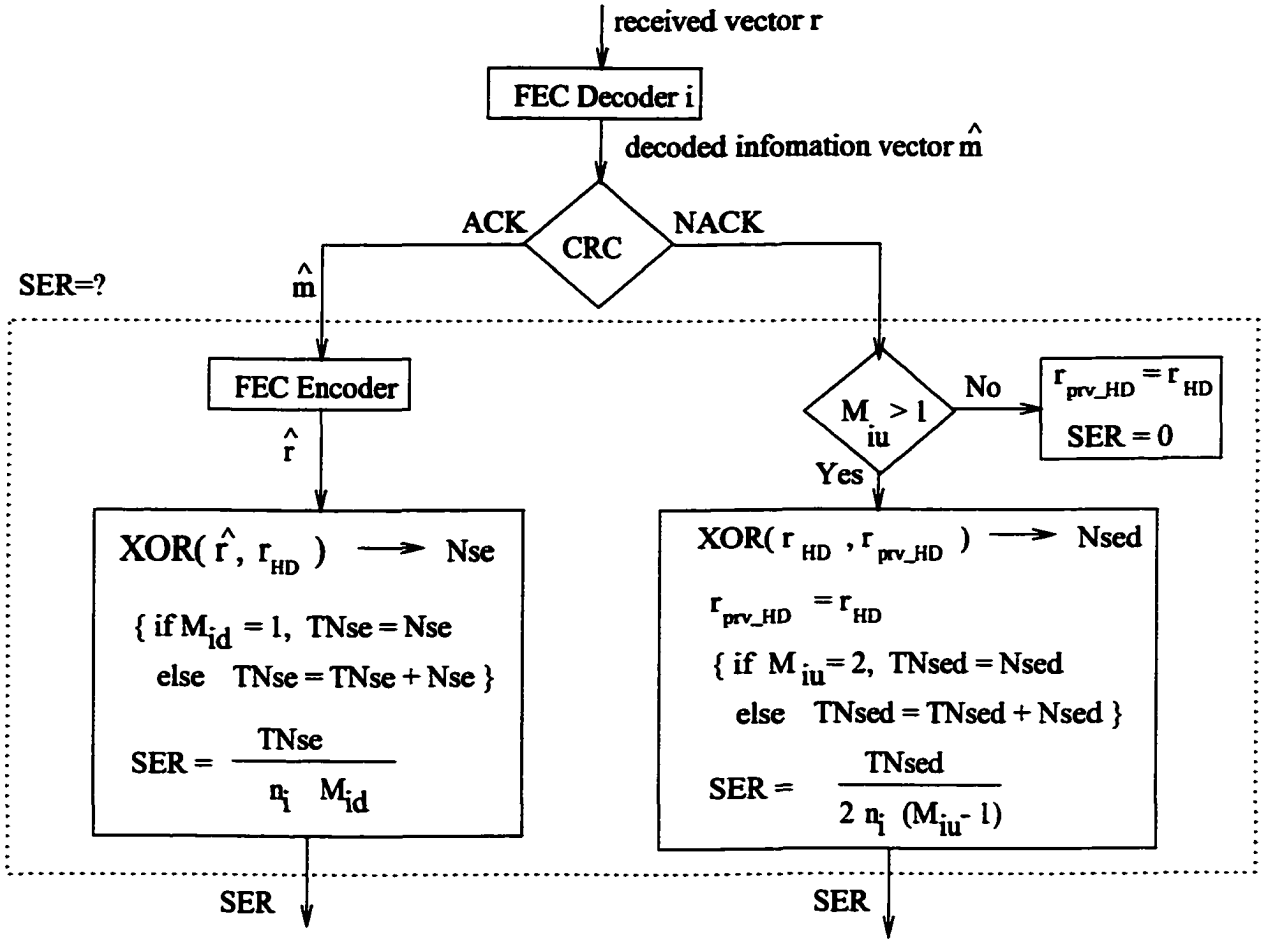

SER = Symbol Error Rate

r_{HD} = Hard Decision of received vector r

$r_{prv\_HD} = r_{HD}$ of previous packet in error

Nse = Number of symbol error per codeword length

TNse = Total Number of symbol error per codeword length

Nsed = Number of symbol error per double codeword length

TNsed = Total Number of symbol error per double codeword length

Figure 10.3. *Proposed channel error rate estimation*

is stored for future use in channel error rate estimation. If the previous packet is also erroneous (then $M_{iu} = 2$), the HD's of the current and previous erroneous packets are XOR-ed to estimate the bit errors in a combined double packet length interval. Any estimated bit error(s) within a symbol causes an estimated symbol error. The estimated bit errors are transformed to estimated symbol errors. Then the estimate of the number of symbol error per double codeword length, $Nsed$, is obtained by averaging over all codewords of the packet. The successive estimates of the number of symbol error per double codeword length are accumulated in $TNsed$. Then the SER (symbol error rate) is estimated by

$$SER = \frac{TNsed}{2n_i(M_{iu} - 1)} \tag{10.6}$$

where n_i is the number of symbols per codeword in mode i. Suppose that after FEC decoding, there be no error detected by CRC. Then the estimate of transmitted packet, $\hat{\mathbf{r}}$, is obtained by FEC-encoding the successfully decoded message and XOR-ed with the HD of the received packet to obtain the estimate of bit errors in the successful packet. Next, the estimated bit errors are transformed to estimated symbol errors in the packet. Then the estimate of the number of symbol error per codeword length, Nse, is obtained by averaging over all codewords of the packet. The successive estimates of Nse are accumulated in $TNse$ and the SER estimate is given by

$$SER = \frac{TNse}{n_i\ M_{id}}. \tag{10.7}$$

Note that $TNse$ and $TNsed$ can be stored in the same memory since only one is required at a time.

10.2.2 Proposed adaptive scheme

Consider an adaptive ARQ scheme with J modes. The operation of proposed adaptive ARQ scheme in mode i, where $2 \leq i \leq J-1$ is shown in Fig. 10.4 and the operations in mode 1 and mode J are shown in Fig. 10.5. While operating in mode i, the receiver decides which mode is the most suitable one for the next transmission
(a) after τ_{id} th continuous successful packet at the receiver (i.e., when $M_{id} = \tau_{id}$) or
(b) after τ_{iu} th continuous unsuccessful packet at the receiver (i.e., when $M_{iu} = \tau_{iu}$).

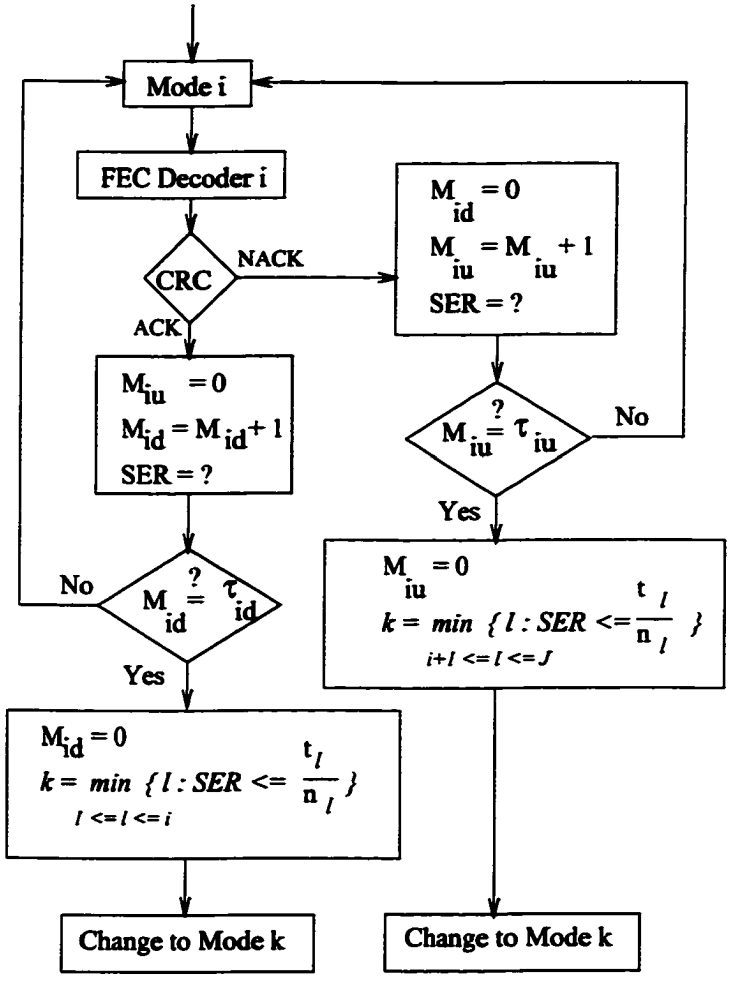

Figure 10.4. *Proposed adaptive ARQ scheme operating in mode i, $2 \leq i \leq J-1$.*

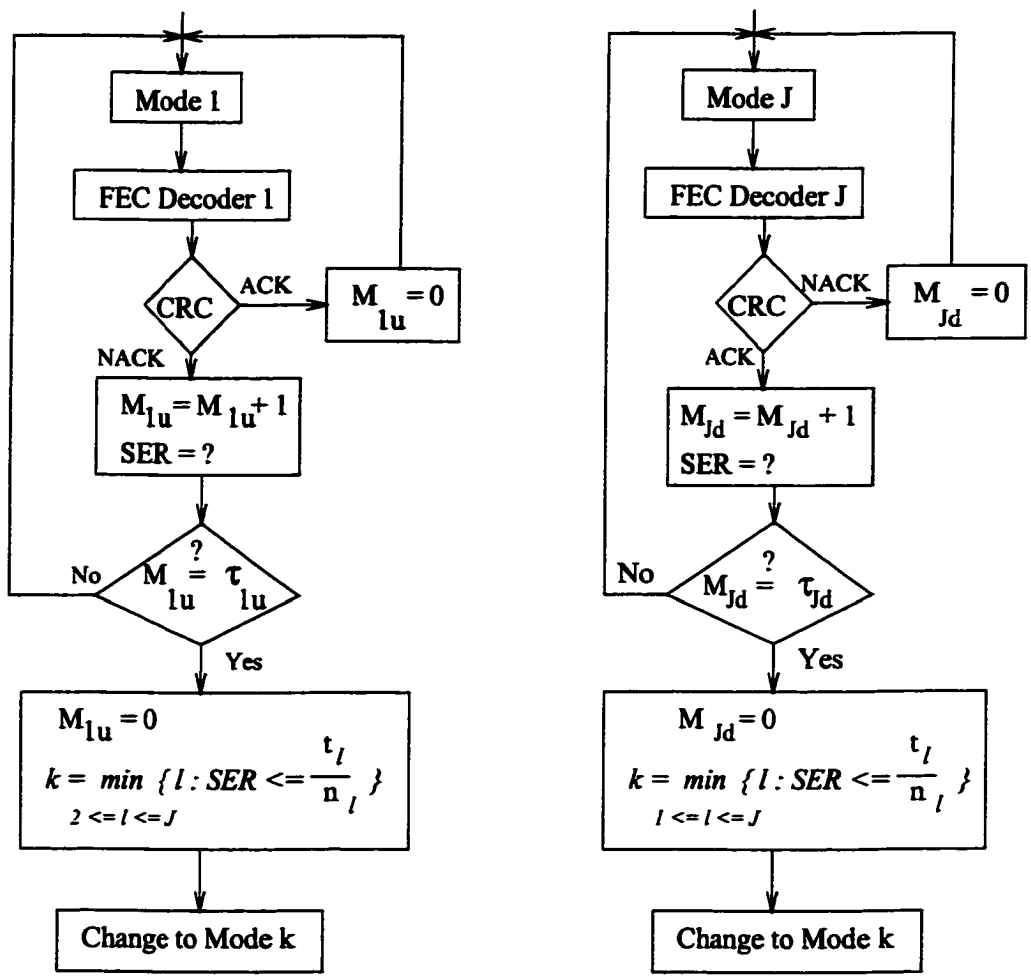

Figure 10.5. *Proposed adaptive ARQ scheme operating in mode 1 and J.*

In the first case, the τ_{id} th successive ACK packet on the feedback channel also contains the information on which mode the next packet is to be transmitted. In the second case, the τ_{iu} th successive NACK packet on the feedback channel also contains the information on which mode the next packet is to be transmitted. In other feedback transmissions, packet doesn't contain the mode number information.

The most suitable mode for the next transmission is chosen as follows. When the successive ACKs in mode i trigger the mode selection procedure, the symbol error rate obtained by the channel error rate estimation is compared against that defined by the error correction capabilities of modes 1 to i, (i.e., $t_1, t_2, \ldots, t_i$), and the most suitable mode k for the next transmission is chosen according to the following

$$k = \min_{1 \le l \le i} \{l : SER \le \frac{t_l}{n_l}\}. \tag{10.8}$$

When the successive NACKs in mode i trigger the mode selection procedure, the symbol error rate obtained by the channel error rate estimation is compared against that defined by the error correction capabilities of modes $i+1$ to J, (i.e., $t_{i+1}, t_{i+2}, ..., t_J$), and the most suitable mode k for the next transmission is chosen according to the following

$$k = \min_{i+1 \le l \le J} \{l : SER \le \frac{t_l}{n_l}\}. \tag{10.9}$$

The proposed adaptive ARQ scheme described above is discussed in a general sense with the parameters $\{\tau_{id}, \tau_{iu}\}$. To find the optimal parameters $\{\tau_{id}, \tau_{iu}\}$ for a practical time-varying multipath fading channel is analytically infeasible. Our choice for these parameters is $\tau_{id} = \tau_{iu} = 2$, ($\tau_{1d}$ and τ_{Ju} are not required). The choice is based on the reasoning that it is much likely for the next packet (new/old) to encounter similar channel condition after two successive packet successes/failures in a slow fading environment. The channel condition for the next packet is hence estimated based on the two successive packets of success/failure. Then the resulted channel error rate estimate for the next packet and the error correction capabilities of the modes are used to choose the most suitable mode for the next packet transmission.

Some differences between the adaptive ARQ schemes described in Section 10.1 and 10.2 are discussed in the following. The scheme of Section 10.1 requires calculation of throughput efficiency expression and optimization of the throughput to find the adaptive system parameters. These parameters are used to determine mode changes.

The channel error rate is indirectly estimated by these parameters. The scheme of Section 10.2 uses fixed adaptive system parameters. These parameters are used for triggering the mode selection procedure not for the mode change. The channel error rate is estimated by XOR-ing method over successive packets the number of which is determined by these parameters. And the error correction capabilities of the operation modes are also used in mode selection.

10.3 Proposed Frequency Hopped Adaptive ARQ Scheme

For circumstances of deep fades in slow fading environment, even stronger FEC code may not be helpful in achieving throughput gain. For example, in very deep fades with long duration, trying to send packets with stronger FEC codes may be useless and power dissipating. For such situations, incorporation of frequency hopping concept into adaptive ARQ scheme is also investigated in this chapter. Usually shadowing effects are caused by terrain environment and hence, hopping the channel frequency into another one may not cure the shadow fading. However, multipath fading in a slow fading environment can be counteracted by frequency hopping since it depends on the carrier frequency.

In conventional FH systems, the carrier frequency is hopped at a fixed rate. In contrast, our proposed frequency hopped adaptive ARQ scheme (FH-Adaptive ARQ) hops the carrier frequency only when it is necessary. For an adaptive ARQ system with J modes, when τ_{Ju} successive packet failures are detected while operating in mode J, frequency hopping is initiated. The required signaling including the new carrier frequency information may be communicated on a dedicated control channel with sufficient error protection. On completion of required signaling, the adaptive system starts to operate with the new carrier frequency in the mode J. Since the packet which is transmitted on a new carrier frequency has already experienced a certain amount of delay, we choose mode J for the system to start operating on new carrier frequency, taking into account the aspect of delay. If the system has no reserved carrier frequencies for FH purpose but is designed to allow frequency hopping to another free user carrier frequency, then the same carrier frequency will be reused

for fully loaded instances. In that situation, FH procedure is performed but actual FH is not accomplished.

Next, the choice of τ_{Ju} value is a tradeoff between counteracting to deep fades and signaling load on the system. The choice of small value, say $\tau_{Ju} = 1$, would more likely counteract deep fades by means of frequency diversity of FH but on the other hand, the more often requirement of signaling would burden the system. The choice of large value would reduce the signaling load on the system but would have less chance of utilizing frequency diversity effect of FH, hence possibly reducing the throughput improvement. In our simulation study, the performance of FH-adaptive ARQ for different choice of FH threshold parameter value τ_{Ju} will also be studied.

10.4 Performance Evaluation by Simulation

10.4.1 System parameters of simulation study

The exact analytical calculation of throughput efficiency of adaptive ARQ schemes in a practical time-varying mobile radio channel is an intractable task and hence, simulation approach is adopted here to evaluate the performance of adaptive ARQ schemes in a typical mobile radio channel. Adaptive stop-and-wait (SW) ARQ schemes with 3 error control codes are considered in our simulation study. Usually packet length is designed based on the application type, channel environment and performance requirement. In our simulation study of adaptive ARQ schemes, without significant effect on the adaptive schemes' performance comparison, we simply assume that one data packet contains only one codeword. We also assume that packets contain only information bits neglecting the synchronization and control bits. All the codes of different modes contain the same length of information bits. In mode 1, which corresponds to low error rate mode Mode-L in [113]-[114], only CRC is used for error detection. Besides CRC, in mode 2 and 3, which correspond to moderate error rate mode Mode-M and high error rate mode Mode-H respectively in [113]-[114], a punctured Reed-Solomon code $RS(21, 15)$ and a Reed-Solomon code $RS(31, 15)$ are used for error correction respectively. BPSK modulation with coherent detection is considered.

The throughput efficiencies of the adaptive ARQ scheme with stationary chan-

nel assumption, the proposed adaptive ARQ scheme, and nonadaptive ARQ schemes using each code of adaptive ARQ schemes mentioned above are compared for the mobile speeds of 1 km/hr, 10 km/hr and 50 km/hr and long-term SNR (signal-to-noise ratio) range of 5 dB to 25 dB. The long-term SNR is defined based on the long interval of 2^{19} samples (i.e., approximately 36.41 seconds at 14.4 kHz). The carrier frequency of 900 MHz and the data rate of 14.4 kbps are used. The round-trip delay of 2 RS symbol intervals is assumed. In throughput evaluation, perfect error detection of CRC is assumed and the CRC parity bits are not included in throughput calculation. The perfect feedback channel is assumed. The parameters of the adaptive ARQ scheme with stationary channel assumption are $(\alpha, \beta, \gamma, \lambda) = (1, 5, 2, 5)$ [113]. For the proposed scheme, the round trip delay associated with the occasions of ACK/NACK containing mode number information is larger than the other occasions of normal ACK/NACK, and for illustration, is assumed 3 RS symbol interval. ARQ scheme which includes FH concept when required, is also investigated in the same environment. For FH-adaptive ARQ scheme, the FH setup time, comprised of the signaling (handshaking) time and round trip delay for a complete frequency hopping, is assumed for illustration as one packet length in mode 3 plus two normal round trip delay.

As a comparison to the proposed FH-adaptive ARQ scheme, non-adaptive FH system is also evaluated. Three cases of non-adaptive FH system using CRC, CRC + RS(21,15) and CRC + RS(31,15), respectively are considered. The carrier frequency is hopped at the start of each packet and the new channel is assumed to have an identically distributed, independent multipath Rayleigh fading. Moreover, partial band interference, which typically exists for FH systems, is not included in the throughput evaluation of non-adaptive FH system. The round trip delays are the same as those of non-adaptive ARQ schemes.

10.4.2 Channel Model

Mobile radio channel is typically characterized by multipath fading and shadowing. In our simulation, multipath fading is modeled with Rayleigh distribution. Doppler spread induced by the motion of a mobile terminal, which corresponds to the time correlation of the fading gain samples, is also included. Jake's Doppler spectrum is

assumed and the correlated Rayleigh fading gain samples are generated by using the method of [109]. The shadowing effect which causes slower variation of the short term median strength of the received signal is usually modeled with lognormal distribution, i.e., the short term median strength of the received signal $\gamma(t)$ can be expressed as

$$\gamma(t) = 10^{-\xi(t)/10} \tag{10.10}$$

where $\xi(t)$ is a time-correlated Gaussian random process. In our simulation, the method of [110] is used for lognormal shadowing where the lognormal shadowing is modeled as a Gaussian white noise process which is filtered with first order lowpass filter. With this model, the discrete-time samples of $\xi(t)$ are given by

$$\xi_{k+1} = \varepsilon \cdot \xi_k + (1-\varepsilon) \cdot \nu_k \tag{10.11}$$

where ν_k is a zero mean white Gaussian random variable with variance Ω_ν^2, ε is a parameter that controls the spatial correlation of the shadowing and given by

$$\varepsilon = \varepsilon_D^{vT_s/D}. \tag{10.12}$$

The parameter ε_D is the correlation between two points separated by a spatial distance of D, v is the velocity of the mobile terminal, T_s is the sampling period. For typical suburban propagation at 900 MHz, it has been suggested in [110] that $\Omega_\xi \approx 7.5\ dB$ with a correlation $\varepsilon_D \approx 0.82$ and $D = 100$.

10.4.3 Performance of Proposed Adaptive ARQ scheme

To illustrate the tracking capability of the proposed adaptive ARQ scheme, the short-term average throughputs are presented in Figs. 10.6-10.8 as a function of time for the mobile speed of 50 km/hr, 10 km/hr and 1 km/hr, respectively. For comparison, the adaptive ARQ scheme with stationary channel assumption [114] and conventional ARQ schemes with single error control codes are also included in these figures. The short-term throughput is obtained by averaging over every 0.1 second interval.

From the figures, it is observed that for very slow fading case of $v = 1\ km/hr$, the short-term throughput is mainly determined by the multipath fading effect. As the fading rate increases, the effects of shadowing on throughput performance become prominent as can be seen in the cases of v =10 km/hr and 50 km/hr.

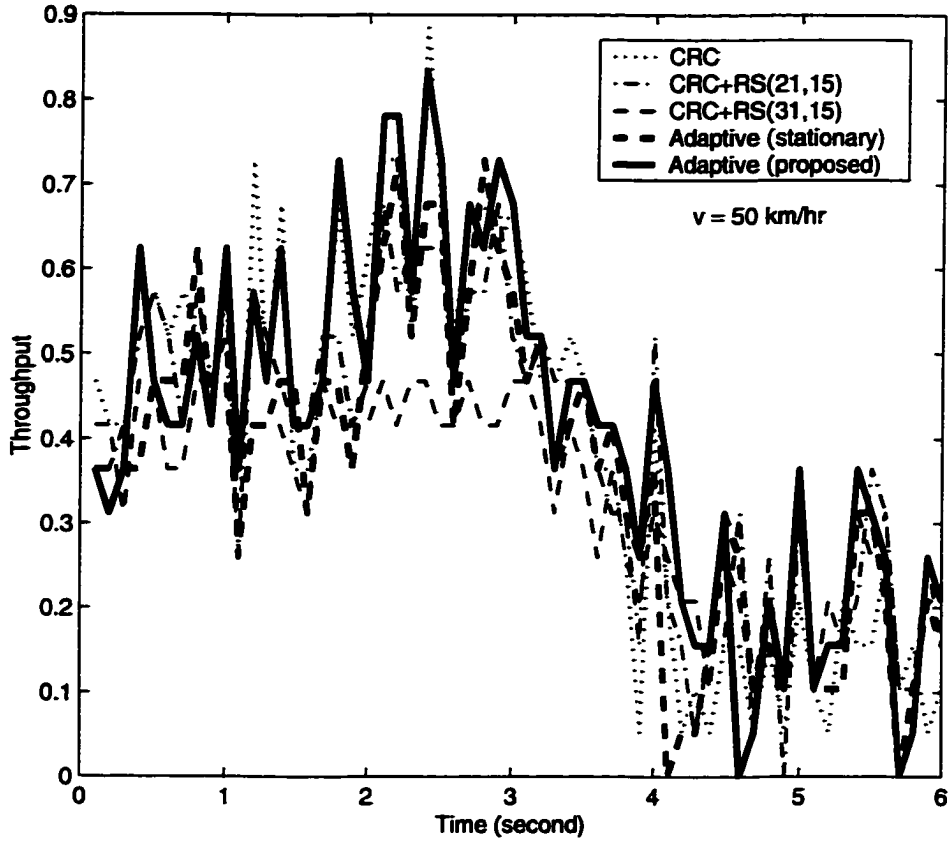

Figure 10.6. *Short-term throughput of the adaptive and nonadaptive ARQ schemes for mobile speed of 50 km/hr and long term SNR of 10 dB*

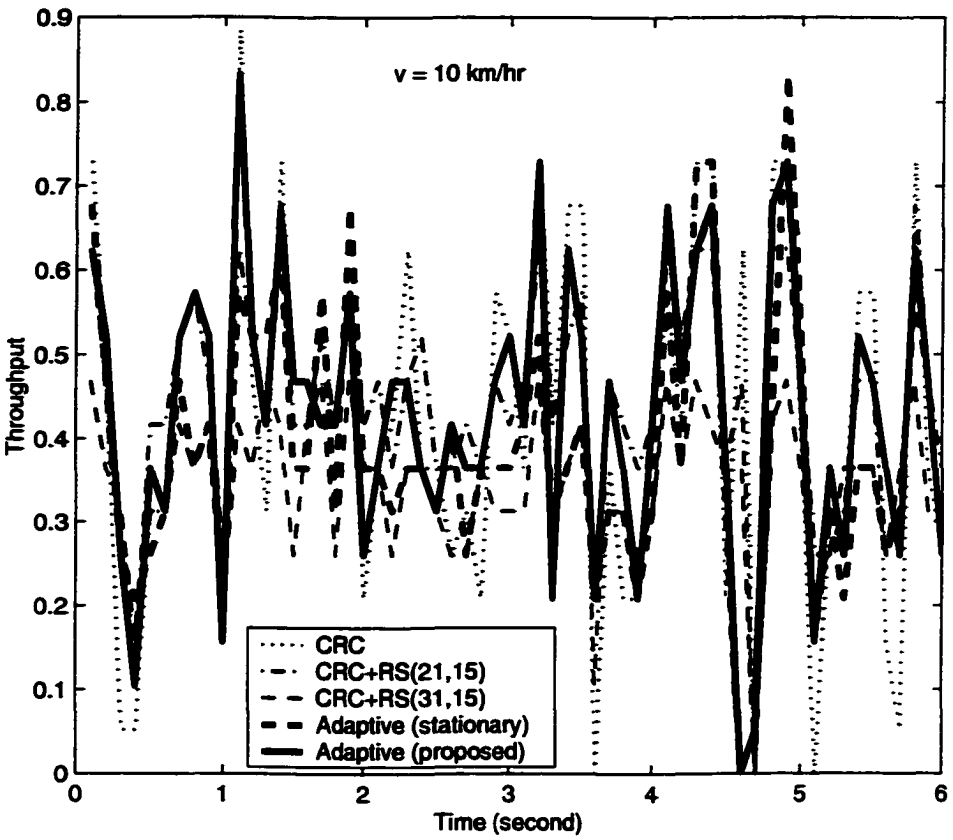

Figure 10.7. *Short-term throughput of the adaptive and nonadaptive ARQ schemes for mobile speed of 10 km/hr and long term SNR of 10 dB*

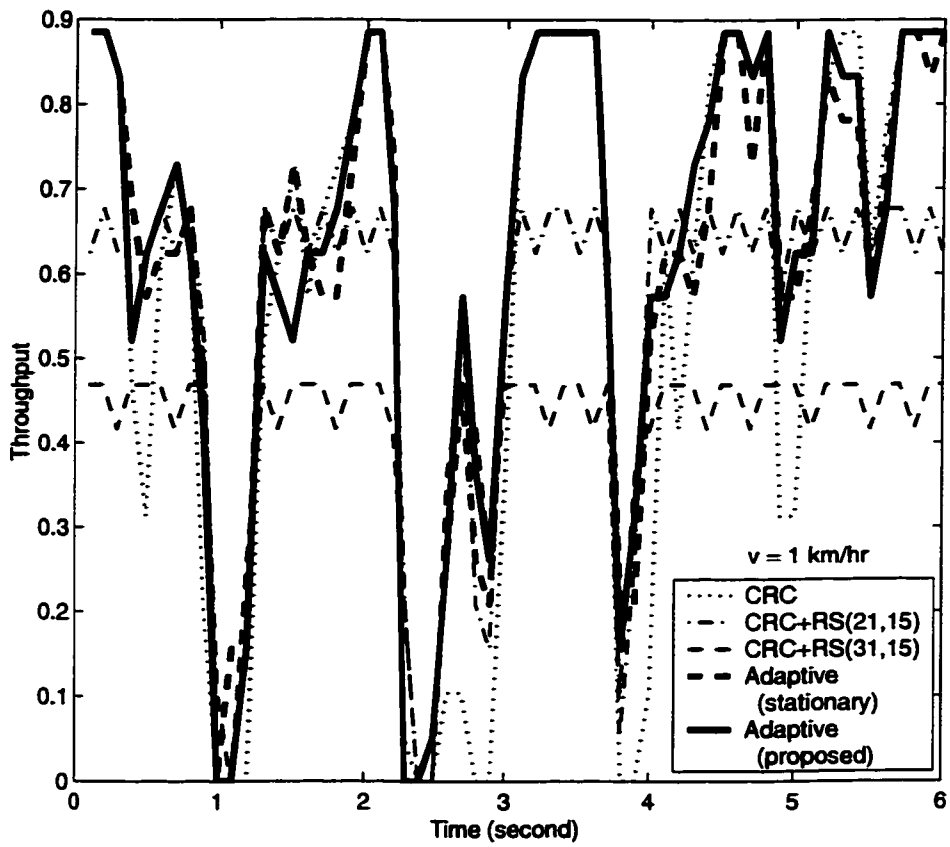

Figure 10.8. *Short-term throughput of the adaptive and nonadaptive ARQ schemes for mobile speed of 1 km/hr and long term SNR of 10 dB*

Regarding the tracking capability to channel conditions, it is observed that both adaptive schemes (proposed one and the one with stationary channel assumption) can track the channel variations quite well for all fading rates considered, especially for slower fading cases. As expected, both adaptive schemes can adapt to multipath fading more closely for very slow fading case than faster fading cases. The tracking trends of both adaptive schemes for faster fading cases cannot follow multipath fading quite closely but they follow the shadowing effect.

For very slow fading rate case of $v = 1$ km/hr, the channel tracking performances of both adaptive schemes are almost the same as illustrated in Fig. 10.8. However, as fading rate increases, the channel tracking of proposed adaptive scheme behaves differently from that of the other scheme. More specifically, for faster fading rates, the proposed adaptive scheme can track the channel variations closer than the other as can be observed in Figs. 10.6 and 10.8.

The throughput performances of the adaptive and nonadaptive ARQ schemes as a function of long-term SNR are shown in Figs. 10.9, 10.10 and 10.11 for the mobile speeds of 50 km/hr, 10 km/hr and 1 km/hr, respectively. Both adaptive schemes show throughput improvement over nonadaptive schemes. For both adaptive schemes, more throughput improvement is observed in slower fading rate cases. This is due to the fact that the adaptive schemes yield better tracking capability over the channel with slower variations. For the cases of mobile speed 1 km/hr and 10 km/hr, both adaptive schemes improve throughput with respect to nonadaptive schemes over all SNR values considered.

When comparing two adaptive schemes, at very slow fading case, e.g., 1 km/hr mobile speed, the proposed scheme has slightly better performance for SNR values greater than 15 dB but slightly worse performance for SNR values less than 15 dB. As an overall evaluation over all SNR values considered, both schemes perform almost the same for mobile speed of 1 km/hr. In faster fading rate cases of mobile speed 10 km/hr and 50 km/hr, the proposed scheme slightly outperforms the adaptive scheme with stationary channel assumption, as an overall. This (slightly) better throughput performance of the proposed scheme indicates the (slightly) better channel tracking capability of the proposed scheme over the other. This fact can also be observed from the short-term throughput figures for faster fading cases. In brief, the proposed

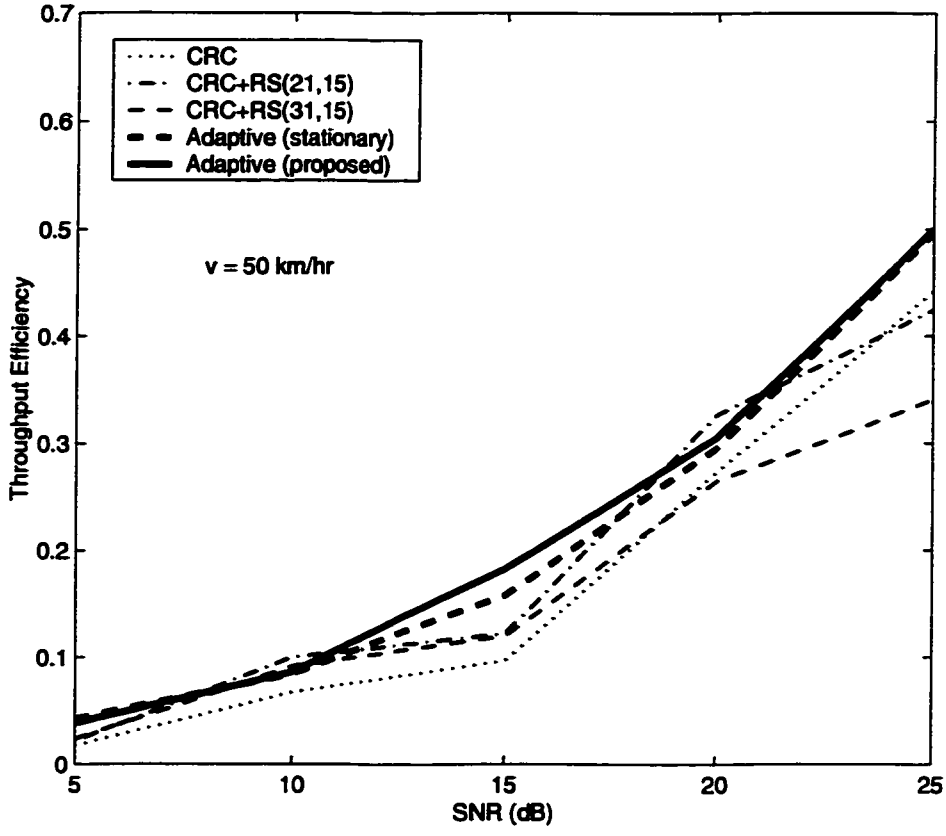

Figure 10.9. *Throughput comparison of adaptive and nonadaptive ARQ schemes for mobile speed of 50 km/hr*

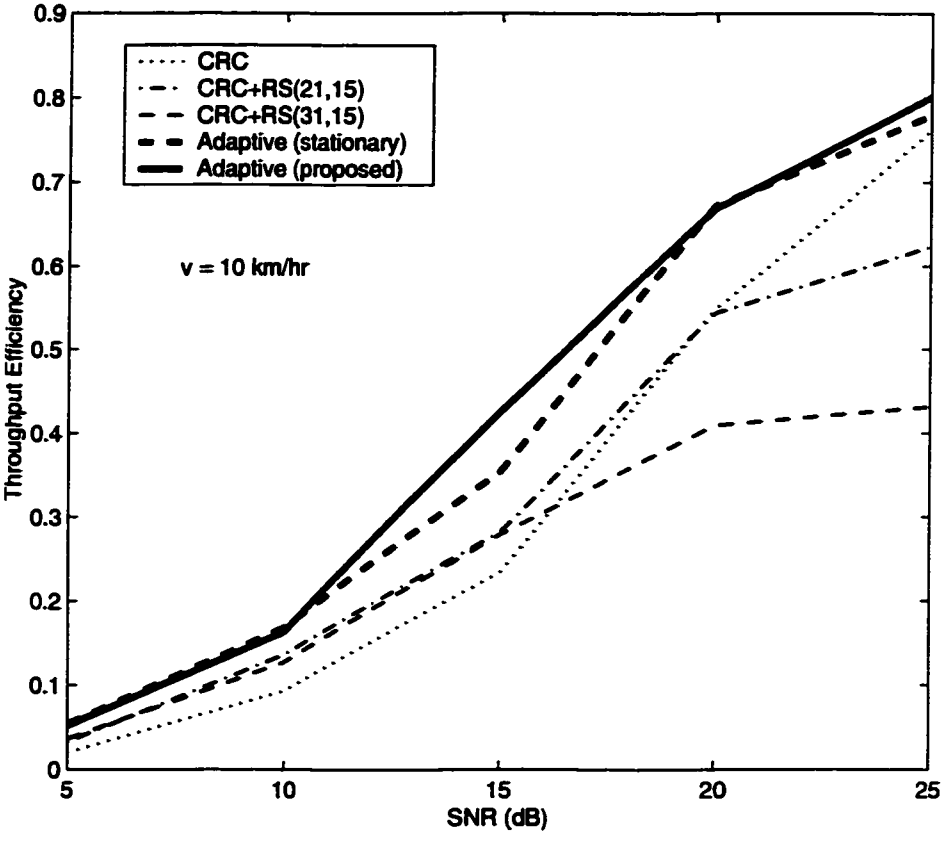

Figure 10.10. *Throughput comparison of adaptive and nonadaptive ARQ schemes for mobile speed of 10 km/hr*

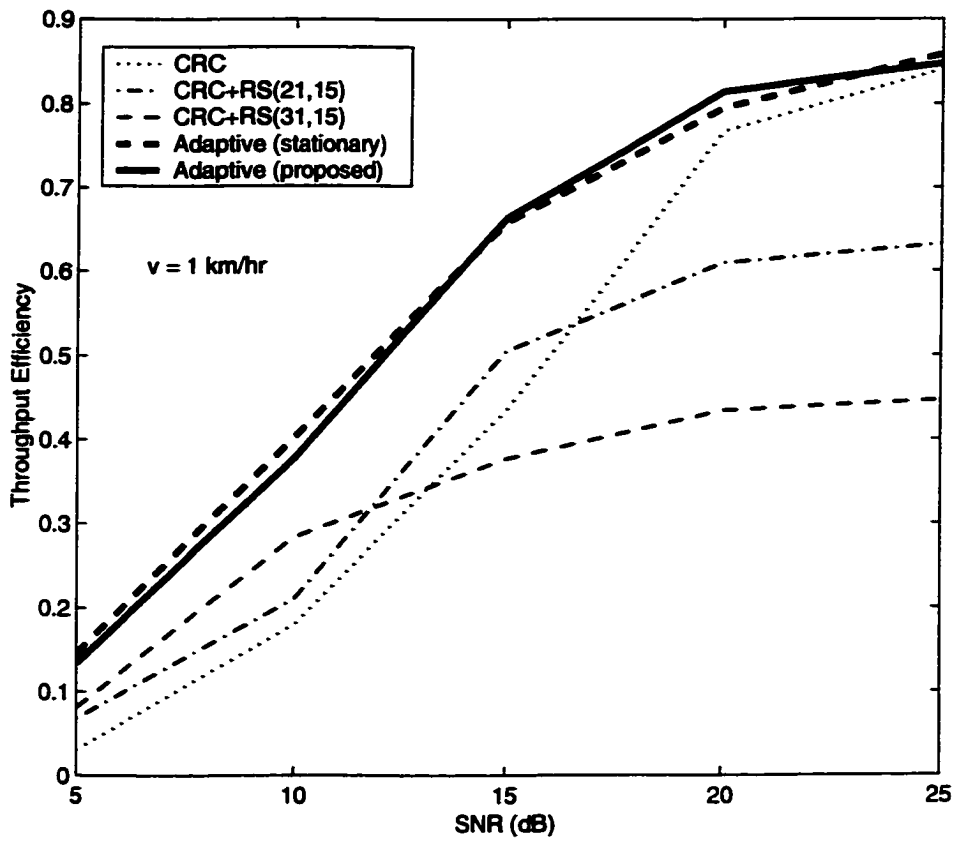

Figure 10.11. *Throughput comparison of adaptive and nonadaptive ARQ schemes for mobile speed of 1 km/hr*

adaptive ARQ scheme has a similar performance for slow fading cases and a slightly better performance for fast fading cases than the adaptive ARQ scheme of [114]; but does not require the tedious design task involved in [114].

10.4.4 Performance of Proposed FH-Adaptive ARQ scheme

In this Section, the throughput performances of Adaptive ARQ scheme with and without frequency hopping are studied. In simulation of a FH-Adaptive ARQ scheme, we assume that there be always a new carrier frequency for FH and the multipath Rayleigh fading channel response for each new carrier frequency be independent and identically distributed (*i.i.d.*). However, since shadow fading is mainly determined by terrain nature, the packet will face the same shadow fading regardless of carrier frequency. Since FH is applied to counteract deep fades in very slow multipath fading environment, only the case with 1 km/hr mobile speed will be considered.

Fig. 10.12 shows the throughput performance of the proposed adaptive ARQ scheme without FH and the proposed FH-Adaptive ARQ scheme with different values of FH threshold parameter τ_{Ju}. More throughput improvements are observed at lower SNR values. Since more deep fades occur at lower SNR values, the effect of FH becomes more dominant in throughput efficiency and brings about more throughput gain. Smaller FH threshold parameter value achieves larger throughput improvement since frequency diversity is applied with less delay. At high SNR values, throughput improvements of FH are almost the same for different values of FH threshold parameter. Since the probability of deep fade occurrence is very low at high SNR region, the FH, which is performed when encountering deep fades, has no significant effect on the average throughput. Consequently, at high SNR region FH-Adaptive ARQ gives almost the same throughput for different values of FH threshold parameter. Due to the same reason, FH-Adaptive ARQ scheme does not achieve significant throughput improvement over Adaptive ARQ scheme at high SNR region. However, the throughput improvement achieved by FH-Adaptive ARQ is quite significant at long term SNR region of less than 20 dB for the system considered.

Fig. 10.13 shows the corresponding percentages of average number of FH per successful packet, denoted by $FH\%$, for different values of FH threshold parameter. The $FH\%$ indicates some measure of average signaling load on the system caused by

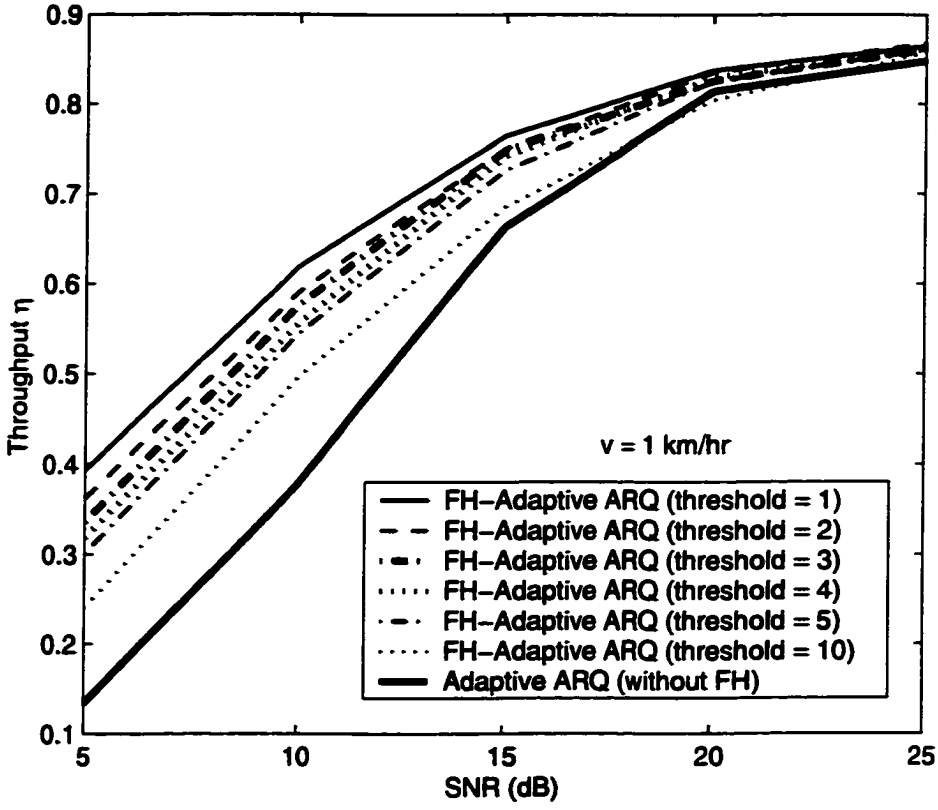

Figure 10.12. *Throughput comparison of proposed adaptive ARQ schemes with and without FH*

FH, in other words, some measure of system resource usage on the control channel by FH. As expected, the average signaling load is quite high at low SNR values for all FH threshold parameter values, with the more signaling load for the smaller FH threshold parameter value. The additional resource usage on the control channel by the FH-adaptive ARQ scheme may require more system resources for the control channel. The optimal FH threshold parameter value taking into account the whole system's capacity and throughput would depend on many system parameters and should be evaluated at system level rather than the level and scope considered in this chapter.

Taking into account the signaling load of FH setup, the system resource usage of the proposed FH-adaptive ARQ scheme can be evaluated in terms of the overall throughput performance which is defined as the ratio of the number of information bits

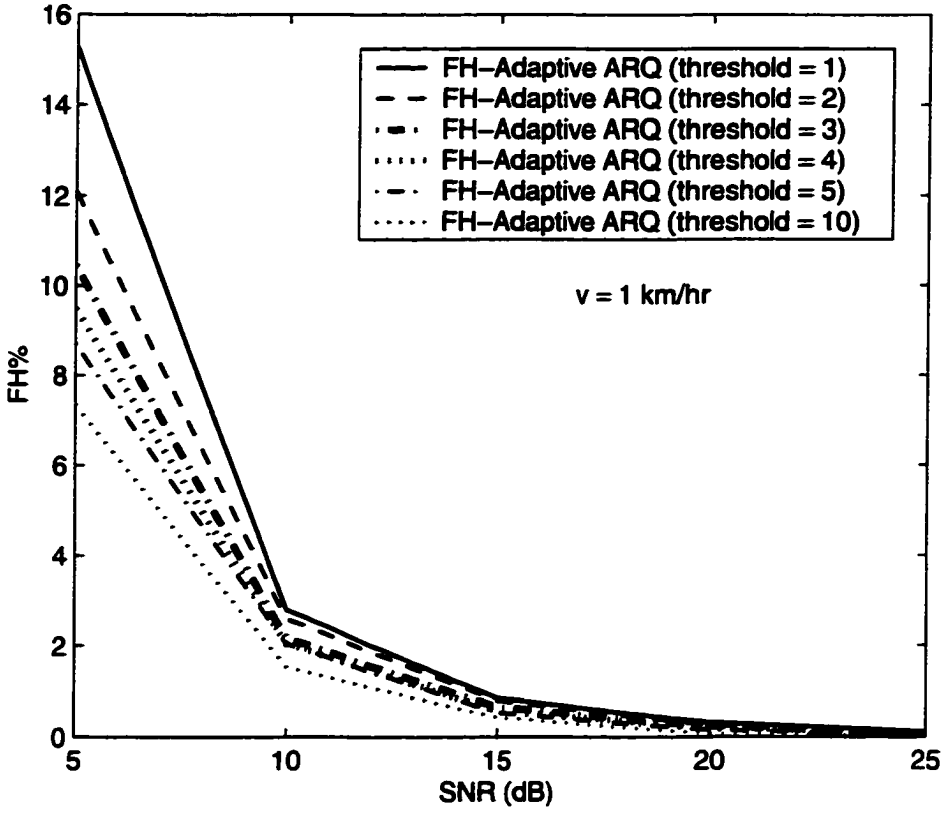

Figure 10.13. *The average number of frequency hopping per successful packet (FH%) in FH-Adaptive ARQ scheme for different values of FH threshold parameter*

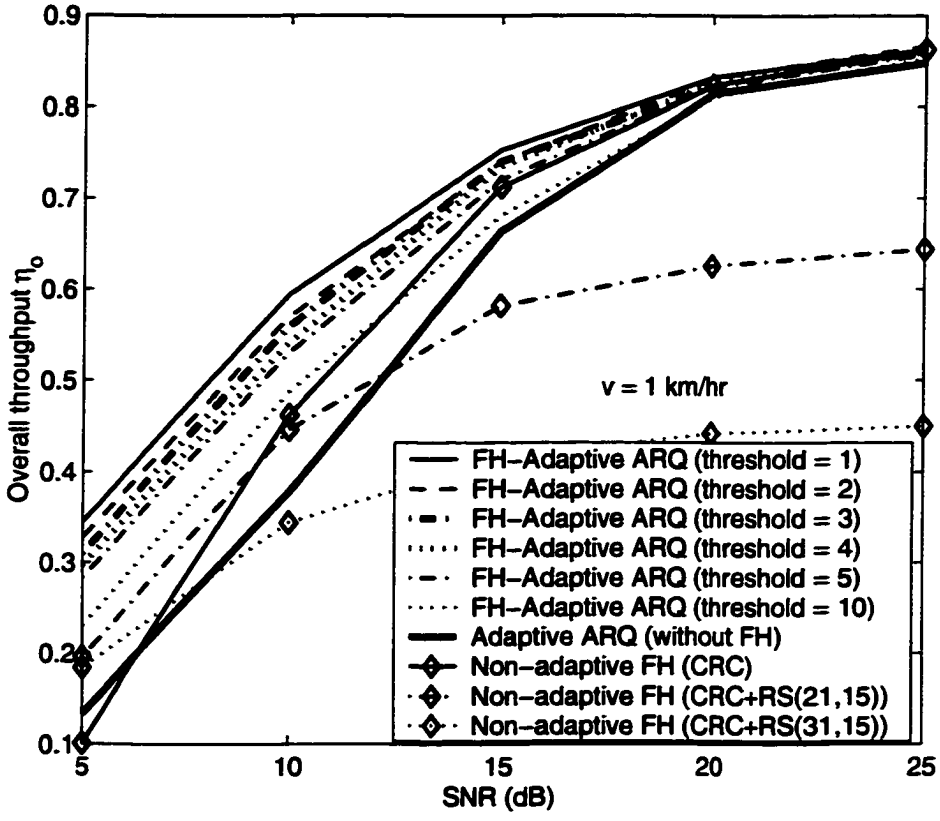

Figure 10.14. *Overall throughput comparison of proposed adaptive ARQ schemes with and without FH and non-adaptive FH*

in a packet to the sum of the average number of bits that would have been transmitted on traffic channel and the average number of bits that would have been transmitted on FH setup control channel for a successful reception of those information bits. Let the FH setup time in terms of the number of bits that would have been transmitted be R and the average throughput on the traffic channel be η. Then the overall throughput η_o of the proposed FH-adaptive ARQ scheme can be given by $\eta_o = (\frac{FH\%\cdot R}{100\cdot K} + \frac{1}{\eta})^{-1}$. The overall throughputs for different FH threshold parameter values are shown in Fig. 10.14. By comparing Fig. 10.12 and Fig. 10.14, it can be seen that although the overall throughputs are less than the traffic channel throughputs and the throughput differences for different FH threshold parameter values become smaller in Fig. 10.14, the throughput curves follow similar trend for different FH threshold parameter values and smaller FH threshold parameter value still gives a better performance. Hence, in terms of system resource usage, FH threshold parameter value of 1 offers the best performance.

Also shown in Fig. 10.14 are the throughput performances of random non-adaptive FH system with different error correction codes. Since no partial band interference is included, the results of random non-adaptive FH system are quite optimistic. Even compared with those optimistic results of non-adaptive FH system, the performance of FH-adaptive ARQ scheme is significantly better. The performance gain of FH-adaptive ARQ over non-adaptive FH with CRC is negligible at very high SNR values but becomes prominently significant for lower SNR values. It may be explained as follows. At high SNR values, the probability of deep fade occurrence is very low and frequency diversity effect does not have significant impact on throughput performance, on the other hand, FH-adaptive ARQ would almost always use CRC at high SNR values; hence both approaches would perform almost the same. For low SNR values, the deep fade occurs more frequently and noise effect also becomes significant; and consequently, both frequency diversity and adaptive code diversity have much more impact on throughput performance. Hence, improvement of having both diversities over having one diversity is greater for lower SNR values. Similarly, the gain of FH-adaptive ARQ over non-adaptive FH with CRC + RS codes can be ascribed to the unnecessary use of stronger error correcting code in non-adaptive FH for high SNR values, and having both frequency diversity and adaptive code diversity in FH-

adaptive ARQ while having only frequency diversity in non-adaptive FH for low SNR values, respectively.

10.5 Conclusions

Adaptive ARQ schemes are quite effective for throughput enhancement in time-varying mobile channel environments. In this chapter, we consider ARQ scheme with adaptive error correcting codes, particularly Reed-Solomon codes. We proposed a channel error rate estimation required for adaptive ARQ implementation by making use of XOR-ing, which is originally applied in [117] and then in [116]. With the proposed channel error rate estimation, we also propose an adaptive scheme that adapts the error correcting code according to channel conditions, as an alternative to [113]-[114]. The proposed adaptive ARQ scheme circumvents the tedious throughput calculation and optimization for choosing adaptive system parameters required in [113]-[114]. In terms of throughput efficiency, the proposed scheme has similar or slightly better performance than [113]-[114].

As an enhancement in counteracting long deep fades, we also investigate the incorporation of FH concept into adaptive ARQ scheme. We investigate the impact of the choice of FH threshold parameter value on the throughput performance and the imposed signaling load on the system. Our results show that FH-adaptive ARQ scheme is quite efficient in counteracting long deep fades at the expense of some signaling load on the system. In terms of system resource usage or overall throughput of the FH-adaptive ARQ scheme, the FH threshold parameter value of 1 gives the best result. The FH-adaptive ARQ also significantly outperforms the random non-adaptive FH system and hence, it is a promising technique for capacity enhancement.

Chapter 11

Conclusions

In this chapter, a brief summary of the results described in the previous chapters is presented and suggestions for further research are given.

11.1 Summary of the Dissertation

This dissertation focuses on two main areas: the first addresses issues in OFDM systems and the second addresses adaptive ARQ schemes. The significance of OFDM technology has been justified by its adoption in many standards for current and future wireless communications. Our contributions in OFDM technology will expectedly have direct impact on those current and future OFDM applications. In order to provide highly reliable performance to current and future wireless applications in slowly time-varying channel environments, adaptive ARQ schemes have attracted much research attention and will play a crucial role in ensuring the required high reliability. Our contributions in adaptive ARQ schemes are expected to play some role for those high performance services. The detailed contributions are presented in the following.

In Chapter 2, timing synchronization in OFDM systems is addressed. We discuss some drawbacks of the existing OFDM timing synchronization methods and propose two approaches which overcome those drawbacks. The first approach uses a sliding window averaging and the second approach is based on the training symbol design and its corresponding timing metric. Both approaches are simple to implement and are of similar complexity to the existing methods. Both proposed approaches achieve performance improvement over the existing methods and the second proposed approach has a better performance.

In Chapter 3, channel estimation in OFDM systems is addressed. The performance of an existing time-domain-based channel estimation namely frequency pilot time average (FPTA) method is analyzed. Our analysis points out that the time-domain pilot to noise ratio as defined in [53] is not an appropriate measure for a comparison of different channel estimation methods. We propose an approximate linear minimum mean square error (LMMSE) type time-domain-based channel estimation called MST which employs intra-symbol time averaging and most significant tap selection. The proposed method well outperforms the FPTA method. The relationship, similarities, and differences between the proposed method and other existing methods are also presented. The proposed method has a similar performance to the LMMSE method (which is the best among the existing methods) but less complexity.

In Chapter 4, a reduced complexity channel estimation for OFDM systems with transmit diversity is proposed. The channel estimation for systems with transmit diversity typically imposes high complexity which is one of the main concerns particularly for mobile terminals. Hence, a reduced complexity method is much desirable. By exploiting the correlation of the subchannel responses, the proposed reduced complexity method achieves much complexity reduction. The sizes of the matrix inverse and the FFT's required in the channel estimation at every OFDM data symbol are reduced by half of the existing method for OFDM systems with non-constant modulus subcarrier symbols or constant-modulus subcarrier symbols with some guard tones. The complexity reduction of hallf FFT's size and some matrix multiplication is still achieved for constant modulus subcarrier symbols with no guard tones. The price for the complexity reduction is just a slight BER degradation and for the channels with relatively small dellay spreads, the BER performance of the proposed method becomes quite comparable to the existing method.

Moreover, an alternative approach for the number of significant taps required in the channel estimation is described which achieves a comparable performance to the case with the known suitable number of significant taps. This approach would be useful for the case where the knowledge of a suitable number of significant taps is not available. Furthermore, the impact of non-sample-spaced channel paths on the channel estimation is analyzed and a simple modification which reduces the lost leakage of the non-sample-spaced channel paths is also proposed. This modification

gives a substantial performance improvement to both the existing method and the proposed reduced complexity method without any added complexity.

In Chapter 5, a robust symbol timing and carrier frequency synchronization for OFDM systems is presented. Usually, timing synchronization and frequency synchronization are addressed separately. Only a few have addressed joint time and frequency synchronization. However, little attention has been given to the sync detection. Our proposed method considers all aspects of timing synchronization, frequency synchronization, sync detection, and the peak factor of the training symbol. The proposed method is based on one training symbol specifically designed to have a steep roll-off timing metric. The proposed timing metric also provides a robust sync detection capability while most timing synchronization methods lack this capability. Both time domain (TD) training and frequency domain (FD) training are investigated. Our results show that TD training generally outperforms FD training. For FD training, low peak-to-average power ratio of the training is also taken into consideration. The channel estimation based on the designed training symbol is also incorporated to give fine timing and frequency offset estimates.

For fine frequency estimation, two approaches are presented. The first one is based on the suppression of the interference introduced to frequency estimation in multipath dispersive channel by the training symbol pattern. The second one is based on maximum likelihood (ML) principle and does not suffer any interference. The proposed timing and frequency synchronization method achieves some improvement over the existing timing and frequency synchronization. A new performance measure for timing estimation, i.e. the plot of signal to timing-error-introduced average interference power ratio versus timing estimate shift, is introduced. A simple approach to find the optimal setting of the timing estimator is presented. This new performance measure and the proposed approach to find the optimal setting of the timing estimator would be quite useful in practice for designing optimal or near optimal synchronization methods.

In Chapter 6, a joint timing synchronization, frequency synchronization and channel estimation is proposed. No methods addressing all these three tasks together are observed in the research literature of OFDM. Since the synchronization and channel estimation tasks can affect each other, the idea of jointly addressing these tasks is

much desirable. We develop a two-stage realizable maximum likelihood (ML) based scheme for a joint timing and frequency synchronization and channel estimation. At the first stage, coarse timing and frequency offset estimates are obtained. Based on these estimates, the channel response estimate is obtained and ML realization is performed at the second stage which may be iterated for further improvement.

This two-stage algorithm reduces the complexity in realizing ML principle. A means of further complexity reduction by an adaptive scheme is also presented which achieves almost the same BER performance and much complexity reduction. The analysis and simulation results of the performance of our proposed method are also presented. The proposed joint synchronization and channel estimation scheme is rather general and can be applied not only in multicarrier systems but also in single carrier systems.

In Chapter 7, we address some fundamental questions such as "under what conditions, if any, can a bandlimited function take infinite values between finite samples?", "does an arbitrary sequence $\{x_n\}$ represent the samples of a bandlimited function?", "what are the requirements for sampling a bandlimited function?", and "how much the peak factors of a continuous signal and its sampled signal can differ ?". In order to answer them, we present several bounds of bandlimited periodic and non-periodic functions and some aspects on the sampling theorem and sampling series beyond the scope of the Shannon's sampling theorem.

For a bandlimited periodic signal, the amplitude is bounded by the total power and the number of constituent harmonic tones. The signal variation is bounded by the total power and the bandwidth. For a bandlimited non-periodic signal, the amplitude and variation are bounded by the total energy and the bandwidth. For an OFDM signal, the peak factor ratio of the continuous signal to the sampled signal is upperbounded by the number of tones. Analogously, for a single-carrier signal, this peak factor ratio is upperbounded by the number of samples. Using an arbitrarily chosen data sequence for the sampling series may not necessarily result in a bandlimited signal of interest for communications systems.

In Chapter 8, we present peak-to-average power ratio (PAPR) behavior of some Reed-Muller codes in OFDM systems. PAPR problem is one of the main issues in OFDM and a coding approach for both PAPR reduction and error correction

has recently emerged as one of the promising techniques. Based on the recognition of the connection between Golay complementary sequences and second-order cosets of RM(1,m) codes, this approach enjoys both tight PAPR control and good error correction capability. However, for an OFDM system with large number of carriers, the code rate of this approach becomes too small. Hence, we consider higher order cosets of RM(1,m) codes beyond its original constraint to second order cosets. In fact, finding a code with low PAPR, good error correction, and reasonable code rate is a really challenging task.

In this dissertation, we have studied PAPR behavior of second-order cosets for m = 4 and 5, and third-order cosets for m = 4 of RM(1,m) codes in OFDM system in order to explore the possibility of including third-order cosets. We have observed that for PAPR at most 4, all 52 second order coset representatives for $m = 4$, all 702 second order coset representatives for $m = 5$, and 240 third order coset representatives out of 265 for $m = 4$ follow some regular patterns. The regularities in the observed PAPR behavior suggests that in order to increase the code rate, it is possible to include the third order cosets of RM(1,m) codes in the approach using RM codes in OFDM system. However, further research is required in order to include third order cosets in a systematic way which allows both efficient encoding and decoding processes.

In Chapter 9, a simple and efficient stop-and-wait (SW) automatic repeat-request (ARQ) scheme with adaptive error control is investigated. In this scheme, the channel state information (CSI) is extracted by monitoring the contiguous positive acknowledgment (ACK) or negative acknowledgment (NAK) messages. Exploiting this CSI, we adapt the coding strategy to the changes in the channel condition, and thus improve the throughput efficiency. In order to facilitate the throughput analysis and parameters optimization, we model the adaptive system by a Markov chain. Using this analytical model and assuming a static channel, an exact throughput expression for the adaptive ARQ protocol is derived and suboptimal adaptive system parameters are obtained.

It also points out that the conventional throughput expression of an adaptive ARQ scheme, which is expressed as the average of the throughputs in all modes of the adaptive system, is not an exact expression but an approximate one. The obtained design parameters are applied for the adaptive system in a typical time-

varying mobile radio channel characterized by Rayleigh multipath fading on top of lognormal shadowing. For slow fading channels, the proposed adaptive system can track the channel variations very well, hence, much throughput improvement can be achieved over conventional nonadaptive SW-ARQ schemes for almost all SNR values considered. The simulation results also confirm the applicability of the adaptive system parameters so-obtained by the throughput analysis in a static channel, to a time-varying mobile radio channel.

In Chapter 10, a robust adaptive ARQ scheme with adaptive error correcting codes is proposed. For link adaptation, we propose a robust channel sensing algorithm by making use of XOR-ing. With the proposed channel sensing algorithm and the information of the error correcting capabilities of the codes, an adaptive scheme that adapts its error correcting codes according to the channel conditions is presented. This proposed scheme circumvents a tedious throughput calculation and optimization for choosing the adaptive system parameters required in our previous proposed approach of Chapter 9. In terms of the throughput efficiency, this proposed approach has similar or slightly better performance than the previous proposed method.

Moreover, as an enhancement in counteracting long deep fades, we introduce an adaptive frequency hopping (FH) concept into the adaptive ARQ system. This proposed FH-adaptive ARQ scheme achieves significant throughput improvement over the adaptive ARQ schemes and the random non-adaptive FH systems. Hence, it is a promising technique for capacity enhancement of wireless data networks.

11.2 Suggestions for further work

The following are interesting topics which may be pursued for future work. Some are already in progress.

- The proposed synchronization and channel estimation methods are based on the systems with continuous transmission or burst mode with TDMA. With OFDM technology, another multiple access scheme namely orthogonal frequency division multiple access (OFDMA) can also be implemented. The synchronization and channel estimation issues in OFDMA are of interest for future wireless systems such as broadband wireless access systems currently being standardized

by the IEEE Metropolitan Area Network (MAN) standards committee [118].

- From our results, it can be observed that if some information of the channel is utilized in the synchronization and channel estimation, performance improvement can be achieved. Hence, it is of interest to find synchronization and channel estimation algorithms that can extract the required information of any type of channel and utilize it in the synchronization and channel estimation. The desirable aspect is the algorithms should work for different channel environments without requiring any prior knowledge of the channel.
- So far, OFDM synchronization algorithms are proposed for system with single transmit antenna. Due to the diversity advantage, transmit diversity has gained more and more application in current and future wireless communication systems. Hence, it is of much interest to investigate the OFDM synchronization algorithms for systems with transmit diversity.
- A desirable and challenging task in OFDM systems is to find a code which has low PAPR, good error correction capability, reasonable code rate, and efficient encoding/decoding process. A recent development in this trend is to use the second-order cosets of first-order Reed-Muller codes. However, for an OFDM system with a large number of subcarriers, the code rate becomes too small. Our results in this trend show that higher order cosets of first-order Reed-Muller codes with low PAPR have some regular patterns. Hence, it would be quite interesting and fruitful if a general pattern can be found such that an efficient encoding/decoding can be realized while keeping good error correction, low PAPR, and reasonable code rate.
- In the proposed adaptive ARQ schemes, only stop-and-wait (SW) ARQ scheme is considered. For short range wireless communications where the round trip delay is quite small, SW ARQ can be an efficient mechanism due to its implementation simplicity and small storage requirement. However, for wider range wireless communications, other ARQ schemes such as selective repeat (SR) would be more efficient although they have quite larger implementation complexity and larger storage requirement. Hence, the extension of the proposed adaptive schemes to other ARQ mechanisms would be of interest.
- Another interesting issue is efficient resource management for OFDMA systems.

Since in OFDMA systems, the radio resources are both in subcarrier domain and time domain, it would be quite interesting to devise an efficient resource management which takes into account the required QoS, data rate, the channel conditions for each user, etc.

Bibliography

[1] R. W. Chang, "Synthesis of band-limited orthogonal signals for multichannel data transmission," *Bell Systems Technical Journal*, vol. 45, pp. 1775–1796, Dec. 1966.

[2] B. R. Saltzberg, "Performance of an efficient parallel data transmission system," *IEEE Transactions on Communications*, vol. 15, pp. 805–811, Dec. 1967.

[3] S. Darlington, "On digital single-sideband modulators," *IEEE Transactions on Circuit Theory*, vol. 17, pp. 409–414, Aug. 1970.

[4] S. B. Weinstein and P. M. Ebert, "Data transmission by frequency division multiplexing using the discrete fourier transform," *IEEE Transactions on Communications*, vol. 9, pp. 628–634, Oct. 1971.

[5] A. Peled and A. Ruiz, "Frequency domain data transmission using reduced computational complexity algorithms," *Proceedings of IEEE International Conference on Acoustic, Speech and Signal Processing, Denver, CO.*, pp. 964–967, 1980.

[6] M. L. Doelz, E. T. Helad, and D. L. Martin, "Binary data transmission techniques for linear systems," *Proceedings of the IRE*, vol. 45, pp. 656–661, May 1957.

[7] R. R. Mosier and R. G. Clabaugh, "Kinplex, a bandwidth-efficient binary transmission system," *AIEE Transactions (Part I: Communications and Electronics)*, vol. 76, pp. 723–728, Jan. 1958.

[8] G. C. Porter, "Error-distribution and diversity performance of a frequency-differential PSK HF modem," *IEEE Transactions on Communication Technology*, vol. 16, pp. 723–728, Jan. 1958.

[9] M. S. Zimmerman and A. L. Kirsch, "The AN/GSC-10(KATHRYN) variable rate data modem for HF radio," *IEEE Transactions on Communication Technology*, vol. 15, pp. 197–205, Apr. 1967.

[10] P. A. Bello, "Selective fading limitations of the kathryn modem and some system design considerations," *IEEE Transactions on Communication Technology*, vol. 13, pp. 320–333, Sept. 1965.

[11] B. Hirosaki, "An orthogonally multiplexed QAM system using the discrete

fourier transform," *IEEE Transactions on Communications*, vol. 29, pp. 982–989, Jul. 1981.

[12] B. Hirosaki et. al., "A 19.2 kbps voiceband data modem based on orthogonally multiplexed QAM techniques," *Proceedings of IEEE International Conference on Communications*, pp. 21.1.1–5, 1985.

[13] L. J. Cimini Jr., "Analysis and simulation of a digital mobile channel using orthogonal frequency division multiplexing," *IEEE Transactions on Communications*, vol. 33, no. 7, pp. 665–675, Jul. 1985.

[14] M. Alard and R. Lassalle, "Principles of modulation and channel coding for digital broadcasting for mobile receivers," *EBU Technical Review*, , no. 224, pp. 168–190, Aug. 1987.

[15] J. A. C. Bingham, "Multicarrier modulation for data transmission: An idea whose time has come," *IEEE Communications Magazine*, vol. 29, no. 5, pp. 5–14, May 1990.

[16] B. Le Floch, R. Halbert-Lassale, and D. Castelain, "Digital sound broadcasting to mobile receivers," *IEEE Transactions on Consumer Electronics*, vol. 35, no. 3, pp. 493–503, Aug. 1989.

[17] J. C. Rault, D. Castelain, and B. Le Floch, "The coded orthogonal frequency division multiplexing (COFDM) technique, and its application to digital radio broadcasting towards mobile receivers," *Proceedings of IEEE Globecom*, Dec. 1989.

[18] P. Hoeher, "TCM on frequency-selective land-mobile fading channels," *Proceedings of* 5^{th} *Tirrenia International Workshop on Digital Communications, Italy*, Sept. 1991.

[19] P. Hoeher, J. Hagenauer, E. Offer, and C. Rapp, "Performance of an RCPC-coded OFDM-based digital audio broadcasting (DAB) system," *Proceedings of IEEE Globecom*, pp. 2.1.1–7, Dec. 1991.

[20] ITU-R, "Systems for terrestrial digital sound broadcasting to vehicular, portable and fixed receivers in the frequency range 30-3,000 mhz, recommendation bs.1114.," .

[21] ITU-R, "Systems for terrestrial digital sound broadcasting to vehicular, portable and fixed receivers in the frequency range 1,400-2,700 mhz, recommendation bo.1130.," .

[22] J. F. Helard and B. Le Floch, "Trellis coded orthogonal frequency division multiplexing for digital video transmission," *Proceedings of IEEE Globecom*, Dec. 1991.

[23] B. Sueur et. al., "Digital terrestrial broadcasting of audiovisual signals," *Proceedings of SPECTRUM 20/20 Symposium, Toronto*, Oct. 1989.

[24] R. Monnier et. al., "Digital television broadcasting with high spectral efficiency," *Proceedings of International Broadcasting Conference*, pp. 380–384, 1992.

[25] J. J. Gledhill, S. V. Anikhindi, and P. A. Avon, "The transmission of digital television in the UHF band using orthogonal frequency division multiplexing," *Proceedings of the 6th International IEE Conference on Digital Processing of Signals in Communications*, pp. 175–180, Sept. 1991.

[26] N. K. Lodge and A. G. Mason, "A rugged and flexible digital modulation scheme for terrestrial high definition television," *Proceedings of 1992 NAB HDTV World Conference*, pp. 359–366, 1992.

[27] M. Saito, S. Moriyama, and O. Yamada, "A digital modulation method for terrestrial digital TV broadcasting using trellis coded OFDM and its performance," *Proceedings of IEEE Globecom*, pp. 1694–1698, Dec. 1992.

[28] M. Uehara, M. Takada, and T. Kuroda, "Transmission scheme for the terrestrial ISDB system," *IEEE Transactions onConsumer Electronics*, vol. 45, no. 1, pp. 101–106, Feb. 1999.

[29] American National Standards Institute (ANSI), "Asymmetric digital subscriber line (ADSL) metallic interface," *Draft American National Standars for Telecommunications*, Dec. 1995.

[30] L. J. Cimini Jr. and N. R. Sollenberger, "OFDM with diversity and coding for advanced cellular internet services," *Proceedings of IEEE Globecom*, pp. 305–309, Nov. 1997.

[31] L. J. Cimini Jr., J. C. Chuang, and N. R. Sollenberger, "Advanced cellular internet services," *IEEE Communications Magazine*, vol. 36, no. 10, pp. 150–159, Oct. 1998.

[32] J. C. Chuang and N. R. Sollenberger, "Wideband wireless data access based on OFDM and dynamic packet assignment," *Wireless Communications and Networking Conference*, pp. 757–761, Sept. 1999.

[33] ETSI, "Broadband radio access networks (BRAN); HIPERLAN type 2; physical (PHY) layer technical specification," *ETSI TS 101 475 v1.1.1 (2000-04)*, 2000.

[34] IEEE LAN/MAN Standards Committee, "Wireless LAN medium access control (MAC) and physical layer (PHY) specifications: High-speed physical layer in the 5 GHz band," *IEEE Standard 802.11a*, 1999.

[35] "Multimedia Mobile Access Communication (MMAC)," *http://www.arib.or.jp/mmac/e/index.htm.*

[36] R. D. J. van Nee and G. Awater, "New high-rate wireless LAN standards," *IEEE Communications Magazine*, pp. 82–88, Dec. 1999.

[37] "Wireless indoor flexible high bit-rate modem architecture (WIND-FLEX)," *http://www.vtt.fi/ele/research/els/projects/windflex.htm.*

[38] J-J. van de Beek, M. Sandell, and P.O. Börjesson, "ML estimation of time and frequency offset in OFDM systems," *IEEE Transactions on Signal Processing*, vol. 45, no. 7, pp. 1800–1805, July 1997.

[39] D. Landström, J.M. Arenas, J.J van de Beek, P.O. Börjesson, M-L.Boucheret, and P.Ödling, "Time and frequency offset estimation in OFDM systems employing pulse shaping," *Proceedings of International Conference on Universal Personal Communications, San Diego, CA, USA*, pp. 279–283, Oct. 1997.

[40] D. Lee and K. Cheun, "A new symbol timing recovery algorithm for OFDM systems," *IEEE Transactions on Consumer Electronics*, vol. 43, no. 3, pp. 767–775, Aug. 1997.

[41] M. Speth, F. Classen, and H. Meyr, "Frame synchronization of OFDM systems in frequency selective fading channels," *Proceedings of IEEE Vehicular Technology Conference, Phoenix, Arizona, USA*, pp. 1807–1811, May 1997.

[42] M. Speth, D. Daecke, and H. Meyr, "Minimum overhead burst synchronization for OFDM based broadband transmission," *Proceedings of Global Telecom. Conf., Sydney, Australia*, pp. 2777–2782, Nov. 1998.

[43] L. Hazy and M. El-Tanany, "Synchronization of OFDM systems over frequency selective fading channels," *Proceedings of IEEE Vehicular Technology Conference, Phoenix, Arizona, USA*, pp. 2094–2098, May 1997.

[44] T.M. Schmidl and D.C. Cox, "Robust frequency and timing synchronization for OFDM," *IEEE Transactions on Communications*, vol. 45, no. 12, pp. 1613–1621, Dec. 1997.

[45] B. McNair, L.J. Cimini Jr., and N. Sollenberger, "A robust timing and frequency offset estimation scheme for orthogonal frequency division multiplexing (OFDM) systems," *Proceedings of IEEE Vehicular Technology Conference, Houston, Texas, USA*, pp. 690–694, May 1999.

[46] D. Landström, S.K. Wilson, J.J. van de Beek, P. Ödling, and P.O. Borjesson, "Symbol time offset estimation in coherent OFDM systems," *Proceedings of Intl Conf. on Communications, Vancouver, BC, Canada*, pp. 500–505, June 1999.

[47] Y. Li, N. Seshadri, and S. Ariyavisitakul, "Channel estimation for OFDM systems with transmitter diversity in mobile wireless channels," *IEEE Journal on Select. Areas in Communications*, vol. 17, no. 3, pp. 461–470, Mar. 1999.

[48] Y. Li, L.J. Cimini Jr., and N.R. Sollenberger, "Robust channel estimation for OFDM systems with rapid dispersive fading channels," *IEEE Transactions on Communications*, vol. 46, no. 7, pp. 902–915, Jul. 1998.

[49] M. Speth, S. Fechtel, G. Fock, and H. Meyr, "Broadband transmission using

OFDM: System performance and receiver complexity," *International Zurich Seminar on Broadband Communications, Zurich, Switzerland*, pp. 99–104, Feb. 1998.

[50] F. Classen, M. Speth, and H. Meyr, "Channel estimation units for an OFDM system suitable for mobile communications," *Mobile Kommunikation: ITG-Fachbericht, Munchen, Berlin*, Sept. 1995.

[51] J-J. van de Beek, O. Edfors, M. Sandell, S.K. Wilson, and P.O. Börjesson, "On channel estimation in OFDM systems," *Proceedings of IEEE Vehicular Technology Conf., Chicago, IL*, pp. 815–819, Jul. 1995.

[52] A. Chini, Y. Wu, M. El-Tanany, and S. Mahmoud, "Filtered decision feedback channel estimation for OFDM-based DTV terrestrial broadcasting system," *IEEE Transactions on Broadcasting*, vol. 44, no. 1, pp. 2–11, Mar. 1998.

[53] C. S. Yeh and Y. Lin, "Channel estimation using pilot tones in OFDM systems," *IEEE Transactions on Broadcasting*, vol. 45, no. 4, pp. 400–409, Dec. 1999.

[54] O. Edfors, M. Sandell, J. J. van de Beek, S. K. Wilson, and P. O. Börjesson, "OFDM channel estimation by singular value decomposition," *IEEE Transactions on Communications*, vol. 46, no. 7, pp. 931–939, Jul. 1998.

[55] S. M. Kay, *Fundamentals of statistical signal processing-Estimation theory*, Prentice Hall PTR, 1st edition, 1993.

[56] ETSI, "Digital video broadcasting (DVB): Framing, channel coding and modulation for digital terrestrial television," *ETSI EN300 744 V1.3.1 Draft (2000-08)*, 2000.

[57] L. J. Cimini Jr., B. Daneshrad, and N. R. Sollenberger, "Clustered OFDM with transmitter diversity and coding," *IEEE Global Telecommunications Conf., London, U.K.*, pp. 703–707, Nov. 1996.

[58] A. Wittneben, "A new bandwidth efficient transmit antenna modulation diversity scheme for linear digital modulation," *IEEE International Conf. on Communications, Geneva, Switerland*, pp. 1630–1634, Jun. 1993.

[59] J. H. Winters, "The diversity gain of transmit diversity in wireless systems with rayleigh fading," *IEEE International Conf. on Communications, Chicago, IL*, pp. 1121–1125, Jun. 1994.

[60] V. Tarokh, N. Seshadri, and A. R. Calderbank, "Space-time codes for high data rate wireless communication: Performance analysis and code construction," *IEEE Transactions on Information Theory*, pp. 744–765, Mar. 1998.

[61] D. Agarwal, V. Tarokh, A. Naguib, and N. Seshadri, "Space-time coded OFDM for high data rate wireless communication over wideband channels," *Proceedings of IEEE Vehicular Technology Conference, Ottawa, Canada*, pp. 2232–2236, May 1989.

[62] K. Pahlavan and A. H. Levesque, *Wireless Information Networks, Chapter 6*, John Wiley & Sons, Inc., 1st edition, 1995.

[63] P.H. Moose, "A technique for orthogonal frequency division multiplexing frequency offset correction," *IEEE Transactions on Communications*, vol. 42, no. 10, pp. 2908–2914, Oct. 1994.

[64] M. Morelli and U. Mengali, "An improved frequency offset estimator for OFDM applications," *IEEE Communications Letters*, pp. 75–77, Mar. 1999.

[65] B. Yang, K. B. Letaief, R. S. Cheng, and Z. Cao, "Timing recovery for OFDM transmission," *IEEE Journal on Selected Areas in Communications*, pp. 2278–2290, Nov. 2000.

[66] T. Keller, L. Piazzo, P. Mandarini, and L. Hanzo, "Orthogonal frequency division multiplex synchronization techniques for frequency-selective fading channels," *IEEE Journal on Selected Areas in Communications*, vol. 19, no. 6, pp. 999–1008, Jun. 2001.

[67] F. Daffara and O. Adami, "A new frequency detector for orthogonal multicarrier transmission techniques," *Proceedings of IEEE Vehicular Technology Conference, Chicago, Illinois, USA*, pp. 804–809, Jul. 1995.

[68] H. Minn, M. Zeng, and V. K. Bhargava, "On timing offset estimation for OFDM systems," *IEEE Communications Letters*, vol. 4, no. 7, pp. 242–244, Jul. 2000.

[69] S. A. Fechtel and H. Meyr, "Improved frame synchronization for spontaneous packet transmission over frequency-selective radio channels," *International Symposium on Personal, Indoor and Mobile Radio Communications, The Hague, Netherlands*, pp. 353–357, 1994.

[70] M. Speth, S. A. Fechtel, G. Fock, and H. Meyr, "Optimum receiver design for wireless broad-band systems using OFDM-part i," *IEEE Transactions on Communications*, vol. 47, no. 11, pp. 1668–1677, Nov. 1999.

[71] A. Czylwik, "Synchronization for single carrier modulation with frequency domain equalization," *Proceedings of IEEE Vehicular Technology Conference' 98, Ottawa, Canada*, pp. 2277–2281, 1998.

[72] P. R. Chevillat, D. Maiwald, and G. Ungerboeck, "Rapid training of a voiceband data-modem receiver employing an equalizer with fractional-t spaced coefficients," *IEEE Transactions on Communications*, vol. COM35, pp. 869–876, Sept. 1987.

[73] S. H. Müller-Weinfurtner, "On the optimality of metrics for coarse frame synchronization in OFDM: a comparison," *International Symposium on Personal, Indoor and Mobile Radio Communications, Boston*, pp. 533–537, 1998.

[74] U. Lambrette, M. Speth, and H. Meyr, "Ofdm burst frequency synchronization

by single carrier training data," *IEEE Communications Letters*, vol. 1, no. 2, pp. 46–48, Mar. 1997.

[75] M.J.E. Golay, "Complementary series," *IRE Transactions on Information Theory*, vol. IT-7, pp. 82–87, Apr. 1961.

[76] R.D.J. van Nee, "OFDM codes for peak-to-average power reduction and error correction," *Proceedings of Global Telecom. Conf., London*, pp. 740–744, Nov. 1996.

[77] M. Morelli and U. Mengalli, "'carrier-frequency estimation for transmissions over selective channels," *IEEE Transactions on Communications*, vol. 48, no. 9, pp. 1580–1589, Sept. 2000.

[78] F. Classen and H. Meyr, "Frequency synchronization algorithms for OFDM systems suitable for communication over frequency selective fading channels," *Proceedings of IEEE Vehicular Technology Conference, Stockholm, Sweden*, pp. 1655–1659, Jun. 1994.

[79] M. Luise and R. Reggiannini, "Carrier frequency acquisition and tracking for OFDM systems," *IEEE Transactions on Communications*, vol. 44, no. 11, pp. 1590–1598, Nov. 1996.

[80] B. Yang, K. B. Letaief, R. S. Cheng, and Z. Cao, "Channel estimation for OFDM transmission in multipath fading channels based on parametric channel modeling," *IEEE Transactions on Communications*, vol. 49, no. 3, pp. 467–479, Mar. 2001.

[81] S. A. Fechtel and H. Meyr, "Fast frame synchronization, frequency offset estimation and channel acquisition for spontaneous transmission over unknown frequency-selective radio channels," *International Symposium on Personal, Indoor and Mobile Radio Communications, Yokohama, Japan*, pp. 229–233, 1993.

[82] M. H. Meyrs and L. E. Franks, "Joint carrier phase and symbol timing recovery for PAM systems," *IEEE Transactions on Communications*, vol. 28, pp. 1121–1129, Aug. 1980.

[83] C. Tellambura, "Use of m-sequence for OFDM peak-to-average power ratio reduction," *IEE Electronics Letters*, vol. 33, no. 15, pp. 1300–1301, Jul. 1997.

[84] D. Wulich, "Comments on the peak factor of sampled and continuous signals," *IEEE Communications Letters*, vol. 4, no. 7, pp. 213–214, Jul. 2000.

[85] A. V. Oppenheim and R. W. Schafer, *Discrete-time signal processing*, Prentice-Hall International, Inc., 1989.

[86] A. Papoulis, "Limits on bandlimited signals," *Proceedings of of IEEE*, vol. 44, no. 10, pp. 1677–1686, Oct. 1967.

[87] A. Papoulis, "Truncated sampling expansions," *IEEE Transactions on Automatic Control*, pp. 604–605, Oct. 1967.

[88] C. E. Shannon, "Communications in the presence of noise," *Proceedings of of IRE*, vol. 37, pp. 12–21, Jan. 1949.

[89] A. J. Jerri, "The shannon sampling theorem-its various extensions and applications: A tutorial review," *Proceedings of IEEE*, vol. 65, no. 11, pp. 1565–1596, Nov. 1977.

[90] L. L. Campbell, "Sampling theorem for the fourier transform of a distribution with bounded support," *SIAM Journal of Applied Mathematics*, vol. 16, pp. 626–636, May 1968.

[91] E. Pfaffelhuber, "Sampling series for band-limited generalized functions," *IEEE Transactions on Information Theory*, vol. IT-7, no. 6, pp. 650–654, Nov. 1971.

[92] A. J. Jerri, "On the equivalence of kramer's and shannon's sampling theorems," *IEEE Transactions on Information Theory*, pp. 497–499, Jul 1969.

[93] X. Li and Jr. L.J. Cimini, "Effects of clipping and filtering on the performance of OFDM," *Proceedings of IEEE Vehicular Technology Conference*, pp. 1634–1638, 1997.

[94] D. Wulich and L. Goldfeld, "Reduction of peak factor in orthogonal multicarrier modulation by amplitude limiting and coding," *IEEE Transactions on Communications*, vol. 47, no. 1, pp. 18–21, Jan. 1999.

[95] A.E. Jones, T.A. Wilkinson, and S.K. Barton, "Block coding scheme for reduction of peak to mean envelope power ratio of multicarrier transmission schemes," *IEE Electronics Letters*, vol. 30, no. 25, pp. 2098–2099, Dec. 1994.

[96] S.J. Shepherd, P.W.J. van Eetvelt, C.W. Wyatt Millington, and S.K. Barton, "Simple coding scheme to reduce peak factor in QPSK multicarrier modulation," *IEE Electronics Letters*, vol. 31, no. 14, pp. 1131–1132, Jul. 1995.

[97] R.W. Bauml, R.F.H. Fischer, , and J.B. Huber, "Reducing the peak-to-average power ratio of multicarrier modulation by selected mapping," *IEE Electronics Letters*, vol. 32, no. 22, pp. 2056–2057, Oct. 1996.

[98] D.J.G. Mestdagh and P.M.P. Spruyt, "A method to reduce the probability of clipping in DMT-based transceivers," *IEEE Transactions on Communications*, vol. 44, no. 10, pp. 1234–1238, Oct. 1996.

[99] Muller and J.B. Huber, "A novel peak power reduction scheme for OFDM," *International Symposium on Personal, Indoor and Mobile Radio Communications*, pp. 1090–1094, 1997.

[100] M. Friese, "Multicarrier modulation with low peak-to-average power ratio," *IEE Electronics Letters*, vol. 32, no. 8, pp. 713–714, Apr. 1996.

[101] A.E. Jones and T.A. Wilkinson, "Combined coding for error control and increased robustness to system nonlinearities in OFDM," *Proceedings of IEEE Vehicular Technology Conference*, pp. 904–908, 1996.

[102] J.A. Davis and J. Jedwab, "Peak-to-mean power control and error correction for OFDM transmission using golay sequences and Reed-Muller codes," *IEE Electronics Letters*, vol. 33, no. 4, pp. 267–268, Feb. 1997.

[103] H. Ochiai and H. Imai, "Block coding scheme based on complementary sequences for multicarrier signals," *IEICE Transactions Fundamentals*, pp. 2136–2143, 1997.

[104] J.A. Davis and J. Jedwab, "Peak-to-mean power control in OFDM, Golay complementary sequences and Reed-Muller codes," *Technical Report HPL-97-158, Hewlett-Packard Labs., Bristol*, Dec. 1997.

[105] K.G. Paterson, "Generalized Reed-Muller codes and power control in OFDM modulation," *Technical Report HPL-98-57, Hewlett-Packard Labs., Bristol*, Mar. 1998.

[106] A. C. Martins and J. C. Alves, "ARQ protocols with adaptive block size perform better over a wide range of bit error rates," *IEEE Transactions on Communications*, pp. 737–739, Jun. 1990.

[107] S. Kallel and C. Leung, "Analysis of memory and incremental redundancy arq schemes over a nonstationary channel," *IEEE Transactions on Communications*, vol. 40, pp. 1474–1480, Sept. 1992.

[108] Y. Yao, "An effective Go-Back-N ARQ scheme for variable error rate channels," *IEEE Transactions on Communications*, pp. 20–23, Jan. 1995.

[109] D. J. Young and N. C. Beaulieu, "On the generation of correlated rayleigh random variates by inverse discrete fourier transform," *Proceedings of International Conference on Universival Personal Communications, Cambridge, Massachusetts*, pp. 231–235, Sept. 1996.

[110] M. Gudmundson, "Correlation model for shadow fading in mobile radio systems," *IEE Electronics Letters*, vol. 27, pp. 2145–2146, Nov. 1991.

[111] S. Hara, A. Ogino, M. Araki, M. Okada, and N. Morinaga, "Throughput performance of SAW-ARQ protocol with adaptive packet length in mobile packet data transmission," *IEEE Transactions on Vehicular Technology*, pp. 561–569, Aug. 1996.

[112] M. Rice and S. B. Wicker, "A sequential scheme for adaptive error control over slowly varying channels," *IEEE Transactions on Communications*, pp. 1533–1543, February/March/April 1994.

[113] M. Zeng, H. Minn, and V. K. Bhargava, "An efficient ARQ protocol for adaptive

error control over time-varying channel," *International Symposium on Communications (ISCOM), Kaohsiung, Taiwan*, pp. 72–76, Nov. 1999.

[114] H. Minn, M. Zeng, A. Annamalai, and V. K. Bhargava, "An efficient ARQ protocol for adaptive error control over time-varying channels," *An International Journal of Wireless Personal Communications, Kluwer Academic Publishers*, vol. 17, no. 1, pp. 3–20, Apr. 2001.

[115] M. Rice and S. B. Wicker, "Adaptive error control for slowly varying channels," *IEEE Transactions on Communications*, pp. 917–925, February/March/April 1994.

[116] S.S. Chakraborty, M. Liinaharja, and E.Y-Juuti, "An adaptive ARQ scheme with packet combining for time varying channels," *IEEE Communications Letters*, vol. 3, no. 2, pp. 52–54, Feb. 1999.

[117] P. Sindhu, "Retransmission error control with memory," *IEEE Transactions on Communications*, vol. COM-25, no. 5, pp. 473–479, May 1977.

[118] IEEE LAN/MAN Standards Committee, "IEEE 802.16 a/b (draft)," *Broadband Wireless Access: IEEE MAN standard*, 2001.